TU/e EINDHOVEN UNIVERSITY OF TECHNOLOGY

Self-assembling auto-fluorescent amphiphiles : nano-sized platform technology for multi-purpose cellular targeting

Citation for published version (APA):
Petkau - Milroy, K. (2012). *Self-assembling auto-fluorescent amphiphiles : nano-sized platform technology for multi-purpose cellular targeting*. [Phd Thesis 1 (Research TU/e / Graduation TU/e), Biomedical Engineering]. Technische Universiteit Eindhoven. https://doi.org/10.6100/IR733401

DOI:
10.6100/IR733401

Document status and date:
Published: 01/01/2012

Document Version:
Publisher's PDF, also known as Version of Record (includes final page, issue and volume numbers)

Please check the document version of this publication:

• A submitted manuscript is the version of the article upon submission and before peer-review. There can be important differences between the submitted version and the official published version of record. People interested in the research are advised to contact the author for the final version of the publication, or visit the DOI to the publisher's website.
• The final author version and the galley proof are versions of the publication after peer review.
• The final published version features the final layout of the paper including the volume, issue and page numbers.

Link to publication

General rights
Copyright and moral rights for the publications made accessible in the public portal are retained by the authors and/or other copyright owners and it is a condition of accessing publications that users recognise and abide by the legal requirements associated with these rights.

• Users may download and print one copy of any publication from the public portal for the purpose of private study or research.
• You may not further distribute the material or use it for any profit-making activity or commercial gain
• You may freely distribute the URL identifying the publication in the public portal.

If the publication is distributed under the terms of Article 25fa of the Dutch Copyright Act, indicated by the "Taverne" license above, please follow below link for the End User Agreement:

www.tue.nl/taverne

Take down policy
If you believe that this document breaches copyright please contact us at:

openaccess@tue.nl

providing details and we will investigate your claim.

Download date: 16. Nov. 2023

Self-assembling auto-fluorescent amphiphiles

Nano-sized platform technology for multi-purpose cellular targeting

PROEFSCHRIFT

ter verkrijging van de graad van doctor aan de
Technische Universiteit Eindhoven, op gezag van de
rector magnificus, prof.dr.ir. C.J. van Duijn, voor een
commissie aangewezen door het College voor
Promoties in het openbaar te verdedigen
op maandag 25 juni 2012 om 16.00 uur

door

Katja Petkau-Milroy

geboren te Froenze, Kirgizië

Dit proefschrift is goedgekeurd door de promotor:

prof.dr.ir. L. Brunsveld

A catalogue record is available from the Eindhoven University of Technology Library
ISBN: 978-90-386-3163-9

Cover Design: K. Petkau-Milroy
Printing: Wöhrmann Print Service, Zutphen, the Netherlands

Моим родителям

Table of Contents

1

Bio-active self-assembling nanostructures

Abstract. The regulation of recognition events via dynamic and reversible self-assembly of building blocks in nature has inspired the emergence of supramolecular chemical biology. In this field of research synthetic supramolecular architectures in water are used to study or to interact with biological systems. Since the development of supramolecular chemical biology, several applications for self-assembling nanostructures have been brought forward, ranging from imaging to diagnostics, and from drug delivery to tissue engineering. Many of these applications require the capability of the supramolecular system to actively target specific cell surface receptors. Targeting is typically achieved with ligands, such as small molecules, peptides, proteins, that can be introduced either prior or post the self-assembling process. Advantages of the non-covalent organization of ligands compared to the organization of ligands in a covalent fashion on polymeric scaffolds include the responsive nature of the self-assembly process, the ease of supramolecular synthesis and the possibility to incorporate a multiple array of different ligands through mixing of building blocks. In this chapter an overview over a diversity of self-assembled nanostructures constructed from mono-disperse synthetic building blocks is given; with a particular focus on their design, self-assembly, functionalization with bioactive ligands and possible applications.

1.1 Inspired by Nature

Nature displays a vast array of functional nanostructures, which are constructed via self-assembly[1], a spontaneous organization of disordered molecular units into ordered structures. Examples include the self-assembly of proteins and RNA to form the ribosome – the translationary machinery of the cell – as well as the rapid assembly and disassembly of actin and microtubule filaments and the self-assembly of phospholipids to form cell membranes (Figure 1.1). The most significant advantage of non-covalent self-assemblies is the generation of adaptable and dynamic nano-sized structures, as will be exemplified in the case of a few selected set of examples.

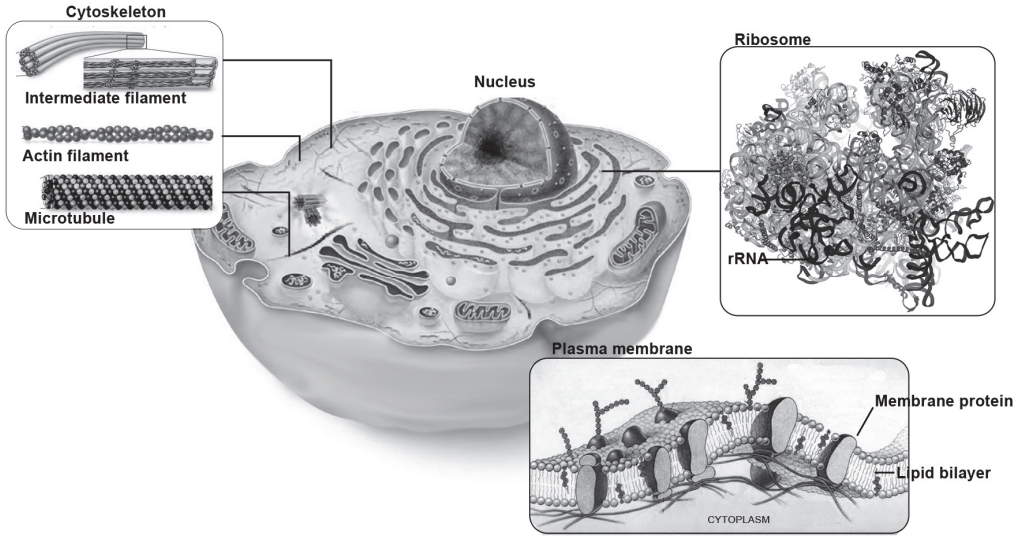

Figure 1.1: Eukaryotic cell; Insets: Cytoskeleton with three major cytoplasmic supramolecular polymers - microtubules, intermediate filaments, and actin filaments; Plasma membrane with transmembrane proteins; Crystal structure of an eukaryotic ribosome[2], a highly complex assembly from more than 50 proteins subunits and several RNAs (black).

Nature frequently uses self-assembly to orchestrate recognition events, in particular in membranes. The cell membrane – a highly selectively permeable barrier consisting of a lipid bilayer with integral proteins – is essential for cell survival and function. The non-covalent self-assembly of transmembrane proteins in the plasma membrane enables dynamic movement and allows for the spontaneous clustering of receptors: a crucial requirement for the function of growth factor-mediated cell signaling[3], for example, or of integrin-mediated cell adhesion[4] and T-cell activation[5]. The phospholipids are asymmetrically distributed between the outer and the inner leaflet of the lipid bilayer and this asymmetric disequilibrial distribution is maintained by energy dependent lipid transporters. The anionic phospholipid, phosphatidylserine (PS), is via this process normally restricted to the inner leaflet (Figure 1.2). However, in dying and activated cells, specific localization is not maintained resulting in the translocation of PS to the outer leaflet[6]; a process only possible through the non-covalent rearrangement of lipid assembly at the

plasma membrane. In nature, this phenomenon triggers the uptake and removal of early apoptotic cells by macrophages bearing PS recognizing receptors. In biochemistry, PS binding probes, for example liposomes displaying several annexin V proteins[7], are now widely used as markers of early apoptotic cells.

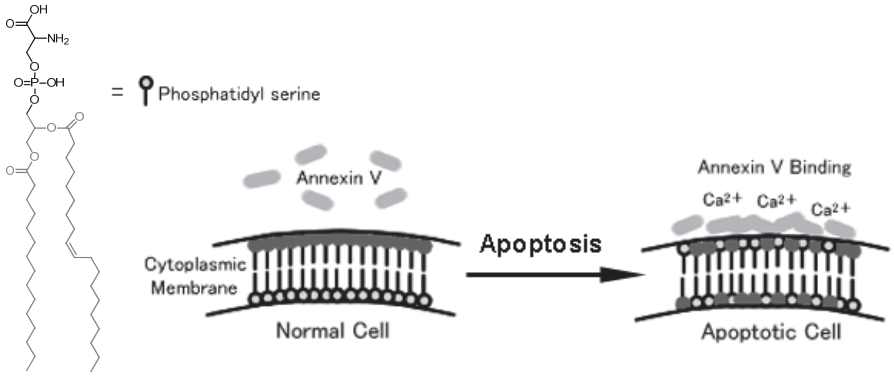

Figure 1.2: Structure of phosphatidyl serine and the binding of annexin V.

The three major cytoplasmic supramolecular polymers - microtubules, intermediate filaments, and actin filaments - spontaneously assemble from short monomers into long uniform structures. The polymerization process is temporally and spatially regulated in response to external stimuli. Microtubules, cytoplasmic tubular fibers, which self-assemble from alternating protein subunits (Figure 1.1), are involved in many cellular functions such as intracellular transport and chromosome segregation during cell division. Motility of cells is regulated via rapid assembly of filamentous actin.[8] The dynamic function of these processes is intrinsically coupled with the capacity of actin and microtubules to rapidly polymerize and depolymerize,[9] a requirement which can only be met with supramolecular assembled systems.

The self-assembly of biomolecules is a consequence of specific, local and non-covalent interactions, which include hydrogen bonding as well as electrostatic and hydrophobic interactions. Since the intrinsic nature of self-assembly is a 'bottom-up' construction of higher-order structure from monomeric building blocks, the final assembly is stabilized by many, relatively weak, non-covalent interactions distributed over the whole molecular volume. At the same time, this intrinsic nature offers an excellent platform for constructing multivalent ligands. Multivalency is a simultaneous interaction between the multiple functionalities of one entity and the complementary functionalities of another. Multivalent interactions are essential for many biological recognition events to enhance binding affinities. Increasing the number of existing interactions or combining diverse molecular interactions leads to high-affinity molecular recognition without the need to evolve stronger and more complex binders.

Using non-covalent self-assembly, nature has created a wide diversity of structures and functions at the cellular and subcellular level, which has inspired the emergence of supramolecular chemistry. Supramolecular chemistry studies the non-covalent interactions in and between molecules, and the resulting multimolecular complexes. Starting with small synthetic supramolecular systems derived from simple building blocks[10], an increased

understanding of intermolecular interactions has led to the supramolecular synthesis of multimolecular architectures with vast arrays of shapes, compositions and functionalities and numerous applications in the field of material science.[11] In most of these cases, however, and in contrast to nature, these supramolecular materials were self-assembled in the solid or gel state or in organic solvents. The development of supramolecular architectures filled with the capacity to assemble under dilute conditions in water or buffered media[12,13] has since opened up the field of supramolecular chemistry to supramolecular chemical biology, where supramolecular chemistry is applied to the study of biological processes.[14]

1.2 Supramolecular chemical biology

1.2.1 *Ligand functionalization of self-assembling materials*

Synthetic supramolecular architectures in water could find diverse applications, ranging from imaging to diagnostics, and from drug delivery to tissue engineering. Many of these applications would require the supramolecular systems capable of actively targeting specific cell surface receptors. Targeting is typically achieved through functionalization of the materials under study with ligands, such as small molecules, peptides, proteins and antibodies. As mentioned above, the intrinsic nature of self-assembled systems – the construction of higher-order structure from monomeric building blocks – could be exploited to facilitate multivalent ligand display. The ligands can either already be part of the monomeric supramolecular building blocks (pre-functionalization) or introduced after self-assembly via (non)covalent attachment to appending reactive groups (post-functionalization).

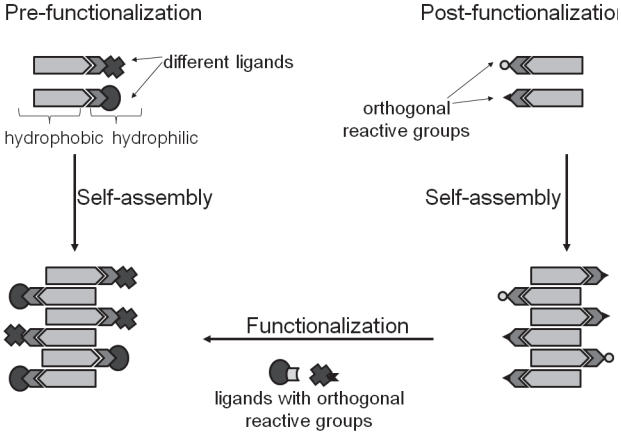

Figure 1.3: Pre- and post-functionalization of self-assembling materials. Using the pre-functionalization approach, heterovalent structures are generated via co-assembly of differently functionalized building blocks. To generate heterovalent structures via post-functionalization the incorporation of several orthogonal reactive groups is required, which can be functionalized with ligand after the assembly.

Combining the bioactive and the self-assembling epitope in one building block, the so-called pre-functionalization approach, enables the generation of nanomaterials with controlled ligand display (Figure 1.3). The ligand density can be tuned through intermixing with building blocks featuring different ligands or those lacking any bioactive epitope.[15] Limitation for the pre-functionalization strategy is the requirement for the bioactive ligands to be compatible with the synthetic preparation of the building block and with the supramolecular synthesis, i.e. the self-assembly process, of the final supramolecular architecture; the introduced ligand should not be hindering the self-assembly. Typically, ligands such as carbohydrates, peptides and aptamers could be suitable for application in the pre-functionalization strategy, because of their robust molecular structures, whereas more environment sensitive ligands such as larger, folded proteins might require an alternative functionalization approach.

The addition of functional epitopes to the bare supramolecular scaffolds post self-assembly would alternatively permit the introduction of a wide range of ligands using both synthetic and enzymatic approaches.[16–19] The non-decorated supramolecular scaffold acts as a versatile platform that can enable rapid functionalization in the aqueous environment in which it is formed. This post-functionalization approach would provide rapid access to diverse applications after functionalization of the supramolecular scaffold without the need of redesign and *de-novo* synthesis. The precise control over the introduced ligand density, however, might be limited to, for example, the reactivity differences on different sites of the scaffold. Orthogonal functional groups could be introduced into the supramolecular building block of the bare self-assembled scaffold to enable the attachment of different functionalities via post-functionalization. The wide array of reactions that can be applied for post-functionalization in aqueous solution, such as NHS-, maleimide-coupling, azide-alkyne cycloaddition, Staudinger ligation and the suicide-enzymes such as SNAP-tag have recently been reviewed.[17,18,20]

1.2.2 *Potential for supramolecular multivalent architectures in biomedicine*

Advantages of the non-covalent organization of ligands compared to the organization of ligands in a covalent fashion on polymeric scaffolds include the responsive nature of the self-assembly process, the ease of supramolecular synthesis and the possibility to incorporate a multiple array of different ligands through mixing of building blocks. Since the development of supramolecular chemical biology, several applications for self-assembling nanostructures have been brought forward.

Many undesired side-effects of small drug molecules amongst others arise from the fact that they are also non-specifically taken up by healthy cells. Typically, only a small percentage of the drug actually reaches the tissue of interest. The selective treatment of diseases with minimal side-effects, the so-called “magic-bullet”, proposed by Paul Ehrlich in 1901,[21] is nowadays for the vast majority of diseases and treatments still under development, for example through active targeted delivery of therapeutics. To improve drug efficacy and safety, it has proved desirable to

encapsulate drugs so as to target them to a specific site of disease.[22] In this case, the drug carrier should allow gradual, or even triggered, release of the drug and be biodegradable. A certain size of approximately 100 nm is beneficial for long circulation times in the body in order to increase drug accumulation at the site of interest. Self-assembling systems of the vesicular sort might combine many of the desired properties of the drug encapsulation strategy with the ability to be functionalized with (several) targeting ligands. Together with liposomes, viral capsids and polymerosomes are promising candidates in this growing research area.[23]

The goal of targeted imaging in diagnostics is to achieve a significant enhancement of contrast at the targeted site in a non-invasive manner. Actively targeted imaging requires the attachment of targeting ligands and imaging probes (fluorophore, contrast agent) to the same molecular entity. The incorporation of several imaging probes, which should be facilitated in self-assembling structures, allows for multimodal imaging: the combination of several imaging techniques to synergistically improve resolution and sensitiviy.[24] Additionally, self-assembling contrast agents might make it possible to combine the benefits of both high and low molecular weight contrast agents, i.e. the high relaxivity and the complete excretion from the body due to disassembly into monomers after dilution over time.

In tissue engineering, self-assembling biomaterials are promising candidates for the construction of cell-interactive (3D) matrices.[25,26] In particular, peptide-based self-assembling materials which are capable to form hydrogels are used to generate adaptable cell-culture matrices (Figure 1.4).[27] The modular self-assembly of proteins, peptides and peptide derivatives into hydrogels enables the independent, simultaneous and systematic tuning of several properties, leading to optimized cell-matrix interactions in cell culture and for regenerative medicine[28]. In contrast, for covalent polymer networks, this optimization of cell-matrix interactions proves to be more difficult. Recently, it was as well shown that the presentation of intermixed binding epitopes led to improved cell adhesion when compared against gels with separately assembled binding epitopes[29], as the density and distribution of adhesive ligands within a substrate can influence integrin clustering and with it cell adhesion, migration and the phenotype.[30]

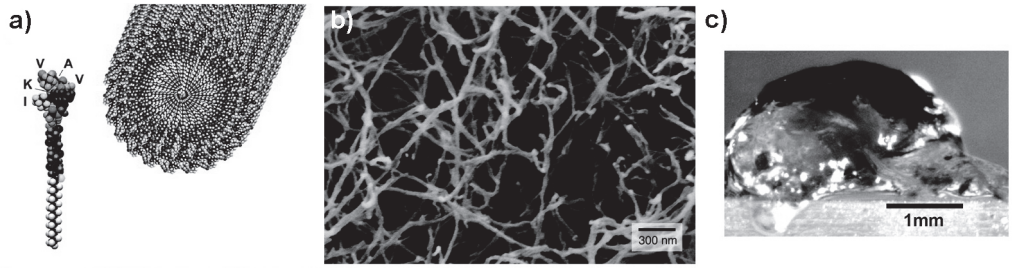

Figure 1.4: a) Molecular graphics illustration of an IKVAV-containing peptide amphiphile molecule and its self-assembly into nanofibers. b) Scanning electron micrograph of an IKVAV nanofiber network formed by adding cell media to a peptide amphiphile aqueous solution. c) Micrograph of an IKVAV nanofiber gel surgically extracted from an enucleated rat eye after intraocular injection of the peptide amphiphile solution. Adapted from reference 30. Reprinted with permission from AAAS.

Apart from the potential biomedical applications of supramolecular biomaterials, the detailed investigation of their self-assembly, especially of *de-novo* designed building blocks, helps with the understanding of how to predict and control the shape and size of self-assembled nanostructures, which remains an imposing challenge in the field of supramolecular chemistry.

Here, the main focus will be to give an overview over a diversity of self-assembled nanostructures, build-up from mono-disperse non-polymeric synthetic building blocks; in particular on their design, self-assembly, functionalization with bioactive ligands and possible applications, which will be illustrated in the case of a few examples. Polymer and block copolymer assemblies (polymersome)[31,32], virus assemblies[33], DNA assemblies[34] as well as non self-assembling nanoparticles[35] are other promising scaffolds used in imaging, targeting and drug delivery applications, which are not dealt with here.

1.3 Self-assembling bioactive nanostructures

The phase separation between hydrophobic and hydrophilic parts of an amphiphilic molecule in water plays an essential role in living systems (e.g for the formation of membranes and protein folding) and is now widely used as a powerful approach towards the fabrication of complex nano-architectures. In aqueous solution, amphiphilic molecules aggregate into micelles if their concentration lies above the critical aggregation concentration (CAC, for natural phospholipids CAC is about 10^{-8} mol/L). Below the CAC defined nanostructures are typically not observed. The micelles of linear amphiphiles might be spherical, cylindrical or plate-shaped and the structure depends on factors such as temperature, concentration and the structure of the amphiphile itself.[36] The structure of an amphiphile refers to the hydrophobic-hydrophilic balance and the geometry of the amphiphile. Disc-shaped amphiphiles, in contrast to linear amphiphiles, form only columnar aggregates due to their molecular geometry.

1.3.1 *Liposomes*

Liposomes, first discovered in 1960s[37], are clinically established drug delivery systems[38] with broad applications in industry and academia.[36] These small self-assembled spherically shaped lipid vesicles are produced from natural nontoxic phospholipids and cholesterol; the lipid bilayer encapsulating an aqueous compartment. Initially used as models to mimic biological membranes[39], liposomes can be easily varied in terms of their composition, size and their ability to encapsulate different ligands, resulting in a large number of applications such as for drug delivery and targeted imaging. A main prerequisite for the aforementioned applications is the functionalization of liposomes with targeting ligands.

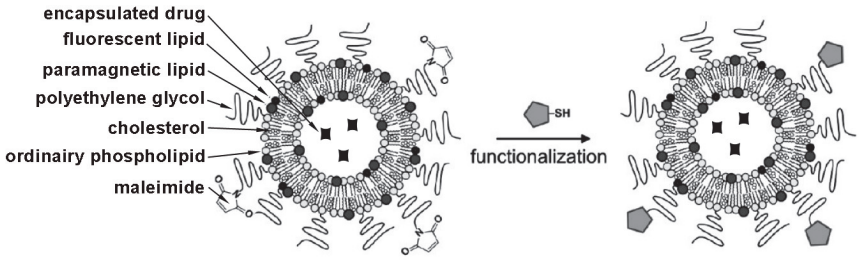

Figure 1.5: Functionalized liposomes. Adapted with permission from reference 40. Copyright (2009) American Chemical Society.

The preparation of liposomes typically involved the evaporation of an organic solvent, rehydration, followed by sonication and then extrusion, a process which limited the types of ligands that could be introduced prior to assembly. This limitation was successfully circumvented though by the introduction of functional reactive groups - using, for example, synthetically functionalized lipids or cholesterol - and post-assembly ligand decoration (Figure 1.5). Liposomes exposing several types of cell recognition ligands, from small molecules such as folic acid to large proteins including antibodies, have already been produced and used.[41] Additionally, the decoration of liposomes with polyethylene glycol (PEG) has helped to elongate in vivo circulation times from a few minutes to several hours and prevent accumulation in the liver and spleen.[42] Liposomes allow not only the inclusion of drugs and imaging agents, but as well of nanocrystals such as iron oxide nanoparticles, gold nanoparticles and quantum dots.[38,40]

In a recent example by Kluza et al. it was shown that simultaneous the targeting of two different receptors ($\alpha_v\beta_3$ integrin and galectin-1), so-called dual-targeting, synergistically improved liposomal uptake.[43] Simultaneous targeting was achieved by post-functionalization with both targeting ligands. Incorporation of fluorescent and paramagnetic lipids enabled simultaneous evaluation and imaging using different techniques. The strong antiproliferative activity of these liposomes shows the potential of theranostics, a combination of diagnostics with therapy.[38]

1.3.2 *Peptidic building blocks*

Protein folding and with it protein function is encoded by 20 natural amino-acids. While based on only a limited set of monomers, unlimited structure diversity can be achieved through sequence adaptations. Besides the extensive use of peptide sequences to mimic the functional domains of large proteins, the ability to program a vast array of structures through changes in sequence via straightforward solid-phase synthesis led to the use of peptides as self-assembling building blocks. In particular, the combination of bioactive and self-assembling epitope generates customized nanomaterials for various biomedical applications.[44,45] Inter- or intramolecular hydrogen bonding between the carbonyl group and nitrogen protons of the amide bond, which is a proton acceptor and donor in one, and the electrostatic and hydrophobic interactions of side-chains are responsible for protein folding, leading to in different structured and unstructured

protein-folding (secondary) motifs. The most common structured motifs are alpha-helices and beta-sheets.

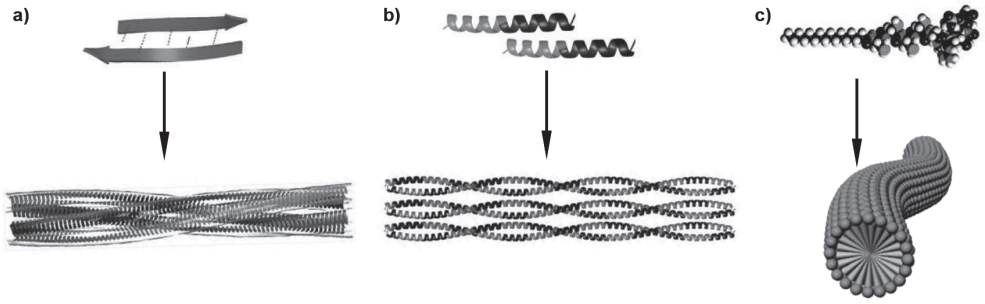

Figure 1.6: Types of peptide-based self-assemblies; a) beta-sheet based self-assembly, b) alpha-helix based self-assembly, c) peptide amphiphiles (based on reference 16).

1.3.2.1 Beta-sheet based self-assembly

Self-assembling beta-sheet structures, also referred to as amyloid-like structures, are mostly designed through alternating placement of positively charged, hydrophobic and negatively charged amino acids. Electrostatic interactions between oppositely charged amino acid side-chains and solvophobic effects between hydrophobic side chains drive the proper interchain backbone hydrogen bonding.[46] The ability of these beta-sheets to pair via edge-to-edge and face-to-face packing leads to the formation of beta-sheet ribbons and tapes, which can bundle through lateral interactions into thicker fibers (Figure 1.6 a).[47] Through sophisticated design, up to four different peptides were shown to co-assemble into one fibril[48], indicating the possibility to incorporate diverse functionalities through co-assembly.

The beta-sheet based self-assembled materials can have one or both of their *N*- or *C*-termini free, which allows for functionalization with ligands. Next to the introduction of proteins through recombinant protein-peptide fusions[49,50], the building blocks for beta-sheet fibrils were decorated with peptides[51–53], biotin[54] and carbohydrates[55,56] prior to self-assembly.[16,57] The introduction of hydrophilic ligands at the *N*- or *C*-termini, however, can influence the self-assembly process, as shown for the functionalization with PEG.

As an example, Lim et al. have synthesized amphiphiles consisting of a beta-sheet forming peptide (FKFEFKFE) and either linear or dendritic mannose functionalized PEG chains (Figure 1.7). The dendritic PEG chains interfered with the self-assembly process, leading to the premature termination of fibrils.[55] Decoration with linear PEG chains led to a stronger association of the beta-sheet bilayer and to more stable fibers. When testing the inhibition in bacterial motility of *E.Coli*, similar inhibition was observed for all fibrils. However, the formation of bacterial clusters by interconnecting the pili of different bacteria was only induced by the long nanoribbons formed by **1**, **2** and **3**. The inhibition of bacterial motility could additionally be fine-tuned through co-assembly of **3** with the same building-block displaying non binding glucose.[56]

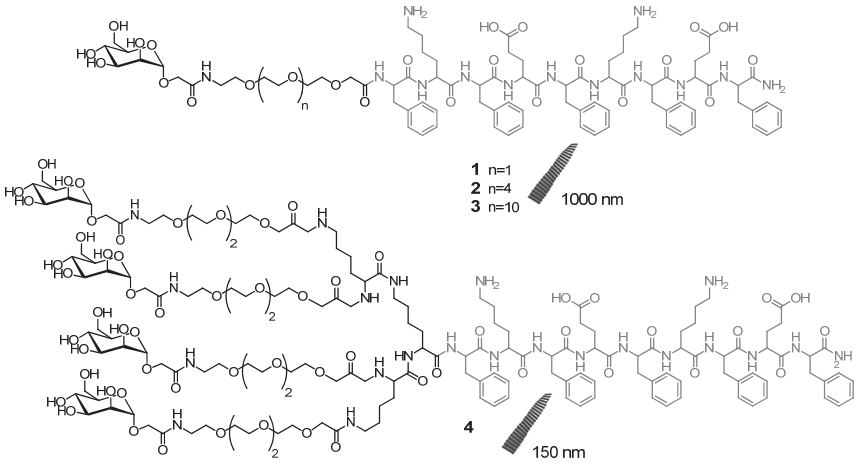

Figure 1.7: Nanoribbons formed by mannose functionalized beta-sheet based amphiphiles.[55]

1.3.2.2 Alpha-helical self-assembly

A key building-block of natural peptides, the alpha-helix, is a right-handed helix which is stabilized by intramolecular backbone hydrogen bonding between the carbonyl group (i) and the amide hydrogen four residues further along the chain (i+4). The HPPHPP amino acid pattern, with H being a hydrophobic and P a polar amino acid, creates amphiphilic structures. Alpha-helices have 3.6 residues per turn, which aligns each third residue on top of each other (Figure 1.8a). Introducing a pattern of polar and hydrophobic amino acids three residues apart generates an amphiphilic helix. The hydrophobic faces of several amphiphilic helices (residues a and d) can wrap around one another forming a so-called coiled-coil with the polar faces (residues b, c and f) exposed to the environment.[58] According to the well-established sequence-to-structure rules, three to five heptad repeats of HPPHPP are required to form stable structures.[59] For the assembly into long and thick fibrils, the amphiphilic alpha-helices are designed with 'overhangs', which enables end-to-end assembly (Figure 1.6 b).[60]

Figure 1.8: a)Helical wheel diagram and peptide sequences used by the group of Woolfson for self-assembly; y = lysine ε-azide, x = allylglycine.

The pre-functionalization of coiled-coil based self-assembling peptide fibers, developed by the group of Woolfson, via the intermixing of bare and ligand bearing peptides showed only poor incorporation of the ligand bearing peptide (~ 0.5% of total peptide). The alpha-helical peptides form crystalline-like assemblies, which do not favor introduction of "molecular defects" like the ligand. For the incorporation of ligands, the same research group then applied the post-

functionalization approach. Modified amino acids carrying azide and alkene moieties were introduced at the f position, furthest away from the coiled-coil interface (Figure 1.8). This led in the most cases to the formation of alpha-helical fibers. Using copper-catalyzed azide-alkyne cycloaddition and the photoinitiated thiol-ene reaction, the self-assembled fibers were decorated with different ligands and dual-functionalization of fibers assembled from mixtures of **8** and **7** with biotin and a dye was successfully achieved, laying the ground for further applications.[61]

The incorporation of an RGD sequence into longer alpha-helical coiled-coil peptides by Villard et al. reduced the size of the formed oligomers from around 80 to 5 self-assembling monomers, highlighting the sensitivity of the alpha-helical based system to structural changes. Immobilized on a substrate, these short self-assembling peptides were capable of promoting integrin $\alpha V\beta 3$-dependent cell adhesion.[62]

1.3.2.3 Peptide amphiphiles

Over the last decade Stupp and coworkers have developed a class of amphiphilic molecules, the so-called peptide amphiphiles (PAs), which self-assemble into cylindrical micelles in dilute aqueous solutions (Figure 1.6 c).[63,64] The PAs consist of an alkyl chain linked to a peptide segment. The peptide segment itself features a structuring element followed by a charged amino acid and finally the bioactive epitope.

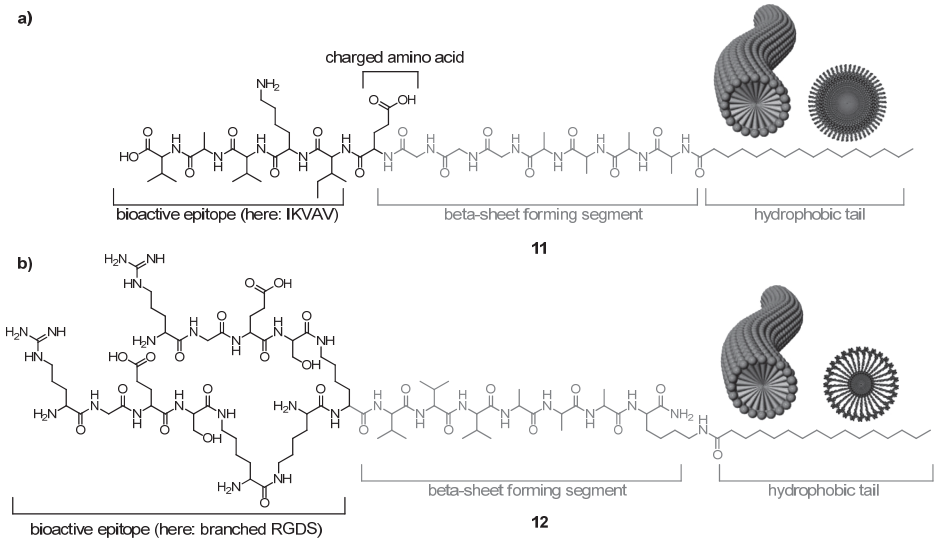

Figure 1.9: a) Salt and pH sensitive PA **11** bearing an IKVAV peptide motif and cross-section through the cylindrical micelle formed; b) Branched PA **12** with two linear RGDS sequences as bioactive epitope; Cross-section through the cylindrical micelles formed (adapted from reference 65, Copyright (2007), with permission from Elsevier).

The structuring peptide segment is composed of β-sheet forming hydrophobic amino acids. Through intermolecular hydrogen bonding the peptide segment stabilizes and dictates the final shape of the self-assembly, as the lipid tail alone favors the formation of spherical and not

cylindrical micelles. Furthermore, the charged amino acid provides enhanced solubility in water, while repulsive charge-charge interactions prevent the amphiphiles from assembling, unless the charge is shielded through adjustment of pH or salt concentration. This has enabled applications in regenerative medicine, as unassembled PAs can be combined with for example growth factors and cells, which upon injection into tissue form a gel network encapsulating the desired payload, through shielding of the charge by electrolytes.[66]

Incorporation of the neurite-promoting laminin-derived epitope IKVAV (**11**, Figure 1.9 a) at high densities on the surface of the assembled nanostructures induced rapid and selective differentiation of neural progenitor cells into neurons. The selective differentiation was even greater when compared to cells cultured with laminin, presumably due to higher epitope densities (Figure 1.4).[30] In vivo, when injected in a mouse spinal cord injury model, the regeneration of the injury was facilitated.[66]

Displaying the cell-adhesion epitope RGDS, the artificial PA matrix enhanced cell adhesion and receptor clustering compared to fibronectin. Signal accessibility was varied through changes in molecular architecture by utilizing (double-)branched PAs (**12**, Figure 1.9 b). The self-assembled structure was not changed, underlining the stability of the design, allowing incorporation of different types of peptide sequences. The lower packing densities of branched PAs (see micelle cross-section Figure 1.9) led to increased epitope motion, improving cell adhesion, spreading and migration. A lower packing density of linear PAs could as well be achieved, through mixing with a PA lacking the bioactive epitope.[65]

Both examples show that the high density display of the hydrophilic bioactive epitope on the surface of the assembled nanostructure outperforms protein containing matrixes. At the same time, the supramolecular assembly of these PAs allows tunability of ligand density either through changes in design or via simple intermixing of different peptide amphiphiles. A detailed overview of further applications of PAs, for example in drug encapsulation, magnetic resonance imaging, mineralization, surface patterning, angiogenesis can be found in reference [67,68].

1.3.3 *Self-assembly driven by non-peptidic units*

Combining the features of lipids with the functions of bioactive peptides, the group of Lee has investigated the influence of lipid composition on the stability and morphology of peptide-lipid conjugates. Tat, a cell-penetrating peptide was coupled to hydrophobic lipid dendrimers. Functionalized with one stearic acid, **13** did not self-assemble in water. Two stearic acids were required for the assembly into spherical micelles (**14**) and cylindrical micelles were observed using the tetrameric lipid dendrimer (**15**). Changing from dimeric to tetrameric lipid dendrimers as well lowered the CAC almost 10-fold, from 208 μM for **14** to 21 μM for **15** (Figure 1.10). The encapsulated dye Nile Red was efficiently delivered into the cytoplasm of HeLa cells.[69] The same group has as well self-assembled Tat using a short beta-sheet forming peptide, instead of a lipid tail, and observed self-assembly at low concentrations.[51] The self-assembly of Stupp's peptide

amphiphiles, containing a beta-sheet forming segment next to a lipid tail, resulted in stable cylindrical micelles no matter which (branched) peptide sequence was introduced, highlighting the higher stability of beta-sheet based self-assembly. On the other hand, a larger diversity in morphology can be obtained using lipid-based systems.

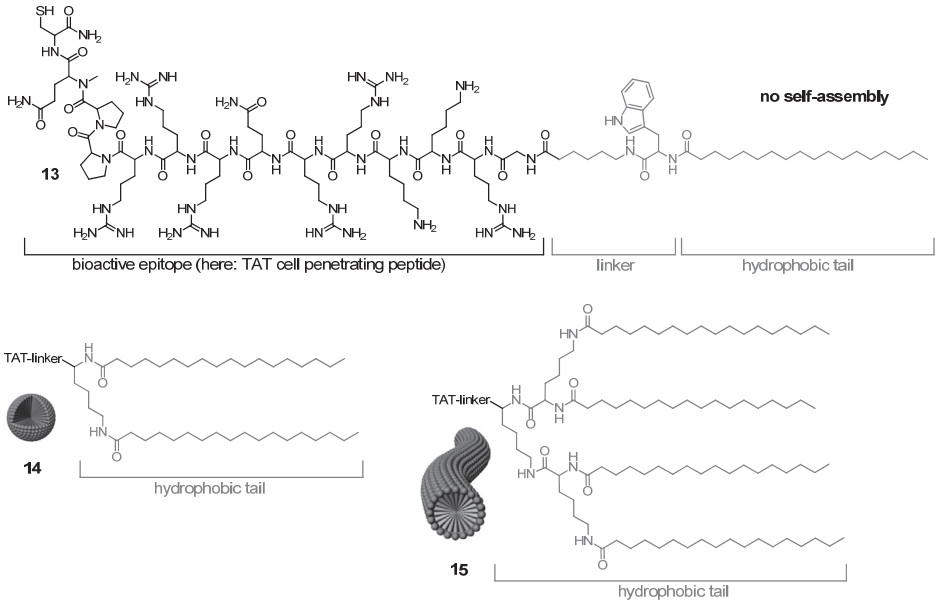

Figure 1.10: Lipid based self-assembly of the cell-penetrating peptide Tat.[69]

To study multivalent carbohydrate-mediated interactions the group of Lee has developed a library of self-assembled nanostructures based on mannose functionalized aromatic rod-coil amphiphiles with a hydrophobic tetra(*p*-phenylene) segment (Figure 1.11). By systematic variation of the volume fraction between the hydrophobic and hydrophilic segments different self-assembling morphologies ranging from spherical vesicles (**16**) and micelles (**17**) to cylindrical micelles (**18**) were achieved.[70,71] These systems function as very effective multivalent ligands for the lectin concanavalin A and *E. coli* bacteria. A 1800-fold increase in relative inhibitory potency compared with a-D-methyl mannose was observed for the self-assembly with the highest curvature, the spherical micellar architectures (**17**), underlining the effect of the supramolecular architecture on the binding activity.

The dendritic amphiphile **19** self-assembled in mannose coated cylindrical micelles with a length of about 200 nm (Figure 1.11). Addition of the hydrophobic guest molecule Nile Red triggered the reversible transformation of these cylindrical micelles into spheres.[72] This supramolecular self-assembling system thus is able to respond to external signals and provides a rapid and reversible entry to different topologies. Binding studies with the lectin concanavalin A showed that both objects, cylindrical micelles and spheres, function as polyvalent inhibitors, but the motility of *E.Coli* bacteria is better inhibited with cylindrical micelles. These results demonstrate that the ability to systematically alter and control the self-assembled structures in shape and size by molecular design can provide control of the biological activities of

supramolecular materials especially as the strength and efficiency of polyvalent interactions are dependent on the shape and the surface properties of the interaction system.

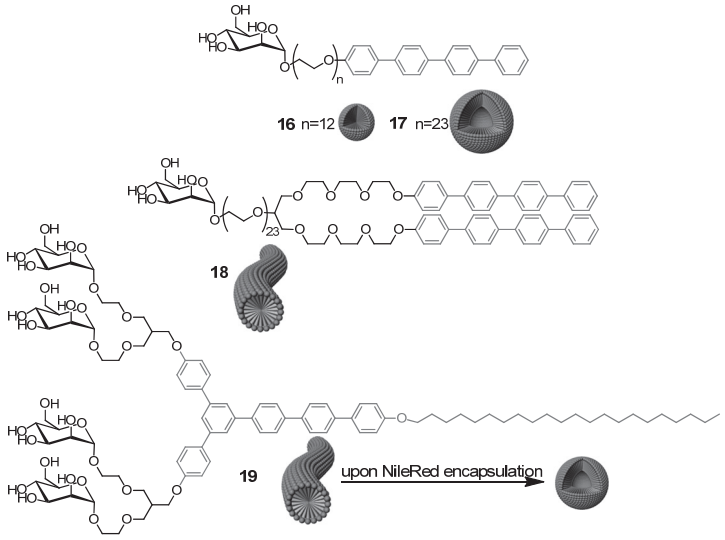

Figure 1.11: Mannose-decorated aromatic rod-coil amphiphiles.[71,72] Adapted with permission from reference 71. Copyright (2005) American Chemical Society.

1.3.4 *Pseudopolyrotoxanes*

A major question in the field of molecular recognition, the role of flexibility and adaptability in binding events, was studied using pseudopolyrotaxenes. Polyrotaxanes are defined as a molecular assembly, in which several cyclic molecules are threaded onto a linear chain capped with bulky end-groups. In pseudopolyrotaxanes the linear chain is not capped with bulky end-groups. In contrast to previously discussed supramolecular assemblies, this supramolecular polymer does not have a strongly defined topological shape. The non-covalently threaded cyclic molecules may rotate and slide along the polymeric chain facilitating the adjustment of ligand positioning to the encountered polyvalent target. This mobility should eliminate the spatial mismatching between ligands and receptors, which can occur at high ligand densities in covalently functionalized multivalent polymers[73], when the geometry of receptors does not fit the spacing between the ligands.

The groups of Stoddart and Kim have studied pseudopolyrotaxanes as adaptable multivalent inhibitors. Pseudopolyrotaxanes consist as well of several cyclic molecules which are threaded onto a linear chain, but this chain is not capped with bulky end-groups. Both groups have used a polyviologen AB-copolymer, consisting of alternating decamethylene (A) and positively charged bipyridinium (B) segments, but different cyclic molecules. The group of Stoddart pioneered in this field using lactose functionalized α-CD[74–76], whereas the group of Kim used mannose functionalized cucurbit[6]uril (CB[6]) (Figure 1.13).[77] Stabilized by the hydrophobic interactions inside their cavities, both cyclic molecules predominantly rest on the decamethylene segments. The flanking charged bipyridinium segments act as electronic “speed bumps”, reducing the

translational movement. In case of cucurbit[6]urils an additional charge-dipole interaction between bipyridinium unit and the CB[6] portal oxygen atoms stabilizes the assembly and no appreciable dethreading is observed after a long period of time.[78] By contrast, cyclodextrins undergo measurable degrees of dethreading within hours after sample dilution, due to the lack of stabilizing charge-dipole interactions as present in the case of CB[6].

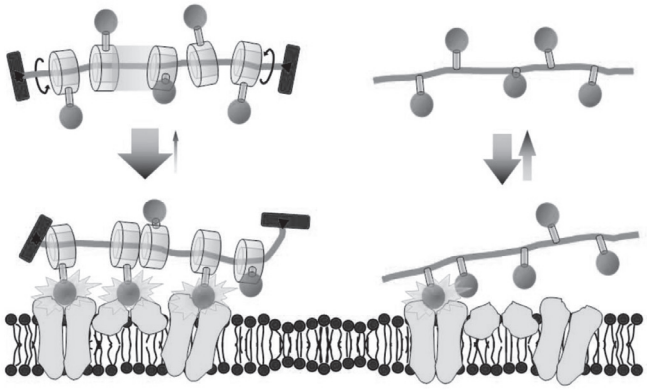

Figure 1.12: Adjustment of ligand positioning of pseudopolyrotaxanes (left) and covalent polymers (right). From reference 79. Reprinted with permission from John Wiley and Sons.

The pseudopolyrotaxane from the group of Stoddart consists of a polyviologen-AB-copolymer with 17 viologen units (**20**) fully threaded with mono-lactose functionalized α-cyclodextrin **21**. Their ability to inhibit the binding of galectin-1 to T-cells was assessed using the T-cell agglutination assay. The lactose binding sites in galectin-1 are located on opposite faces of the protein and therefore only small valency corrected inhibition enhancements are observed for example for dendrimeric systems.[74] This pseudopolyrotoxanes, when compared with lactose bearing polymer, showed a 6-fold valency corrected enhancement in a T-cell agglutination assay. Further, the influence of the length of the polyviologen chain and the degree of threading was investigated. A longer polyviologen chain, which can bridge longer distances, was observed to be more effective in the T-cell agglutination assay. On the other hand, a lower degree of threading led to enhanced inhibitory properties.

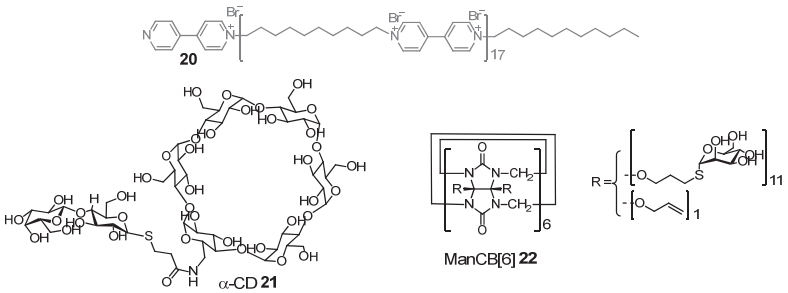

Figure 1.13: Pseudopolyrotoxanes building blocks.

In the pseudopolyrotaxane system of Kim et al. each cucurbit[6]uril was functionalized with on average eleven mannose moieties. Different amounts of these mannosylated CB[6]s (ManCB[6],

22) were mixed with polyviologen generating three mannose functionalized pseudopolyrotaxanes bearing 3, 5 or 10 ManCB[6] (Figure 1.13). For control experiments galactose and glycose functionalized pseudopolyrotaxanes were prepared. In both a bacterial aggregation and a hemagglutination assay the mannose pseudopolyrotaxanes systems were much more effective than ManCB[6] alone. As well here, the pseudopolyrotaxane threaded with only three ManCB[6] was the most potent inhibitor, showing a 300 times higher inhibitory potency than monomeric methyl-α-D-mannose, probably by providing the proper density of mannose. This pseudopolyrotaxane was able to inhibit the adhesion of ORN178 bacteria to urinary epithelial cells, a model of urinary tract infection.

1.3.5 *Metal-ligand coordination*

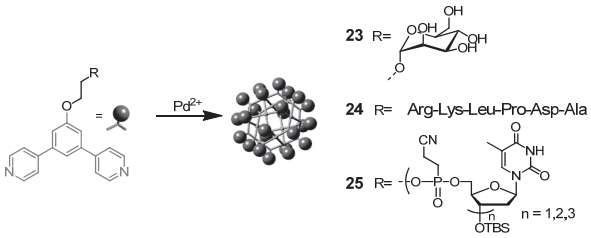

Figure 1.14: Metal-ligand coordinated self-assembly. Parts adapted with permission from reference 82. Copyright (2007) American Chemical Society.

Using well-defined metal–ligand coordinated spheres the group of Fujita obtained supramolecular polyvalent self-assemblies of a different type of topology. Here the formation of a well-defined metal–organic framework of 12 paladium (II) ions with 24 1,3-bis(4-pyridyl)phenyl groups is the main driving force of self-assembly. Incorporation of different bioactive ligands into this organic building block yielded spheres with precisely 24 hexapeptides[80], DNA oligonucleotides[81] or carbohydrates[82] at the periphery (Figure 1.14). The spheres coated with different saccharides such as α-mannopyranoside, α-galactopyranoside, α- and β-glycopyranoside were used to study the formation of aggregates upon lectin binding. Concanavalin A, a α-mannopyranoside and α-glycopyranoside binding lectin, formed aggregates only with α-mannopyranoside or α-glycopyranoside coated spheres. Addition of an excess of a corresponding carbohydrate reversed the formation of colloidal aggregates. Peanut agglutinin (PNA), a galactose-binding lectin, formed aggregates only with β-galactose coated spheres, indicating that the lectins recognize the terminal carbohydrate units of the spheres. This system shows a high potential for the generation of spheres with encapsulated compounds, such as drugs, which can be released upon cell recognition by the bioactive ligand attached to this supramolecular platform.

1.3.6 *Disc-shaped amphiphiles*

In contrast to linear amphiphiles such as phospholipids and peptide amphiphiles, the self-assembly of C_3-symmetrical disc-shaped molecules selectively leads to the formation of one type of aggregate: columnar stacks.

The discotic amphiphiles described by Besenius et al. consist of a C_3-symmetrical benzene-1,3,5-tricarboxamide core, a motif that self-assembles into triple hydrogen bonded helices. Extension of the core with (fluorinated) phenylalanine and aminobenzoate moieties stabilizes the assembly through additional π–π interactions and solvophobic effects and shielding of the core (Figure 1.15).[84] The discotic scaffold itself (**26**) self-assembles into columnar structures of 50-75 nm at millimolar concentrations, which increases in length with concentration. To yield supramolecular contrast agents for magnetic resonance imaging (MRI), different chelating ligands were introduced at the periphery. The increasing ionic character of the introduced ligands led, through electrostatic repulsion, to the formation of small nearly spherical structures of around eleven monomers.[85] Functionalization with peptides led as well to changes in morphology and stability of the supramolecular polymers. Long and very stable rods were formed with a tendency to form bundles.[83] Dilution of peptide-functionalized discotics with Gd(III)-DOTA functionalized discotics prevented the peptide induced secondary interactions. These results again underline that introduction of a ligand can have a big influence on the self-assembly of a supramolecular scaffold and at the same allowing to tune the length/shape of self-assembly by balancing attractive and repulsive forces.

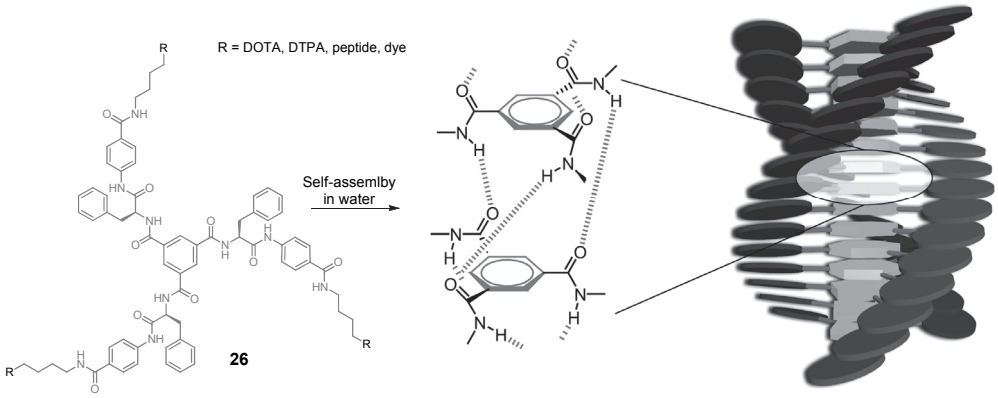

Figure 1.15: Fluorinated phenylalanine containing discotic amphiphiles (based on reference 83).

The discotics studied in this thesis consist of an extended aromatic core of three 2,2′-bipyridine-3,3′-diamine molecules linked to a central benzene-1,3,5-tricarbonyl unit.[89,90] This inner core is surrounded by three gallic acid moieties functionalized with in total nine ethylene glycol chains which induce water-solubility and shield the hydrophobic core. The discotics are intrinsically fluorescent, which was used for detection using Förster resonance energy transfer (FRET) and to confirm the presence of self-assembling structures, as the fluorescent lifetime of the monomers increases upon self-assembly into columnar polymer.[91] The self-assembly of these discotics is based on strong intramolecular hydrogen bonding between the amide N-H groups and

neighboring bipyridine N-atoms, which pre-organize the molecules into an on average planar C_3-symmetrical conformation, allowing the molecules to form long stacks primarily through π-π stacking (Figure 1.16).[88,92] The introduction of functional groups at the periphery of the ethylene oxide tails enabled functionalization with bioactive ligands. The discotic bearing three azide functionalities was decorated with three mannose moieties (**27**) which led to selective binding to *E.Coli* bacteria, which display the mannose binding FimH receptor.[87] The multivalent display of mannose ligands induced enhanced binding affinity through multivalency as quantified using an enzyme-linked lectin assay. Functionalization of amine bearing discotics with biotin (**28**) enabled the display of streptavidin, a biotin-binding protein, along the supramolecular polymer.[86] Förster resonance energy transfer (FRET) between differently labeled streptavidins indicated the approximation of those proteins along the supramolecular polymer. The bare scaffold itself in both examples did not show any unspecific interactions with proteins and bacteria. These proofs-of-principle show the possibility to utilize the discotic scaffold as a platform, which can be flexibly decorated with different ligands.

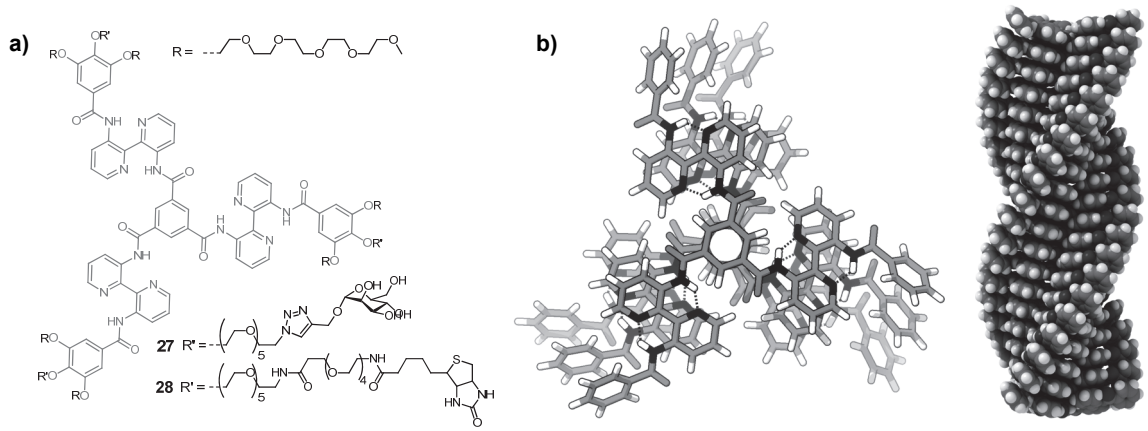

Figure 1.16: Discotic self-assembling structures with an extended aromatic core functionalized with the ligands mannose and biotin.[86,87] b) Ball-and-stick model trimer and filled-space model side view of self-assembling discotics.[88]

1.4 Aim and outline of this thesis

As discussed in this chapter, supramolecular chemistry allows the rapid formation of nano-sized architectures. For the self-assembly in water amphiphilic molecules emerged as versatile building blocks which can be programmed to self-assemble into a wide range of different topologies. The ability to decorate the generated nano-structures with bioactive epitopes led to applications in the biomedical field. Applications in tissue engineering, imaging and protein clustering are arising. Their success strongly depends on the ability to fine-tune the density and display of bioactive epitopes - creating more complex heterovalent structures - while not interfering with the self-assembly process. Therefore, the development of self-assembling structures is strongly coupled to a detailed understanding of the self-assembling properties of the system; its dynamics, stability and its susceptibility to changes.

The aim of this thesis is to explore the characteristics and the potential of self-assembling nanostructures based on disc-shaped and linear auto-fluorescent amphiphilic molecules. The focus is on insights into the generation of complex heterovalent structures through dynamic intermixing of ligand functionalized building blocks.

Chapter 2 describes the synthesis of different discotic scaffolds bearing either a single or multiple functional groups. These discotics offer versatile platforms for the introduction of bioactive ligands. The functionalization with peptides, carbohydrates, small molecules and fluorescent dyes is shown using both amide coupling and copper-catalyzed azide-alkyne cycloaddition.

The self-assembling multivalency of discotics bearing a single ligand is explored in chapter 3. The ability of the monovalent biotin-discotic to bind several monovalent streptavidin proteins in the self-assembled state is investigated. The self-assembling multivalency is quantified using the monovalent mannose-discotic in the enzyme linked lectin assay. Additionally, the possibility to generate heterovalent supramolecular polymers is studied using mixtures of monovalent biotin- and fluorescein-discotics.

In chapter 4 covalent post-functionalization of the self-assembled discotics with fluorescent proteins using the SNAP-tag technology is explored. Covalent and monovalent attachment of two FRET-pairing fluorescent proteins enables to follow the dynamic intermixing of supramolecular polymers into heterovalent protein assemblies using FRET.

Chapter 5 evaluates the cellular uptake of amine-decorated discotics and the dependence of cellular uptake on the peripheral amine density. Additionally, the knowledge about the formation of intermixed supramolecular polymers obtained in chapter 3 and 4 is used to study the possible cellular uptake of non-cell permeable discotics through intermixing with cell-permeable discotic monomers.

Chapter 6 deals with a different self-assembling system, self-assembling π-conjugated oligomer based nanoparticles. Upon microinjection into water, these auto-fluorescent amphiphiles self-assemble into highly-fluorescent amorphous nanoparticles of 80-100 nm offering a great potential as a novel class of targeted multimodal imaging agents.[93] In this chapter the pre- and post-functionalization with functional groups and bioactive ligands is investigated. The binding of the nanoparticles to proteins, bacteria, and magnetic beads is studied in detail, as well as the possibility to fine-tune ligand density and to create heterovalent nanoparticles through intermixing of building blocks prior to self-assembly.

1.5 References

1. Philp, D.; Stoddart, J. F. Self-Assembly in Natural and Unnatural Systems. *Angew. Chem. Int. Ed.* **1996**, *35*, 1154–1196.
2. Ben-Shem, A.; Jenner, L.; Yusupova, G.; Yusupov, M. Crystal Structure of the Eukaryotic Ribosome. *Science* **2010**, *330*, 1203–1209.
3. Taipale, J.; Keski-Oja, J. Growth Factors in the Extracellular Matrix. *FASEB J* **1997**, *11*, 51–59.

4. Miyamoto, S.; Akiyama, S. K.; Yamada, K. M. Synergistic Roles for Receptor Occupancy and Aggregation in Integrin Transmembrane Function. *Science* **1995**, *267*, 883–885.
5. Germain, R. N. T-cell Signaling: The Importance of Receptor Clustering. *Curr. Biol.* **1997**, *7*, R640–R644.
6. Zwaal, R. F. A.; Comfurius, P.; Bevers, E. M. Surface Exposure of Phosphatidylserine in Pathological Cells. *Cell. Mol. Life Sci.* **2005**, *62*, 971–988.
7. Garnier, B.; Bouter, A.; Gounou, C.; Petry, K. G.; Brisson, A. R. Annexin A5-Functionalized Liposomes for Targeting Phosphatidylserine-Exposing Membranes. *Bioconjugate Chem.* **2009**, *20*, 2114–2122.
8. Wear, M. A.; Schafer, D. A.; Cooper, J. A. Actin Dynamics: Assembly and Disassembly of Actin Networks. *Curr. Biol.* **2000**, *10*, R891–R895.
9. Avila, J. Microtubule Dynamics. *FASEB J.* **1990**, *4*, 3284–3290.
10. Pedersen, C. J. Cyclic Polyethers and Their Complexes with Metal Salts. *J. Am. Chem. Soc.* **1967**, *89*, 7017–7036.
11. Ciferri, A. *Supramolecular Polymers*; Taylor & Francis, 2005.
12. Oshovsky, G. V.; Reinhoudt, D. N.; Verboom, W. Supramolecular Chemistry in Water. *Angew. Chem. Int. Ed.* **2007**, *46*, 2366–2393.
13. Ryu, J.-H.; Hong, D.-J.; Lee, M. Aqueous Self-assembly of Aromatic Rod Building Blocks. *Chem. Commun.* **2008**, 1043–1054.
14. Uhlenheuer, D. A.; Petkau, K.; Brunsveld, L. Combining Supramolecular Chemistry with Biology. *Chem. Soc. Rev.* **2010**, *39*, 2817-2826.
15. Gu, F.; Zhang, L.; Teply, B. A.; Mann, N.; Wang, A.; Radovic-Moreno, A. F.; Langer, R.; Farokhzad, O. C. Precise Engineering of Targeted Nanoparticles by Using Self-assembled Biointegrated Block Copolymers. *PNAS* **2008**, *105*, 2586 –2591.
16. Woolfson, D. N.; Mahmoud, Z. N. More Than Just Bare Scaffolds: Towards Multi-component and Decorated Fibrous Biomaterials. *Chem. Soc. Rev.* **2010**, *39*, 3464-3479.
17. Algar, W. R.; Prasuhn, D. E.; Stewart, M. H.; Jennings, T. L.; Blanco-Canosa, J. B.; Dawson, P. E.; Medintz, I. L. The Controlled Display of Biomolecules on Nanoparticles: A Challenge Suited to Bioorthogonal Chemistry. *Bioconjugate Chem.* **2011**, *22*, 825–858.
18. Perrier, T.; Saulnier, P.; Benoît, J. Methods for the Functionalisation of Nanoparticles: New Insights and Perspectives. *Chem. Eur. J.* **2010**, *16*, 11516–11529.
19. Lallana, E.; Sousa-Herves, A.; Fernandez-Trillo, F.; Riguera, R.; Fernandez-Megia, E. Click Chemistry for Drug Delivery Nanosystems. *Pharm. Res.* **2012**, *29*, 1–34.
20. Canalle, L. A.; Löwik, D. W. P. M.; Hest, J. C. M. van Polypeptide–polymer Bioconjugates. *Chem. Soc. Rev.* **2010**, *39*, 329–353.
21. Aschoff, L. *Ehrlich's Seitenkettentheorie Und Ihre Anwendung Auf Die Künstlichen Immunisierungsprozesse, 1866-1942*; G. Fischer.
22. Torchilin, V. P. Multifunctional Nanocarriers. *Adv. Drug. Deliver. Rev.* **2006**, *58*, 1532–1555.
23. Discher, D. E.; Ahmed, F. Polymerosomes. *Annu. Rev. Biomed. Eng.* **2006**, *8*, 323–341.
24. Louie, A. Multimodality Imaging Probes: Design and Challenges. *Chem. Rev.* **2010**, *110*, 3146–3195.
25. Dankers, P. Y. W.; Meijer, E. W. Supramolecular Biomaterials. A Modular Approach Towards Tissue Engineering. *Bull. Chem. Soc. Jpn.* **2007**, *80*, 2047–2073.
26. Collier, J. H. Modular Self-assembling Biomaterials for Directing Cellular Responses. *Soft Matter* **2008**, *4*, 2310–2315.
27. Collier, J. H.; Rudra, J. S.; Gasiorowski, J. Z.; Jung, J. P. Multi-component Extracellular Matrices Based on Peptide Self-assembly. *Chem. Soc. Rev.* **2010**, *39*, 3413.
28. Matson, J. B.; Stupp, S. I. Self-assembling Peptide Scaffolds for Regenerative Medicine. *Chem. Commun.* **2012**, *48*, 26–33.
29. Gasiorowski, J. Z.; Collier, J. H. Directed Intermixing in Multicomponent Self-Assembling Biomaterials. *Biomacromolecules* **2011**, *12*, 3549–3558.

30. Silva, G. A.; Czeisler, C.; Niece, K. L.; Beniash, E.; Harrington, D. A.; Kessler, J. A.; Stupp, S. I. Selective Differentiation of Neural Progenitor Cells by High-Epitope Density Nanofibers. *Science* **2004**, *303*, 1352–1355.
31. Dongen, S. F. M. van; Hoog, H.-P. M. de; Peters, R. J. R. W.; Nallani, M.; Nolte, R. J. M.; Hest, J. C. M. van Biohybrid Polymer Capsules. *Chem. Rev.* **2009**, *109*, 6212–6274.
32. Pack, D. W.; Hoffman, A. S.; Pun, S.; Stayton, P. S. Design and Development of Polymers for Gene Delivery. *Nat Rev Drug Discov* **2005**, *4*, 581–593.
33. Steinmetz, N. F. Viral Nanoparticles as Platforms for Next-generation Therapeutics and Imaging Devices. *Nanomed-Nanotechnol* **2010**, *6*, 634–641.
34. Cutler, J. I.; Auyeung, E.; Mirkin, C. A. Spherical Nucleic Acids. *J. Am. Chem. Soc.* **2012**, *134*, 1376–1391.
35. Themed issue on Nanomedicine *Chem. Soc. Rev.* **2012**, *41*, 2521–3012.
36. Ringsdorf, H.; Schlarb, B.; Venzmer, J. Molecular Architecture and Function of Polymeric Oriented Systems: Models for the Study of Organization, Surface Recognition, and Dynamics of Biomembranes. *Angew. Chem. Int. Ed. Engl.* **1988**, *27*, 113–158.
37. Bangham, A. D.; Horne, R. W. Negative Staining of Phospholipids and Their Structural Modification by Surface-active Agents as Observed in the Electron Microscope. *J. Mol. Biol.* **1964**, *8*, 660–668, IN2–IN10.
38. Al-Jamal, W. T.; Kostarelos, K. Liposomes: From a Clinically Established Drug Delivery System to a Nanoparticle Platform for Theranostic Nanomedicine. *Acc. Chem. Res.* **2011**, *44*, 1094–1104.
39. Bangham, A. D. Surrogate Cells or Trojan Horses. The Discovery of Liposomes. *BioEssays* **1995**, *17*, 1081–1088.
40. Mulder, W. J. M.; Strijkers, G. J.; Tilborg, G. A. F. van; Cormode, D. P.; Fayad, Z. A.; Nicolay, K. Nanoparticulate Assemblies of Amphiphiles and Diagnostically Active Materials for Multimodality Imaging. *Acc. Chem. Res.* **2009**, *42*, 904–914.
41. Forssen, E.; Willis, M. Ligand-targeted Liposomes. *Adv. Drug. Deliver. Rev.* **1998**, *29*, 249–271.
42. Klibanov, A. L.; Maruyama, K.; Torchilin, V. P.; Huang, L. Amphipathic Polyethyleneglycols Effectively Prolong the Circulation Time of Liposomes. *FEBS Lett.* **1990**, *268*, 235–237.
43. Kluza, E.; Schaft, D. W. J. van der; Hautvast, P. A. I.; Mulder, W. J. M.; Mayo, K. H.; Griffioen, A. W.; Strijkers, G. J.; Nicolay, K. Synergistic Targeting of Avβ3 Integrin and Galectin-1 with Heteromultivalent Paramagnetic Liposomes for Combined MR Imaging and Treatment of Angiogenesis. *Nano Lett.* **2010**, *10*, 52–58.
44. Peptide- and Protein-based Materials Themed Issue. *Chem. Soc. Rev.* **2010,** *39*, 3337–3580.
45. Boyle, A. L.; Woolfson, D. N. Rational Design of Peptide-Based Biosupramolecular Systems. In *Supramolecular Chemistry: From Molecules to Nanomaterials*; **2012**, John Wiley & Sons, Ltd.
46. Aggeli, A.; Bell, M.; Carrick, L. M.; Fishwick, C. W. G.; Harding, R.; Mawer, P. J.; Radford, S. E.; Strong, A. E.; Boden, N. pH as a Trigger of Peptide β-Sheet Self-Assembly and Reversible Switching Between Nematic and Isotropic Phases. *J. Am. Chem. Soc.* **2003**, *125*, 9619–9628.
47. Serpell, L. C. Alzheimer's Amyloid Fibrils: Structure and Assembly. *BBA-Mol. Basis Dis.* **2000**, *1502*, 16–30.
48. Takahashi, Y.; Ueno, A.; Mihara, H. Amyloid Architecture: Complementary Assembly of Heterogeneous Combinations of Three or Four Peptides into Amyloid Fibrils. *ChemBioChem* **2002**, *3*, 637–642.
49. Baxa, U.; Speransky, V.; Steven, A. C.; Wickner, R. B. Mechanism of Inactivation on Prion Conversion of the Saccharomyces Cerevisiae Ure2 Protein. *PNAS* **2002**, *99*, 5253–5260.
50. Baldwin, A. J.; Bader, R.; Christodoulou, J.; MacPhee, C. E.; Dobson, C. M.; Barker, P. D. Cytochrome Display on Amyloid Fibrils. *J. Am. Chem. Soc.* **2006**, *128*, 2162–2163.
51. Lim, Y.; Lee, E.; Lee, M. Cell-Penetrating-Peptide-Coated Nanoribbons for Intracellular Nanocarriers. *Angew. Chem. Int. Ed.* **2007**, *46*, 3475–3478.
52. Gras, S. L.; Tickler, A. K.; Squires, A. M.; Devlin, G. L.; Horton, M. A.; Dobson, C. M.; MacPhee, C. E. Functionalised Amyloid Fibrils for Roles in Cell Adhesion. *Biomaterials* **2008**, *29*, 1553–1562.

53. Rudra, J. S.; Tian, Y. F.; Jung, J. P.; Collier, J. H. A Self-Assembling Peptide Acting as an Immune Adjuvant. *PNAS* **2010**, *107*, 622–627.
54. Kodama, H.; Matsumura, S.; Yamashita, T.; Mihara, H. Construction of a Protein Array on Amyloid-like Fibrils Using Co-assembly of Designed Peptides. *Chem. Commun.* **2004**, 2876–2877.
55. Lim, Y.; Park, S.; Lee, E.; Jeong, H.; Ryu, J.-H.; Lee, M. S.; Lee, M. Glycoconjugate Nanoribbons from the Self-Assembly of Carbohydrate–Peptide Block Molecules for Controllable Bacterial Cell Cluster Formation. *Biomacromolecules* **2007**, *8*, 1404–1408.
56. Lim, Y.; Park, S.; Lee, E.; Ryu, J.-H.; Yoon, Y.-R.; Kim, T.-H.; Lee, M. Tunable Bacterial Agglutination and Motility Inhibition by Self-Assembled Glyco-Nanoribbons. *Chem. Asian J.* **2007**, *2*, 1363–1369.
57. Channon, K.; MacPhee, C. E. Possibilities for "smart" Materials Exploiting the Self-assembly of Polypeptides into Fibrils. *Soft Matter* **2008**, *4*, 647.
58. Lupas, A. N.; Gruber, M. The Structure of α-Helical Coiled Coils. In *Fibrous Proteins: Coiled-Coils, Collagen and Elastomers*; Adv. Protein. Chem.; Academic Press, **2005**; Vol. 70, pp. 37–38.
59. Ryadnov, M. G.; Papapostolou, D.; Woolfson, D. N. Nanostructure Design. In; Methods in Molecular Biology; Humana Press, **2008**; Vol. 474, pp. 35–51.
60. Ryadnov, M. G.; Bella, A.; Timson, S.; Woolfson, D. N. Modular Design of Peptide Fibrillar Nano-to Microstructures. *J. Am. Chem. Soc.* **2009**, *131*, 13240–13241.
61. Mahmoud, Z. N.; Gunnoo, S. B.; Thomson, A. R.; Fletcher, J. M.; Woolfson, D. N. Bioorthogonal Dual Functionalization of Self-assembling Peptide Fibers. *Biomaterials* **2011**, *32*, 3712–3720.
62. Villard, V.; Kalyuzhniy, O.; Riccio, O.; Potekhin, S.; Melnik, T. N.; Kajava, A. V.; Rüegg, C.; Corradin, G. Synthetic RGD-containing A-helical Coiled Coil Peptides Promote Integrin-dependent Cell Adhesion. *J. Pept. Sci.* **2006**, *12*, 206–212.
63. Hartgerink, J. D. Self-Assembly and Mineralization of Peptide-Amphiphile Nanofibers. *Science* **2001**, *294*, 1684–1688.
64. Hartgerink, J. D.; Beniash, E.; Stupp, S. I. Peptide-Amphiphile Nanofibers: A Versatile Scaffold for the Preparation of Self-Assembling Materials. *PNAS* **2002**, *99*, 5133–5138.
65. Storrie, H.; Guler, M. O.; Abu-Amara, S. N.; Volberg, T.; Rao, M.; Geiger, B.; Stupp, S. I. Supramolecular Crafting of Cell Adhesion. *Biomaterials* **2007**, *28*, 4608–4618.
66. Tysseling-Mattiace, V. M.; Sahni, V.; Niece, K. L.; Birch, D.; Czeisler, C.; Fehlings, M. G.; Stupp, S. I.; Kessler, J. A. Self-Assembling Nanofibers Inhibit Glial Scar Formation and Promote Axon Elongation After Spinal Cord Injury. *J. Neurosci* **2008**, *28*, 3814–3823.
67. Webber, M. J.; Kessler, J. A.; Stupp, S. I. Emerging Peptide Nanomedicine to Regenerate Tissues and Organs. *J. Intern. Med.* **2010**, *267*, 71–88.
68. Cui, H.; Webber, M. J.; Stupp, S. I. Self-assembly of Peptide Amphiphiles: From Molecules to Nanostructures to Biomaterials. *Biopolymers* **2010**, *94*, 1–18.
69. Lim, Y.; Lee, E.; Lee, M. Controlled Bioactive Nanostructures from Self-Assembly of Peptide Building Blocks. *Angew. Chem. Int. Ed.* **2007**, *46*, 9011–9014.
70. Kim, B.-S.; Yang, W.-Y.; Ryu, J.-H.; Yoo, Y.-S.; Lee, M. Carbohydrate-coated Nanocapsules from Amphiphilic Rod-coil Molecule: Binding to Bacterial Type 1 Pili. *Chem. Commun.* **2005**, 2035-2037.
71. Kim, B.-S.; Hong, D.-J.; Lee, E.; Bae, J.; Lee, M. Controlled Self-Assembly of Carbohydrate Conjugate Rod-Coil Amphiphiles for Supramolecular Multivalent Ligands. *J. Am. Chem. Soc.* **2005**, *127*, 16333–16337.
72. Ryu, J.-H.; Lee, E.; Lim, Y.; Lee, M. Carbohydrate-Coated Supramolecular Structures: Transformation of Nanofibers into Spherical Micelles Triggered by Guest Encapsulation. *J. Am. Chem. Soc.* **2007**, *129*, 4808–4814.
73. Hasegawa, T.; Kondoh, S.; Matsuura, K.; Kobayashi, K. Rigid Helical Poly(glycosyl Phenyl Isocyanide)s: Synthesis, Conformational Analysis, and Recognition by Lectins. *Macromolecules* **1999**, *32*, 6595–6603.
74. Nelson, A.; Belitsky, J. M.; Vidal, S.; Joiner, C. S.; Baum, L. G.; Stoddart, J. F. A Self-Assembled Multivalent Pseudopolyrotaxane for Binding Galectin-1. *J. Am. Chem. Soc.* **2004**, *126*, 11914–11922.

75. Belitsky, J. M.; Nelson, A.; Hernandez, J. D.; Baum, L. G.; Stoddart, J. F. Multivalent Interactions Between Lectins and Supramolecular Complexes: Galectin-1 and Self-Assembled Pseudopolyrotaxanes. *Chem. Biol.* **2007**, *14*, 1140–1151.
76. Belitsky, J. M.; Nelson, A.; Stoddart, J. F. Monitoring Cyclodextrin–polyviologen Pseudopolyrotaxanes with the Bradford Assay. *Org. Biomol. Chem.* **2006**, *4*, 250-256.
77. Kim, J.; Ahn, Y.; Park, K. M.; Lee, D.-W.; Kim, K. Glyco-pseudopolyrotaxanes: Carbohydrate Wheels Threaded on a Polymer String and Their Inhibition of Bacterial Adhesion. *Chem. Eur. J.* **2010**, *16*, 12168–12173.
78. Choi, S.; Lee, J. W.; Ko, Y. H.; Kim, K. Pseudopolyrotaxanes Made to Order: Cucurbituril Threaded on Polyviologen. *Macromolecules* **2002**, *35*, 3526–3531.
79. Yui, N.; Ooya, T. Molecular Mobility of Interlocked Structures Exploiting New Functions of Advanced Biomaterials. *Chem. Eur. J.* **2006**, *12*, 6730–6737.
80. Ikemi, M.; Kikuchi, T.; Matsumura, S.; Shiba, K.; Sato, S.; Fujita, M. Peptide-coated, Self-assembled M12L24 Coordination Spheres and Their Immobilization onto an Inorganic Surface. *Chem. Sci.* **2010**, *1*, 68-71.
81. Kikuchi, T.; Sato, S.; Fujita, M. Well-Defined DNA Nanoparticles Templated by Self-Assembled M12L24 Molecular Spheres and Binding of Complementary Oligonucleotides. *J. Am. Chem. Soc.* **2010**, *132*, 15930–15932.
82. Kamiya, N.; Tominaga, M.; Sato, S.; Fujita, M. Saccharide-Coated M12L24 Molecular Spheres That Form Aggregates by Multi-interaction with Proteins. *J. Am. Chem. Soc.* **2007**, *129*, 3816–3817.
83. Besenius, P.; Goedegebure, Y.; Driesse, M.; Koay, M.; Bomans, P. H. H.; Palmans, A. R. A.; Dankers, P. Y. W.; Meijer, E. W. Peptide Functionalised Discotic Amphiphiles and Their Self-assembly into Supramolecular Nanofibres. *Soft Matter* **2011**, *7*, 7980–7983.
84. Besenius, P.; den Hout, K. P. van; Albers, H. M. H. G.; Greef, T. F. A. de; Olijve, L. L. C.; Hermans, T. M.; Waal, B. F. M. de; Bomans, P. H. H.; Sommerdijk, N. A. J. M.; Portale, G. *et al.* Controlled Supramolecular Oligomerization of C3-Symmetrical Molecules in Water: The Impact of Hydrophobic Shielding. *Chem. Eur. J.* **2011**, *17*, 5193–5203.
85. Besenius, P.; Portale, G.; Bomans, P. H. H.; Janssen, H. M.; Palmans, A. R. A.; Meijer, E. W. Controlling the Growth and Shape of Chiral Supramolecular Polymers in Water. *PNAS* **2010**, *107*, 17888–17893.
86. Müller, M. K.; Petkau, K.; Brunsveld, L. Protein Assembly Along a Supramolecular Wire. *Chem. Commun.* **2010**, 310–312.
87. Müller, M. K.; Brunsveld, L. A Supramolecular Polymer as a Self-Assembling Polyvalent Scaffold. *Angew. Chem. Int. Ed.* **2009**, *48*, 2921–2924.
88. Metzroth, T.; Hoffmann, A.; Martin-Rapun, R.; Smulders, M. M. J.; Pieterse, K.; Palmans, A. R. A.; Vekemans, J. A. J. M.; Meijer, E. W.; Spiess, H. W.; Gauss, J. Unravelling the Fine Structure of Stacked Bipyridine Diamine-derived C3-discotics as Determined by X-ray Diffraction, Quantum-chemical Calculations, Fast-MAS NMR and CD Spectroscopy. *Chem. Sci.* **2011**, *2*, 69–76.
89. Palmans, A. R. A.; Vekemans, J. A. J. M.; Fischer, H.; Hikmet, R. A.; Meijer, E. W. Extended-Core Discotic Liquid Crystals Based on the Intramolecular H-Bonding in N-Acylated 2,2′-Bipyridine-3,3′-diamine Moieties. *Chem. Eur. J.* **1997**, *3*, 300–307.
90. Brunsveld, L.; Lohmeijer, B. G. G.; Vekemans, J. A. J. M.; Meijer, E. W. Chirality Amplification in Dynamic Helical Columns in Water. *Chem. Commun.* **2000**, 2305–2306.
91. Brunsveld, L.; Zhang, H.; Glasbeek, M.; Vekemans, J. A. J. M.; Meijer, E. W. Hierarchical Growth of Chiral Self-Assembled Structures in Protic Media. *J. Am. Chem. Soc.* **2000**, *122*, 6175–6182.
92. Palmans, A. R. A. Supramolecular Structures Based on the Intramolecular H-bonding in the 3,3′-di(acylamino)-2,2′-bipydridine Unit, Technische Universiteit Eindhoven: Eindhoven, **1997**.
93. Abbel, R.; Weegen, R. van der; Meijer, E. W.; Schenning, A. P. H. J. Multicolour Self-assembled Particles of Fluorene-based Bolaamphiphiles. *Chem. Commun.* **2009**, 1697-1699.

2

Synthesis and functionalization of discotics

Abstract. The design, synthesis and functionalization of discotics based on three 2,2′-bipyridine-3,3′-diamine molecules linked to a central benzene-1,3,5-tricarbonyl unit are described. A poly-amine discotic with nine peripheral amines groups is synthesized and characterized, which is envisaged to induce cellular uptake. Additionally, for functionalization with ligands, a key requirement for biological applications such as targeted imaging, several discotics bearing a single functional group at their periphery are synthesized. Two strategies are described to functionalize these discotics with different ligands such as carbohydrates, peptides, dyes and small molecules. On the one hand amine bearing discotics are functionalized using amide coupling. On the other hand the functionalization of azide and propargyl bearing discotics via copper-catalyzed azide-alkyne cycloaddition is evaluated. Especially the discotic bearing one amine functionality at the periphery is shown to be an excellent scaffold for ligand attachment, leading to a rapid and facile generation of discotics carrying a single biotin, benzylguanine, mannose, and dye functionality, which are used in the following chapters to study the self-assembling multivalency and the dynamic intermixing of self-assembling discotic scaffolds.

2.1 Introduction

A wide diversity of structure and function at cellular and subcellular level in nature is created via non-covalent self-assembly. This spontaneous organization of molecular units into ordered structures generates dynamic nanostructures. The non-covalent self-assembly of the cell membrane for example enables the dynamic and adaptable supramolecular display of transmembrane proteins. These proteins translate external stimuli into intracellular signal transduction cascades and spatial organization of these proteins is often crucial for their functioning, for example the clustering of receptors as response to stimuli.[1–3] To interact with dynamic natural processes, an adoptable and dynamic scaffold is therefore advantageous. This has led to an emergence in the use of a wide range of supramolecular scaffolds: for imaging[4–6], protein-recognition[7–9] or medicine[10–14]. Dynamic supramolecular scaffolds mostly based on amphiphilic monomers[15,16] are envisioned to bridge the gap between high molecular weight rigid polymers and dynamic natural systems.[17]

The supramolecular self-assembling system used here is based on disc-shaped molecules which self-assemble in water into columnar polymers. These so-called discotics[18] consist of an extended aromatic core of three 2,2′-bipyridine-3,3′-diamine molecules linked to a central benzene-1,3,5-tricarbonyl unit (Figure 2.1 a).[19] This core is surrounded by three gallic acid moieties, which can be functionalized with for example alkoxy or polyethylene glycol (PEG) chains. The self-assembly capabilities and properties of discotics are not only determined by the nature of the rigid core; the nine peripheral tails also induce solubility and determine the polarity of the discotics.

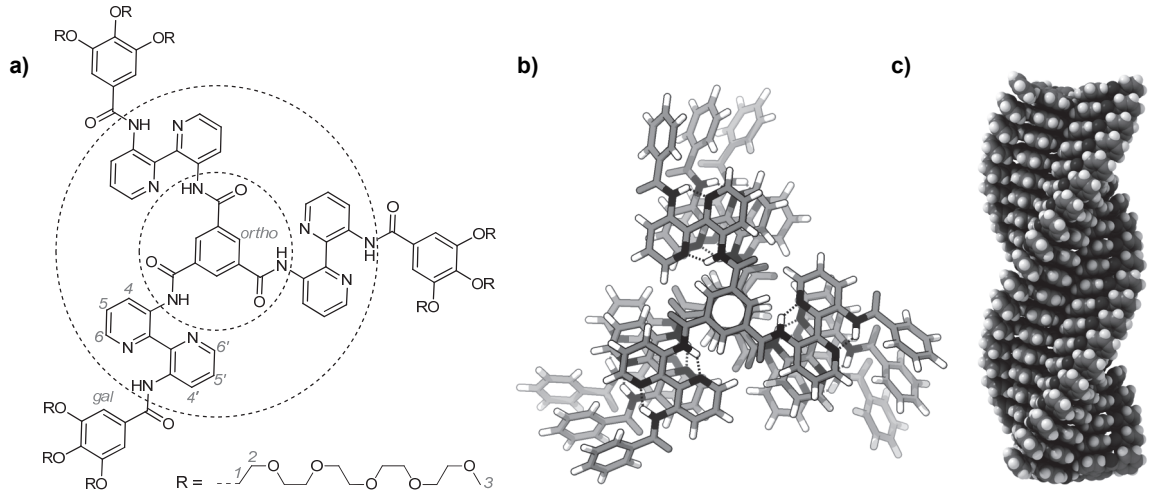

Figure 2.1: a) Structure of the **Inert-Disc**; b) Ball-and-stick model trimer[20]; c) Filled-space model side view of 20-mer.[20]

Since the first introduction of alkoxy functionalized 3,3′-bis(acylamino)-2,2′-bipyridine based discotics by Palmans et al. in the late 90s[19], the self-assembly in solution[21–24] and gel state[25] was studied and applications as conductive supramolecular fibers are still emerging[26,27]. The development of a water-soluble discotic, the so-called **Inert-Disc**, functionalized with ethylene

glycol tails, in the year 2000 by Brunsveld et al.[23] opened up new opportunities for its use in biological applications. For this purpose, bioactive ligands need to be introduced at the periphery of the scaffold. Recently, in the pioneering work of Müller et al.[8], the introduction of functional groups at the periphery of the ethylene glycol tails was shown. This enabled functionalization with the bioactive ligand, mannose, and led to specific and multivalent binding of the mannose functionalized supramolecular polymer to proteins and *E.Coli* bacteria. In the absence of the ligand, no unspecific interactions of the bare discotic scaffold itself were observed. The ethylene glycol chains not only ensure water-solubility, they render the discotics biocompatible by preventing unspecific interactions with biological matter.[28,29]

2.2 Self-assembling properties of discotics

In contrast to linear amphiphiles, such as phospholipids and peptide amphiphiles, the self-assembly of C_3-symmetrical disc-shaped molecules selectively leads to the formation of one type of aggregate: columnar stacks. The degree of oligomerization gradually increases with the monomer concentration and typically, no critical aggregation concentration is observed. The self-assembly of these discotics is based on strong intramolecular hydrogen bonding between the amide N-H groups and neighboring bipyridine N-atoms. This can be observed experimentally by a downfield shift in the ^{1}H-NMR ($CDCl_3$) signal corresponding to the amide protons, from normally 6-9 ppm[30] to approximately 15 ppm (Figure 2.2 a).

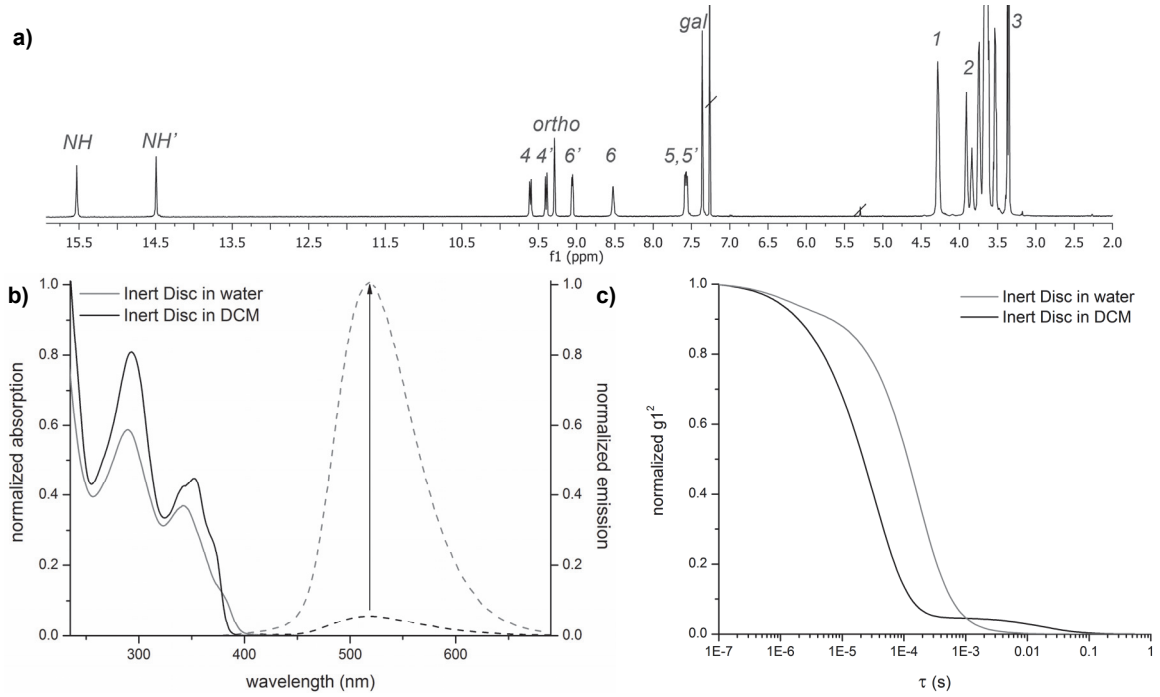

Figure 2.2: a) ^{1}H-NMR spectra of **Inert-Disc** in $CDCl_3$ at 20°C (for assignment see Figure 2.1a); b) Absorption and emission (dashed, λ_{ex} = 350 nm) spectra of **Inert-Disc**(10 μM) in H_2O and DCM at 20 °C; c) DLS correlation spectra of **Inert-Disc** (10 μM) in H_2O and DCM at 20 °C at 140°.

The intramolecular hydrogen bonding pre-organizes the molecules into a propeller-like conformation, which allows the molecules to form long stacks primarily through π-π stacking (Figure 2.1 b).[20,31] In apolar or polar aprotic solvents such as chloroform, dichloromethane, THF, and DMF discotics are typically molecularly dissolved at low concentrations, whereas in polar protic solvents, such as methanol, ethanol and water, the discotics self-assemble.[32] The molecularly dissolved and self-assembled state can be visualized using UV/Vis and fluorescence spectroscopy and dynamic light scattering (DLS) (Figure 2.2 b&c). A shorter correlation function, corresponding to smaller particles, is obtained during DLS measurements of molecularly dissolved discotics in dichloromethane compared to self-assembled discotics in water. Upon self-assembly, a red-shift in the UV/Vis spectra and an increase in fluorescence intensity can be observed.[23] The intrinsic fluorescence with a large Stokes shift of the discotics is attributed to the intramolecular double proton transfer within the bipyridine-diamine groups.[22] Upon self-assembly, due to the decreased motion of the molecules within the self-assembling structure, the fluorescent lifetime increases from 0.3 to 4 ns.[33] Therefore, next to using the auto-fluorescence of these discotics for detection, the emission intensity can indicate the existence of the self-assembled state.

2.3 Design and Synthesis

The synthesis of the C_3-symmetric discotics was based on selective consecutive acylation of the two amino groups of 2,2′-bipyridine-3,3′-diamine, to form *N*-monoacylated 2,2′-bipyridine-3,3′-diamine wedges, which were unified with the benzene-1,3,5-tricarbonyl core at the last step. This convergent approach greatly facilitates the isolation of the discotic in high purity, as only the final compound self-assembles in polar protic solvents.

To enable diverse biological applications, such as receptor targeting or imaging, robust, reliable and general methods were sought to functionalize the discotics with a diverse array of ligands. For this purpose, strategies based on either pre- or post-functionalization are generally applied, as discussed in chapter 1. In contrast to the pre-functionalization approach, where the ligand is incorporated during the synthesis of the self-assembling building block, the post-functionalization strategy introduces the ligand after self-assembly. Due to the linearity of the synthesis, pre-functionalization of the discotics would require the *de novo* introduction of individual ligands at some stage prior to the formation of the discotics. To circumvent this inefficiency, discotics bearing orthogonal functional groups at their extremities were engineered that would in principle enable the introduction of a diverse range of ligands, be it in organic solvents, in which the discotics are molecularly dissolved, or water, which favors dynamic self assembly. Either way, functionalization at the periphery of the discotic, and therefore remote from the critical self-assembling interactions, should in principle accommodate a range of different ligands to suit the intended applications, such as small lipophilic drug molecules, more polar peptides, and large functional macromolecules such as proteins and antibodies.

To decorate the periphery of discotics with orthogonal functionality, a synthetic strategy which allows for selective introduction of modified PEG side chains was needed. To this end, it was previously shown that selective protection of methyl gallate led to the introduction of functional glycol side chains *para* to the methyl ester group, and the formation of multivalent C_3-symmetric discotics with three amine or azide functionalities.[7,8] In this case, complete post-functionalization with different small ligands such as carbohydrates and biotin was demonstrated. However, the attachment of larger charged molecules, such as the Texas Red dye, led to an inseparable mixture of thrice-, twice- and mono-functionalized discotics.[34] Therefore, discotics bearing a single functional group at their periphery were designed. Their synthesis will be described in section 2.3.2. While offering a non-sterically hindered platform for the attachment of high molecular weight ligands, these discotics enable as well the investigation of self-assembling multivalency. The synthesis of discotics bearing nine amine groups will be presented in section 2.3.3. These poly-amine building blocks were not envisaged for the purpose of ligand functionalization, but rather for use as charged supramolecular wires that might induce cellular uptake, bacterial clustering or aggregation of α-synuclein. In section 2.4 the functionalization of discotics with different ligands using amide-coupling and copper-catalyzed azide-alkyne cycloaddition will be discussed.

2.3.1 *Synthesis of building blocks*

Glycol side-chains bearing either an azide, propargyl or Boc-protected amine functionality were prepared according to a divergent strategy starting from hexaethylene glycol **2** (Scheme 2.1).

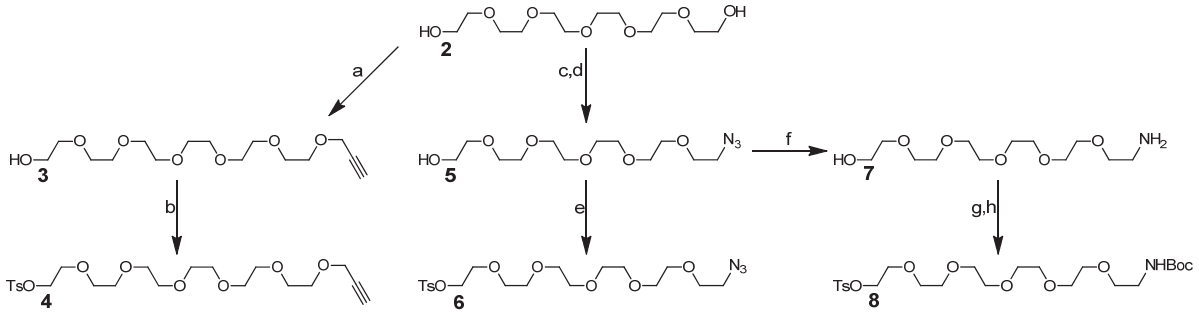

Scheme 2.1: Synthesis of functionalized ethylene glycol chains. Reagents and conditions: a) NaH, propargyl bromide, THF, 0°C to RT, 3 h, 11%; b) TsCl, NEt_3, CH_2Cl_2, RT, 18 h, 29%; c) TsCl, Ag_2O, KI, CH_2Cl_2, 0 °C, 1 h, 80%.; d) NaN_3, DMF, 20°C, 16 h, 79%; e) TsCl, NEt_3, CH_2Cl_2, RT, 18 h, 66%; f) PPh_3, THF, 0 °C to RT, 16 h, 98%; g) Boc_2O, CH_2Cl_2, 0 °C to RT, 16 h, 92%; h) TsCl, NEt_3, CH_2Cl_2, RT, 16 h, 84%.

For the synthesis of propargyl derived building block **4**, Williamson etherification synthesis using stoichiometric amounts of NaH and propargyl bromide was followed by tosylation under standard conditions.[35] Of note here was the tendency for products and by-products – such as double propargylated, double tosylated or non-reacted hexaethylene glycol – to co-elute, which

required the use of extensive purification via extraction and column chromatography, leading to diminished yields. For the synthesis of azide and amine bearing building blocks **6** and **8** protocols previously described by Müller et al.[34] were followed with some minor adjustments. First, the azide functionality was introduced via mono-tosylation of **2** followed S_N2 by NaN_3. Here, double tosylation was suppressed using silver oxide[36] resulting in isolated yields of up to 80%. Alcohol **5** could then be converted either to tosylate **6** for the synthesis of azide-bearing discotics, or alternatively to building block **8**, via azide reduction with PPh_3 to form amine **7** followed by Boc protection and tosylation to generate **8** in high yields, in readiness for the synthesis of amine-bearing discotics.

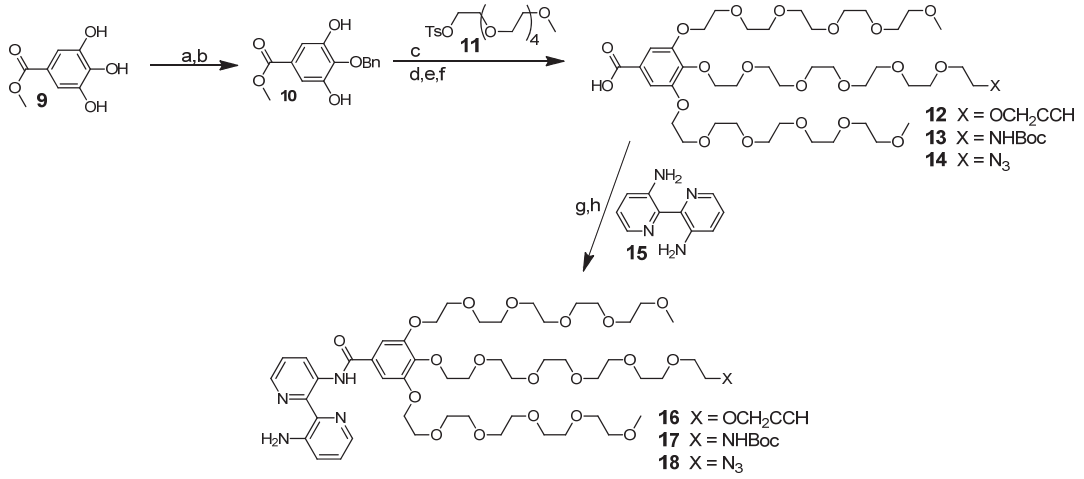

Scheme 2.2: Synthesis of bipyridine wedges **16, 17** and **18.** Reagents and conditions: a) NEt_3, Ac_2O, 0 °C, 4 h 85%; b) i) BnCl, KI, K_2CO_3, DMF, 40 °C, 18 h; ii) K_2CO_3, MeOH/H_2O, 0 °C, 30 min, 57% over 2 steps; c) K_2CO_3, DMF, 70 °C, 16 h, 61% ; d) Pd/C, cat. HCl, EtOH, H_2 (50 bar), 24 h, 94%; e) **4, 6** or **8**, K_2CO_3, DMF, 70 °C, 12 h; f) KOH, H_2O/EtOH, 70 °C, 3 h, 51 % (**12**), 85 % (**13**), 70 % (**14**) over 2 steps; g) $(COCl)_2$, DMF, CH_2Cl_2, 0 °C, 2 h, quant.; h) **15,** NEt_3, CH_2Cl_2, 0 °C to RT, 16 h, 80 % (**16**), 90 % (**17**), 58 % (**18**).

Next, a highly efficient protection group strategy was used to introduce the modified glycol side chains *para* to the methyl ester group of methyl 3,4,5-trihydroxybenzoate **9** (Scheme 2.2).[37] First, peracetylation using acetic anhydride followed by a one pot sequential deacetylation- and mono-benzylation reaction, selective for the *para*-position, afforded intermediate **10** in a useful 48% yield over the 2 steps. A short sequence of etherification, debenzylation and a second etherification step effectively introduced the different functional PEG-ylated side-chains in a sequential manner – via tosylates **11** and **4**, **6** and **8** – to afford the bipyridine wedges **16**-**18** after straightforward saponification of the methyl benzoate group. Subsequent coupling between 2,2′-biamino-3,3′-bipyridine **15**, and the free acids of either, **12, 13** or **14**, was managed by first pre-forming the acid chloride using oxalyl chloride in the presence of catalytic amount of DMF. The crude acid chloride was diluted in dry dichloromethane and added drop-wise to the 2,2′-biamino-3,3′-bipyridine to form the mono-acylated product in 60-70% yield. Using extra dry triethylamine[38] the yields could be increased to above 90%.

2.3.2 *Synthesis of monovalent discotics*

Statistical methods have traditionally been used for the synthesis of desymmetrized 3,3′-bis(acylamino)-2,2′-bipyridine discotics,[39,40] which has necessitated elaborate chromatographic purification to isolate the pure material. A more convergent approach was recently described starting from bis-acylation of a mono-protected benzene-1,3,5-tricarbonyl core (compound **19**, Scheme 2.3).[41,42] Saponification of the resulting ester using aqueous LiOH gave the intermediate carboxylic acid (**20**)[43], which activated into an acid chloride gives rapid access to different mono-functional discotics through coupling with the appropriate mono-*N*-acylated 2,2′-bipyridine-3,3′-diamine wedge.

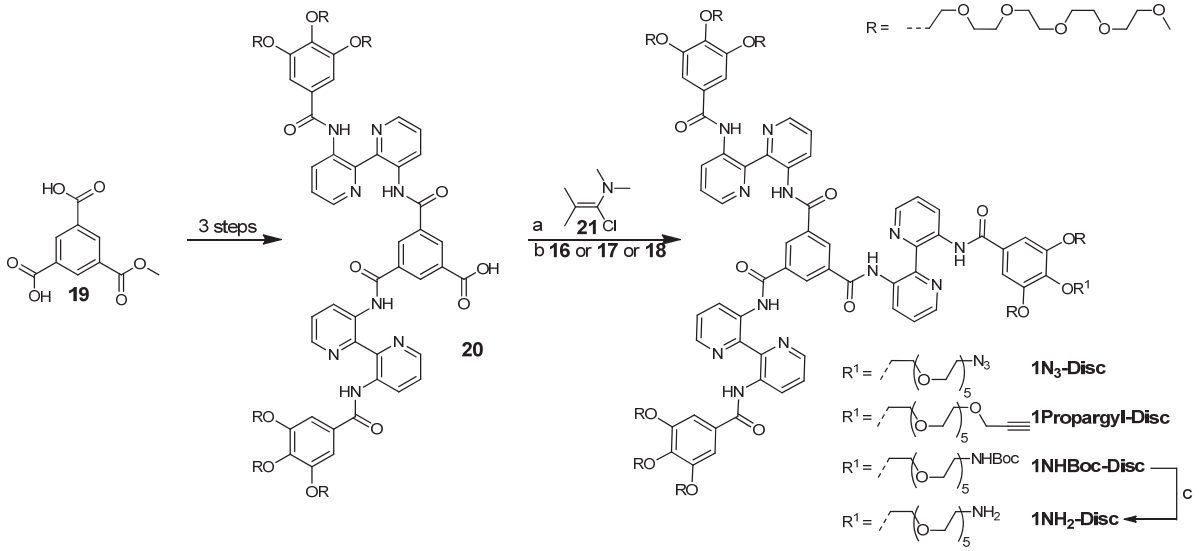

Scheme 2.3: Synthesis of **1N$_3$-Disc**, **1Propargyl-Disc** and **1NH$_2$-Disc**. Reagents and conditions: a) 1-chloro-*N*,*N*,2-trimethylpropenylamine (**21**), RT, 2 h, quant., b) **16, 17** or **18**, NEt$_3$, CH_2Cl_2, RT, 18 h, 77 % (**1Propargyl-Disc**), 45 % (**1N$_3$-Disc**), 77 % (**1NH$_2$-Disc**); c) TFA, CH_2Cl_2, RT, 1 h, quant.

A mild chlorination agent, 1-chloro-*N*,*N*,2-trimethylpropenylamine[44] (known as 'Ghosez's reagent'), was used to convert the carboxylic acid of **20** into an acid chloride in presence of secondary amide functionalities.[45] The formation of the intermediate acid chloride proceeded quantitatively within a few hours and could be conveniently monitored by IR spectroscopy of the crude reaction mixture. The final discotic molecules **1N$_3$-Disc**, **1Propargyl-Disc** and **1NHBoc-Disc** were in each case purified by size-exclusion chromatography (recycling GPC) and characterized using a combination of NMR, IR and mass spectrometry. NMR spectrometry, revealed the presence of strong intramolecular hydrogen bonds, as observed for inert and trivalent discotics (Figure 2.2 a), indicating the presence of an on-average flat conformation.

2.3.3 *Synthesis of 9NH$_2$-Disc*

The synthesis of *C*$_3$-symmetric **9NH$_2$-Disc** (Scheme 2.4), bearing nine peripheral amines, proceeded similar to the synthesis of the **Inert-Disc**.[32] The commercially available methyl 3,4,5-trihydroxybenzoate was alkylated with **8** and the methyl ester saponified to yield **22** in an excellent 84% yield over the two steps. To avoid amine deprotection due to in situ HCl formation, Ghosez's reagent was used in place of oxalyl chloride to convert the carboxylic acid of **22** into the corresponding chloride. Subsequent coupling with 2,2′-biamino-3,3′-bipyridine **15** gave compound **23**, which was reacted with commercially available benzene-1,3,5-tricarbonyl trichloride **24** in the presence of dry triethylamine. Here, a slight excess of **23** was used in an attempt to reach complete three-fold reaction of the inner core. However conversions no greater than 66% were achieved of the desired product with the bis-acylated trimesic acid as a significant by-product. It is interesting to note that under the same reaction conditions no significant hydrolysis was observed during the mono-acylation of 2,2′-biamino-3,3′-bipyridine. The fact that the mono-acylated 2,2′-biamino-3,3′-bipyridine is less nucleophilic than 2,2′-biamino-3,3′-bipyridine, suggests that the decreased reactivity leaves more time for hydrolysis of the acid chloride.

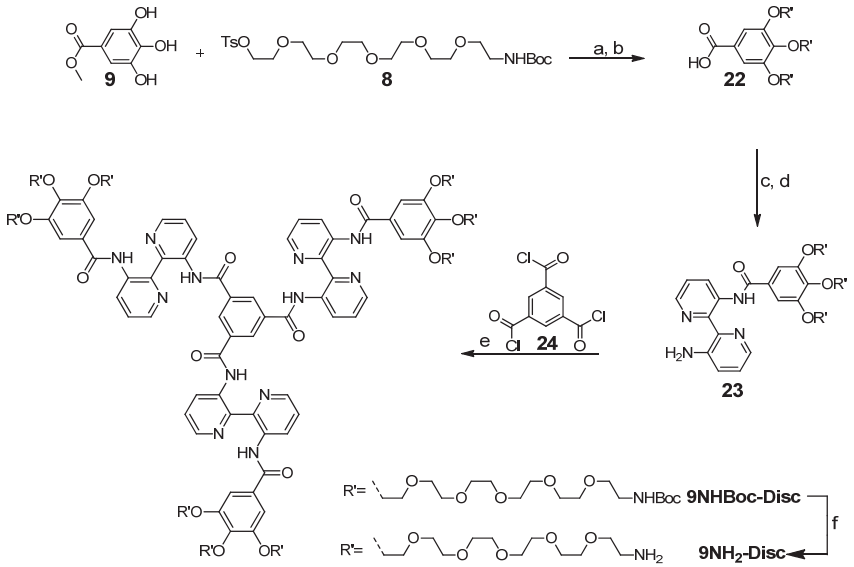

Scheme 2.4: Synthesis of **9NH$_2$-Disc**. Reagents and conditions: a) K_2CO_3, DMF, 70 °C, 10 h, 86 %; b) KOH, EtOH/H_2O 1:1, 80 °C, 3 h, 97 %; c) 1-chloro-*N*,*N*-2-trimethylpropenylamine (Ghosez's reagent, **21**), CH_2Cl_2, 20 °C, 2 h, quant.; d) 2,2′-bipyridine-3,3′-diamine, NEt_3, CH_2Cl_2, 20 °C, 18 h, 61 %; e) **24**, NEt_3, CH_2Cl_2, 5 °C, 18 h, 32 %; f) TFA, CH_2Cl_2, 20 °C, 2 h, 97 %.

Although the excess of **23** could be easily separated using size-exclusion chromatography (BioBeads in dichloromethane), the separation of the bis-acylated impurity from the **9NHBoc-Disc** was not possible; as can be seen by ^{1}H-NMR analysis (Figure 2.3 a). Attempts at purifying using silica chromatography failed to yield the pure discotic. Fortunately, the use of aluminium oxide and a gradient of methanol in dichloromethane resulted in a successful separation (Figure

2.3 b&c). Under these conditions, the carboxylic acid of the side-product is retained on the column, facilitating the separation of the desired product, typically in >95% purity. Such high purity discotics are typically only obtained after purification by recycling-GPC. However, recycling-GPC has its limitations with respect to the scale of the separation and with respect to the incompatibility with amine decorated discotics.[46] The application of the alumina based separation strategy was additionally successfully applied for the purification of **3NHBoc-Disc** and of **1NHBoc-Disc,** as well on a larger scale (500 mg), which highlights the generality of this purification method.

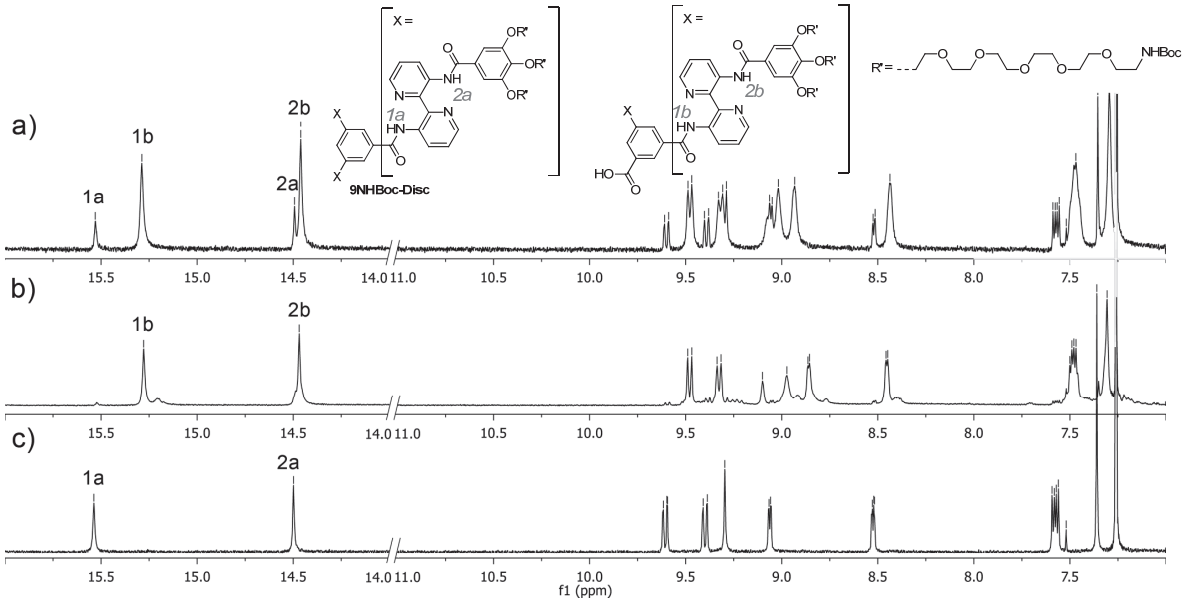

Figure 2.3: a) ^{1}H-NMR spectra in $CDCl_3$ after size-exclusion chromatography with evidence of the bis-acylated by-product; b) ^{1}H-NMR spectrum in $CDCl_3$ of the bis-acylated by-product after alumina column chromatography; c) ^{1}H-NMR spectrum in $CDCl_3$ of **9NHBoc-Disc** after alumina column chromatography. Only the aromatic region is shown for reason of clarity.

At the final step, the Boc-protecting groups were removed using trifluoroacetic acid in dichloromethane. After deprotection, the **9NH$_2$-Disc** showed excellent solubility in water and methanol, but was poorly soluble in non-polar or polar aprotic solvents such as chloroform and dichloromethane, in contrast to the excellent solubility of **1NH$_2$-** and **3NH$_2$-Disc** in the same solvents. This latter point made NMR characterization of the final compounds impossible. Therefore, complete deprotection could only be confirmed by MALDI-ToF.

2.4 Functionalization of discotics

Various biological applications of discotics require their functionalization with a wide array of ligands such as small lipophilic drug molecules, carbohydrates, more polar peptides, and large functional macromolecules such as proteins and antibodies.[47] The non-covalent organization of ligands using a supramolecular scaffold allows fine-tuning of ligand density through either

dynamic adaptation of the system or via the incorporation of different ligands via intermixing of building blocks.[48] At the same time, in contrast for example to small molecules, the dynamic self-assembling properties of the discotics add a degree of complexity to their functionalization. The use of polar solvents favors self-assembly, which increases the density of peripheral discotic functionality and therefore the steric crowding, imposing constraints on the types of reactions and reaction conditions that can be used. In choosing reaction types suitable for studies into discotic functionalization, therefore, only those that have already shown broad applicability to other large macromolecules with diverse ligands, such as proteins, dendrimers, and surfaces were considered. Importantly, the reaction types must also be compatible with solvents that limit the stacking of the discotic molecules, thereby reducing the steric crowding effect.

For this purpose, the Huisgen 1,3-dipolar cycloaddition reaction between azides and alkynes appears to be ideally suited. Especially since the introduction of Cu(I) catalysis,[49,50] this highly versatile ligation reaction has found broad applications in drug discovery, polymer synthesis and controlled surface modifications through its compatibility with a wide range of different molecules such as sugars, peptides, DNA and in light of its orthogonality with respect to other functional groups, high stoichiometric efficiency and importantly, its tolerance of aqueous media and a wide range of organic solvents under standard conditions.[51] Typically, though, the copper catalyzed version is performed using CuI in THF, CH_3CN, or DMSO or with $CuSO_4$/sodium ascorbate in water/alcohol mixtures, depending on the solubility of the substrates. Furthermore, the azide and alkyne components are easy to introduce and are orthogonal to a range of reaction conditions, including peptide cleavage, which means that they can be introduced at different stages of a synthesis.[51,52] Since the advent of copper-catalyzed azide-alkyne cycloaddition, the scope of this powerful methodology was further widened with the emergence of more biologically relevant copper-free variants using ring strained cyclic alkynes, where the relief of strain takes the place of the copper catalyst to drive 1,2,3-triazole formation.[53,54]

In contrast to azide-alkyne cycloaddition, the amide coupling reaction between carboxylic acids and amines is fundamental to life, connecting individual amino acids in the backbone of all proteins. The amine and carboxy groups are as well a common feature in a range of synthetic molecules, including peptides, small drug molecules and polymers.[55] For these reasons in particular, amide coupling was also chosen as a means to introduce diverse ligands. In order for amide coupling to occur under mild conditions, the carboxylic acid must first be activated by converting the OH of the carboxylate into a better leaving group. For this, especially since the introduction of solid-phase peptide synthesis[56], a plethora of coupling reagents have been developed,[57] where the 'activated ester' can either be pre-formed and isolated prior to use (via *N*-hydroxy-succinimide-(NHS) ester, for example),[58] pre-activated prior to the addition of (e.g. *O*-Benzotriazolyl-*N*,*N*,*N'*,*N'*-tetramethyl-uronium-hexafluoro-phosphate or HBTU) or in the presence (e.g. *O*-(7-Azabenzotriazol-1-yl)-*N*,*N*,*N'*,*N'*-tetramethyluronium hexafluorophosphate or HATU) of the amine coupling partner.[55] The correct choice of activation strategy can very much determine the success of an amide coupling reaction, and is an important consideration for

the functionalization of the dynamic discotic molecules. For example, in order to gain better control over the key pre-activation step, it would be more prudent if the amine functionality resided on the discotic molecule and the carboxylic acid on the ligand. In the event of the in situ pre-activation strategy failing, formation of the NHS-ester is more straightforward on the smaller ligand, typically using a combination of NHS/EDC or other carbodiimide coupling reagents. Additionally, multiple NHS-activated ligands and dyes are now commercially available. While the ubiquitous occurrence of carboxylic acids and amines in natural and synthetic substrates offers numerous opportunities for ligand coupling, this non-bioorthogonal coupling might require protection of additional functionalities followed by a deprotection step post amide coupling. Here, for the introduction of ligands via amide coupling reactions, NHS-activation and HBTU pre-activation were explored.

2.4.1 *Functionalization of discotics via amide coupling*

The natural abundance of carboxylic acids in for example drug molecules, peptides and proteins offers the possibility to introduce a wide range of ligands to the **1NH$_2$-Disc** and **3NH$_2$-Disc** via amide coupling. Here, next to bioactive peptide sequences, probes for imaging and ligands for (non-)covalent conjugation of proteins were selected (Scheme 2.5).

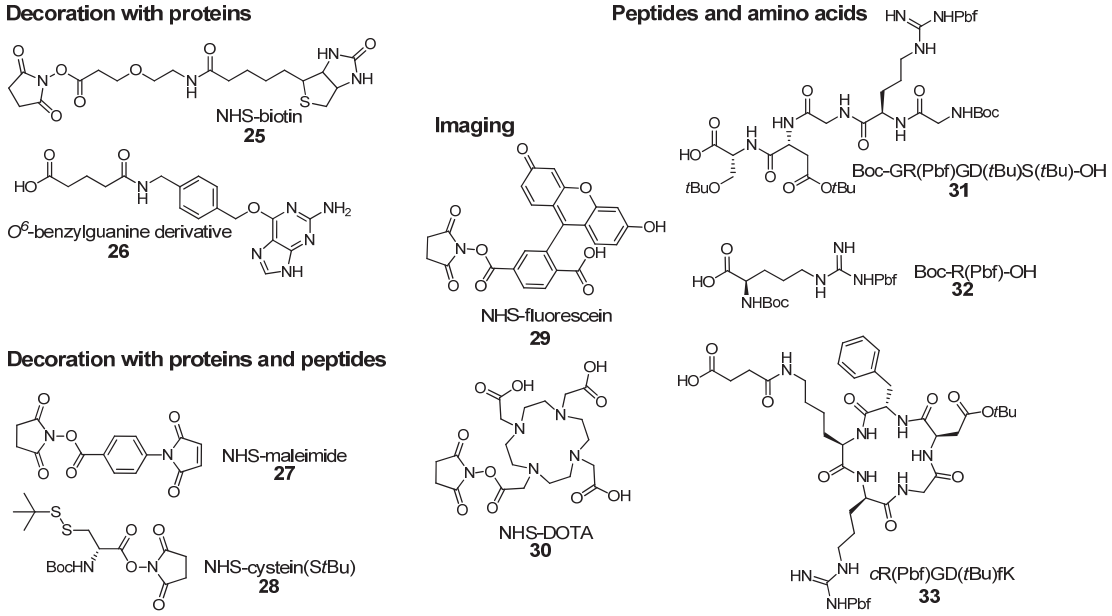

Scheme 2.5: Overview of ligands used for the functionalization of **3NH$_2$-Disc** and **1NH$_2$-Disc**.

As discussed above, two activation strategies were chosen for the functionalization of either the **3NH$_2$-Disc** or the **1NH$_2$-Disc** with bioactive ligands. In all cases, carboxylic acid ligand pre-activated with HBTU or as an NHS ester reacted with the **1NH$_2$-Disc** in a clean and quantitative manner in either dry dichloromethane or DMF as reaction solvent (Table 2.1). The quantitative conversion greatly facilitated the purification, where the excess of ligand was removed using size-

exclusion chromatography (BioBeads in dichloromethane or in DMF). In the case of certain ligands – e,g, (GR(Pbf)GD(*t*Bu)S(*t*Bu), R(Pbf), Cys(S*t*Bu), NHS-maleimide – purification by column chromatography was also possible (Table 2.1). The functionalized monovalent discotics were isolated in 54-98% yield. The functionalization of **3NH$_2$-Disc** with HBTU pre-activated peptides resulted in incomplete conversion and the formation of mixtures of thrice-, twice,- and mono-functionalized discotics, which could not be separated using size-exclusion chromatography. The functionalization of **3NH$_2$-Disc** using NHS-esters was attempted only using NHS-DOTA. However, the highly charged discotics were not detectable by MALDI-ToF. Previously, the functionalization of **3NH$_2$-Disc** with NHS-TexasRed resulted in mixtures of differently functionalized discotics,[34] indicating that this is an attribute of the discotic scaffold and not of the activation strategy used.

Table 2.1: Overview of ligand-functionalized discotics via amide coupling.

starting material[1]	Ligand	equiv.	activation method	conversion (isolated yield)	purification
1NH$_2$-Disc	Biotin	3	NHS	quant. (54%)	SEC
1NH$_2$-Disc	benzylguanine	2	HBTU	quant. (90%)	SEC
1NH$_2$-Disc	Cys(S*t*Bu)	1.6	NHS	quant. (97%)	silica
1NH$_2$-Disc	Maleimide	1.5	NHS	quant. (88%)	SEC/silica
1NH$_2$-Disc	Fluorescein	2	NHS	quant. (89%)	SEC
1NH$_2$-Disc	DOTA	3	NHS	quant. (98%)	SEC
1NH$_2$-Disc	GRGDS	1.5	HBTU	quant. (86%)	silica
1NH$_2$-Disc	*c*RGDfK	2	HBTU	quant. (71%)	SEC
3NH$_2$-Disc	DOTA	6	NHS	--[2]	SEC
3NH$_2$-Disc	R(Pbf)	6	HBTU	95% (53%)[3]	silica
3NH$_2$-Disc	GRGDS	3.3	HBTU	mixtures	--
3NH$_2$-Disc	*c*RGDfK	5	HBTU	mixtures[3]	SEC

[1]All reactions have been performed on a scale of 5-10 mg discotic. [2]The compound was not detectable by MALDI. [3]After side-chain deprotection the compound was not detectable by MALDI.

Functionalization of discotics with whole proteins enables the generation of dynamic protein assemblies. The high affinity of the biotin-streptavidin interaction was frequently applied to generate for example polymer-protein[59] and DNA-protein[60] conjugates. The functionalization of the **3NH$_2$-Disc** with biotin, led to the formation of supramolecular protein assemblies.[7] However, the tetrameric nature of streptavidin and the trivalent nature of the discotics limits the control over stoichiometry. Therefore, monovalent discotics which enable site-specific (non-)covalent conjugation of proteins are sought after.

For non-covalent attachment of streptavidin, the **1NH$_2$-Disc** was functionalized with NHS-biotin (**25**) and, as described for the **3NH$_2$-Disc**[7], the conversion was rapid and quantitative (Table

2.1). In chapter 3, utilizing the recently developed monovalent streptavidin, the multivalent protein display upon self-assembly of **1Biotin-Disc** is investigated.

Covalent and site-specific protein conjugation can be achieved using self-labeling proteins which specifically bind to their suicide ligands.[61] The *O*^{6}-benzylguanine derivative **26** was coupled to the **1NH$_2$-Disc** via in situ pre-activation with HBTU achieving complete conversion. *O*^{6}-benzylguanine is known to react in a rapid and highly selective manner with the mutant of the DNA repair protein *O*^{6}-alkylguanine-DNA alkyltransferase, the so-called SNAP-tag.[62] The generated **1Benzylguanine-Disc** was used for studies into the post-functionalization of discotics with proteins via covalent attachment to SNAP- fusion proteins, which are in detail studied in chapter 4.

To further extend the scope of possible orthogonal methods of ligand attachment, discotics were reacted with NHS esters of maleimide (**27**) and S*t*Bu-protected cysteine (**28**) leading to rapid and quantitative conversion (Table 2.1 and Figure 2.5). In principle, the **1Maleimide-Disc** enables the attachment of ligands bearing reactive thiol groups in a rapid and bioorthogonal manner.[63] This raises the possibility to generate novel discotic-ligand constructs, as cysteine can either be readily coupled to small molecules via amide coupling or, more interesting, expressed in a site selective manner on whole proteins. In a complementary way, the **1Cys(S*t*Bu)-Disc** could be used to functionalize the discotics with peptides and proteins bearing a thioester at the *C*-terminus via native chemical ligation (NCL).[64,65] In this case, the -S*t*Bu protective group serves as a latent form of cysteine, to be removed in situ on treatment with *tris*(2-carboxyethyl)phosphine (TCEP). Previous attempts to functionalize a discotic bearing three fully deprotected cysteines via NCL led to uncontrolled cross-linking of the discotic stacks via disulfide bond and gel formation, which blocked subsequent ligand functionalization.[34] It was envisaged therefore, that in situ deprotection of discotics bearing only one peripheral cysteine would limit disulfide-bridge cross-linking.

NHS-fluorescein **29** was attached quantitatively to a **1NH$_2$-Disc**. With fluorescein as an additional fluorescent read-out, the **1Fluorescein-Disc** was used in chapters 3 and 5 to investigate the formation of mixed supramolecular polymers. Data from UV-Vis spectroscopy measurements revealed an additional absorption between 400 and 500 nm, corresponding to the absorption of fluorescein (Figure 2.4 a). The emission spectrum of the **1Fluorescein-Disc** (λ_{ex} = 350 nm) is shifted from λ_{max} = 510 nm to λ_{max} = 550 nm, the emission maximum of fluorescein (Figure 2.4 c). Due to an overlay of disc emission and fluorescein absorption, Förster resonance energy transfer (FRET) from the disc to the attached dye occurs, leading to a change in the emission profile. Using an excitation wavelength of ≥ 440 nm, the attached fluorescein dye can be selectively excited over the discotics (Figure 2.4 d), indicating that both signals can be separately detected.

With applications relevant to medical imaging, the **3NH$_2$-Disc** and the **1NH$_2$-Disc** were as well functionalized with NHS activated 1,4,7,10-tetraazacyclododecane-1,4,7,10-tetraacetic acid (DOTA) **30**. DOTA is known to chelate metal ions such as gadolinium, indium or gallium, which are used as contrast agents in magnetic resonance imaging (MRI), single-photon emission

computed tomography (SPECT) or positron emission tomography (PET).[66] In light of their intrinsic fluorescence and multivalent self-assembling properties of the discotics molecules, it was hypothesized that dynamic intermixing of targeted discotics with DOTA-functionalized discotics, would produce multimodal, multivalent and multi-targeting imaging agents. Functionalization of the **1NH$_2$-Disc** with **30** proceeded quantitatively. However, the detection of the highly charged high molecular weight discotics generated upon functionalization of **3NH$_2$-Disc** with **30** were not detectable by MALDI-ToF. The restricted solubility of **3DOTA-Disc** in polar aprotic solvents additionally limited their characterization with other techniques such as NMR and GPC.

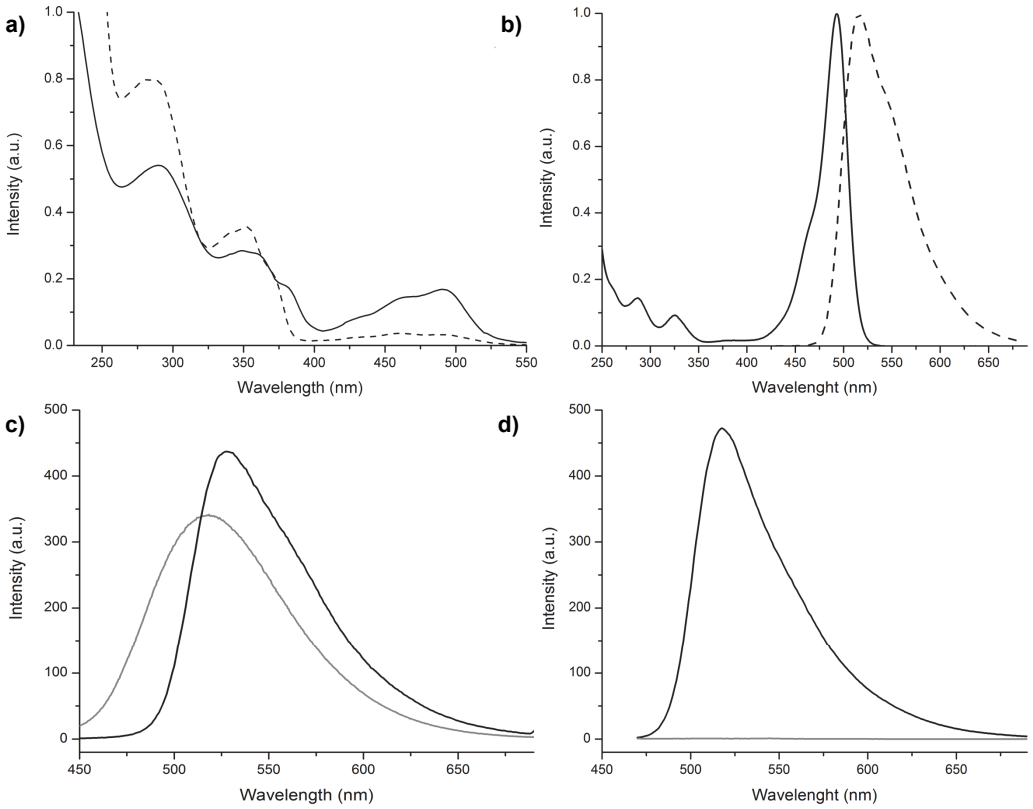

Figure 2.4: a) Absorption spectrum of **1Fluorescein-Disc** in water and chloroform (dashed) at 20 °C showing an additional absorption between 400 and 500 nm. b) Absorption and emission (dashed, λ_{ex} = 420 nm) spectra of fluorescein in water. c) Emission spectra of **1Fluorescein-Disc** (black) and **Inert-Disc** (gray) both 10 μM at 20 °C in water excited at λ_{ex} = 350 nm. d) Emission spectrum of **1Fluorescein-Disc** (black) and **Inert-Disc** (gray) both 10 μM at 20 °C in water excited at λ_{ex} = 460 nm.

The coupling of single amino acids or long peptide sequences to the discotic molecule is an exciting prospect with a myriad of potential applications. For example, peptide sequences corresponding to the active protein binding are commonly used to induce physiologically significant protein-protein interactions. Here the fibronectin derived integrin RGD peptides (linear and cyclic) were selected.[67] Self-assembled peptide amphiphiles displaying the RGDS sequence at high densities were reported to outperform fibronectin induced cell adhesion. Additionally, dynamic adaptation of the binding epitopes could enhance the performance.[68]

For the coupling to amine bearing discotics, protected peptides bearing a free *C*-terminus for coupling were synthesized (see experimental section). Using in situ activation with HBTU, protected peptides and amino acids were ligated to **3NH$_2$-Disc** and **1NH$_2$-Disc.** Functionalization of **1NH$_2$-Disc** with linear and cyclic peptide sequences (e.g. **31** and **33**) proceeded rapidly and quantitatively (Table 2.1), whereas, mixtures of thrice-, double- and mono-functionalized discotics were typically obtained for functionalization of the **3NH$_2$-Disc**, except for the coupling of single amino acids, such as the Pbf protected arginine **32** (Figure 2.5). After coupling and purification, the peptides were readily deprotected with trifluoroacetic acid (TFA). In contrast to **1*c*RGDfK-Disc**, the fully deprotected **3*c*RGDfK-Disc** could not be detected by MALDI-ToF, even though the highly fluorescent solution clearly indicated the presence of the discotic molecule.

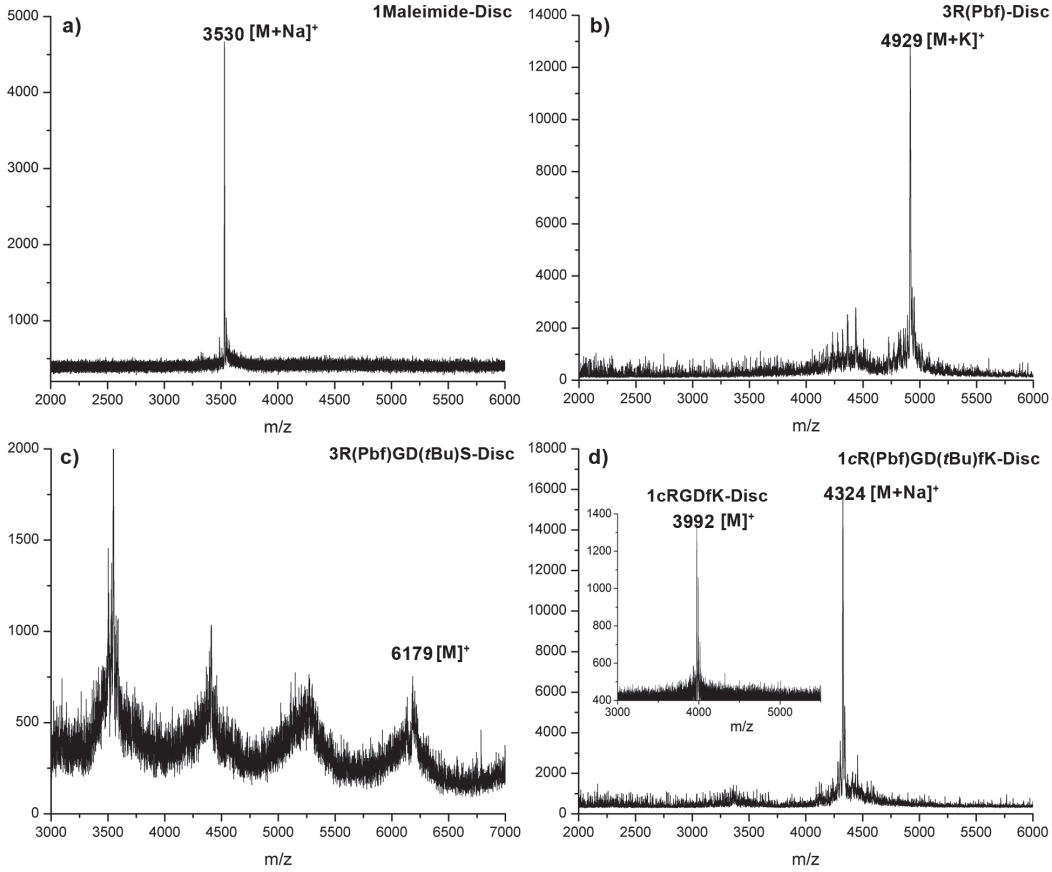

Figure 2.5: MALDI-ToF spectra of crude functionalized discotics. The functionalization of the **1NH$_2$-Disc** with a small ligand (a) as well as with a cyclic peptide (d) proceeds quantitatively, as well as the deprotection of the peptide (d). In contrast, functionalization of **3NH$_2$-Disc** with a linear peptide (c) leads to mixtures of thrice-, twice- and mono-functionalized discotics. The functionalization of **3NH$_2$-Disc** with a single amino acid (b) however proceeded nearly quantitatively.

2.4.2 *Functionalization of discotics via copper-catalyzed azide-alkyne cycloaddition*

Three different discotics – **1N$_3$-Disc**, **3N$_3$-Disc** and **1Propargyl-Disc** – were functionalized with ligands using the Cu(I)[69]-catalyzed azide-alkyne cycloaddition (CuAAC) reaction. The

orthogonality of this reaction with other present functional groups enables the coupling of fully deprotected, ready-to-use, peptides and carbohydrates. At the same time, the poor solubility of fully deprotected peptides and carbohydrates in organic solvents requires water/alcohol mixture as a solvent system for functionalization; a solvent system that leads to self-assembly of discotics and increases the steric crowding.

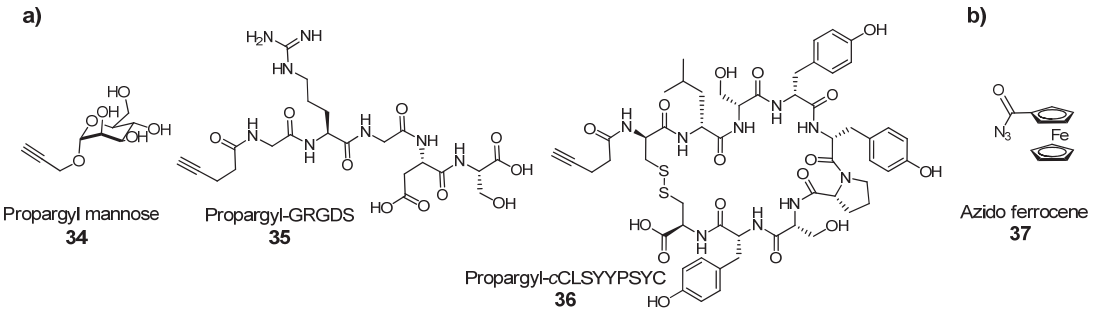

Scheme 2.6: a) Overview of ligands used for the functionalization of **1N$_3$-Disc** and **3N$_3$-Disc**; b) Ligand used for functionalization of **1Propargyl-Disc**.

Generally, in water/alcohol mixtures the catalytic Cu(I) is generated in situ using Cu(II)SO$_4$ and sodium ascorbate as a reducing agent.[51] The presence of a large excess of reducing agent renders the reaction much less susceptible to oxygen and the reaction is often carried out under open-air conditions. Functionalization of **1N$_3$-Disc** with propargyl mannose **34** (Scheme 2.6) under these standard conditions led to a conversion of around 70% after stirring for 16 hours. For **3N$_3$-Disc** 30% conversion within the first hours was reported, whereas complete functionalization took up to four weeks.[8] To achieve rapid and quantitative conversion, several strategies were used to maintain the concentration of Cu(I) at a sufficiently high level during the reaction. To avoid oxidation of Cu(I) to Cu(II), the reaction was performed in degassed solvent under argon atmosphere and in presence of copper turnings.[70] Under these conditions, the quantitative ligation of propargyl mannose **34** to **1N$_3$-Disc** and **3N$_3$-Disc** was achieved within 16 h (Figure 2.7). Following the reaction with IR revealed complete functionalization of the **3N$_3$-Disc** within 4 hours (Figure 2.6) and the presence of only negligible amounts of azide after 2 hours of reaction time, judging by the azide absorbance peak at ~2100 cm^{-1}.

The functionalization of **1N$_3$-Disc** with deprotected peptides **35** and **36** (for synthesis see experimental section) proceeded under the same conditions to 20-40% conversion as judged by MALDI-ToF (Figure 2.7). Using the Cu(I) stabilizing ligand *tris*[(1-benzyl-1*H*-1,2,3-triazol-4-yl)methyl]amine (TBTA) and elongated reaction times did not improve the conversion. For the functionalization of **3N$_3$-Disc** with peptides **35** and **36** IR spectroscopy indicated some consumption of the azide functionality, but it proved impossible to obtain a satisfactory mass spectrum of these highly charged and high-molecular weight discotics (see as well Table 2.1).

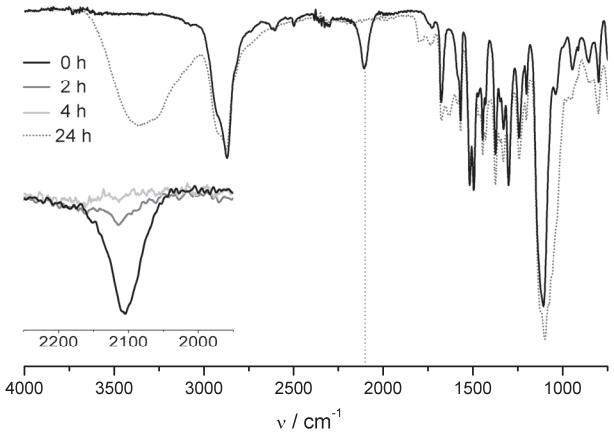

Figure 2.6: IR spectra of **3N$_3$-Disc** (black) and of the crude reaction mixture of **3Mannose-Disc** 16 h after the reaction's start. Inset: IR spectra fragment of **3N$_3$-Disc** and of the crude reaction mixture of **3Mannose-Disc**, 2 and 4 h after the start of the reaction.

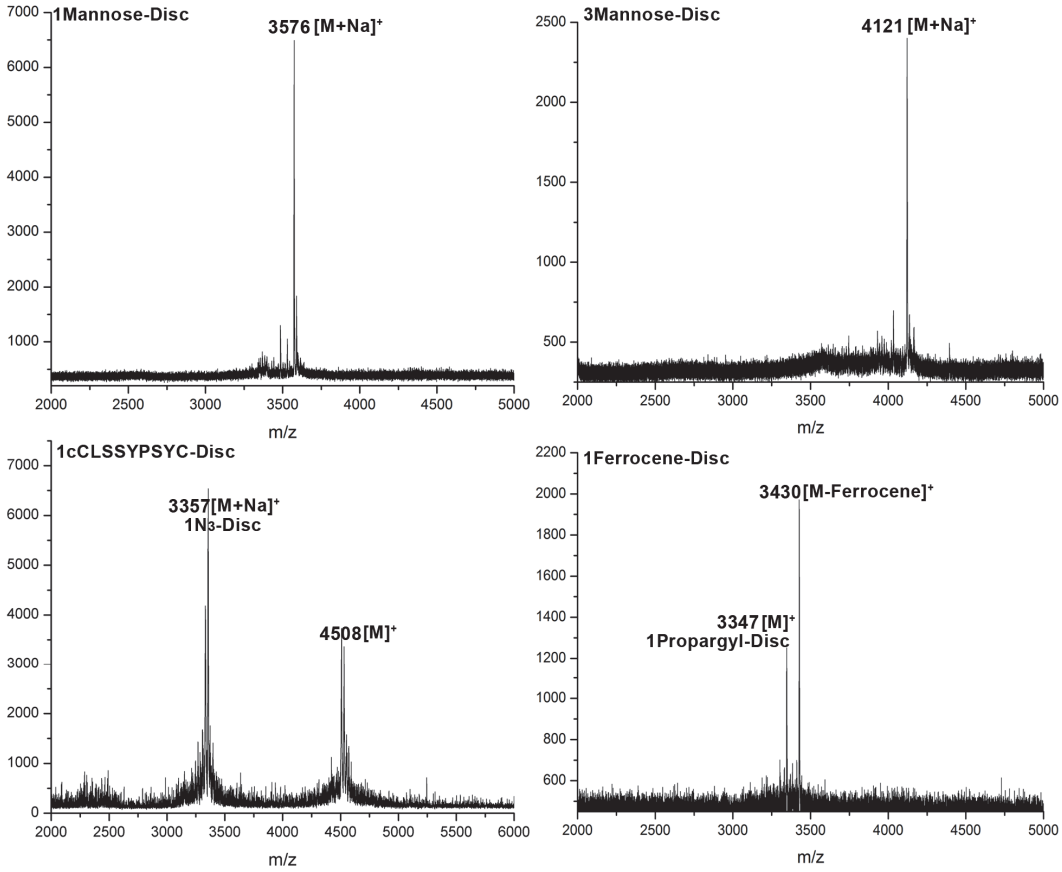

Figure 2.7: MALDI-ToF spectra of crude click reactions.

Coupling of ferrocene azide **37** to the **1Propargyl-Disc** via the CuAAC reaction using the set of optimized conditions resulted in 60% conversion, as judged by thin layer chromatography. Despite its reactivity and orthogonality, the conditions for copper-catalyzed azide-alkyne cycloaddition are substrate dependent and require optimization for each ligand. Optimization

might include the use of microwave irradiation, which was shown to improve the functionalization of highly complex dendritic structures with peptides.[71] Additionally, in view of biological applications, the use of strain promoted cycloaddition[53,54] would be beneficial, as the presence of cytotoxic copper[69] is avoided.

2.5 Conclusions

A novel discotic containing nine amine functionalities as well as monovalent discotics containing a single amine, azide and propargyl group were successfully synthesized. Using aluminium oxide column chromatography the final discotics could be obtained on up to 500 mg scale in over 95% purity.

Two different types of reactions were utilized for ligand functionalization of the discotics: amide coupling and the copper-catalyzed azide alkyne cycloaddition (CuAAC) reaction. Due to the orthogonality of the CuAAC reaction, ligands do not require protecting groups and, for example, unprotected peptides can be directly coupled. Quantitative functionalization with carbohydrates was typically achieved within 4 h by ensuring a high concentration of Cu(I) for the reaction's duration through the use of degassed solvents, a positive inert atmosphere and the addition of copper wire. However, coupling of peptides to **1N$_3$-Disc** proceeded with at best 40% conversion. Using unprotected ligands saves a deprotection step, while at the same time the solubility of the deprotected ligands restricts the reaction conditions to the use of polar protic solvents, which tends to favor the self-assembly of the discotics and the steric crowding of side chain functionality.

In contrast, amine bearing discotics were more readily functionalized with a range of peptidic- and non-peptidic ligands. The functionalization of the **3NH$_2$-Disc**, especially with the larger ligands, led to mixtures of thrice-, double- and mono-functionalized discotics.[34] In principle, such mixtures can be utilized, once an alternative technique for quantitative analysis of the complex mixture can be found, as discotics functionalized with highly charged ligands are difficult to characterize by NMR or MALDI. The **1NH$_2$-Disc** emerged as a versatile non-sterically hindered scaffold for ligand attachment as all ligands used herein were rapidly and quantitatively attached using both, NHS ester and HBTU/DIPEA, activation techniques.

By offering a non-sterically hindered platform for ligand attachment, monovalent discotics display multiple ligands only upon self-assembly into columnar stacks. This multivalency will be investigated as a property of the discotics in the following chapters. Chapter 3 focuses on the quantification of the self-assembling multivalency, while the adaptivity of ligand display is studied in chapter 4.

In all cases where discotic molecules were soluble in $CDCl_3$, the NMR spectroscopy data showed strong intramolecular hydrogen bonding and an on-average planar conformation for both non-functionalized as well as for ligand-functionalized discotics. For those discotics investigated by UV/Vis spectroscopy (**1Biotin-Disc**, **1Fluorescein-Disc**, **1NH$_2$-Disc**, **9NH$_2$-Disc**),

a red-shift in the absorption spectrum in water was observed, which would suggest this to be a general property of all peripherally functionalized discotics. The fluorescence emission of all discotics introduced in this chapter strongly increases in polar protic solvents, as well indicating that the introduction of ligands does not interfere with the self-assembly. Recently, the self-assembly of discotics in water was additionaly confirmed with cryogenic transmission electron microscopy (cryo-TEM) measurements using the **1Ferrocene-Disc**, where the ferrocene ligand greatly increased the contrast of the organic material.

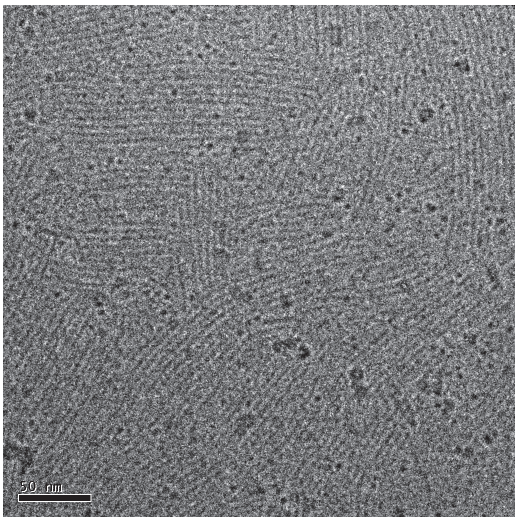

Figure 2.8: Cryo-TEM image of **1Ferrocene-Disc** (1mg/mL in water).

2.6 Experimental

O-Benzotriazolyl-*N,N,N′,N′*-tetra methyl-uronium-hexafluoro-phosphate (HBTU) and *N,N´*-diisopropylethylamine (DIPEA) and trifluoroacetic acid (TFA) were purchased from Biosolve. Dry *N,N´*-dimethylacetamide (DMA), dry *N,N´*-dimethylformamide (DMF), dry triethylamine (NEt_3), copper (II) sulfate, (+)-sodium L-ascorbate, 4-pentynoic acid, trimesic chloride, methyl-3,4,5-trihydroxybenzoate and ferrocene azide were purchased from Sigma-Aldrich. Oxalyl chloride and 1-chloro-*N,N*,2-trimethyl-1-propenylamine were purchased from Acros. NHS-Fluorescein and NHS-PEO_4-biotin were purchased from Pierce, Thermo Scientific. NHS-DOTA and NHS-maleimide were obtained from Symo-Chem. All amino acids and the pre-loaded resins (Fmoc-Ser(tBu)-Wang resin, Fmoc-Phe-Wang resin, Fmoc-Cys(Trt)-Wang resin, H-Ser(tBu)-2-Cl-Trt chloride resin, H-Gly-2-Cl-Trt chloride resin) were purchased from Novabiochem. Deuterated solvents were bought from Cambridge Isotope Laboratories. All solvents and chemicals were used as received. Water was demineralized prior to use. Chloroform, tetrahydrofuran (THF), and dichloromethane (DCM) (HPLC grade) were degassed with argon and purified by passage through activated alumina solvent column prior to use. PEG-containing molecules were dried overnight over P_2O_5 under vacuum prior to the acylation reaction.

Analytical thin layer chromatography (TLC) was carried out using Merck pre-coated silica gel or aluminium oxide plates (60F-254) using ultraviolet light irradiation at 254 or 365 nm. Manual column chromatography was carried out using either Merck 60 Å pore size silica gel (particle size: 63-200 μm) or Merck aluminium oxide (90 active basic, 0.063-0.2 mm, activated with 6 vol% water). Preparative recycling GPC was performed using a Shimadzu system equipped with a Shimadzu LC-10ADvp pump, a Jai-Gel 2.5

H and a Jai-Gel 2 H column in series and a Shimadzu SPD-10AVvp UV/Vis detection system performing detection at 275 nm and 325 nm. HPLC grade chloroform was used as the eluent (with a flow of 3.5 ml/min and manual injection was performed with a volume of 2 ml. One cycle through the system took 1 h.) Manual size-exclusion chromatography was performed on BIO RAD BioBeads S-X1 (200-400 mesh) in a long glass column (1.2 m) at atmospheric pressure and a flow rate less than 1 mL/min in DMF or in dichloromethane. Reversed phase high-pressure liquid chromatography (RP-HPLC) was performed on a Shimadzu LC-8A HPLC system by using a Gemini 5u C18 column. A gradient of water in acetonitrile, both containing 0.1% formic acid was used to elute products. Detection was performed by a Shimadzu SPD-10AV UV-detector (λ = 240 nm).

Matrix assisted laser desorption/ionisation time of flight mass spectra (MALDI-TOF-MS) were measured on a PerSeptive Biosystems Voyager-DE PRO spectrometer with a Biospectrometry workstation using 2-[(2E)-3-(4-tert-butylphenyl)-2-methylprop-2-enylidene]malononitrile (DCTB) and α-Cyano-4-hydroxycinnamic acid (CHCA) as matrix material and THF or MeOH as solvent. M/z values are given in g/mol. General LC-MS analysis: samples were analyzed using a Shimadzu SCL-10 AD VP series HPLC coupled to a diode array detector (Finnigan Surveyor PDA Plus detector, Thermo Electron Corporation) and an Ion-Trap (LCQ Fleet, Thermo Scientific). Analyses were performed using a reversed phase HPLC column (GraceSmart PP18, 50 mm x 2.1 mm, 3µm), using an injection volume of 1-4 µL, a flow rate of 0.20 mL/min and a typically a gradient (5% to 100% in 10 minutes, held at 100% for 1 more minute) of acetonitrile in water (both containing 0.1% formic acid) at 298K. Infrared spectra were recorded as a liquid film on a Perkin Elmer Spectrum One 1600 FT-IR spectrometer, equipped with a Perkin Elmer Universal ATR Sampler Accessory. ^{1}H and ^{13}C NMR spectra were recorded using a Varian Mercury Vx 400 MHz (100 MHz for ^{13}C) NMR spectrometer at 298 K. Chemical shifts are given in parts per million (ppm) and the spectra are calibrated to residual solvent signals of $CDCl_3$ (7.26 ppm (^{1}H) and 77.0 ppm (^{13}C)). Splitting patterns are labeled as s, singlet; d, doublet; dd, double doublet; t, triplet; and m, multiplet.

UV-vis spectra were measured on a Jasco V-650 spectrophometer equipped with a Perkin–Elmer PTP-1 Peltier temperature control system. Fluorescence spectra were recorded on a Varian Cary Eclipse fluorescence spectrophotometer equipped with a Perkin–Elmer PTP-1 Peltier temperature control system. All UV-vis and fluorescence measurements were performed in quartz cuvettes of 10 mm light path (Hellma) and 2 mL minimal volume at 20°C. Dynamic light scattering experiments (DLS) were performed on an ALVCGS-3 Compact Goniometer, in the angular range of 25 to 151 degrees. The incident beam was produced by a HeNe laser operating at 532 nm. The intensity signal was sent to an ALV5000 digital correlator, using a typical acquisition time of 100 s for each angle.

Cryo-TEM measurements were performed by Marcel Koenigs. Samples for cryo-TEM were prepared in a 'Vitrobot' instrument4 (PC controlled vitrification robot, patent applied, Frederik et al 2002, patent licensed to FEI) at room temperature and a relative humidity >95%. In the preparation chamber of the 'Vitrobot' a 4 µl sample was applied on a Quantifoil grid (R 2/2, Quantifoil Micro Tools GmbH; freshly glow discharged just prior to use), excess liquid was blotted away with filters at -2mm for 2 seconds and the thin film thus formed was shot (acceleration about 3 g) into liquid ethane. The vitrified film was transferred to a cryoholder (Gatan 626) and observed at -170 °C in a Tecnai microscope operating at 120 kV. Micrographs were taken at low dose conditions.

Compound **20** was provided by Jolanda Spiering. NHS-Cys(S*t*Bu) was provided by Dr. Christian Haase, propargyl mannose **34**, **3N$_3$-Disc** and **Inert-Disc** were provided by Dr. Marion Müller.

3Biotin-Disc[7], **1Benzylguanine-Disc**[72], **14**[8], **13**[7], **10**[34], **11**[34], **40**[8] and 2,2'-biamino-3,3'-bipyridine **15**[8] were synthesized according to literature.

3,6,9,12,15,18-hexaoxahenicos-20-yn-1-ol (3)

Hexaethylene glycol **2** (5.2 g, 18.5 mmol), dissolved in 20 mL dry THF, was added dropwise at 0 °C to a suspension of sodiumhydride, 60% dispersion in mineral oil (0.776 g, 32.5 mmol) dissolved in 10 mL dry THF. After stirring the reaction mixture for 30 min at rt, propargyl bromide, 80% in toluene (2.97 g, 25 mmol), was added dropwise at 0 °C. The reaction mixture was allowed to warm to room temperature and stirred for 3 h. The solvent was evaporated and extraction with diethyl ether was used to remove doulbe functionalized hexaethylene glycol. Extraction of the aqueous phase with dichloromethane led to an enrichment of unreacted hexaethylene glycol in the aqueous phase. The combined dichloromethane layers were washed with brine, dried over $MgSO_4$ and evaporated *in vacuo*. The enriched crude product was purified by column chromatography (silica, 2%-5% methanol in dichloromethane, R_f = 0.32) affording the pure compound **3** (0.64 g, 2 mmol, 11%). ^{1}H NMR (400 MHz, $CDCl_3$): δ= 4.20 (d, *J* = 2.4 Hz, 2H, CH_2CCH), 3.81 – 3.51 (m, 24H), 2.43 (t, *J* = 2.4 Hz, 1H, CC*H*); ^{13}C NMR (100 MHz, $CDCl_3$): δ= 79.7, 74.5, 72.5, 70.3-70.6, 69.1, 61.7, 58.4; LC-MS(ESI): R_t=4.16 min, m/z calcd ($C_{15}H_{28}O_7$) 320.2; found 321.2 $[M+H]^+$.

3,6,9,12,15,18-hexaoxahenicos-20-yn-1-yl 4-methylbenzenesulfonate (4)

To a solution of **3** (1.39 g, 4.3 mmol) and triethylamine (1.8 mL, 13 mmol) in DCM (25 mL) *p*-toluenesulfonyl chloride (2.48 g, 13 mmol) in DCM (25 mL) was added dropwise. The reaction was stirred over night and then washed with 1N HCl (3 x 100 mL) and brine (100 mL). Drying over $MgSO_4$ and evaporating the solvent *in vacuo* gave the crude product. Purification by column chromatography (alumina, 0%-5% EtOH in chloroform) yielded the pure compound **4** (0.6 g, 1.3 mmol, 29%) as a colorless oil. ^{1}H NMR (400 MHz, $CDCl_3$): δ= 7.80 (d, *J* = 8.3 Hz, 2H), 7.34 (d, *J* = 8.3 Hz, 2H), 4.20 (d, *J* = 2.3 Hz, 2H, CH_2CCH), 4.16 (t, *J* = 5 Hz, 2H), 3.73 – 3.58 (m, 22H), 2.45 (s, 3H), 2.42 (t, *J* = 2.4 Hz, 1H, CC*H*); ^{13}C NMR (101 MHz, $CDCl_3$): δ= 144.92, 133.18, 129.96, 128.13, 79.82, 74.66, 70.90, 70.71, 70.66, 70.55, 69.38, 69.26, 68.84, 58.55, 21.80; LC-MS(ESI): R_t=6.69 min, m/z calcd ($C_{22}H_{34}O_9S$) 474.2; found 475.2 $[M+H]^+$.

2[-2-(2-{2-[2-(2-Hydroxyethoxy)-ethoxy]-ethoxy}-ethoxy)-ethoxy]-ethyl *p*-tosylate (38)

The solution of hexaethyleneglycol **2** (12.5 g, 42.5 mmol) in CH_2Cl_2 (250 mL) was cooled to 0°C. After the addition of KI (1.57 g, 9 mmol) and Ag_2O (12 g, 51.7 mmol), *para*-toluensulfonyl-chloride (8.1 g, 42.5 mmol) was added to the cooled solution. After 1 hour at 0°C all starting material was consumed. Ag_2O was removed via filtration over Celite. After filtration and evaporation of the solvents *in vacuo* the residue was purified by column chromatography (silica, 1-2% methanol in CH_2Cl_2) to **38** as colorless oil (14.7 g, 34 mmol, 80 %). ^{1}H NMR (400 MHz, $CDCl_3$): δ= 7.78 (d, *J*=8.1, 2H), 7.33 (d, *J*=8.0, 2H), 4.15 (dd, 2H), 3.74-3.56 (m, 22H), 2.93 (br, 1H), 2.44 (s, 3H); LC-MS(ESI): R_t=5.56 min, m/z calcd ($C_{19}H_{32}O_9S$) 436.1; found 437.1 $[M+H]^+$. In agreement with literature.[8]

2[-2-(2-{2-[2-(2-Hydroxyethoxy)-ethoxy]-ethoxy}-ethoxy)-ethoxy]- ethyl azide (5)

38 (3.09 g, 7 mmol) and NaN_3 (0.5 g, 8.5 mmol) in DMF (70 mL) were stirred at room temperature over night. Subsequently the solvent was evaporated *in vacuo*. The residue was redissolved in ethylacetate, filtered over Celite and the solvent was again evaporated *in vacuo* to yield pure **5** (1.7 g, 5.5 mmol, 79 %). ^{1}H

NMR (400 MHz, $CDCl_3$): δ= 3.73-3.56 (m, 22H), 3.37 (t, 2H); LC-MS(ESI): R_t=4.09 min, m/z calcd ($C_{12}H_{25}N_3O_6$) 307.1; found 308.1 $[M+H]^+$. In agreement with literature.[8]

2[-2-(2-{2-[2-(2-Hydroxyethoxy)-ethoxy]-ethoxy}-ethoxy)-ethoxy]- ethyl amine (7)

6 (0.54 g, 1.8 mmol) was dissolved in dry THF (7 mL) and cooled to 0°C. PPh_3 (0.51 g, 1.96 mmol) was added after which the mixture was allowed to attain room temperature. The reaction was monitored by LC-Ms. At completion, water (0.7 mL) was added to hydrolyze the intermediate phosphorus adduct. The triphenylphosphine oxide was extracted with toluene and the aqueous layer containing **7** was evaporated yielding **7** (0.5 g, 1.76 mmol, 98%). ^{1}H NMR (400 MHz, $CDCl_3$); δ= 3.75 – 3.57 (m, 20H), 3.52 (t, 2H), 2.86 (t, 2H); LC-MS(ESI): R_t=0.88 min, m/z calcd ($C_{12}H_{27}NO_6$) 281.1; found 282.1 $[M+H]^+$.

2[-2-(2-{2-[2-(2-Hydroxyethoxy)-ethoxy]-ethoxy}-ethoxy)-ethoxy]- ethyl- tert-butyl carbamate (39)

To a solution of **7** (2.85 g, 10 mmol) in dry CH_2Cl_2 (30 mL) di-*tert*-butyl dicarbonate (2.2 g, 10 mmol) was added at 0 °C and stirred for 16 h. The solvent was evaporated *in vacuo* to yield a 95% pure **39** (3.52 g, 9 mmol, 92%). LC-MS(ESI): R_t=6.90 min, m/z calcd ($C_{17}H_{35}NO_8$) 381.1; found 382.0 $[M+H]^+$, 282.1 $[M-Boc]^+$. In agreement with literature.[7]

2[-2-(2-{2-[2-(2-tert-butoxycarbonylamino)-ethoxy)-ethoxy]-ethoxy}-ethoxy)-ethoxy]- ethyl p-tosylate (8)

To a solution of **39** (0.6 g, 1.6 mmol) and triethylamine (0.65 mL, 4.7 mmol) in CH_2Cl_2 *p*-toluenesulfonyl chloride (0.9 g, 4.7 mmol) was added. The reaction was stirred over night and then washed with 1N HCl and brine. Drying over $MgSO_4$ and evaporating the solvent *in vacuo* gave the crude product which was purified by column chromatography (silica, 2-4% methanol in CH_2Cl_2) yielding the pure compound **8** as a colorless oil (0.72 g, 1.3 mmol, 84%). ^{1}H NMR (400 MHz, $CDCl_3$); δ= 7.80 (d, *J* = 8.3 Hz, 2H), 7.34 (d, *J* = 8.0 Hz, 2H), 5.03 (br, 1H), 4.15 (t, 2H), 3.68 (t, 2H), 3.66 – 3.57 (m, 16H), 3.53 (t, *J* = 5.1 Hz, 2H), 3.30 (dd, *J* = 10.4, 5.1 Hz, 2H), 2.45 (s, 3H), 1.44 (s, 9H); LC-MS(ESI): R_t=6.49 min, m/z calcd ($C_{24}H_{41}NO_{10}S$) 535.2; found 536.2 $[M+H]^+$, 558.2 $[M+Na]^+$.

methyl 3,5-bis(2,5,8,11,14-pentaoxahexadecan-16-yloxy)-4-(3,6,9,12,15,18-hexaoxahenicos-20-yn-1-yloxy)benzoate (41)

A mixture of **4** (0.439 g, 0.93 mmol), **40** (0.503 g, 0.77 mmol) and K_2CO_3 (1.064 g, 7.7 mmol) was stirred over night at 70 °C in dry DMF (7 mL). Water (15 mL) was added to the reaction mixture until all K_2CO_3 was dissolved and the reaction mixture was extracted with DCM (4 x 15 mL). The combined organic layers were washed with brine, dried over $MgSO_4$ and evaporated *in vacuo*. The crude product was purified by column chromatography (alumina, 2% ethanol in chloroform, followed by silica, 0% - 7% MeOH in DCM) affording the pure compound **41** (0.412 g, 0.44 mmol, 56 %). ^{1}H NMR (400 MHz, $CDCl_3$): δ= 7.28 (s, 2H, 12), 4.25 – 4.13 (m, 8H), 3.88 (s, 3H), 3.85 (t, *J* = 4 Hz, 4H), 3.78 (t, *J* = 4 Hz, 2H), 3.73 – 3.59 (m, 48H), 3.55 – 3.49 (m, 4H), 3.37 (s, 6H), 2.43 (t, *J* = 2.4 Hz, 1H, CC*H*); ^{13}C NMR (100 MHz, $CDCl_3$): δ= 166.67, 152.40, 142.69, 125.06, 109.15, 79.79, 74.67, 72.52, 72.05, 70.94, 70.78, 70.72, 70.68, 70.63, 70.53, 69.73, 69.22, 68.96, 59.14, 58.51, 52.28: LC-MS(ESI): R_t=6.15 min, m/z calcd ($C_{45}H_{78}O_{21}$) 954.5; found 955.8 $[M+H]^+$.

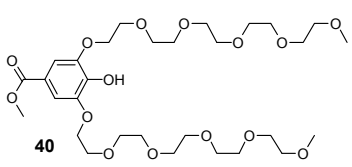

40

3,5-bis(2,5,8,11,14-pentaoxahexadecan-16-yloxy)-4-(3,6,9,12,15,18-hexaoxahenicos-20-yn-1-yloxy)benzoic acid (12)

A solution of **41** (0.314 g, 0.33 mmol) and KOH (0.055 g, 0.99 mmol) in ethanol (4 mL) and water (4 mL) was heated under reflux overnight. Subsequently, the solution was acidified to pH = 2 with concentrated HCl, cooled and extracted with DCM (3 x 10 mL). The organic layer was washed with brine. Drying over $MgSO_4$, evaporating *in vacuo* afforded the pure compound **12** (0.283 g, 0.3 mmol, 91%). ^{1}H NMR (400 MHz, $CDCl_3$): δ= 7.37 (s, 2H), 4.28 – 4.17 (m, 8H), 3.85 (t, *J* = 4.8 Hz, 4H), 3.78 (t, *J* = 5.0 Hz, 2H), 3.74 – 3.59 (m, 48H), 3.59 – 3.53 (m, 4H), 3.38 (s, 6H), 2.43 (t, *J* = 2.2 Hz, 1H, CC*H*); ^{13}C NMR (100 MHz, $CDCl_3$): δ= 168.97, 152.43, 143.23, 124.62, 110.00, 79.78, 74.70, 72.50, 72.08, 71.02, 70.56, 69.87, 69.23, 69.08, 59.12, 58.53; LC-MS(ESI): R_t=6.15 min, m/z calcd ($C_{44}H_{76}O_{21}$) 940.5; found 941.8 $[M+H]^+$.

3,5-bis(2,5,8,11,14-pentaoxahexadecan-16-yloxy)-4-(3,6,9,12,15,18-hexaoxahenicos-20-yn-1-yloxy)-N-(3'-amino-[2,2'-bipyridin]-3-yl)benzamide (16)

A solution of oxalyl chloride (0.05 g, 3.8 mmol, 33 µL) in dry DCM (1 ml) was added dropwise to a solution of **12** (281 mg, 0.299 mmol) containing a catalytic amount of DMF in dry DCM (5 mL) at 0 °C. After stirring the reaction mixture for 1 hour at 0 °C complete conversion into an acid chloride was observed with ^{1}H-NMR. Evaporating the solvent *in vacuo* afforded the crude acid chloride (287 mg, 0.299 mmol, quant.). ^{1}H NMR (400 MHz, $CDCl_3$): δ= 7.39 (s, 2H), 4.28 (t, *J* = 5 Hz, 2H), 4.22 – 4.19 (m, 6H), 3.86 (t, *J* = 5 Hz, 4H), 3.79 (t, *J* = 5.1 Hz, 2H), 3.73 – 3.57 (m, 48H), 3.54 (dd, *J* = 6.1, 3.3 Hz, 4H), 3.37 (s, 6H), 2.43 (t, *J* = 2.4 Hz, 1H, CC*H*). The crude acid chloride was dissolved in dry DCM (4 mL) and added dropwise to a stirred solution of 2,2'-bipyridyl-3,3'-diamine **15** (0.061 g, 0.33 mmol) and triethylamine (124 µL, 0.89 mmol) in dry CH_2Cl_2 (4 mL) at room temperature. After stirring overnight at room temperature, the crude reaction mixture was washed with aqueous NaOH solution, water and brine. After drying over $MgSO_4$, the solvent was evaporated *in vacuo*. The crude product was purified by column chromatography (alumina, 0% - 2% ethanol in chloroform, followed by silica, 0% - 7% MeOH in DCM) to afford pure **16** (275 mg, 0.24 mmol, 75%). ^{1}H NMR (400 MHz, $CDCl_3$): δ= 14.39 (s, 1H), 9.22 (d, *J* = 8.5 Hz, 1H), 8.34 (d, *J* = 4.5 Hz, 1H), 8.05 (d, *J* = 1.3 Hz, 1H), 7.32 (s, 3H), 7.15 (s, 2H), 6.58 (s, 2H, *NH*$_2$), 4.25 (dd, *J* = 10.8, 5.6 Hz, 6H), 4.20 (s, 2H), 3.88 (t, *J* = 4.8 Hz, 4H), 3.81 (t, *J* = 4.8 Hz, 2H), 3.76 – 3.58 (m, 48H), 3.56 – 3.51 (m, 4H), 3.36 (s, 6H), 2.43 (s, 1H, CC*H*); ^{13}C NMR (100 MHz, $CDCl_3$): δ= 165.86, 152.77, 145.27, 143.79, 142.18, 140.99, 138.69, 136.27, 135.20, 130.98, 128.75, 125.47, 124.44, 122.90, 108.03, 79.78, 74.69, 72.60, 72.08, 70.98, 70.81, 70.77, 70.72, 70.66, 70.56, 69.87, 69.43, 69.27, 59.17, 58.55; LC-MS(ESI): R_t=5.38 min, m/z calcd ($C_{54}H_{84}N_4O_{20}$) 1108.57; found 1109.9 $[M+H]^+$.

3'-(4-{2[-2-(2-{2-[2-(2-tert-butoxycarbonylamino-ethoxy)-ethoxy]-ethoxy}-ethoxy)-ethoxy]-ethyl}-3,5-bis[2-(2-{2-[2-(2-methoxyethoxy)-ethoxy]-ethoxy}-ethoxy)-ethoxy]-benzoylamino)-2,2'-bipyridine-3-amine (17)

i) A solution of 1-chloro-2,*N*,*N*-trimethylpropenylamine **21** (Ghosez's reagent, 57 mg 0.427 mmol) in dry DCM (0.6 mL) was added dropwise via a syringe pump to a solution of **13** (0.2402 g, 0.240 mmol) in dry DCM (1.85 mL) over a period of 1 hour. After addition, NMR and IR confirmed complete conversion to the corresponding acid chloride (0.240 mmol, quant.). The solvent and the excess of Ghosez's reagent were removed *in vacuo* and the acid chloride was re-dissolved in dry DCM (1.2 mL) for the following reaction step. ^{1}H-NMR (400MHz, $(CD_3)_2CO$): δ = 7.46 (s, 2H), 5.85 (s, 1H), 4.37 - 4.33 (m, 2H), 4.32 - 4.25 (m, 4H), 3.92 - 3.85 (m, 4H), 3.83 - 3.77 (m, 2H), 3.73 - 3.52 (m, 44H), 3.52 – 3.43 (m, 6H), 3.28 (s, 6H), 3.21 (q, *J* = 5.4 Hz, 2H), 1.40 (s, 9H); IR (ATR): ν = 2875, 1750 (COCl), 1716 ($COOC(CH)_3$), 1107 cm^{-1}.

ii) The re-dissolved acid chloride was added dropwise via a syringe pump to a stirred solution of 2,2′-bipyridyl-3,3′-diamine **15** (50.2 mg, 0.27 mmol) and triethylamine (5 µL, 0.36 mmol, from a capsule)[38] in dry DCM (1.1 mL) within 1 h at room temperature. The reaction continued overnight and the solvent was evaporated *in vacuo*. The crude product was purified by column chromatography (alumina, 0%-1% EtOH in chloroform, R_f = 0.32 (1% EtOH)) to yield pure **17** (0.252 g, 0.216 mmol, 90%). ^{1}H NMR (400 MHz, $CDCl_3$): δ= 14.39 (s, 1H), 9.21 (dd, *J* = 8.5, 1.6 Hz, 1H), 8.33 (dd, *J* = 4.6, 1.6 Hz, 1H), 8.04 (dd, *J* = 3.7, 2.3 Hz, 1H), 7.34 – 7.29 (m, 3H), 7.18 – 7.12 (m, 2H), 6.58 (s, 2H), 5.07 (s, 1H), 4.25 (dd, *J* = 10.9, 5.6 Hz, 6H), 3.88 (t, *J* = 5 Hz, 4H), 3.81 (t, *J* = 5 Hz, 2H), 3.76 – 3.68 (m, 6H), 3.68 – 3.56 (m, 38H), 3.56 – 3.49 (m, 6H), 3.36 (s, 6H), 3.30 (dd, *J* = 10.1, 5.2 Hz, 2H), 1.44 (s, 9H). LC-MS(ESI): R_t = 6.69 min, m/z calcd ($C_{56}H_{91}N_5O_{21}$) 1169.6; found 1170.9 $[M+H]^+$. In agreement with literature.[7]

3′-(4-{2[-2-(2-{2-[2-(2-Azido-ethoxy)-ethoxy]-ethoxy}-ethoxy)-ethoxy]-ethyl}-3,5-bis[2-(2-{2-[2-(2-methoxyethoxy)-ethoxy]-ethoxy}-ethoxy)-ethoxy]-benzoylamino)-2,2′-bipyridine-3-amine (18)

i) A solution of oxalyl chloride (47 µL, 0.54 mmol) in dry CH_2Cl_2 (1.2 ml) was added dropwise to a solution of **14** (380 mg, 0.41 mmol) containing a catalytic amount of DMF in dry CH_2Cl_2 (3 mL) at 0°C. The reaction mixture was stirred overnight at room temperature in the absence of light. The solvent and the excess of Ghosez's reagent were removed *in vacuo* and the acid chloride was re-dissolved in dry DCM (1.2 mL) for the following reaction step. ^{1}H-NMR (400MHz, CD_3CN): δ = 7.42 (s, 2H), 4.29 – 4.23 (m, 2H), 4.23 – 4.17 (m, 4H), 3.85 – 3.79 (m, 4H), 3.76 – 3.71 (m, 2H), 3.67 – 3.49 (m, 44H), 3.47 – 3.41 (m, 4H), 3.34 (s, 2H), 3.28 (s, 6H); IR (ATR): ν = 2875, 2102.96 (N_3), 1749 (COCl), 1107 cm^{-1}.

ii) The re-dissolved acid chloride (0.41 mmol) was added dropwise via a syringe pump to a stirred solution of 2,2′-bipyridyl-3,3′-diamine **15** (114 mg, 0.62 mmol) and triethylamine (6 µL, 0.41 mmol) in dry DCM (1.5 mL) within 1 h at room temperature. The reaction was continued overnight. The hydrolyzed acid chloride (**14**) was removed using acid-base extraction; the organic phase was washed with 0.1 M aqueous NaOH solution. Subsequently, the organic phase was washed with brine, dried over $MgSO_4$ and the solvent was evaporated *in vacuo*. The crude product was purified by column chromatography (silica, EtOAc followed by 5% methanol in CH_2Cl_2) yielding **18** (0.26 g, 0.23 mmol, 58%). ^{1}H NMR (400 MHz, $CDCl_3$): δ= 14.39 (s, 1H), 9.21 (dd, *J* = 8.5, 1.5 Hz, 1H), 8.33 (dd, *J* = 4.6, 1.5 Hz, 1H), 8.04 (dd, *J* = 3.6, 2.3 Hz, 1H), 7.30 (m, 3H), 7.14 (m, 2H), 6.57 (s, 2H), 4.24 (dd, *J* = 10.7, 5.6 Hz, 6H), 3.87 (t, *J* = 4.9 Hz, 4H), 3.81 (t, *J* = 4.9 Hz, 2H), 3.76 – 3.68 (m, 6H), 3.68 – 3.56 (m, 38H), 3.53 (dd, *J* = 5.7, 3.5 Hz, 6H), 3.38 (m, 2H), 3.36 (s, 6H). LC-MS(ESI): R_t = 6.29 min, m/z calcd ($C_{51}H_{81}N_7O_{19}$) 1095.6; found 1096.9 $[M+H]^+$.

3,5-Bis{{3′-{3,4,5-tris[2-(2-{2-[2-(2-methoxyethoxy)-ethoxy]-ethoxy}-ethoxy)-ethoxy]benzoyl- amino}-2,2′-bipyridyl-3-aminocarbonyl}}-benzoic acid chloride (42)

A solution of 1-chloro-*N*,*N*,2-trimethyl-1-propenylamine (0.020 g, 0.147 mmol) in dichloromethane (0.5 mL) was added dropwise in 40 minutes to **20** (0.122 g, 0.098 mmol) dissolved in dry dichloromethane (2.5 mL). The progress of the reaction was monitored by IR. When no carboxylic acid was left, the mixture was concentrated and dried *in vacuo* to remove the excess of 1-chloro-*N*,*N*,2-trimethyl-1-propenylamine and the residue **42** was used as such in the next step. IR (ATR): ν = 2870, 1759 (C=OCl), 1672, 1568, 1097 cm^{-1}.

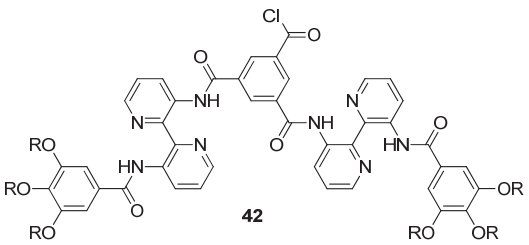

42

1Propargyl-Disc

A solution of crude **42** (0.123 mmol) in dry dichloromethane (1.2 mL) was added dropwise in 50 min using a syringe pump to a stirred solution of mono-propargyl **16**(0.151 g, 0.136 mmol) and triethylamine (25 μL, 0.184 mmol) in dry dichloromethane (1 mL) and the reaction was continued overnight under Argon. The solvent was evaporated and the excess of mon-propargyl **16** was removed using size-exclusion chromatography (Recycling-GPC in chloroform), obtaining pure **1Propargyl-Disc** (32 mg, 77%). IR (ATR): ν = 3514, 2920, 2853, 1672, 1568, 1105 cm^{-1}; ^{1}H NMR ($CDCl_3$): δ=15.52 (s, 3H), 14.50 (s, 3H), 9.61 (s, 3H), 9.39 (s, 3H), 9.28 (s, 3H), 9.06 (s, 3H), 8.53 (s, 3H), 7.57 (s, 6H), 7.36 (s, 6H), 4.25 (d, *J* = 39.0 Hz, 23H), 3.60 (d, *J* = 47.7 Hz, 181H), 3.36 (s, 28H), 2.44 (s, 1H); ^{13}C NMR ($CDCl_3$): δ=165.87, 164.12, 152.76, 142.34, 141.56, 137.54, 137.50, 136.15, 130.65, 130.00, 129.58, 124.79, 108.07, 79.73, 72.03, 70.82, 70.73, 70.63, 70.11, 69.75, 59.19; MALDI- TOF MS: m/z calcd ($C_{163}H_{244}N_{12}O_{61}$) 3347.73; found 3370.40 $[M+Na]^+$, 3386.33 $[M+K]^+$.

1NHBoc-Disc

A solution of crude **42** (0.073 mmol) in dichloromethane (1.2 mL) was added dropwise in 30 min to a stirred solution of monoamine **17** (0.094g, 0.08 mmol) and triethylamine (15 μL, 0.11 mmol) in dichloromethane (0.5 mL) and the reaction was continued overnight. The reaction mixture was washed with 0.1 M aqueous NaOH (2 x 3 mL) and brine (1 x 3 mL). The organic layer was dried with $MgSO_4$, filtered and concentrated *in vacuo*. The excess of monoamine **17** was removed using size-exclusion chromatography (Recycling-GPC in chloroform), obtaining pure **1NHBoc-Disc** (191 mg, 77%). IR (ATR): ν = 2873, 1738, 1715, 1672, 1568, 1097 cm^{-1}. ^{1}H-NMR ($CDCl_3$): δ= 15.53 (s, 3H), 14.49 (s, 3H), 9.60 (d, *J* = .5 Hz, 3H), 9.39 (d, *J* = 8.5 Hz, 3H), 9.28 (s, 3H), 9.05 (d, *J* = 4.5 Hz, 3H), 8.52 (d, *J* = 4.5 Hz, 3H), 7.57 (dd, *J* = 8.5, 4.5 Hz, 6H), 7.35 (s, 6H), 5.03 (s, 1H, N*H*Boc), 4.27 (dd, *J* = 10.8, 5.5 Hz, 18H), 3.90 (t, *J* = 4.8 Hz, 12H), 3.83 (t, *J* = 4.8 Hz, 6H), 3.74 (q, *J* = 4.8 Hz, 18H), 3.70 – 3.59 (m, 110H), 3.53 (dd, *J* = 10.4, 5.4 Hz, 18H), 3.37 (s, 6H), 3.35 (s, 18H), 3.30 (d, *J* = 5.2 Hz, 2H, C*H*$_2$NHBoc), 1.43 (s, 9H). ^{13}C NMR ($CDCl_3$): δ=165.96, 164.25, 156.11 (C=OBoc), 152.88, 142.53, 142.41, 141.68, 141.60, 140.91, 137.67, 137.58, 136.28, 130.71, 130.11, 130.04, 129.71, 124.84, 124.49, 112.73, 108.19, 79.25 (*C*(CH_3)$_3$), 72.65, 72.05, 70.98, 70.81, 70.64, 70.36, 69.87, 69.55, 59.15 (OCH_3), 40.55 (CH_2NH), 28.57 (CH_3). MALDI- TOF MS: m/z calcd ($C_{165}H_{251}N_{13}O_{62}$) 3408.81; found 3431.68 $[M+Na]^+$, 3309.18 $[(M-Boc)+H]^+$.

1NH$_2$-Disc

To a stirring solution of **1NHBoc-Disc** (33.7 mg, 0.099 mmol) in dichloromethane (2 mL) trifluoroacetic acid (TFA, 0.2 mL) was added dropwise and the reaction was continued for 2 hours at room temperature before TFA was co-evaporated with toluene. After drying, the pure **1NH$_2$-Disc** was obtained as a sticky yellow compound (34 mg, quantitative). ^{1}H-NMR ($CDCl_3$): δ= 15.53 (s, 2H), 15.49 (s, 1H), 14.49 (s, 3H), 9.60 (d, *J* = 8.5 Hz, 3H), 9.38 (m, 3H), 9.28 (s, 3H), 9.06 (d, *J* = 3.2 Hz, 3H), 8.52 (d, *J* = 3.2 Hz, 2H), 8.49 (d, *J* = 3.2 Hz, 1H), 7.57 (dd, *J* = 8.5, 4.5 Hz, 6H), 7.36 (s, 4H), 7.33 (s, 2H), 4.28 (dd, *J* = 10.0, 5.3 Hz, 18H), 3.97 – 3.88 (m, 12H), 3.88 – 3.80 (m, 6H), 3.79 – 3.71 (m, 18H), 3.70 – 3.58 (m, 110H), 3.59 – 3.48 (m, 18H), 3.37 (s, 6H), 3.36 (s, 18H), 3.23 (s, C*H*$_2$NH$_2$, 2H). ^{13}C NMR ($CDCl_3$): δ= 165.95, 164.23, 152.85, 152.71, 142.42, 142.39, 141.73, 141.68, 141.43, 140.91, 137.65, 137.57, 136.26, 131.20, 130.74, 130.11, 129.70, 124.84, 124.49, 108.12, 107.37, 72.64, 72.03, 71.99, 70.95, 69.99, 69.85, 69.70, 69.51, 69.15, 67.18, 59.14(OCH_3), 59.12(OCH_3), 40.23(CH_2NH_2), 29.82(CH_3). MALDI- TOF MS: m/z calcd ($C_{160}H_{243}N_{13}O_{60}$) 3308.69; found 3309.77$[M+H]^+$, 3331.66 $[M+Na]^+$.

1N$_3$-Disc

A solution of crude **42** (0.098 mmol) in dichloromethane (2 mL) was added dropwise in 50 min to a stirred solution of monoamine **18** (0.138g, 0.110 mmol) and triethylamine (20 μL, 0.147 mmol) in dichloromethane (2 mL) and the reaction was continued overnight. The reaction mixture was washed with water (1 x 3 mL) and brine (1 x 3 mL). The organic layer was dried with $MgSO_4$, filtered and concentrated *in vacuo.* The excess of monoamine **18** was removed using size-exclusion chromatography (Recycling-GPC in chloroform), obtaining pure **1N$_3$-Disc** (44 mg, 45%). IR (ATR): ν = 2873, 2101(*N*$_3$), 1671, 1568, 1097 cm^{-1}. ^{1}H-NMR ($CDCl_3$): δ= 15.53 (s, 3H), 14.49 (s, 3H), 9.60 (d, *J* = 8.4 Hz, 3H), 9.40 (d, *J* = 8.4 Hz, 3H), 9.28 (s, 3H), 9.06 (d, *J* = 4.4 Hz, 3H), 8.52 (d, *J* = 4.4 Hz, 3H), 7.57 (dd, *J* = 8.5, 4.5 Hz, 6H), 7.36 (s, 6H), 4.27 (dd, *J* = 10.7, 5.4 Hz, 18H), 3.90 (t, *J* = 4.7 Hz, 12H), 3.83 (t, *J* = 4.8 Hz, 6H), 3.74 (dd, *J* = 10.1, 4.9 Hz, 18H), 3.71 – 3.60 (m, 110H), 3.53 (dd, *J* = 9.9, 4.9 Hz, 18H), 3.46 – 3.33 (m, 26H). ^{13}C NMR ($CDCl_3$): δ= 165.96, 164.25, 152.88, 142.53, 142.41, 141.68, 137.67, 137.58, 136.28, 130.71, 130.04, 129.70, 124.84, 124.49, 108.19, 72.65, 72.06, 70.98, 70.81, 70.77, 70.73, 70.71, 70.66, 70.64, 70.17, 69.88, 69.55, 59.16 (OCH_3), 50.82 (CH_2N_3). MALDI- TOF MS: m/z calcd ($C_{160}H_{241}N_{15}O_{60}$) 3332.63; found 3357.46 $[M+Na]^+$.

Methyl 3,4,5-tris[2-(2-{2-[2-(2-tert-butoxycarbonylamino-ethoxy)-ethoxy]-ethoxy}-ethoxy)-ethoxy]-benzoat (43)

A mixture of **8** (0.7 g, 1.3 mmol), methyl 3,4,5-trihydroxybenzoate **9** (0.07 g, 0.4 mmol, 1) and K_2CO_3 (0.55 g, 4 mmol) was stirred for 10 hours at 70 °C in dry DMF (3 mL). Water (5 mL) was added and the reaction mixture was extracted with CH_2Cl_2 (4 x 20 mL). The combined organic layers were washed with brine, dried over $MgSO_4$ and evaporated *in vacuo*. The crude product was purified by column chromatography (alumina, 1% ethanol and 1% triethyl amine in chloroform, R_f = 0.4) affording the pure compound **43** (0.44 g, 0.35 mmol, 86%). ^{1}H-NMR ($CDCl_3$): δ = 7.29 (s, 2H), 5.07 (s, 3H, N*H*Boc), 4.20 (dt, *J* = 9.9, 5.1 Hz, 6H), 3.88 (s, 3H), 3.87 – 3.83 (m, 4H), 3.81 – 3.76 (m, 2H), 3.73 – 3.58 (m, 50H), 3.53 (t, *J* = 5.1 Hz, 6H), 3.30 (dd, *J* = 10.1, 5.0 Hz, 6H), 1.44 (s, 27H). ^{13}C-NMR ($CDCl_3$): δ = 166.71, 156.15, 152.43, 142.69, 125.12, 109.18, 79.29, 72.55, 70.95, 70.77, 70.71, 70.67, 70.39, 69.76, 68.97, 52.32, 40.52, 28.58; LC-MS(ESI): R_t=7.20min, m/z calcd ($C_{59}H_{107}N_3O_{26}$) 1274.5; found 1296.8 $[M+Na]^+$, 1175.0 $[M-Boc]^+$.

3,4,5-Tris[2-(2-{2-[2-(2-tert-butoxycarbonylamino-ethoxy)-ethoxy]-ethoxy}-ethoxy)-ethoxy]-benzoic acid (22)

To a solution of the methyl ester **43** (0.4 g, 0.314 mmol) in ethanol (3 mL) was added KOH (0.05 mg, 0.94 mmol) dissolved in water (3 mL). The mixture was refluxed for 3 hours. Monitoring by TLC showed the disappearance of the ester. After cooling to room temperature the aqueous phase was acidified with aqueous 1 M HCl to pH 2-3 and extracted with dichloromethane (3 x 6 mL). The combined organic layers were washed with brine, dried over $MgSO_4$ and evaporated i*n vacuo* to afford the pure acid **22** as thick oil (0.386 g, 0.31 mmol, 97%). ^{1}H-NMR ($CDCl_3$): δ = 7.39 (s, 2H), 5.09 (s, 3H, N*H*Boc), 4.22 (t, *J* = 4.8 Hz, 6H), 3.5 (t, *J* = 4.7 Hz, 4H), 3.78 (t, *J* = 4.9 Hz, 2H), 3.74 – 3.58 (m, 48H), 3.55 (dd, *J* = 9.8, 4.8 Hz, 6H), 3.31 (d, *J* = 3.7 Hz, 6H), 1.44 (s, 27H). ^{13}C-NMR ($CDCl_3$): δ = 166.88, 156.13, 152.24, 142.72, 125.16, 109.59, 79.19, 72.39, 70.83, 70.68, 70.65, 70.56, 70.51, 70.50, 70.25, 69.70, 68.88, 40.38, 28.46. LC-MS(ESI): R_t = 6.84min, m/z calcd ($C_{58}H_{105}N_3O_{26}$) 1260.5; found 1282.7 $[M+Na]^+$, 1160.9 $[M-Boc]^+$.

3′-{3,4,5-Tris[2-(2-{2-[2-(2-tert-butoxycarbonylamino-ethoxy)-ethoxy]-ethoxy}-ethoxy)-ethoxy]-benzoylamino}-2,2′-bipyridine-3-amine (23)

a) To a solution of the carboxylic acid **22** (0.15 g, 0.15 mmol) in dry dichloromethane (1.5 mL) the Ghosez's reagent **21** (0.03 g, 30 μL, 0.225 mmol) was added dropwise at room temperature. Monitoring by ^{1}H NMR showed a complete conversion into the acid chloride after 1 hour. The solvent and the excess of Ghosez's reagent were removed *in vacuo* and the acid chloride was redissolved in dry DCM (1 mL) for the following reaction step. ^{1}H NMR ($CDCl_3$): δ = 7.39 (s, 2H), 4.98 (s, 3H, N*H*Boc), 4.28 (t, *J* = 4.9 Hz, 2H), 4.21 (t, *J* = 4.8 Hz, 4H), 3.86 (t, *J* = 4.8 Hz, 4H), 3.79 (t, *J* = 4.8 Hz, 2H), 3.75 – 3.57 (m, 48H), 3.53 (t, *J* = 5.1 Hz, 6H), 3.30 (t, *J* = 5.1 Hz, 6H), 1.44 (s, 27H).

b) To a solution of 2,2′-bipyridine-3,3′-diamine **15** (334 mg, 0.18 mmol, 5) and triethyl amine (32 μL, 0.225 mmol) in dry dichloromethane (1 mL) the crude acid chloride (0.15 mmol) redissolved in dry dichloromethane (1 mL) was added dropwise over the period of 2 hours using a syringe pump. After addition the reaction mixture was stirred at room temperature for 18 hours. Subsequently, the reaction mixture was diluted with dichloromethane (2 mL) and washed with aqueous NaOH solution to remove the hydrolyzed starting material. The combined organic layers were washed with brine, dried over $MgSO_4$ and evaporated i*n vacuo.* The crude product was purified by column chromatography (alumina, 1% ethanol in chloroform, R_f = 0.37) affording the pure compound **23** (0.13 g, 0.091 mmol, 61%). ^{1}H-NMR ($CDCl_3$): δ= 14.39 (s, 1H), 9.21 (dd, *J* = 8.5, 1.5 Hz, 1H), 8.33 (dd, *J* = 4.6, 1.6 Hz, 1H), 8.04 (t, *J* = 2.9 Hz, 1H), 7.32 (s, 3H), 7.14 (d, *J* = 3.2 Hz, 2H), 6.59 (s, 2H, NH_2), 5.04 (s, 3H, N*H*Boc), 4.24 (dd, *J* = 11.0, 5.7 Hz, 6H), 3.87 (t, *J* = 4.9 Hz, 4H), 3.81 (t, *J* = 5.0 Hz, 2H), 3.71 (dd, *J* = 9.0, 3.7 Hz, 6H), 3.68 – 3.56 (m, 42H), 3.51 (t, *J* = 4.7 Hz, 6H), 3.29 (d, *J* = 4.5 Hz, 6H), 1.43 (s, 27H); ^{13}C NMR ($CDCl_3$): δ= 165.82, 156.12, 152.74, 145.28, 143.76, 142.15, 140.98, 138.64, 136.22, 135.12, 130.97, 128.72, 125.43, 124.41, 122.88, 108.03, 79.25, 72.58, 70.95, 70.78, 70.75, 70.69, 70.64, 70.34, 69.84, 69.41, 40.50, 28.56; LC-MS(ESI): R_t = 7.80min, m/z calcd ($C_{68}H_{113}N_7O_{25}$) 1428.7; found 1428.7 $[M]^+$, 1451.6 $[M+Na]^+$.

N, N′, N′′ -Tris{3[3′-(3,4,5-tris{2-(2-{2-[2-(2- tert-butoxycarbonylamino-ethoxy)-ethoxy]-ethoxy}-ethoxy)-ethoxy})-benzoylamino]-2,2′-bipyridyl}benzene-1,3,5-tricarboxamide (9NHBoc-Disc)

To a solution of 2,2′-bipyridine-3,3′-diamine-wedge **23** (70 mg, 0.05 mmol) and triethyl amine (14 μL, 0.1 mmol) in dry dichloromethane (1 mL) trimesic chloride **24** (4 mg, 2.7 μL, 0.015 mmol, 7) dissolved in dry dichloromethane (0.5 mL) was added dropwise at 5 °C over the period of 2 hours using a syringe pump. After addition the reaction mixture was stirred at room temperature for 18 hours. Using BioBeads S-X1 size-exclusion chromatography the excess of **23** was separated. The twice reacted side-product was separated via column chromatography (alumina, 5% ethanol and 0.1% formic acid in dichloromethane) affording the pure compound 8 (21 mg, 4.7 μM, 32%); silica, 10% MeOH in DCM; R_f(**9NHBoc-Disc**) = 0.49, R_f(bi-acylated side-product) = 0.46; alumina, 5% MeOH, 0,1% formic acid in DCM; R_f(**9NHBoc-Disc**) = 0.42, R_f(bi-acylated side product) = 0 – 0.3; ^{1}H-NMR ($CDCl_3$): δ= 15.53 (s, 3H), 14.49 (s, 3H), 9.60 (d, *J* = 8.4 Hz, 3H), 9.39 (d, *J* = 8.5 Hz, 3H), 9.29 (s, 3H), 9.05 (d, *J* = 4.1 Hz, 3H), 8.52 (d, *J* = 4.0 Hz, 3H), 7.57 (dd, *J* = 8.4, 4.5 Hz, 6H), 7.35 (s, 6H), 5.08 (s, 9H, N*H*Boc), 4.27 (dd, *J* = 10.3, 5.4 Hz, 18H), 3.90 (t, *J* = 4.5 Hz, 12H), 3.83 (t, *J* = 4.8 Hz, 6H), 3.74 (dd, *J* = 9.5, 4.6 Hz, 18H), 3.70 – 3.55 (m, 126H), 3.52 (dd, *J* = 9.9, 4.9 Hz, 18H), 3.29 (t, *J* = 4.8 Hz, 18H), 1.43 (d, *J* = 5.0 Hz, 81H). ^{13}C NMR ($CDCl_3$): δ= 165.97, 164.28, 156.13, 154.78, 152.88, 148.41, 142.43, 141.71, 137.68, 137.60, 136.31, 130.77, 130.07, 129.74, 127.80, 124.87, 124.52, 121.06, 108.15, 79.27, 72.66, 70.97, 70.81, 70.78, 70.71, 70.66, 70.37, 69.87, 69.53, 41.11, 40.51, 28.58. MALDI-ToF-MS: m/z calcd ($C_{213}H_{339}N_{21}O_{78}$) 4442.06; found 4464.9 $[M+Na]^+$.

N, N′, N′′ -Tris{3[3′-(3,4,5-tris{2-(2-{2-[2-(2-amino-ethoxy)-ethoxy]-ethoxy}-ethoxy)-ethoxy})-benzoylamino]-2,2′-bipyridyl}benzene-1,3,5-tricarboxamide (9NH$_2$-Disc)

To a solution of **9NHBoc-Disc** (17.8 mg, 4 μmol) in dichloromethane (2 mL) trifluoroacetic acid (200 μL) was added dropwise and the reaction mixture was stirred at room temperature for 2 hours. Trifluoroacetic acid was co-evaporated with toluene. The deprotected discotic was redissolved in water and freeze-dried. MALDI confirmed complete deprotection, affording the pure compound 9 (13.3 mg, 3.8 μM, 97%). MALDI-ToF-MS: m/z calcd ($C_{168}H_{267}N_{21}O_{60}$) 3541.02; found 3541.46 $[M]^+$.

N,N′,N′′-Tris{3[3′-(4-{2[-2-(2-{2-[2-(2-tert-butoxycarbonylamino-ethoxy)-ethoxy]-ethoxy}-ethoxy)-ethoxy]-ethyl}-3,5-bis[2-(2-{2-[2-(2-methoxyethoxy)-ethoxy]-ethoxy}-ethoxy)-ethoxy]-benzoylamino]-2,2′-bipyridyl}benzene-1,3,5-tricarboxamide (3NHBoc-Disc)

To a solution of **17** (251 mg, 0.215 mmol) and triethylamine (60 μL, 0.43 mmol) in dry DCM (0.5 mL), a solution of trimesic chloride (17.1 mg, 0.065 mmol) in dry DCM (0.15 mL) was added dropwise within 1 hour via a syringe pump at room temperature. Stirring was continued overnight. To remove the excess of **17** the crude reaction mixture was purified by size exclusion chromatography (BioBeads in DCM). After removing the di-ester side-product via column chromatography (alumina, 5% MeOH with 0.1% formic acid in DCM; R_f (3NHBoc-Disc) = 0.69; R_f (side-product) = 0-0.16) the desired product **3NHBoc-Disc** was obtained (139 mg, 0.038 mmol, 59%). ^{1}H NMR (400 MHz, $CDCl_3$): δ= 15.51 (s, 3H), 14.48 (s, 3H), 9.58 (dd, *J* = 8.5, 1.4 Hz, 3H), 9.37 (dd, *J* = 8.6, 1.4 Hz, 3H), 9.25 (s, 3H), 9.04 (dd, *J* = 4.6, 1.5 Hz, 3H), 8.50 (dd, *J* = 4.5, 1.5 Hz, 3H), 7.55 (dd, *J* = 8.5, 4.6 Hz, 6H), 7.34 (s, 6H), 5.04 (s, 3H), 4.26 (dd, *J* = 11.0, 5.6 Hz, 18H), 3.93 – 3.86 (t, *J* = 4.5 Hz, 12H), 3.85 – 3.78 (t, *J* = 4.9 Hz, 6H), 3.77 – 3.56 (m, 132H), 3.51 (dt, *J* = 4.3, 3.7 Hz, 18H), 3.34 (s, 18H), 3.29 (dd, *J* = 10.5, 5.3 Hz, 6H), 1.42 (s, 27H). MALDI-ToF-MS: m/z calcd ($C_{191}H_{286}N_{22}O_{69}$) 3667.1; found 3689.5 $[M+Na]^+$, 3705.53 $[M+K]^+$. In agreement with literature.[7]

1Biotin-Disc

A solution of NHS-biotin **25** (4.2 mg, 7.2 μmol) in dry dichloromethane (0.2 mL) was added dropwise to a solution of **1NH$_2$-Disc** (7.9 mg, 2.4 μmol) and triethyl amine (10 μL, 72 μmol) in dry dichloromethane (0.5 mL) and the reaction was continued overnight. Full conversion was observed with TLC (silica, dichloromethane with 10% methanol, stained with Seebach reagent, R_f=0.27). After concentrating the reaction mixture *in vacuo*, the **1Biotin-Disc** was purified via size-exclusion chromatography (BioBeads, SX-1 in DMF) yielding pure compound (5 mg, 1.3 μmol, 54%). ^{1}H-NMR ($CDCl_3$): δ= 15.53 (s, 3H), 14.49 (s, 3H), 9.60 (d, *J* = 7.5 Hz, 3H), 9.39 (d, *J* = 8.6 Hz, 3H), 9.29 (s, 3H), 9.06 (d, *J* = 4.4 Hz, 3H), 8.52 (d, *J* = 3.5 Hz, 3H), 7.57 (dd, *J* = 8.4, 4.6 Hz, 6H), 7.36 (s, 6H), 6.84 (s, 1H), 6.61 (s, 1H), 5.56 (s, 1H), 5.12 (s, 1H), 4.49 (dd, *J* = 6.9, 5.5 Hz, 1H), 4.33 (m, 1H), 4.27 (dd, *J* = 10.7, 5.6 Hz, 18H), 3.90 (t, *J* = 4.7 Hz, 12H), 3.83 (t, *J* = 4.7 Hz, 6H), 3.76 – 3.51 (m, 174H), 3.43 (m, 5H), 3.37 (s, 6H), 3.35 (s, 18H), 3.20 – 3.09 (m, 1H), 2.91 (dd, *J* = 12.8, 5.1 Hz, 1H), 2.72 (d, *J* = 12.8 Hz, 1H), 2.48 (t, *J* = 6.1 Hz, 2H), 2.21 (t, *J* = 6.9 Hz, 2H), 2.03 (s, 1H), 1.88 (s, 6H), 1.80 – 1.28 (m, 6H). ^{13}C NMR ($CDCl_3$): δ= 173.16, 171.51, 165.98, 164.26, 152.88, 142.52, 142.41, 141.69, 140.89, 137.68, 137.58, 136.30, 130.71, 130.09, 129.61, 124.85, 124.36, 108.18, 72.66, 72.07, 72.05, 70.98, 70.81, 70.77, 70.71, 70.66, 70.64, 69.88, 69.55, 67.47, 61.90, 60.21, 59.16, 55.44, 40.65, 39.31, 37.01, 35.82, 28.19, 25.36. MALDI-ToF MS: m/z calcd ($C_{181}H_{278}N_{16}O_{67}S$) 3782.28; found 3804.81 $[M+Na]^+$, 3820.80 $[M+K]^+$. During storage, oxidation of the biotin was observed with MALDI-ToF MS: m/z calcd ($C_{181}H_{278}N_{16}O_{68}S$) 3795.85; found 3796.5 $[M]^+$.

1Maleimide-Disc

Using a few drops of TEA the pH of the solution of **1NH$_2$-Disc** (11 mg, 3.3 μmol) in dry DCM (1 mL) was adjusted to 8 and NHS-maleimide **27** (1.46 mg, 3.6 μmol) dissolved in dry DCM (0.5 mL) was slowly added. The reaction was continued at room temperature overnight and TLC confirmed full conversion (silica, 10% MeOH in DCM, R_f = 0.43). The solvent was evaporated *in vacuo* and the crude product was first purified by size exclusion chromatography (BioBeads in DMF) followed by column chromatography (silica, 0% - 10% MeOH in DCM) a affording **1Maleimide-Disc** (11.1 mg, 3.2 μmol, 88%). MALDI-ToF-MS: m/z calcd ($C_{171}H_{248}N_{14}O_{63}$) 3505.6; found 3530.4 $[M+Na]^+$.

1Cys(S*t*Bu)-Disc

Using a few drops of TEA the pH of the solution of **1NH$_2$-Disc** (10 mg, 3 μmol) in dry DMF (1 mL) was adjusted to 8 and NHS-Cys(S*t*Bu) **28** (2 mg, 4.8 μmol) dissolved in dry DMF (0.5 mL) was slowly added. The reaction was continued at room temperature overnight and TLC confirmed full conversion (silica, 10% MeOH in DCM, R_f = 0.5). The solvent was evaporated *in vacuo* and the crude product was first purified by column chromatography (silica, 0% - 15% MeOH in DCM) affording **1Cys(S*t*Bu)-Disc** (10.8 mg, 3 μmol, 97%). MALDI-ToF-MS: m/z calcd ($C_{172}H_{264}N_{14}O_{63}S_2$) 3597.7; found 3622.5 $[M+Na]^+$, 3638.4 $[M+K]^+$.

1Fluorescein-Disc

The pH of a solution of **1NH$_2$-Disc** (10 mg, 3 μmol) in dry DCM (2 mL) was adjusted to 8 using a few drops of TEA. NHS-fluorescein **29** (3,3 mg, 7 μmol) dissolved in dry DCM (2 mL) was added dropwise and the reaction continued overnight in the dark, at room temperature and under Argon atmosphere. The crude reaction mixture was purified using size-exclusion chromatography (BioBeads in DCM) affording **1Fluorescein-Disc** (9.8 mg, 2.6 mmol, 89%).

^{1}H-NMR ($CDCl_3$): δ= 15.52 (s, 2H), 15.46 (d, *J* = 6.1 Hz, 2H), 14.49 (s, 3H), 9.60 (d, *J* = 7.8 Hz, 2H), 9.56 (d, *J* = 7.1 Hz, 1H), 9.38 (ddd, *J* = 8.6, 3.5, 1.4 Hz, 2H), 9.34 (dd, *J* = 6.6, 1.5 Hz, 1H), 9.27 (s, 3H), 9.07 – 9.02 (m, 2H), 9.02 – 8.98 (m, 1H), 8.52 (dd, *J* = 4.5, 1.4 Hz, 2H), 8.50 (dd, *J* = 4.6, 1.3 Hz, 1H), 8.44 (s, 1H, *NH*), 8.16 (dd, *J* = 8.0, 2.8 Hz, 1H), 8.03 (d, *J* = 8.1 Hz, 1H), 7.63 – 7.48 (m, 6H), 7.35 (s, 4H), 7.30 (s, 2H), 7.04 – 6.91 (m, 2H), 6.76 – 6.49 (m, 4H), 4.28 (d, *J* = 14.1 Hz, 8H), 4.25 – 4.16 (m, 4H), 4.14 – 3.48 (m, 170H), 3.35 (m, 26H). MALDI-ToF-MS: m/z calcd ($C_{181}H_{253}N_{13}O_{66}$) 3664.7; found 3667.6 $[M+H]^+$, 3689.6 $[M+Na]^+$.

1DOTA-Disc

Using a few drops of TEA the pH of the solution of **1NH$_2$-Disc** (11 mg, 3.3 μmol) in dry DMF (1 mL) was adjusted to 8 and NHS-DOTA **30** (5.4 mg, 9 μmol) dissolved in dry DMF (0.5 mL) was slowly added. The reaction was continued at room temperature overnight and TLC confirmed full conversion (silica, 10% MeOH in DCM, R_f = 0). The solvent was evaporated *in vacuo* and the crude product was purified by size exclusion chromatography (BioBeads in DMF) affording **1DOTA-Disc** (12 mg, 3.2 μmol, 98%). MALDI-ToF-MS: m/z calcd ($C_{176}H_{269}N_{27}O_{67}$) 3692.82; found 3694.3 $[M+H]^+$, 3717.2 $[M+Na]^+$.

^{1}H NMR (400 MHz, $CDCl_3$): δ= 15.51 (s, 3H), 14.49 (s, 3H), 9.59 (d, *J* = 8.0 Hz, 3H), 9.37 (d, *J* = 8.9 Hz, 3H), 9.23 (s, 3H), 9.05 (s, 3H), 8.49 (s, 3H), 7.65 – 7.46 (m, 6H), 7.34 (s, 6H), 4.27 (d, *J* = 4.4 Hz, 18H), 3.91 (t, *J* = 5.0 Hz 12H), 3.83 (t, *J* = 5.0 Hz 6H), 3.78 – 3.44 (m, 158H), 3.36 (d, *J* = 7.8 Hz, 32H), 2.57 (m, broad, 20H), 1.25 (s, 6H), 0.87 (s, 2H, 1).

3DOTA -Disc

Using a few drops of TEA the pH of the solution of **3NH$_2$-Disc** (10 mg, 2.9 μmol) in dry DMF (1 mL) was adjusted to 8 and NHS-DOTA **30** (9 mg, 17.8 μmol) dissolved in dry DMF (0.5 mL) was slowly added. The reaction was continued at room temperature overnight. The solvent was evaporated *in vacuo* and the crude product was purified using size-exclusion chromatography (BioBeads in DMF) yielding three fluorescent fractions. No mass was detectable by MALDI-ToF-MS.

1c*R*(Pbf)GD(*t*Bu)fK-Disc

33 (6 mg, 6 μmol) dissolved in dry DMF (0.5 mL) was pre-activated with HBTU (2.16 mg, 5.7 μmol) and DIPEA (2 μL, 12 μmol) for 30 minutes and subsequently added to **1NH$_2$-Disc** (10 mg, 3 μmol) dissolved in dry DMF (1 mL). The reaction was followed with TLC (silica, 10% MeOH in DCM, Rf = 0.19) and after 18 hours at room temperature the solvent was evaporated and the reaction mixture purified using size-exclusion chromatography (BioBeads in DMF) yielding 1cR(Pbf)GD(tBu)fK-Disc (9.2 mg, 2.1 μmol, 71%). MALDI-ToF-MS: m/z calcd ($C_{208}H_{310}N_{22}O_{72}S$) 4300.1; found 4324.4 $[M+Na]^+$.

1*c*RGDfK-Disc

For deprotection, the **1*c*R(Pbf)GD(tBu)fK-Disc** was dissolved in 0.5 mL DCM and TIS (40 μL) was added as a scavenger. Subsequently TFA (1.5 mL) was added and after 2 hours at room temperature TFA was co-evaporated with toluene affording **1*c*RGDfK-Disc** (10.4 mg, 2.6 μmol, quant.) MALDI-ToF-MS: m/z calcd ($C_{191}H_{286}N_{22}O_{69}$) 3991.9; found 3992.4 $[M+H]^+$.

3*c*R(Pbf)GD(*t*Bu)fK-Disc

33 (16.6 mg, 16 μmol) dissolved in dry DMF (0.4 mL) was pre-activated with HBTU (6.2 mg, 16 μmol) and DIPEA (5.7 μL, 33 μmol) for 30 minutes and subsequently added to **3NH$_2$-Disc** (13.8 mg, 4 μmol) dissolved in dry DMF (0.5 mL). The reaction was continued for 18 hours at room temperature. Subsequently the solvent was evaporated and the reaction mixture purified using size-exclusion chromatography (BioBeads in DMF) yielding a mixture of thrice, double and mono-functionalized peptide discotic. 3cR(Pbf)GD(tBu)fK-Disc (7 mg). MALDI-ToF-MS: m/z calcd ($C_{306}H_{450}N_{42}O_{96}S_3$) 6345.4; found 6344.9 $[M]^+$.

3R(Pbf)-Disc

R(Pbf) **32** (6.8 mg, 13 μmol) dissolved in dry DMF (0.4 mL) was pre-activated with HBTU (4.8 mg, 13 μmol) and DIPEA (4.4 μL, 24 μmol) for 30 minutes and subsequently added to **3NH$_2$-Disc** (6.3 mg, 2 μmol) dissolved in dry DMF (0.6 mL). The reaction was continued for 18 hours at room temperature. Subsequently the solvent was evaporated and the reaction mixture purified using column chromatography (silica, 5-10% MeOH in CH_2Cl_2, R_f=0.65) yielding pure **3R(Pbf)-Disc** (5.1 mg, 1 μmol, 53%).MALDI-ToF-MS: m/z calcd ($C_{234}H_{357}N_{27}O_{78}S_3$) 4889.4; found 4929.6 $[M+K]^+$.

1Mannose-Disc

A 1:1 mixture of water and *t*-buthanol was degassed prior to the reaction. After dissolving **1N$_3$-Disc** (15mg, 4.5 μmol) and propargyl mannose **34** (2.4 mg, 11 μmol) in the water/*t*-buthanol mixture (3 mL), $CuSO_4$ (15 μL of a 20 mM stock solution in degassed water, 100 μM) and subsequently sodium ascorbate (150 μL of a 100 mM stock solution in degassed water, 5 mM) and a small piece of copper wire were added. The reaction mixture was stirred at room temperature and under Argon for 16 hours. Complete conversion was

observed with IR and after evaporation of solvents the crude reaction mixture was purified with size-exclusion chromatography (BioBeads SX-1, in dichloromethane) yielding pure **1Mannose-Disc** (12.5 mg, 78%). IR (ATR): ν = 3366, 2875, 1723, 1676, 1568, 1107 cm^{-1}. ^{1}H-NMR ($CDCl_3$): δ= 15.51 (s, 3H), 14.49 (s, 3H), 9.59 (d, *J* = 8.5 Hz, 3H), 9.38 (d, *J* = 8.5 Hz, 3H), 9.26 (s, 3H), 9.05 (d, *J* = 4.3 Hz, 3H), 8.50 (d, *J* = 4.3 Hz, 3H), 7.83 (s, 1H, triazole), 7.56 (dd, *J* = 8.5, 4.3 Hz, 6H), 7.35 (s, 6H), 4.96 (s, 1H, mannose), 4.79 (d, *J* = 11.9 Hz, 1H, mannose), 4.67 (d, *J* = 12.7 Hz, 1H, mannose), 4.54 (s, 2H, mannose), 4.27 (dd, *J* = 9.7, 5.2 Hz, 18H), 3.99 – 3.46 (m, 168H), 3.36 (d, *J* = 6.8 Hz, 26H). ^{13}C NMR ($CDCl_3$): δ=165.95, 164.21, 152.86, 152.77, 144.22, 142.42, 142.35, 142.07, 141.66, 140.90, 137.66, 137.59, 136.23, 130.92, 130.75, 130.08, 129.69, 124.83, 124.51, 108.11, 107.91, 99.59, 72.64, 72.04, 72.00, 71.62, 70.96, 70.87, 70.79, 70.75, 70.71, 70.69, 70.63, 70.55, 69.86, 69.79, 69.52, 69.39, 67.99, 60.74, 59.15 (OCH_3), 50.38, 44.52, 29.83, 26.65. MALDI- ToF MS: m/z calcd ($C_{169}H_{255}N_{15}O_{66}$) 3552.89; found 3576.08 $[M+Na]^+$.

3Mannose-Disc

A 1:1 mixture of water and *t*-buthanol was degassed prior to the reaction. After dissolving **3N$_3$-Disc** (8.7 mg, 2.5 μmol) and propargyl mannose **34** (3.3 mg, 15 μmol) in the water/*t*-buthanol mixture (2 mL), $CuSO_4$ (10 μL of a 20 mM stock solution in degassed water, 100 μM) and subsequently sodium ascorbate (100 μL of a 100 mM stock solution in degassed water, 5 mM) and a small piece of copper wire were added. The reaction mixture was stirred at room temperature under Argon and the conversion was followed with IR. Complete conversion was observed after 4 hours and after evaporation of solvents the crude reaction mixture was purified with size-exclusion chromatography (BioBeads SX-1, in DMF) yielding pure **3MannoseDisc** (8.4mg, 82%). IR (ATR): ν = 3366, 2875, 1723, 1676, 1568, 1107 cm^{-1}. MALDI-ToF MS: m/z calcd ($C_{189}H_{285}N_{21}O_{78}$) 4096.90; found 4120.29 $[M+Na]^+$, 4135.21$[M+K]^+$. In agreement with literature.[8]

1Ferrocene-Disc

A 1:1 mixture of water and *t*-butanol was degassed prior to the reaction. After dissolving **1Propargyl-Disc** (5mg, 1.5 μmol) and ferrocene azide **37** (0.8 mg, 3 μmol) in the water/*t*-butanol mixture (2 mL), $CuSO_4$ (10 μL of a 20 mM stock solution in degassed water, 100 μM) and subsequently sodium ascorbate (100 μL of a 100 mM stock solution in degassed water, 5 mM) and a small piece of copper wire were added. The reaction mixture was stirred at 40 °C and under Argon for 12 hours. Conversion stopped after around 70% of the product was formed, as observed with TLC (silica, 10% MeOH in DCM, R_f(1Ferrocene-Disc)=0.44 (fluorescent and brown), R_f(1Propargyl-Disc)=0.5 (only fluorescent)). After evaporation of solvents the excess of ferrocene azide was removed using size-exclusion chromatography (BioBeads SX-1, in DMF) yielding **1Ferrocene-Disc** (5.5 mg, as a 7:3 mixture with 1Propargyl-Disc). MALDI- TOF MS: m/z calcd ($C_{174}H_{253}FeN_{15}O_{62}$) 3600.65; found 3430.8 $[M-Ferrocene]^+$.

Solid phase peptide synthesis:

The peptides were synthesized manually by solid phase peptide synthesis[56] applying the Fmoc strategy[73] and either using the 2-chlorotrityl chloride resin[74], for later coupling of a protected peptide to amine discotics, or the Wang resin, for coupling of a deprotected peptide via click chemistry to azide discotics. Both resin types were purchased pre-loaded with the first amino acid and all sequences were synthesized from *C*- to *N*-terminus on a 200 μmol scale after swelling the resin in NMP for 30 minutes. Coupling reactions were performed using, relative to the resin loading, 4 equiv. of *N*-Fmoc-protected amino acid activated in situ with 4 equiv. of HBTU and 16 equiv. of DIPEA in NMP for 30 min. *N*-Fmoc protecting

groups were removed by treatment with a piperidine/NMP solution (1:4) for 10 min. Between each step the resin was washed several times with NMP and the steps were repeated until the desired peptide sequence was completed.

Peptides for click chemistry:

The complete sequence of the peptide was synthesized using the general procedure described above. To the free *N*-terminus of the completed resin-bound peptide 4-pentynoic acid was coupled in situ activated with HBTU and DIPEA as described above. The resin was subsequently washed with NMR, DCM and dried under vacuum for 10 minutes. Cleavage from the resin and side chain deprotection was carried out for 2 hour using a cleavage cocktail containing TFA/TIS/H_2O/EDT (94:2:2:2). The cleaved resin was filtered and washed with TFA and the combined filtrated were precipitated with cold Et_2O and the re-dissolved precipitate was lyophilized. The crude fully deprotected peptides obtained were analyzed by LC-MS and, if necessary, purified on a preparative column.

Pentynoic-GRGDS-OH (35): (16.5 mg, 15%) LC-MS(ESI): R_t = 0.87 min, m/z calcd ($C_{22}H_{34}N_8O_{10}$) 570.2; found 571.3 $[M+H]^+$.

Pentynoic-CLSYYPSYC-OH: (13.6 mg, 5.7%) LC-MS(ESI): R_t = 5.13 min, m/z calcd ($C_{55}H_{71}N_9O_{16}S2$) 1177.4; found 1178.8 $[M+H]^+$.

For the oxidation, the peptide was dissolved in a 0.01 m ammonium bicarbonate buffer (pH 8) at a concentration of 0.1 mg/mL to prevent formation of dimers. The solution was vigorously stirred under exposure to air overnight. LC-MS confirmed complete oxidation to a cyclic peptide.

Oxidized pentynoic-CLSYYPSYC-OH (36): LC-MS(ESI): R_t = 4.95 min, m/z calcd ($C_{55}H_{69}N_9O_{16}S2$) 1175.4; found 1176.8 $[M+H]^+$.

Peptides for amide coupling:

The sequence of the peptide missing the last amino acid was synthesized using the general procedure described above. The last amino acid coupled to these peptides was *N*-Boc-protected. The resin was subsequently washed with NMR, DCM and dried under vacuum for 10 minutes. To cleave the side-chain and *N*-terminus protected peptide from the resin, the resin was treated twice with HFIP/DCM[75] (10 mL, 3:7 v/v) or TFE/DCM (10 mL, 1:4 v/v) for 45 min. The cleaved resin was filtered and washed with cleavage solution and the combined filtrated were concentrated and white solid peptides were obtained by precipitation from a mixture of cold ether and hexane. The crude protected peptides obtained were analyzed by LC-MS and, if necessary, purified on a preparative column.

Boc-GR(Pbf)GD(tBu)S(tBu)-OH: (17.4 mg, 9%) LC-MS(ESI): R_t = 6.85 min, m/z calcd ($C_{43}H_{70}N_8O_{14}S$) 954.5; found 955.8 $[M+H]^+$.

***c*R(Pbf)GD(*t*Bu)fK(COOH)**:

The linear peptide sequence H-Asp(OtBu)-D-Phe-Lys(Alloc)-Arg(Pbf)-Gly-OH **31**, was synthesized on a glycine pre-loaded 2-chlorotrityl chloride resin and cleaved from the resin with TFE/DCM (10 mL, 1:4 v/v) using general procedures described above. (140 mg, 0.14 mmol, 69%) LC-MS(ESI): R_t = 6.00 min, m/z calcd ($C_{48}H_{71}N_9O_{13}S$) 1013.5; found 1014.9 $[M+H]^+$.

Subsequently, the peptide was cyclized under dilute conditions. The linear D(tBu)fK(Alloc)R(Pbf)G peptide (140 mg, 0.14 mmol) was dissolved in dry DMF (3 mL) and added dropwise using a syringe pump over a period of 2 hours to a solution of PyBOP (110 mg, 0.21 mmol) and DIPEA (144 μL, 0.83 mmol) in a mixture

of dry DCM (11 mL) and dry DMF (28 mL). LC-MS confirmed complete conversion of the linear peptide (0.14 mmol, quant.). LC-MS(ESI): R_t = 7.25 min, m/z calcd ($C_{48}H_{69}N_9O_{12}S$) 995.5; found 996.8 $[M+H]^+$.

After evaporating the solvent the crude cyclic peptide (0.14 mmol) was dissolved in a mixture of dry DCM (6 mL) and dry DMF (2 mL) and after addition of morpholine (200 μL) and acetic acid (400 μL), $Pd(PPh_3)_4$ (55 mg, 47 μmol) was added. After 2 hours at room temperature the solvent mixture was evaporated and LC-MS confirmed complete Lys deprotection (0.14 mmol, quant.). LC-MS(ESI): R_t = 5.50 min, m/z calcd ($C_{44}H_{65}N_9O_{10}S$) 911.46; found 912.8 $[M+H]^+$.

The free amine group of the lysine side-chain was reacted with succinic anhydride to yield a fully protected peptide with one carboxylic acid function for attachment to amine discotics. The crude peptide (0.14 mmol) was dissolved in dry DMF (3 mL) and TEA (60 μL, 0.4 mmol) and succinic anhydride (25 mg, 0.25 mmol) were added. After 2 hours at room temperature LC-MS confirmed complete conversion and the crude peptide was purified using column chromatography (silica, 2%-20% MeOH, 0.1% formic acid in DCM, R_f = 0.28 (10% MeOH in DCM)) affording pure peptide **33** (84.2 mg, 82 μmol, 59% after 3 steps). LC-MS(ESI): R_t = 6.53 min, m/z calcd ($C_{48}H_{69}N_9O_{13}S$) 1011.5; found 1012.8 $[M+H]^+$.

2.7 References

1. Taipale, J.; Keski-Oja, J. Growth Factors in the Extracellular Matrix. *FASEB J.* **1997**, *11*, 51–59.
2. Miyamoto, S.; Akiyama, S. K.; Yamada, K. M. Synergistic Roles for Receptor Occupancy and Aggregation in Integrin Transmembrane Function. *Science* **1995**, *267*, 883–885.
3. Germain, R. N. T-cell Signaling: The Importance of Receptor Clustering. *Curr. Biol.* **1997**, *7*, R640–R644.
4. Bull, S. R.; Guler, M. O.; Bras, R. E.; Meade, T. J.; Stupp, S. I. Self-Assembled Peptide Amphiphile Nanofibers Conjugated to MRI Contrast Agents. *Nano Lett.* **2005**, *5*, 1–4.
5. Besenius, P.; Portale, G.; Bomans, P. H. H.; Janssen, H. M.; Palmans, A. R. A.; Meijer, E. W. Controlling the Growth and Shape of Chiral Supramolecular Polymers in Water. *PNAS* **2010**, *107*, 17888–17893.
6. Mulder, W. J. M.; Strijkers, G. J.; Tilborg, G. A. F. van; Cormode, D. P.; Fayad, Z. A.; Nicolay, K. Nanoparticulate Assemblies of Amphiphiles and Diagnostically Active Materials for Multimodality Imaging. *Acc. Chem. Res.* **2009**, *42*, 904–914.
7. Müller, M. K.; Petkau, K.; Brunsveld, L. Protein Assembly Along a Supramolecular Wire. *Chem. Commun.* **2010**, 310–312.
8. Müller, M. K.; Brunsveld, L. A Supramolecular Polymer as a Self-Assembling Polyvalent Scaffold. *Angew. Chem. Int. Ed.* **2009**, *48*, 2921–2924.
9. Kim, B.-S.; Hong, D.-J.; Bae, J.; Lee, M. Controlled Self-Assembly of Carbohydrate Conjugate Rod−Coil Amphiphiles for Supramolecular Multivalent Ligands. *J. Am. Chem. Soc.* **2005**, *127*, 16333–16337.
10. Silva, G. A.; Czeisler, C.; Niece, K. L.; Beniash, E.; Harrington, D. A.; Kessler, J. A.; Stupp, S. I. Selective Differentiation of Neural Progenitor Cells by High-Epitope Density Nanofibers. *Science* **2004**, *303*, 1352–1355.
11. Webber, M. J.; Tongers, J.; Newcomb, C. J.; Marquardt, K.-T.; Bauersachs, J.; Losordo, D. W.; Stupp, S. I. Supramolecular Nanostructures That Mimic VEGF as a Strategy for Ischemic Tissue Repair. *PNAS* **2011**, *108*, 13438–13443.
12. Webber, M. J.; Kessler, J. A.; Stupp, S. I. Emerging Peptide Nanomedicine to Regenerate Tissues and Organs. *J. Intern. Med.* **2010**, *267*, 71–88.
13. Webber, M. J.; Han, X.; Prasanna Murthy, S. N.; Rajangam, K.; Stupp, S. I.; Lomasney, J. W. Capturing the Stem Cell Paracrine Effect Using Heparin-presenting Nanofibres to Treat Cardiovascular Diseases. *J Tissue Eng Regen Med* **2010**, *4*, 600–610.

14. Tysseling-Mattiace, V. M.; Sahni, V.; Niece, K. L.; Birch, D.; Czeisler, C.; Fehlings, M. G.; Stupp, S. I.; Kessler, J. A. Self-Assembling Nanofibers Inhibit Glial Scar Formation and Promote Axon Elongation After Spinal Cord Injury. *J. Neurosci* **2008**, *28*, 3814–3823.
15. Cavalli, S.; Albericio, F.; Kros, A. Amphiphilic Peptides and Their Cross-disciplinary Role as Building Blocks for Nanoscience. *Chem. Soc. Rev.* **2010**, *39*, 241-263.
16. Cui, H.; Webber, M. J.; Stupp, S. I. Self-assembly of Peptide Amphiphiles: From Molecules to Nanostructures to Biomaterials. *Biopolymers* **2010**, *94*, 1–18.
17. Uhlenheuer, D. A.; Petkau, K.; Brunsveld, L. Combining Supramolecular Chemistry with Biology. *Chem. Soc. Rev.* **2010**, *39*, 2817.
18. Laschat, S.; Baro, A.; Steinke, N.; Giesselmann, F.; Hägele, C.; Scalia, G.; Judele, R.; Kapatsina, E.; Sauer, S.; Schreivogel, A. *et al.* Discotic Liquid Crystals: From Tailor-Made Synthesis to Plastic Electronics. *Angew. Chem. Int. Ed.* **2007**, *46*, 4832–4887.
19. Palmans, A. R. A.; Vekemans, J. A. J. M.; Fischer, H.; Hikmet, R. A.; Meijer, E. W. Extended-Core Discotic Liquid Crystals Based on the Intramolecular H-Bonding in N-Acylated 2,2′-Bipyridine-3,3′-diamine Moieties. *Chem. Eur. J.* **1997**, *3*, 300–307.
20. Metzroth, T.; Hoffmann, A.; Martin-Rapun, R.; Smulders, M. M. J.; Pieterse, K.; Palmans, A. R. A.; Vekemans, J. A. J. M.; Meijer, E. W.; Spiess, H. W.; Gauss, J. Unravelling the Fine Structure of Stacked Bipyridine Diamine-derived C3-discotics as Determined by X-ray Diffraction, Quantum-chemical Calculations, Fast-MAS NMR and CD Spectroscopy. *Chem. Sci.* **2011**, *2*, 69–76.
21. Palmans, A. R. A.; Vekemans, J. A. J. M.; Havinga, E. E.; Meijer, E. W. Sergeants-and-Soldiers Principle in Chiral Columnar Stacks of Disc-Shaped Molecules with C3 Symmetry. *Angew. Chem. Int. Ed.* **1997**, *36*, 2648–2651.
22. Brunsveld, L.; Zhang, H.; Glasbeek, M.; Vekemans, J. A. J. M.; Meijer, E. W. Hierarchical Growth of Chiral Self-Assembled Structures in Protic Media. *J. Am. Chem. Soc.* **2000**, *122*, 6175–6182.
23. Brunsveld, L.; Lohmeijer, B. G. G.; Vekemans, J. A. J. M.; Meijer, E. W. Chirality Amplification in Dynamic Helical Columns in Water. *Chem. Commun.* **2000**, 2305–2306.
24. Palmans, A. R. A.; Meijer, E. W. Amplification of Chirality in Dynamic Supramolecular Aggregates. *Angew. Chem. Int. Ed.* **2007**, *46*, 8948–8968.
25. Martín-Rapún, R.; Byelov, D.; Palmans, A. R. A.; Jeu, W. H. de; Meijer, E. W. Lyomesophases of C3-Symmetrical Bipyridine-Based Discs in Alkanes: An X-ray Diffraction Study. *Langmuir* **2009**, *25*, 8794–8801.
26. Danila, I.; Riobé, F.; Puigmartí-Luis, J.; Pino, Á. P. del; Wallis, J. D.; Amabilino, D. B.; Avarvari, N. Supramolecular Electroactive Organogel and Conducting Nanofibers with C3-symmetrical Architectures. *J. Mater. Chem.* **2009**, *19*, 4495–4504.
27. Danila, I.; Riobé, F.; Piron, F.; Puigmartí-Luis, J.; Wallis, J. D.; Linares, M.; Ågren, H.; Beljonne, D.; Amabilino, D. B.; Avarvari, N. Hierarchical Chiral Expression from the Nano- to Mesoscale in Synthetic Supramolecular Helical Fibers of a Nonamphiphilic C3-Symmetrical π-Functional Molecule. *J. Am. Chem. Soc.* **2011**, *133*, 8344–8353.
28. Harris, J. M.; Chess, R. B. Effect of Pegylation on Pharmaceuticals. *Nat Rev Drug Discov* **2003**, *2*, 214–221.
29. Caliceti, P.; Veronese, F. M. Pharmacokinetic and Biodistribution Properties of Poly(ethylene Glycol)-protein Conjugates. *Adv. Drug. Deliver. Rev.* **2003**, *55*, 1261–1277.
30. Hesse, M.; Meier, H.; Zeeh, B. *Spectroscopic Methods in Organic Chemistry*; G. Thieme, **1997**.
31. Palmans, A. R. A. Supramolecular Structures Based on the Intramolecular H-bonding in the 3,3′-di(acylamino)-2,2′-bipydridine Unit, Technische Universiteit Eindhoven, **1997**.
32. Brunsveld, L. Supramolecular Chirality, Technische Universiteit Eindhoven, **2001**.
33. Toele, P.; Gorp, J. J. van; Glasbeek, M. Femtosecond Fluorescence Studies of Self-Assembled Helical Aggregates in Solution. *J. Phys. Chem. A* **2005**, *109*, 10479–10487.
34. Müller, M. K. Supramolecular Multivalency, Technische Universität Dortmund, **2009**.
35. Gill, H. S.; Tinianow, J. N.; Ogasawara, A.; Flores, J. E.; Vanderbilt, A. N.; Raab, H.; Scheer, J. M.; Vandlen, R.; Williams, S.-P.; Marik, J. A Modular Platform for the Rapid Site-Specific Radiolabeling of

Proteins with 18F Exemplified by Quantitative Positron Emission Tomography of Human Epidermal Growth Factor Receptor 2. *J. Med. Chem.* **2009**, *52*, 5816–5825.

36. Bouzide, A.; Sauvé, G. Highly Selective silver(I) Oxide Mediated Monoprotection of Symmetrical Diols. *Tetrahedron Letters* **1997**, *38*, 5945–5948.
37. Zhu, J.; Chastanet, J.; Beugelmans, R. Selective Hydroxy Group Protection of Gallic Acid. *Synthetic. Commun.* **1996**, *26*, 2479–2486.
38. Sigma-Aldrich; 90338 Triethylamine for Protein Sequence Analysis, Ampule, ≥99.5%.
39. Pieterse, K. Electron-deficient Materials Based on Azaheterocycles: Towards Supramolecular Electronics, Technische Universiteit Eindhoven, **2001**.
40. Houtem, M. H. C. J. van; Martín-Rapún, R.; Vekemans, J. A. J. M.; Meijer, E. W. Desymmetrization of 3,3′-Bis(acylamino)-2,2′-bipyridine-Based Discotics: The High Fidelity of Their Self-Assembly Behavior in the Liquid-Crystalline State and in Solution. *Chem. Eur. J.* **2010**, *16*, 2258–2271.
41. Houtem, M. H. C. J., van 3,3′-Bis(acylamino)-2,2′-bipyridine Discotics: Desymmetrization and Functionalization, Technische Universiteit Eindhoven, **2010**.
42. Petkau-Milroy, K.; Uhlenheuer, D. A.; Spiering, A. J. H.; Vekemans, J. A. J. M.; Brunsveld, L. Dynamic Protein Assembly Through Site-Selective Attachment and Display on a Supramolecular Wire. *submitted*.
43. This compound was provided by J. Spiering. For synthesis see reference 42.
44. Ghosez, L.; Haveaux, B.; Viehe, H. G. Alkyl and Aryl α-Chloro Enamines. *Angew. Chem. Int. Ed. Engl.* **1969**, *8*, 454–455.
45. Gillies, E. R.; Dolain, C.; Léger, J.-M.; Huc, I. Amphipathic Helices from Aromatic Amino Acid Oligomers. *J. Org. Chem.* **2006**, *71*, 7931–7939.
46. Only **1NHBoc-**, **1N$_3$-**, **1Prop-** and **3N$_3$-Disc** were compatible with recycling-GPC purification in chloroform. The presence of a single free amine or even of three Boc protected amines led to smearing on the size-exclusion column, rendering the purification and analysis of **1NH$_2$-**, **3NHBoc-** or **9NHBoc-Disc** using recycling-GPC futile.
47. Forssen, E.; Willis, M. Ligand-targeted Liposomes. *Adv. Drug. Deliver. Rev.* **1998**, *29*, 249–271.
48. Collier, J. H.; Rudra, J. S.; Gasiorowski, J. Z.; Jung, J. P. Multi-component Extracellular Matrices Based on Peptide Self-assembly. *Chem. Soc. Rev.* **2010**, *39*, 3413-3424.
49. Tornøe, C. W.; Christensen, C.; Meldal, M. Peptidotriazoles on Solid Phase: [1,2,3]-Triazoles by Regiospecific Copper(I)-Catalyzed 1,3-Dipolar Cycloadditions of Terminal Alkynes to Azides. *J. Org. Chem.* **2002**, *67*, 3057–3064.
50. Rostovtsev, V. V.; Green, L. G.; Fokin, V. V.; Sharpless, K. B. A Stepwise Huisgen Cycloaddition Process: Copper(I)-Catalyzed Regioselective "Ligation" of Azides and Terminal Alkynes. *Angew. Chem. Int. Ed.* **2002**, *41*, 2596–2599.
51. Meldal, M.; Tornøe, C. W. Cu-Catalyzed Azide−Alkyne Cycloaddition. *Chem. Rev.* **2008**, *108*, 2952–3015.
52. Lallana, E.; Sousa-Herves, A.; Fernandez-Trillo, F.; Riguera, R.; Fernandez-Megia, E. Click Chemistry for Drug Delivery Nanosystems. *Pharm. Res.* **2012**, *29*, 1–34.
53. Agard, N. J.; Prescher, J. A.; Bertozzi, C. R. A Strain-Promoted [3 + 2] Azide−Alkyne Cycloaddition for Covalent Modification of Biomolecules in Living Systems. *J. Am. Chem. Soc.* **2004**, *126*, 15046–15047.
54. Debets, M. F.; Doelen, C. W. J. van der; Rutjes, F. P. J. T.; Delft, F. L. van Azide: A Unique Dipole for Metal-Free Bioorthogonal Ligations. *ChemBioChem* **2010**, *11*, 1168–1184.
55. Valeur, E.; Bradley, M. Amide Bond Formation: Beyond the Myth of Coupling Reagents. *Chem. Soc. Rev.* **2009**, *38*, 606-631.
56. Merrifield, R. B. Solid Phase Peptide Synthesis. I. The Synthesis of a Tetrapeptide. *J. Am. Chem. Soc.* **1963**, *85*, 2149–2154.
57. El-Faham, A.; Albericio, F. Peptide Coupling Reagents, More Than a Letter Soup. *Chem. Rev.* **2011**, *111*, 6557–6602.
58. Anderson, G. W.; Zimmerman, J. E.; Callahan, F. M. N-Hydroxysuccinimide Esters in Peptide Synthesis. *J. Am. Chem. Soc.* **1963**, *85*, 3039-3039.

59. Griffith, B. R.; Allen, B. L.; Rapraeger, A. C.; Kiessling, L. L. A Polymer Scaffold for Protein Oligomerization. *J. Am. Chem. Soc.* **2004**, *126*, 1608–1609.
60. Saccà, B.; Niemeyer, C. M. Functionalization of DNA Nanostructures with Proteins. *Chem. Soc. Rev.* **2011**, *40*, 5910-5921.
61. Hinner, M. J.; Johnsson, K. How to Obtain Labeled Proteins and What to Do with Them. *Curr. Opin. Biotech.* **2010**, *21*, 766–776.
62. Keppler, A.; Gendreizig, S.; Gronemeyer, T.; Pick, H.; Vogel, H.; Johnsson, K. A General Method for the Covalent Labeling of Fusion Proteins with Small Molecules in Vivo. *Nat Biotech* **2003**, *21*, 86–89.
63. Becer, C. R.; Hoogenboom, R.; Schubert, U. S. Click Chemistry Beyond Metal-Catalyzed Cycloaddition. *Angew. Chem. Int. Ed.* **2009**, *48*, 4900–4908.
64. Hackenberger, C. P. R.; Schwarzer, D. Chemoselective Ligation and Modification Strategies for Peptides and Proteins. *Angew. Chem. Int. Ed.* **2008**, *47*, 10030–10074.
65. Flavell, R. R.; Muir, T. W. Expressed Protein Ligation (EPL) in the Study of Signal Transduction, Ion Conduction, And Chromatin Biology. *Acc. Chem. Res.* **2008**, *42*, 107–116.
66. Tanaka, K.; Fukase, K. PET (positron Emission Tomography) Imaging of Biomolecules Using metal–DOTA Complexes: a New Collaborative Challenge by Chemists, Biologists, and Physicians for Future Diagnostics and Exploration of in Vivo Dynamics. *Org. Biomol. Chem.* **2008**, *6*, 815–828.
67. Pierschbacher, M. D.; Ruoslahti, E. Variants of the Cell Recognition Site of Fibronectin That Retain Attachment-promoting Activity. *PNAS* **1984**, *81*, 5985-5988.
68. Storrie, H.; Guler, M. O.; Abu-Amara, S. N.; Volberg, T.; Rao, M.; Geiger, B.; Stupp, S. I. Supramolecular Crafting of Cell Adhesion. *Biomaterials* **2007**, *28*, 4608–4618.
69. 2,2′-bipyridine-3,3′-diamine is known to be an excellent chelator for copper ions (C. R. Rice et al. *Eur. J. Inorg. Chem.* **2002**, 2002, 8, 1985-1997). Addition of copper to alkoxy functionalized discotics in organic solvents leads to complete quenching of fluorescence. Chelation induces a change in bipyridine confirmation, distorting the planar orientation of the molecule. For PEG-functionalized discotics in water, copper chelation was not observed. The solutions remained fluorescent and no copper-adducts were detected by MALDI-ToF mass spectrometry.
70. The concentrations of copper sulfate and sodium ascorbate and the order of addition were adopted from: Hong, V.; Presolski, S.; Ma, C.; Finn, M.G. *Angew. Chem. Int. Ed*. **2009,** 48, 9879–9883.
71. Rijkers, D. T. S.; Esse, G. W. van; Merkx, R.; Brouwer, A. J.; Jacobs, H. J. F.; Pieters, R. J.; Liskamp, R. M. J. Efficient Microwave-assisted Synthesis of Multivalent Dendrimeric Peptides Using Cycloaddition Reaction (click) Chemistry. *Chem. Commun.* **2005**, 4581–4583.
72. Uhlenheuer, D. A. Supramolecular Control over Protein Assembly, Technische Universiteit Eindhoven, **2011**.
73. Carpino, L. A.; Han, G. Y. 9-Fluorenylmethoxycarbonyl Function, a New Base-sensitive Amino-protecting Group. *J. Am. Chem. Soc.* **1970**, *92*, 5748–5749.
74. Barlos, K.; Gatos, D.; Kallitsis, J.; Papaphotiu, G.; Sotiriu, P.; Wenqing, Y.; Schäfer, W. Darstellung Geschützter Peptid-fragmente Unter Einsatz Substituierter Triphenylmethyl-harze. *Tetrahedron Lett.* **1989**, *30*, 3943–3946.
75. Bollhagen, R.; Schmiedberger, M.; Barlos, K.; Grell, E. A New Reagent for the Cleavage of Fully Protected Peptides Synthesised on 2-chlorotrityl Chloride Resin. *J. Chem. Soc., Chem. Commun.* **1994**, 2559–2560.

3

Self-assembling multivalency of monovalent discotics

Abstract. In the previous chapter the synthesis and functionalization of novel discotics bearing a single functional group was described. Here the self-assembly of these intrinsically monovalent discotics into columnar wires is investigated. Enzyme-linked lectin assay is used to quantify the enhancement in binding affinity upon self-assembly of the discotic displaying a single mannose moiety. Compared with the non self-assembling counterpart, a three-fold increase in binding activity is observed, which can be accredited to the multivalent ligand display upon self-assembly. The ability of discotics functionalized with a single biotin to display several monovalent streptavidin proteins along the supramolecular stack is confirmed using Förster resonance energy transfer and SDS-PAGE. The self-assembly of the monovalent discotics into supramolecular polymers generates a multivalent system. Additionally, the dynamic intermixing of monomers between the self-assembling stacks lead to the formation of heterovalent structures, as confirmed using mixtures of fluorescein and biotin functionalized discotics.

3.1 Introduction

Multivalent interactions, simultaneous interactions between multiple functionalities on one entity and complementary functionalities on another, are essential in many biological recognition events including for example cell-cell contacts to enhance binding affinities.[1] The multivalent interactions are especially prevalent in glycobiology to ensure high-avidity interactions between lectins (carbohydrate-binding proteins) and their ligands, which typically display only low affinity interactions of the isolated entity.[2–4] Increasing the number of existing interactions leads to high-affinity molecular recognition without the need to evolve stronger binders. In the field of biochemistry this concept has been successfully applied for the development of highly potent synthetic binders.[5–7] The enhanced binding is exhibited through statistical rebinding due to an increased local concentration (Figure 3.1 c) and/or via chelation, an entropic effect which favors the binding of a second ligand after translational and rotational penalties were already paid by the first binding event (Figure 3.1 b).[2]

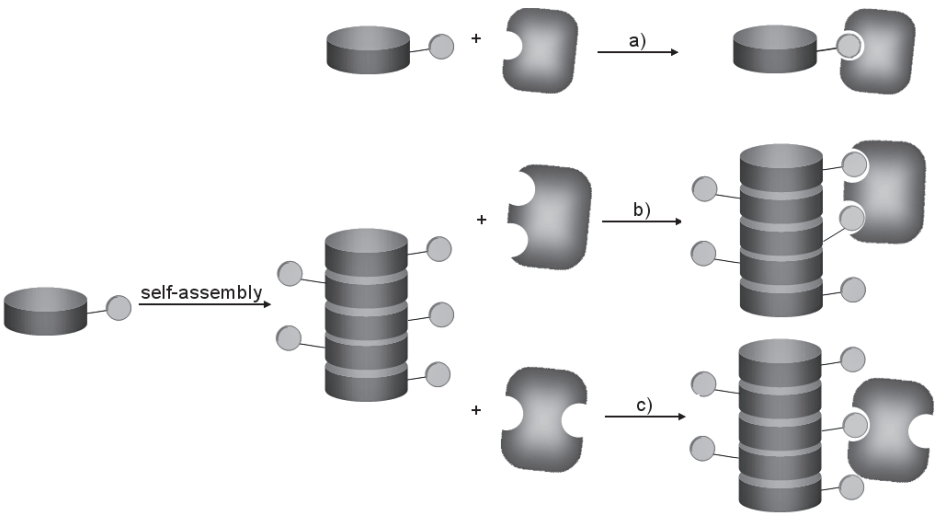

Figure 3.1: a) Monovalent binding; After self-assembly into a multivalent ligand; b) binding via a chelation mechanism, c) enhanced binding through high local concentration of ligand.

Recently, next to using covalent scaffolds, self-assembling scaffolds were applied to organize multiple ligands.[8–10] Self-assembly is the spontaneous association of molecules into well-defined structures, held together by non-covalent interactions.[11] Nature frequently uses self-assembly to organize recognition events, in particular in membranes, where receptors or ligands can cluster to spontaneously generate a multivalent region.[12] The advantages of the non-covalent compared to covalent organization of ligands include the responsive nature of the self-assembly, ease of supramolecular synthesis and the possibility to incorporate multiple and different ligands in a single step through mixing of building blocks.

Monovalent discotics, especially the **1NH$_2$-Disc**, were shown to be an excellent platform for the attachment of different types of ligands in the previous chapter. For the envisaged applications of

ligand-functionalized discotics in for example targeted imaging the display of multiple ligands is necessary for high selectivity.[13,14] The use of discotics as a platform for protein assembly similarly requires the presence of multiple binding sites or attachment points. Therefore, it is of fundamental interest to understand the self-assembly of intrinsically monovalent discotics into columnar wires and the resulting multivalent ligand display.

Previously it has been shown that the self-assembly of trivalent **3Mannose-Disc** leads to selective binding to *E.Coli* bacteria, which display the mannose binding FimH receptor.[15] The enhanced binding affinity through multivalency was as well confirmed and quantified using an enzyme-linked lectin assay. Functionalization of **3NH$_2$-Disc** with biotin enabled the display of streptavidin, a biotin-binding protein, along the supramolecular stack.[16] Förster resonance energy transfer (FRET) between differently labeled streptavidins showed that upon binding of multiple streptavidins to the supramolecular platform interactions between the differently labeled streptavidins could be induced.

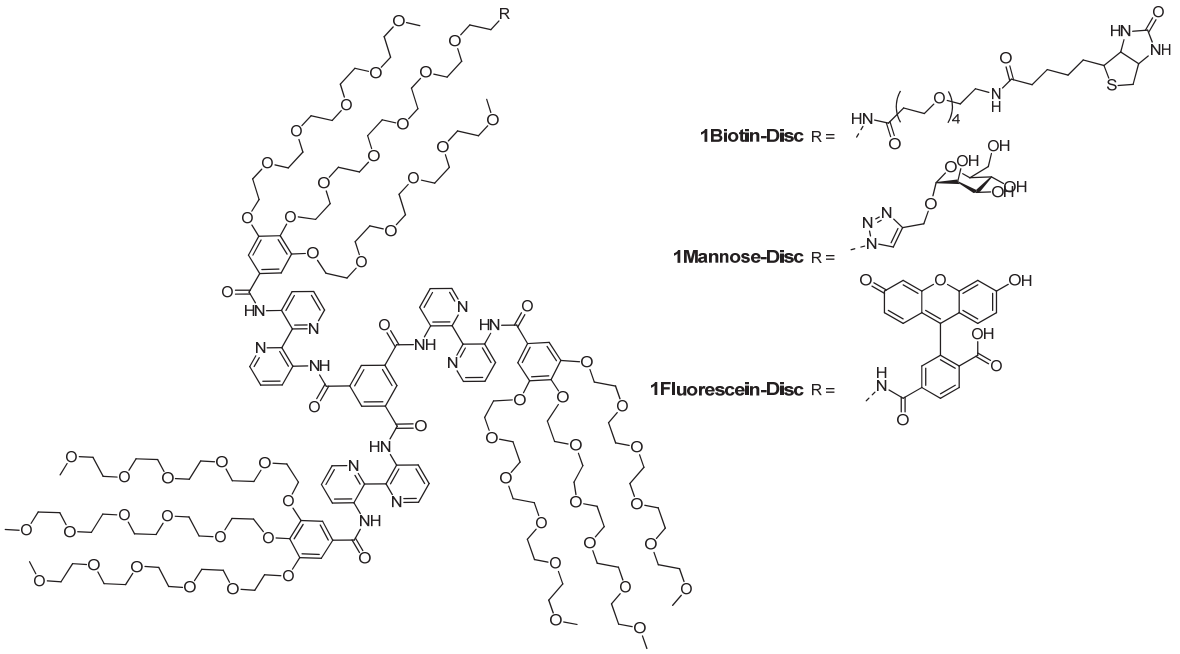

Scheme 3.1: Structures of monovalent discotics used in this chapter.

Here the monovalent variants of these two well studied systems, **1Biotin-Disc** and **1Mannose-Disc** are applied to understand the self-assembling multivalency of discotics (Scheme 3.1). On the one hand the self-assembling multivalency of **1Mannose-Disc** will be quantified using the enzyme-linked lectin assay. On the other hand the possibility to display multiple streptavidins on supramolecular stacks based on **1Biotin-Disc** will be investigated. Additionally, using mixtures of **1Fluorescein-Disc** and **1Biotin-Disc** the formation of heterovalent supramolecular polymers via co-assembly of monovalent discotics is studied.

3.2 Results and Discussion

3.2.1 *Self-assembling multivalency of 1Mannose-Disc*

Oligosaccharides are important mediators of complex cellular events. Next to immune response and fertilization, early events in bacterial and viral infections are controlled by protein-carbohydrate interactions.[1] Most saccharides bind to their receptors only weakly, with association constants seldom beyond the micromolar range. To achieve high binding affinities in competitive aqueous environments nature uses multivalency, through using receptors with multiple clustered binding sites on the one hand and branched polymeric carbohydrates on the other.[17] This has inspired the design of inhibitors to block protein-carbohydrate interactions.[5] Many scaffolds ranging from dendrimers, polymers, micelles, vesicles to nanoparticles and nanotubes were applied to enhance the potency of carbohydrates as inhibitors or effectors.[3] At the same time a wide range of assays has been developed to evaluate the protein-carbohydrate binding constants. The most common assays are the inhibition of hemagglutination assay (HIA), enzyme-linked lectin assay (ELLA), isothermal titration microcalorimetry (ITC) and surface plasmon resonance (SPR).[2] The obtained half-maximal inhibitory concentration (IC_{50}) is highly dependent on the type of assay used and discrepancies between the derived IC_{50} values from different methods are common as each assay reports on one aspect of multivalent binding.[18] HIA is often used to determine aggregation and precipitation properties of multivalent polymers[19,20], but high aberration in IC_{50} values only permit rough classification of binding affinity. In contrast to dendritic structures, the dynamic properties of a self-assembling multivalent polymer do not allow the use of ITC and SPR. In ITC the carbohydrate containing ligand is titrated to a solution of a lectin. In SPR the carbohydrate containing ligand is flown over an immobilized lectin, in both cases resulting in a dilution of the ligand. In a dynamic supramolecular polymer this might lead to changes in length of the assembly which might influence the results.

To quantify the binding of the supramolecular polymer self-assembled from monovalent mannose functionalized discotics, an enzyme linked lectin assay (ELLA) was performed. The assay is based on competitive binding inhibition of a lectin to immobilized polymeric saccharide by carbohydrate-functionalized ligands. Experiments using horseradish peroxidase labeled concanavalin A (ConA-HRP) as the lectin and mannan as the immobilized polymeric ligand were carried out in 96-well plates as illustrated in Figure 3.2. ConA, a widely applied lectin with binding specificity for mannose, is a tetramer at neutral pH[21] and the tetrahedral orientation of the four binding sites leads to a distance of 6-7 nm between them.[22]

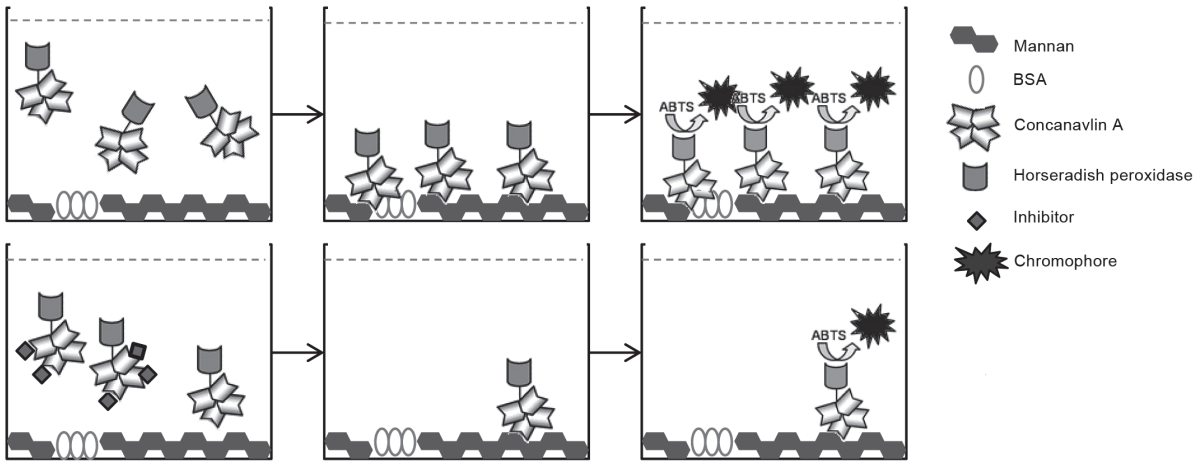

Figure 3.2: Cartoon illustrating the binding of concanavalin A-horseradish peroxidase conjugate (ConA-HRP) to a mannan coated surface (top) and inhibition of this binding by an inhibitor (bottom).

Optimal concentration of ConA was evaluated prior to the inhibition experiments (see experimental part). After pre-incubation of ConA-HRP with different concentrations of **1Mannose-Disc**, **3Mannose-Disc** and **Inert-Disc,** binding of ConA-HRP to mannan coated plates was measured. A pro-dye substrate is converted by the horseradish peroxidase and the development of color, which is proportional to the concentration of retained lectin and inversely proportional to the affinity of the soluble ligand, is read out spectrophotometrically (Figure 3.3). **Inert-Disc** was used as control for unspecific binding of the supramolecular scaffold and α-D-methyl mannose served as the monovalent reference compound. To exclude any interference of disc absorption in the read-out process, the spectrophotometric measurements were performed at two different wavelengths; at 340 nm and 415 nm. Measurements during incubation with a mixture of ConA-HRP and inhibitor (**1Mannose-Disc**, **3Mannose-Disc**, **Inert-Disc**, α-D-methyl mannose) revealed no interference of disc absorption at 415 nm. At the same time, measurements at 340 nm could be used to control the dilution series of discotics (Figure 3.3 a). After a washing step, followed by incubation with a pro-dye substrate, no absorption at 340 nm was detected confirming that there was no unspecific binding of the discotics to the mannan coated plates. As could already be observed during the experiment (see Figure 3.3 d), all mannose-functionalized inhibitors led to a decreased absorption at 415 nm at higher concentrations which corresponds to inhibition of lectin binding. The non-affected absorption signal at 415 nm in the case of the **Inert-Disc** confirms that there is no unspecific binding of the bare discotic scaffold.

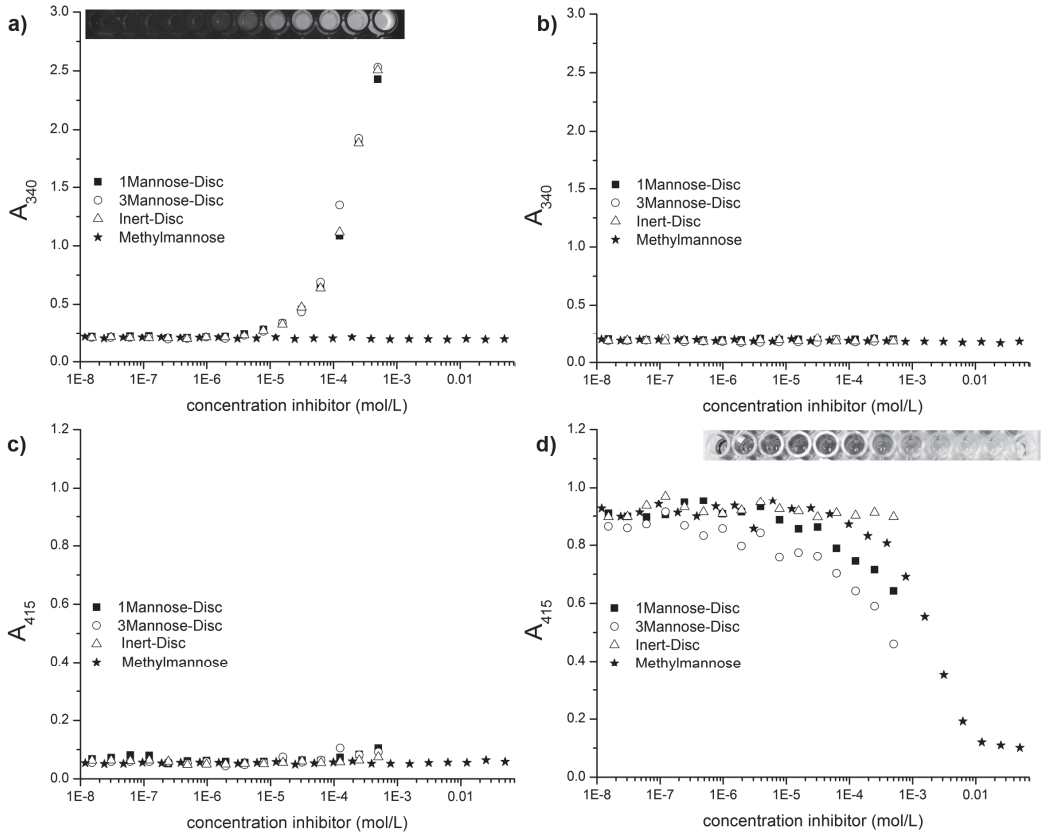

Figure 3.3: a) & b) Absorption of the 96 well plate at 340 nm during incubation with inhibitor-lectin mixtures (a) and after washing and incubation with ABTS (b); Inset: dilution series of discotics under UV-irradiation (λ_{ex} = 350 nm); c) & d) Absorption of the 96 well plate at 415 nm during incubation with inhibitor-lectin mixtures (c) and after washing and incubation with ABTS (d); The wavelength of 340 nm corresponds to the absorbance of disc. At 415 nm, the absorption peak of the pro-dye ABTS, no disc absorption is observed.

The inhibition of ConA-HRP binding was measured in three independent experiments and after substraction of background absorption the inhibition in % was calculated (see experimental section). Plotting the inhibition in % against the concentration of inhibitor enabled the calculation/extrapolation of the half maximal inhibitory concentration (IC_{50}) from these inhibition curves (Figure 3.4). The IC_{50} of 1950 μM for α-D-methyl mannose is in agreement with literature, where IC_{50} values between 1300 and 3900 μM are normally reported.[18,23] Both, the **3Mannose-Disc** and the **1Mannose-Disc**, showed a stronger inhibition than the monovalent non self-assembling reference (Figure 3.4 a).[24] To inhibit 24% of lectin binding to mannan a 781 μM concentration of α-D-methyl mannose is required, which is a 3.1 times higher concentration than in the case of **1Mannose-Disc** (250 μM for 24% inhibition). The stronger inhibitory power of the **1Mannose-Disc** can be attributed to the self-assembling multivalency of this monovalent disc.

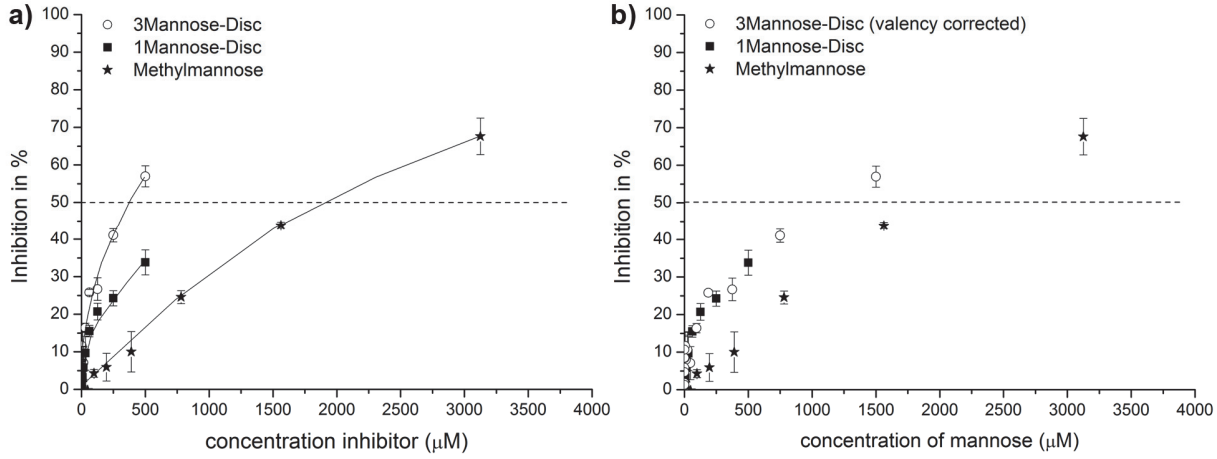

Figure 3.4: a) Inhibition curves of **1Mannose-Disc**, **3Mannose-Disc** and α-D-methyl mannose**.** b) The Inhibition curve of **3Mannose-Disc** is valency corrected. Dashed line represents the half-maximal inhibition.

This enhancement in binding activity of compounds of equal valency is known as the cluster glycoside effect.[2] The valency corrected inhibition of **3Mannose-Disc** however perfectly overlays with the inhibition achieved through the **1Mannose-Disc** (Figure 3.4 b), showing no further enhancement in the cluster glycoside effect through the two additionally appending mannose moieties. Probably, the appending mannose moieties are not able to chelate the far apart oriented binding sites of ConA. Most enhancements in binding affinity towards ConA, are based on statistical rebinding. Only for larger polyvalent systems the chelation of far apart oriented binding sites of ConA was reported, which led to the strongest cluster glycoside effects.[3,25] Activity on an inhibitor depends on its ability to occupy multiple binding sites; however, a potent effector of biological processes is determined by its ability to cluster receptors.[25] The ELLA assay however does not distinguish effects arising from receptor clustering; there different types of assays are required to determine the ability of receptor clustering.[26]

3.2.2 *Self-assembling multivalency of 1Biotin-Disc*

Protein assembly regulates a plethora of biological processes. Signal transduction as well as immune-response depends on the spontaneous clustering of proteins in the membrane.[27–29] Self-assembled protein fibers (actin, tubulin) play an essential role in motility and stabilization of cells.[30] At the same time, miss regulation of protein assembly can lead to diseases[31] such as Alzheimer's disease. A lot of research has focused on the elucidation of assembly mechanisms and their biological function. Additionally, self-assembling protein nanostructures emerged as novel materials for (bio)nanotechnology, enabling the generation of for example bioactive hydrogels and nanometer-scale electronics.[32,33]

Previously it was shown that functionalization of **3NH$_2$-Disc** with biotin enabled the display of streptavidin, a biotin-binding protein, along the supramolecular stack.[16] Förster resonance energy

transfer (FRET) between differently labeled streptavidins, indicated that upon binding of multiple streptavidins to the supramolecular platform interactions between the differently labeled streptavidins could be induced**.** Streptavidin is a tetrameric protein of 52.8 kDa which interacts strongly and specifically with biotin (Kd = 4 x 10^{-14} M)[34]. The tetrameric binding however can cause cross-links between several supramolecular wires (Figure 3.5b). To investigate self-assembling multivalency of the monovalent **1Biotin-Disc** a monovalent streptavidin is required. As the biotin binding sites lie at the interface between the subunits[35], disruption of the tetramer interface is always accompanied by a dramatic decrease in binding affinity[36]. An alternative approach was developed by Howarth et al.[37,38] to generate a monovalent streptavidin with a single femtomolar biotin binding site. They have generated a so-called 'dead'-subunit containing three mutations in the biotin binding site (N23A, S27D, S45A) with a diminished binding affinity (K_d = 1.2 x 10^{-3} M). The wild-type, or 'alive'-subunit, was equipped with a 6His tag. Combining the 'dead'- and 'alive'-subunits in a molar ratio of 3:1 and refolding them allows the subsequent separation of the different statistically formed streptavidins via nickel-nitrilotriacetic acid (Ni-NTA) column using increasing concentrations of imidazole. In this way a monovalent streptavidin (mSA), a tetrameric streptavidin construct with a single biotin binding site, was generated and randomly labeled with Cy3 for FRET studies.[39]

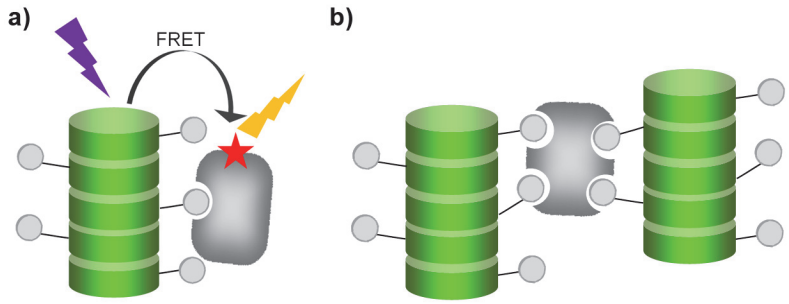

Figure 3.5: a) Binding of the monovalent streptavidin to biotin functionalized supramolecular wires and energy transfer from the auto-fluorescent polymer to Cy3-labeled streptavidin. b) Cross-linking between supramolecular wires caused through binding of tetravalent streptavidin.

FRET is a non-radiative energy transfer between two fluorescent molecules. The fact, that the efficiency of energy transfer highly depends on the distance between the donor and acceptor molecule,[40] led to an extensive use of this technique as a so-called "molecular ruler" to study protein-protein interactions.[41–43] Due to a spectral overlap of the absorbance spectrum of Cy3 with the emission spectrum of the discotics, a requirement for energy transfer, Cy3 serves as an acceptor. Subsequently, the protein assembly of Cy3-labeled monovalent and tetravalent streptavidin (Cy3-mSA and Cy3-tSA) proteins on supramolecular wires of **1Biotin-Disc** was investigated using FRET (Figure 3.5). The binding of streptavidin to biotin decorated supramolecular wires should bring the dye-labeled protein in close proximity to the auto-fluorescent discotic scaffold and enable energy transfer from the discotic to the Cy3, leading to an increase in acceptor signal (575 nm) and a simultaneous decrease in donor signal (525 nm).

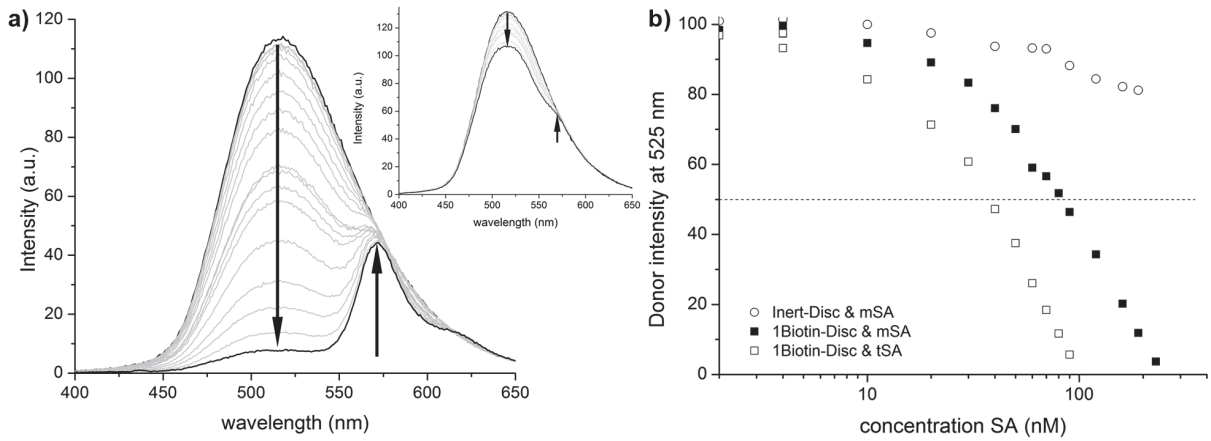

Figure 3.6: a) Emission spectra of the titration of monovalent Cy3-labelled streptavidin (0 nM – 270 nM) to **1Biotin-Disc** (1 μM). Inset: Emission spectra of the titration of monovalent Cy3-labelled streptavidin (0 nM – 270 nM) to **Inert-Disc** (1 μM). b) Normalized decrease in disc intensity at 525 nm upon addition of Cy3-labelled streptavidin, either monovalent or tetravalent, to **1Biotin-Disc** and **Inert-Disc** (both 1 μM); Dashed line represents the intensity, where half of the donor intensity is quenched.

Indeed, upon addition of Cy3-labeled monovalent and tetravalent streptavidin to **1Biotin-Disc** an increase in acceptor signal (575 nm) and a simultaneous decrease in donor signal (525 nm) is observed (Figure 3.6 a). No significant energy transfer was observed for the non-biotinylated **Inert-Disc**, which was used as a control, underlining that FRET is selectively induced through the binding of Cy3-labeled streptavidins to the appending biotins on the supramolecular scaffold. As expected, less tSA was required to fully quench the emission of the donor compared to mSA, as the tSA might lead to more efficient energy transfer through cross-linking between the wires. Plotting the decrease in donor intensity against the concentration of added streptavidin shows that for Cy3-tSA only 0.04 equivalents (40 nM) suffice to quench half of the donor fluorescence (Figure 3.6 b). This indicates that at this concentration 12 discotics are quenched by one Cy3 labeled streptavidin (donor : acceptor ratio is 25 to 1 and half of donor is quenched). In the case of the monovalent streptavidin, only 0.09 equivalents (90 nM) of Cy3-mSA suffice to quench half of the donor fluorescence. Assuming a 1 to 1 binding of the monovalent protein to the monovalent discotic 0.5 equivalents would be required to achieve this effect, when the discotics would be molecularly dissolved. This implies that at this concentration the fluorescence of approximately 5 discotics is quenched by one Cy3-SA acceptor fluorophore (donor : acceptor ratio is 11 to 1 and half of donor is quenched), strongly suggesting multivalency of the discotics upon self-assembly.

Additionally, the ability of self-assembled **1Biotin-Disc** to bind monovalent streptavidin(s) was investigated using non-denaturing sodium dodecyl sulfate polyacrylamide gel electrophoresis (SDS-PAGE).[44] In this widely used technique proteins are separated according to their electrophoretic mobility. The electrophoretic mobility is a function of the length and of the charge of the protein. Even distribution of charge per mass unit is guaranteed through binding of SDS,

enabling the separation of proteins according to their size. Denaturation of streptavidin through addition of a reducing agent (β-mercaptoethanol) and heating to 95 °C (a standard procedure for SDS-PAGE) would lead to the dissociation of the subunits and the simultaneous dissociation of bound biotin. Therefore a non-denaturing approach was chosen to visualize the binding of monovalent streptavidin to the supramolecular wire. Prior to electrophoresis the **1Biotin-Disc** was incubated with monovalent streptavidin and as a control with dead streptavidin, the tetramer consisting only of 'dead'-subunits. The semi-native SDS gel was imaged under UV-illumination (λ_{ex} = 350 nm) and subsequently the proteins were stained with Coomassie blue (Figure 3.7).

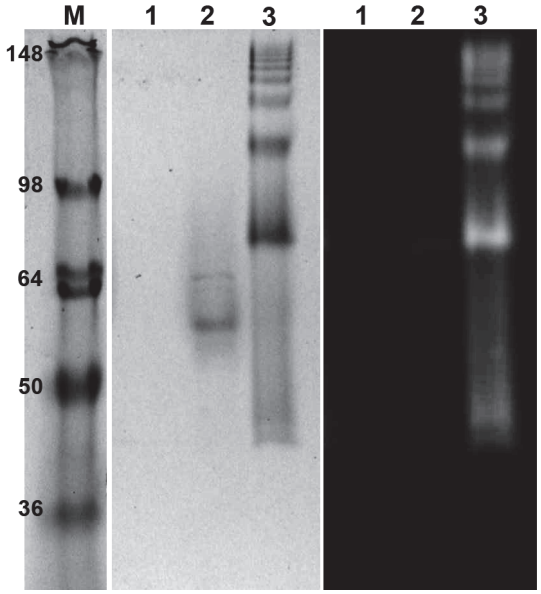

Figure 3.7: Non-denaturing SDS-Gel stained with Coomassie blue (left) and under UV-illumination (right, λ_{ex}=350 nm) before staining. Lane 1: **1Biotin-Disc**, lane 2: dead streptavidin with **1Biotin-Disc**, lane 3: monovalent streptavidin with **1Biotin-Disc**. Concentration of **1Biotin-Disc** was 10 μM and of the dead and monovalent streptavidin 0.4 mg/mL.

The **1Biotin-Disc** itself, with a molecular weight of 3.5 kDa, was not detectable. Dead streptavidin incubated with **1Biotin-Disc** showed one non-fluorescent band corresponding to the tetravalent streptavidin of 55 kDa. In the case of the mixture of monovalent streptavidin with **1Biotin-Disc** several higher mass protein bands were observed, which at the same time featured fluorescence when excited at 350 nm, resulting from the bound **1Biotin-Disc**. This can be explained through the binding of several monovalent streptavidins to a supramolecular wire consisting of several self-assembling **1Biotin-Discs**. This observation at the same time suggests that the protein-decorated supramolecular wires formed through self-assembly of discotics are at least partially stable under the SDS-PAGE conditions. The occurrence of multiple protein lanes as well indicates the assembly of multiple discotics into longer stacks.

3.2.3 *Heterovalency through intermixing*

The major advantage of supramolecular polymers is their non-covalent nature, which allows generating heterovalent polymers via co-assembly of different monomers.[45–47] Without the need for repeated synthesis a vast array of materials is accessible via this so-called supramolecular synthesis, facilitating the fine-tuning of ligand density and composition. Both of these factors, ligand density and composition, were shown to be crucial for good performances in regenerative medicine[48,49] and targeted imaging[13]. At the same time, the possibilities to investigate the intermixing of self-assembling systems are rather limited. Commonly, model-ligands, such as biotin or a fluorophore, are used to study the formation of mixed assemblies. Introduction of biotin can be confirmed through the labeling with streptavidin coated gold nanoparticles via transmission electron microscopy (TEM)[47,50]. Energy transfer[51] and anisotropy measurements[46] can be applied upon functionalization with fluorophores. Both of these model ligands are combined here to study the intermixing of monovalent discotics into heterovalent supramolecular polymers and their interaction with multivalent particles, streptavidin coated magnetic beads. The utilization of magnetic beads provides a rapid and reliable method to remove unbound discotics, whereas the intrinsic fluorescence of discotics and the additional fluorescent signal of fluorescein enable visualization with confocal microscopy.

FRET measurements (see 3.2.2) revealed specific interaction of streptavidin with **1Biotin-Disc**. Incubation of **1Biotin-Disc** with magnetic streptavidin beads as well confirmed this observation, as after incubation and washing, the beads were stained green (Figure 3.8 a). Subsequently, mixtures of **1Fluorescein-Disc** (in a 1 to 1 ratio) with either **1Biotin-Disc** or **Inert-Disc** were prepared. To ensure intermixing between the different supramolecular polymers through monomer exchange, these mixtures were pre-incubated either for 3 hours at 37 °C or overnight at room temperature and subsequently incubated for 1 hour with streptavidin coated magnetic beads, washed and imaged. The mixture of **Inert-/1Fluorescein-Disc** was used as a control to visualize any unspecific interactions of the discotic scaffold or the attached fluorophore with the streptavidin coated magnetic beads. No unspecific binding was observed, as no signal, neither from the disc nor from the fluorescein was detected (Figure 3.8 c). In contrast, both the fluorescein and disc fluorescence could be detected when streptavidin coated magnetic beads were incubated with the **1Biotin-/1Fluorescein-Disc** mixture (Figure 3.8 b), indicating the presence of both types of discotics by virtue of their hetero-self-assembly. This confirms the assumption, that via co-assembly of streptavidin binding discs with non-streptavidin binding discs, intermixed polymers are generated. Using both pre-equilibration conditions, intermixed polymers were observed, indicating a rather fast intermixing process.

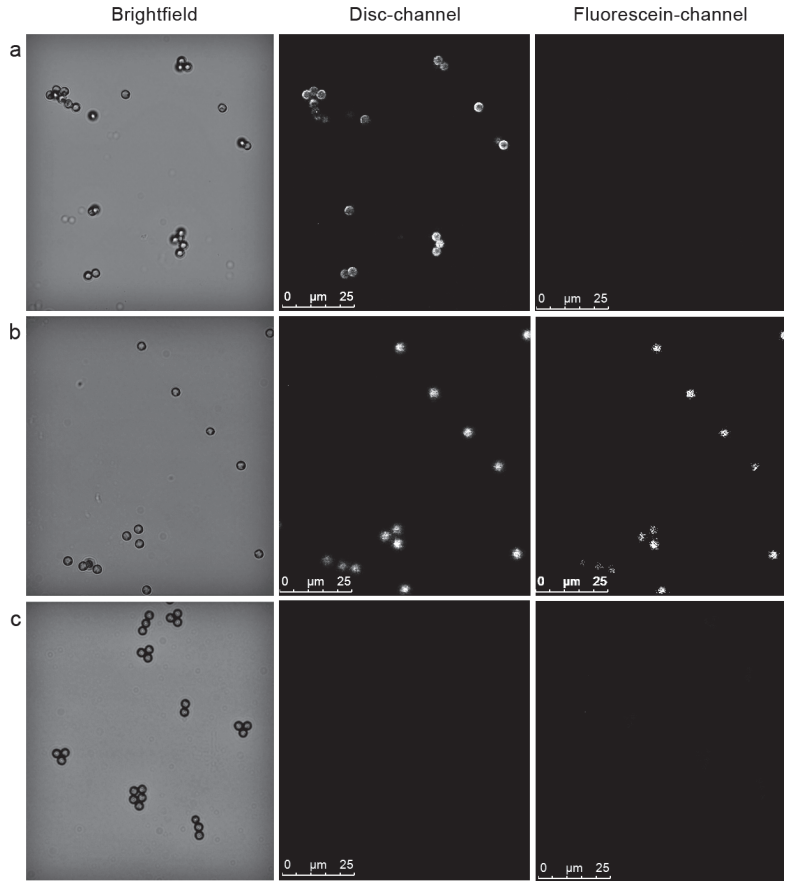

Figure 3.8: Microscopic images of streptavidin coated magnetic beads incubated with **1Biotin-Disc** (a), a 1:1 mixture of **1Biotin-Disc** and **1Fluorescein-Disc** (b) and with a 1:1 mixture of **Inert-Disc** and **1Fluorescein-Disc** (c).

3.3 Conclusions

Future applications of discotics will highly depend on the possibility to functionalize discotics with a wide array of ligands and at the same time on the ability to form multi- and heterovalent supramolecular polymers. In chapter 2 the **1NH$_2$-Disc** emerged as a versatile non-sterically hindered scaffold for ligand attachment, here the multivalency upon self-assembly has been probed with a number of monovalent ligand-functionalized discotics. On the one hand, **1Mannose-Disc** was shown to inhibit the binding of the lectin concanavalin A to a polysaccharide in an ELLA assay, displaying a 3-fold larger inhibitory activity than its non self-assembling counterpart. On the other hand, the possibility to display several monovalent streptavidin proteins using **1Biotin-Disc** was confirmed with FRET measurements and semi-native SDS-PAGE. The self-assembly into supramolecular polymers not only generated a multivalent, but as well a heterovalent system by simple intermixing of several differently-functionalized building blocks, as shown using mixtures of **1Biotin-** and **1Fluorescein-Disc** incubated with streptavidin coated magnetic beads. The possibility to generate multivalent and

heterovalent supramolecular stacks starting from monovalent discotic, which can readily be functionalized with ligands, has a great potential in view of advanced biological applications, for example in the field of targeted imaging.

3.4 Experimental

Bio-safe Coomassie Brilliant Blue was purchased from BioRad. Streptavidin, mannan, α-D-methyl mannose, ABTS and ConA-HRP were purchased from Sigma. Streptavidin coated magnetic beads (Dynabeads® MyOne™ Streptavidin M270) and SeeBlue® Plus2 pre-stained standard were purchased from Invitrogen. Sodium dodecyl sulfate (SDS) was purchased from Merck. NHS-Cy3 was purchased from Lumiprobe. Plasmids for the 'dead'- and 'alive'-subunit were obtained from A. Y. Ting (MIT) and monovalent streptavidin was expressed by Michael Sonntag and Alexander Colditz following a published protocol.[37] The synthesis of **1Biotin-Disc**, **3Biotin-Disc**, **1Fluorescein-Disc**, **1Mannose-Disc** and **3Mannose-Disc** is described in chapter 2.

Enzyme Linked Lectine Assay (ELLA)[52]*:*
Determination of Enzyme concentration:
Costar® 96 well plates (EIA/RIA, Corning, NY) were coated with 100 µL/well of mannan (10 µg/mL in 0.01 M PBS, pH = 7.3 with 0.1 mM Mn^{2+} and Ca^{2+}) overnight at room temperature. Subsequently each well was washed three times with 300 µL washing buffer (PBS with 0.05 % (v/v) Tween) (PBST). This washing procedure was repeated after each incubation step throughout the assay. The wells were then blocked for 1 h at 37 °C using 150 µL/well of BSA (1% in PBS). Washing was repeated as described. Afterwards the plates were incubated for 1 h at 37 °C with serial dilutions of Horseradish Peroxidase labeled Concanavalin A (ConA-HRP) ranging from 0.1 mg/mL to 0.05 µg/mL in PBS (pH = 7.3 with 0.1 mM Mn^{2+} and Ca^{2+}). The washing step was repeated and 50 µL/well of ABTS (0.25 mg/mL) in citrate buffer (0.2 M, pH = 4.0 with 0.015 % (v/v) H_2O_2) were added. Color development was stopped after 20 min by adding 50 µL/well of 1M H_2SO_4. Light absorption was measured at 415 nm. The concentration of ConA-HRP with the readout between 0.8 and 1 was used for inhibition studies (Figure 3.9).

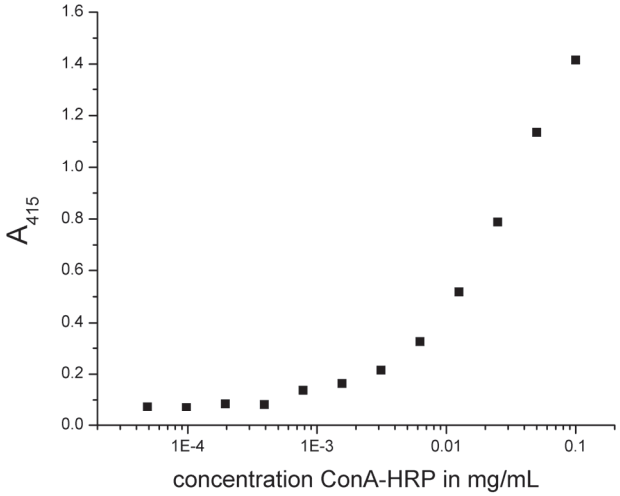

Figure 3.9: Determination of ConA-HRP concentration for inhibition experiments. Absoprtion at 415 nm of the ABTS converted with HRP.

Inhibition Experiments:
Costar® 96 well plates (EIA/RIA, Corning, NY) were coated, washed and blocked as described above. Independently, 60 µL/well of serial dilutions of inhibitor (methyl-α-D-mannopyranoside, **1Mannose-Disc**, **3Mannose-Disc** or **Inert-Disc**) were prepared in a Falcon 96 well plate (U-Bottom, flexible plate, Becton Dickinson). To each of these wells 60 µL of ConA-HRP was added and incubated for 1 h at 37 °C. 100 µL/well of these inhibitor-lectin mixtures were transferred to the mannan coated plate and incubated for 1 h at 37 °C. Before and after the washing step after this incubation the absorption at 340 nm and 415 nm was measured to control the concentration of Disc and to ensure that there is no unspecific Disc absorption at 415 nm. The wells were than treated with ABTS and the color development was stopped after 20 min. Absorption was measured at 415 nm and as a control at 340 nm. The inhibition of ConA-HRP binding was measured in three independent experiments and after substraction of background absorption the inhibition in % was calculated: % Inhibition = {[A_{415}(no inhibitor) – A_{415}(with inhibitor)] / A_{415}(no inhibitor)} x 100

Random labeling of streptavidin with Cy3-NHS:
The concentration of monovalent and tetravalent streptavidin in PBS was adjusted to 3mg/mL (determined by NanoDrop; mass: 55kDa, extinction coefficient: 200.000). 0.723mg Cy3-NHS was dissolved in 10µl DMF. The pH of the mSA and tSA in PBS was set to 8.5. 5µl of Cy3-NHS in DMF was added to both reaction mixtures. The reaction was performed overnight at room temperature and in the dark. The excess of dye was removed through dialysis.

FRET measurements:
Cy3 labeled monovalent or tetravalent streptavidin (4 µM in PBS) was titrated to **1Biotin-Disc** or **3Biotin-Disc** or **Inert-Disc** (each 1 µM in PBS) in serial concentrations from 2 nM to 310 nM at 20 °C. After each addition the solution in the cuvette was intermixed by turning the closed cuvette several times upside-down. Fluorescence- (λ_{ex} = 340 nm, λ_{em} = 400 - 650 nm) spectra were measured after each titration step.

Semi-native SDS-PAGE:
Semi-native SDS-PAGE electrophoresis was performed on a Mini-PROTEAN 3 electrophoresis system (Biorad, Hercules, California). The gel consisted of an 8% separating gel and a 5% stacking gel. The running buffer contained 25mM Tris, 250mM Glycine, and 0,1% (w/v) SDS in H_2O. Monovalent and dead streptavidin were incubated for about 16 hours at room temperature with different concentrations of **1Biotin-Disc** and **3Biotin-Disc**. To avoid protein denaturation no β-mercaptoethanol was added to the samples and the samples were not heated up to 95 °C. Sample buffer (100mM Tris-HCl, 20% (v/v) glycerol, 4% (w/v) SDS, 0,2% (w/v) bromophenol blue, pH 6,8 in Millipore H_2O) was added (1:3) was added to the samples and electrophoresis was run at room temperature at 80 V for 30 min and then at 140V for 60 min. The protein bands were stained with Coomassie Brilliant Blue.
30% Acrylamide mix (30% Acrylamide/Bis Solution, 29:1 (3.3%C));
Running-gel buffer (1,5 M Tris-HCl (pH 8,8) in Millipore H_2O);
Stacking-gel buffer (1,0 M Tris-HCl (pH 6,8) in Millipore H_2O).

Confocal microscopy:

Discotics (all 10 μM) were mixed in a 1 to 1 ratio and incubated either at 37° C for 3 hours or at room temperature for 24 hours. Streptavdidn coated magnetic beads were thoroughly vortexed and 50 μL of the beads suspension were washed three times with 200 μL PBS buffer prior to use. In the end the beads were resuspended in 140 μL buffer. 20 μL of the streptavidin magnetic beads suspension was mixed with 20 μL of discotic mixtures and incubated for 1 h at room temperature. After washing the beads four times with 40 μL of PBS, the beads were resuspendent in 15 μL of PBS and mounted on a glassslide and sealed with nail polish. The beads were imaged on a Leica TCS SP5 AOBS equipped with an HCX PL APO CS x63/1.2 NA water immersion lens. Discotics were excited with a Chameleon Multiphoton laser using 760 nm laser pulses. Fluorescein was excited with a Whitelight laser at 488 nm. During imaging with Multiphoton laser the pinhole was fully opened, whereas otherwise it was closed to 1 airy unit. Fluorophore emission bands were detected in the following ranges: discotics, 500–550 nm and fluorescein, 496–520 nm.

3.5 References

1. Mammen, M.; Choi, S.; Whitesides, G. M. Polyvalent Interactions in Biological Systems: Implications for Design and Use of Multivalent Ligands and Inhibitors. *Angew. Chem. Int. Ed.* **1998**, *37*, 2754–2794.
2. Lundquist, J. J.; Toone, E. J. The Cluster Glycoside Effect. *Chem. Rev.* **2002**, *102*, 555–578.
3. Pieters, R. J. Maximising Multivalency Effects in Protein–carbohydrate Interactions. *Org. Biomol. Chem.* **2009**, *7*, 2013–2025.
4. Deniaud, D.; Julienne, K.; Gouin, S. G. Insights in the Rational Design of Synthetic Multivalent Glycoconjugates as Lectin Ligands. *Org. Biomol. Chem.* **2011,** *9*, 966–979.
5. Pieters, R. J. Toward Multivalent Carbohydrate Drugs. *Drug Discov. Today* **2009**, *6*, e27–e31.
6. Kitov, P. I.; Sadowska, J. M.; Mulvey, G.; Armstrong, G. D.; Ling, H.; Pannu, N. S.; Read, R. J.; Bundle, D. R. Shiga-like Toxins Are Neutralized by Tailored Multivalent Carbohydrate Ligands. *Nature* **2000**, *403*, 669–672.
7. Rao, J.; Lahiri, J.; Isaacs, L.; Weis, R. M.; Whitesides, G. M. A Trivalent System from Vancomycin·d-Ala-D-Ala with Higher Affinity Than Avidin·Biotin. *Science* **1998**, *280*, 708–711.
8. Lim, Y.; Lee, M. Self-assembled Multivalent Carbohydrate Ligands. *Org. Biomol. Chem.* **2007**, *5*, 401-405.
9. Cui, H.; Webber, M. J.; Stupp, S. I. Self-assembly of Peptide Amphiphiles: From Molecules to Nanostructures to Biomaterials. *Biopolymers* **2010**, *94*, 1–18.
10. For further examples see chapter 1.
11. Philp, D.; Stoddart, J. F. Self-Assembly in Natural and Unnatural Systems. *Angew. Chem. Int. Ed.* **1996**, *35*, 1154–1196.
12. Miyamoto, S.; Akiyama, S. K.; Yamada, K. M. Synergistic Roles for Receptor Occupancy and Aggregation in Integrin Transmembrane Function. *Science* **1995**, *267*, 883–885.
13. Kluza, E.; Schaft, D. W. J. van der; Hautvast, P. A. I.; Mulder, W. J. M.; Mayo, K. H.; Griffioen, A. W.; Strijkers, G. J.; Nicolay, K. Synergistic Targeting of Avβ3 Integrin and Galectin-1 with Heteromultivalent Paramagnetic Liposomes for Combined MR Imaging and Treatment of Angiogenesis. *Nano Lett.* **2010**, *10*, 52–58.
14. Englund, E. A.; Wang, D.; Fujigaki, H.; Sakai, H.; Micklitsch, C. M.; Ghirlando, R.; Martin-Manso, G.; Pendrak, M. L.; Roberts, D. D.; Durell, S. R. *et al.* Programmable Multivalent Display of Receptor Ligands Using Peptide Nucleic Acid Nanoscaffolds. *Nat Commun* **2012**, *3*, 614.
15. Müller, M. K.; Brunsveld, L. A Supramolecular Polymer as a Self-Assembling Polyvalent Scaffold. *Angew. Chem. Int. Ed.* **2009**, *48*, 2921–2924.
16. Müller, M. K.; Petkau, K.; Brunsveld, L. Protein Assembly Along a Supramolecular Wire. *Chem. Commun.* **2010**, 310–312.

17. Lee, Y. C.; Lee, R. T. Carbohydrate-Protein Interactions: Basis of Glycobiology. *Acc. Chem. Res.* **1995**, *28*, 321–327.
18. Corbell, J. B.; Lundquist, J. J.; Toone, E. J. A Comparison of Biological and Calorimetric Analyses of Multivalent Glycodendrimer Ligands for Concanavalin A. *Tetrahedron-Asymmetr.* **2000**, *11*, 95–111.
19. Kanai, M.; Mortell, K. H.; Kiessling, L. L. Varying the Size of Multivalent Ligands: The Dependence of Concanavalin A Binding on Neoglycopolymer Length. *J. Am. Chem. Soc.* **1997**, *119*, 9931–9932.
20. Disney, M. D.; Zheng, J.; Swager, T. M.; Seeberger, P. H. Detection of Bacteria with Carbohydrate-Functionalized Fluorescent Polymers. *J. Am. Chem. Soc.* **2004**, *126*, 13343–13346.
21. Bittiger, H.; Schnebli, H. P. *Concanavalin A as a Tool*; Wiley, 1976.
22. Kanellopoulos, P. N.; Pavlou, K.; Perrakis, A.; Agianian, B.; Vorgias, C. E.; Mavrommatis, C.; Soufi, M.; Tucker, P. A.; Hamodrakas, S. J. The Crystal Structure of the Complexes of Concanavalin A with 4′-Nitrophenyl-α-d-mannopyranoside and 4′-Nitrophenyl-α-d-glucopyranoside. *J. Struct. Biol.* **1996**, *116*, 345–355.
23. Lindhorst, T. K.; Kötter, S.; Kubisch, J.; Krallmann-Wenzel, U.; Ehlers, S.; Křen, V. Effect of p-Substitution of Aryl α-D-Mannosides on Inhibiting Mannose-Sensitive Adhesion of Escherichia Coli – Syntheses and Testing. *Eur. J. Org. Chem.* **1998**, *1998*, 1669–1674.
24. Due to restricted solubility the maximal measured concentrations for discotics did not exceed 500 μM and at this concentration the 1Mannose-Disc did not yet inhibit 50% of ConA-HRP binding, so that IC_{50} values can only be extrapolated.
25. Gestwicki, J. E.; Cairo, C. W.; Strong, L. E.; Oetjen, K. A.; Kiessling, L. L. Influencing Receptor−Ligand Binding Mechanisms with Multivalent Ligand Architecture. *J. Am. Chem. Soc.* **2002**, *124*, 14922–14933.
26. Cairo, C. W.; Gestwicki, J. E.; Kanai, M.; Kiessling, L. L. Control of Multivalent Interactions by Binding Epitope Density. *J. Am. Chem. Soc.* **2002**, *124*, 1615–1619.
27. Germain, R. N. T-cell Signaling: The Importance of Receptor Clustering. *Curr. Biol.* **1997**, *7*, R640–R644.
28. Pawson, T.; Nash, P. Assembly of Cell Regulatory Systems Through Protein Interaction Domains. *Science* **2003**, *300*, 445 –452.
29. Taipale, J.; Keski-Oja, J. Growth Factors in the Extracellular Matrix. *FASEB J* **1997**, *11*, 51–59.
30. Pollard, T. D.; Cooper, J. A. Actin, a Central Player in Cell Shape and Movement. *Science* **2009**, *326*, 1208 –1212.
31. Eisenberg, D.; Nelson, R.; Sawaya, M. R.; Balbirnie, M.; Sambashivan, S.; Ivanova, M. I.; Madsen, A. Ø.; Riekel, C. The Structural Biology of Protein Aggregation Diseases: Fundamental Questions and Some Answers. *Acc. Chem. Res.* **2006**, *39*, 568–575.
32. Scheibel, T. Protein Fibers as Performance Proteins: New Technologies and Applications. *Curr. Opin. Biotech.* **2005**, *16*, 427–433.
33. Patolsky, F.; Weizmann, Y.; Willner, I. Actin-based Metallic Nanowires as Bio-nanotransporters. *Nat Mater* **2004**, *3*, 692–695.
34. Michael Green, N. [5] Avidin and streptavidin. In *Avidin-Biotin Technology*; Academic Press, **1990**; Vol. 184, pp. 51–67.
35. Sano, T.; Cantor, C. R. Intersubunit Contacts Made by Tryptophan 120 with Biotin Are Essential for Both Strong Biotin Binding and Biotin-induced Tighter Subunit Association of Streptavidin. *PNAS* **1995**, *92*, 3180–3184.
36. Qureshi, M. H.; Wong, S.-L. Design, Production, and Characterization of a Monomeric Streptavidin and Its Application for Affinity Purification of Biotinylated Proteins. *Protein Express. Purif.* **2002**, *25*, 409–415.
37. Howarth, M.; Chinnapen, D. J.-F.; Gerrow, K.; Dorrestein, P. C.; Grandy, M. R.; Kelleher, N. L.; El-Husseini, A.; Ting, A. Y. A Monovalent Streptavidin with a Single Femtomolar Biotin Binding Site. *Nat Meth* **2006**, *3*, 267–273.
38. Howarth, M.; Ting, A. Y. Monovalent Streptavidin Expression and Purification. *Nat Protoc* **2008**, *10.1038/nprot.2008.81*.
39. Expression, purification and labeling of mSA was performed by Michael Sonntag and Alexander Colditz. The plasmids for the "dead"- and "alive"-subunit were obtained from A.Y. Ting (MIT).

40. Lakowicz, J. R. *Principles of Fluorescence Spectroscopy*; Springer, **2006**.
41. Maurel, D.; Comps-Agrar, L.; Brock, C.; Rives, M.-L.; Bourrier, E.; Ayoub, M. A.; Bazin, H.; Tinel, N.; Durroux, T.; Prezeau, L. *et al.* Cell-surface Protein-protein Interaction Analysis with Time-resolved FRET and Snap-tag Technologies: Application to GPCR Oligomerization. *Nat Meth* **2008**, *5*, 561–567.
42. Huebsch, N. D.; Mooney, D. J. Fluorescent Resonance Energy Transfer: A Tool for Probing Molecular Cell-biomaterial Interactions in Three Dimensions. *Biomaterials* **2007**, *28*, 2424–2437.
43. VanVeller, B.; Swager, T. M. Biocompatible Post-polymerization Functionalization of a Water Soluble Poly(p-phenylene Ethynylene). *Chem. Commun.* **2010**, 5761–5763.
44. Shapiro, A. L.; Viñuela, E.; Maizel Jr., J. V. Molecular Weight Estimation of Polypeptide Chains by Electrophoresis in SDS-polyacrylamide Gels. *Biochem. Bioph. Res. Co.* **1967**, *28*, 815–820.
45. Petkau-Milroy, K.; Uhlenheuer, D. A.; Spiering, A. J. H.; Vekemans, J. A. J. M.; Brunsveld, L. Dynamic Protein Assembly Through Site-Selective Attachment and Display on a Supramolecular Wire. *submitted*.
46. Besenius, P.; Goedegebure, Y.; Driesse, M.; Koay, M.; Bomans, P. H. H.; Palmans, A. R. A.; Dankers, P. Y. W.; Meijer, E. W. Peptide Functionalised Discotic Amphiphiles and Their Self-assembly into Supramolecular Nanofibres. *Soft Matter* **2011**, *7*, 7980–7983.
47. Gasiorowski, J. Z.; Collier, J. H. Directed Intermixing in Multicomponent Self-Assembling Biomaterials. *Biomacromolecules* **2011**, *12*, 3549–3558.
48. Webber, M. J.; Tongers, J.; Newcomb, C. J.; Marquardt, K.-T.; Bauersachs, J.; Losordo, D. W.; Stupp, S. I. Supramolecular Nanostructures That Mimic VEGF as a Strategy for Ischemic Tissue Repair. *PNAS* **2011**, *108*, 13438 –13443.
49. Tysseling-Mattiace, V. M.; Sahni, V.; Niece, K. L.; Birch, D.; Czeisler, C.; Fehlings, M. G.; Stupp, S. I.; Kessler, J. A. Self-Assembling Nanofibers Inhibit Glial Scar Formation and Promote Axon Elongation After Spinal Cord Injury. *J. Neurosci* **2008**, *28*, 3814–3823.
50. Mahmoud, Z. N.; Gunnoo, S. B.; Thomson, A. R.; Fletcher, J. M.; Woolfson, D. N. Bioorthogonal Dual Functionalization of Self-assembling Peptide Fibers. *Biomaterials* **2011**, *32*, 3712–3720.
51. See chapter 4.
52. Gouin, S. G.; Vanquelef, E.; García Fernández, J. M.; Ortiz Mellet, C.; Dupradeau, F.-Y.; Kovensky, J. Multi-Mannosides Based on a Carbohydrate Scaffold: Synthesis, Force Field Development, Molecular Dynamics Studies, and Binding Affinities for Lectin Con A. *J. Org. Chem.* **2007**, *72*, 9032–9045.

4

Dynamic protein assembly on a supramolecular polymer

Abstract. Dynamic protein assembly on supramolecular columnar wires is achieved through site-specific covalent conjugation of fluorescent proteins fused to a SNAP-tag to monovalent O^6-benzylguanine bearing self-assembling discotics. The covalent protein conjugation, confirmed with several analytical techniques such as SDS-PAGE and LC-MS, leads to Förster resonance energy transfer (FRET) from the auto-fluorescent discotic scaffold to the yellow fluorescent protein (YFP) and allows on-line monitoring of the conjugation. At the same time the protein conjugation does not interfere with the self-assembling process, leading to a multivalent protein display on a supramolecular wire, as visualized via FRET from CFP to YFP. The system maintains its intermixing dynamics, which allows the formation of hetero-functionalized supramolecular protein-conjugated polymers through exchange of the protein-functionalized discotics over time.

K. Petkau-Milroy, D.A. Uhlenheuer, A.J.H. Spiering, Jef A. J. M. Vekemans, Luc Brunsveld, *submitted*

4.1 Introduction

Supramolecular assembly of proteins in cells and on their membranes controls a diversity of biological processes such as gene transcription or signal transduction.[1–4] This has inspired researchers to create similar artificial architectures using next to small molecules[5–7] a wide range of dendritic[8–10] and polymeric[11–14] scaffolds. Nature, in contrast, brings proteins together on dynamic supramolecular platforms. Therefore, synthetic systems which similarly provide a dynamic framework for protein assembly are needed. Such systems will provide entry to architectures with dynamic properties and functions alike their biologically inspired counterparts.

Due to their responsive nature, supramolecular assemblies offer a promising synthetic platform for bridging the gap to the dynamic biological systems.[15] Ease of assembly, tunability and the potential to incorporate multiple copies of different active units are further advantages of self-assembled systems ranging from micellar-like architectures to completely synthetic nanostructures.[16–21] Recently, a class of auto-fluorescent C_3-symmetrical amphiphilic discotics which spontaneously assemble into supramolecular columnar stacks in water[22] and can be functionalized with different biological ligands which bind to target proteins was reported.[23,24] This class of molecules opens up the opportunity to generate synthetic biological architectures for dynamic protein display. Herein a mono-functionalized oligo(ethylene oxide)-decorated discotic molecule, equipped with one O^6-benzylguanine moiety is used (Figure 4.1 a). This discotic molecule allows for site-specific, monovalent, and covalent protein conjugation, in contrast to protein attachment via multiple-site ligand-receptor interactions, for example of the biotin-avidin type.[6,11,25,26] Two fluorescent proteins (yellow and cyan fluorescent protein) are separately attached to the monovalent discotic scaffold (Figure 4.1 b). These supramolecular protein conjugates self-assemble into supramolecular wires displaying proteins on their periphery. This bioinspired synthetic architecture acts as a dynamic platform, allowing fluorescent proteins to come together and exchange position, resulting in optimized energy transfer (Figure 4.1 c), alike protein assembly on biological counterparts.

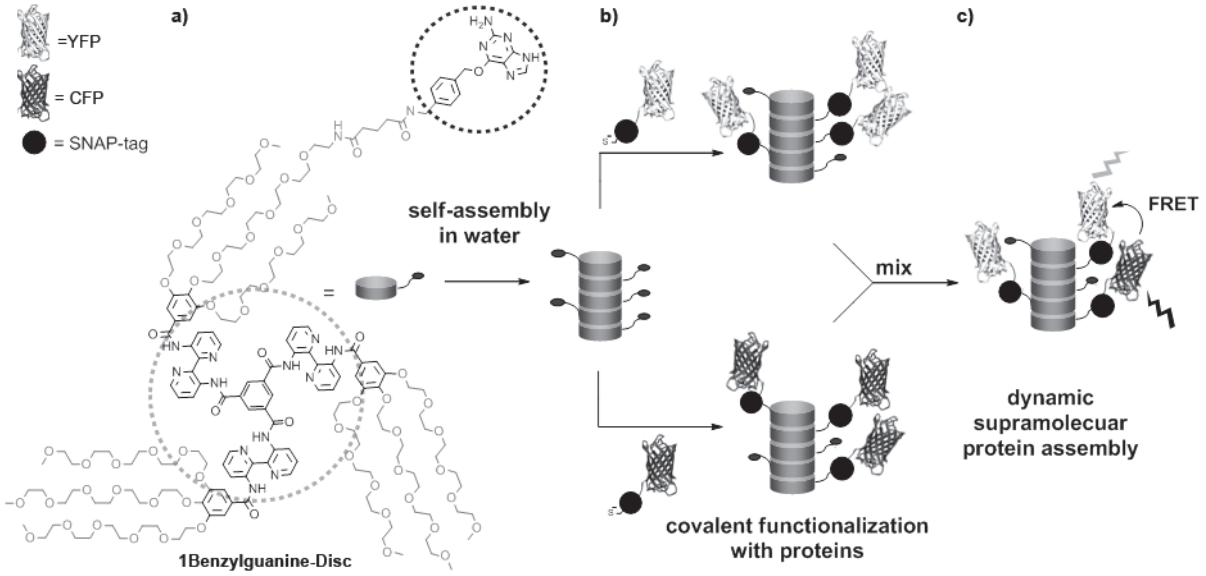

Figure 4.1: a) Structure of the monofunctional discotic (**1Benzylguanine-Disc**) carrying a single *O*^{6}-benzylguanine moiety for conjugation to SNAP-tag fusion proteins. In water these discotics self-assemble to form auto-fluorescent columnar stacks, displaying moieties for conjugation at their periphery. b) Site-selective covalent functionalization of the supramolecular polymer with cyan and yellow fluorescent protein (CFP and YFP) fused to a SNAP-tag. c) The dynamic intermixing of protein-functionalized supramolecular polymers leads to reassembly bringing the two different proteins into close proximity, resulting in Förster resonance energy transfer (FRET).

4.2 Results and Discussion

4.2.1 *Design and Synthesis*

The synthesis of the **1Benzylguanine-Disc** is described in chapter 2. Briefly, *O*^{6}-(4-glutaryl-amidomethyl)-benzylguanine[27] was in situ activated with HBTU and reacted with the monovalent **1NH$_2$-Disc**. Introduction of a single reactive protein ligation site into the discotic scaffold was envisaged to reduce the steric crowding during the ligation and to enable detailed studies on the exchange of discotic monomers using FRET.

4.2.2 *Functionalization of discotics with fluorescent proteins*

The specific reaction of *O*^{6}-benzylguanine with the SNAP-tag, a genetically encoded protein tag developed by K. Johnsson and co-workers which can be fused to the protein of interest[28], provides an entry for site-selective covalent attachment of proteins to **1Benzylguanine-Disc**. The 21 kDa SNAP-tag irreversibly transfers the alkyl group from *O*^{6}-benzylguanine derivatives carrying a ligand of interest,[29] in this case the disc, to one of its cysteine residues resulting in covalent linkage between the SNAP-tag and disc. Besides labeling purified SNAP-tag fusion

proteins, this genetically encoded tag can as well be used for cell-surface[30] and intracellular labeling[31] allowing future intracellular applications.

Both yellow and cyan fluorescent protein were expressed and purified as SNAP-tag fusion proteins (YFP-SNAP and CFP-SNAP respectively).[32] The proteins were conjugated to **1Benzylguanine-Disc** in phosphate buffer at 37 °C and at micromolar concentrations. The auto-fluorescence of the discotics (λ_{exc}=340 nm, λ_{em}=510 nm, dashed line in Figure 4.2 a) makes these supramolecular polymers ideal FRET donors for the YFP protein (λ_{exc}=500 nm) and allows on-line monitoring of the functionalization of **1Benzylguanine-Disc**.[32,33] Fluorescence spectroscopy measurements revealed an increase of the YFP emission at 527 nm during the protein conjugation reaction (Figure 4.2). Incubation of YFP-SNAP with **Inert-Disc**[34], showed no appearance of FRET. These results strongly indicate that the observed energy transfer in case of the **1Benzylguanine-Disc** with SNAP-YFP is specifically due to the covalent protein attachment.

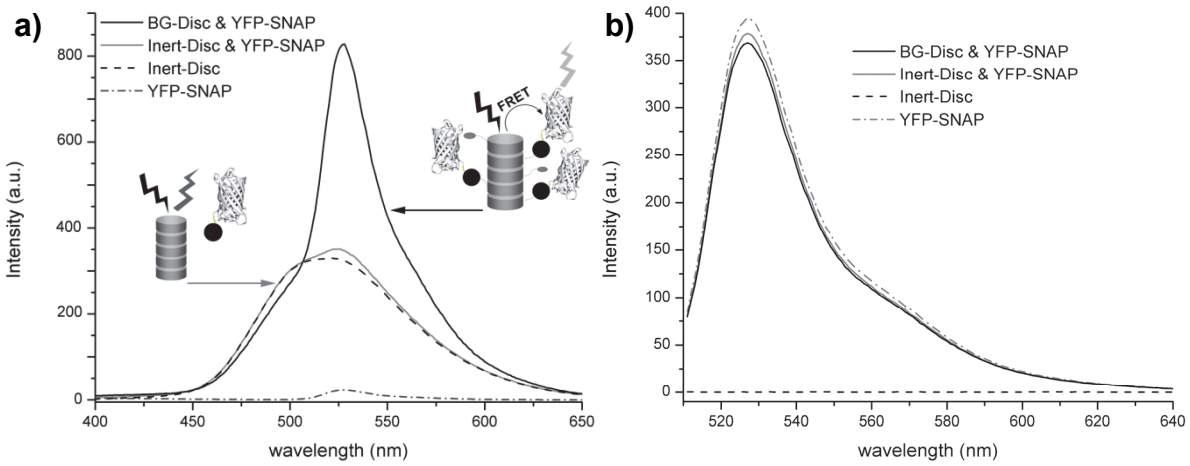

Figure 4.2: a) Fluorescence emission spectra (λ_{exc} = 340 nm) of YFP-SNAP (dash-dot), **Inert-Disc** (dashed), a mixture of YFP-SNAP and **Inert-Disc** (gray) and of a mixture of YFP-SNAP and **1Benzylguanine-Disc** (black) after 3 hours of ligation at 37 °C. Concentration of YFP-SNAP is 1 μM and of discotics 20 μM. b) The same four samples after 3 hours of ligation at 37 °C excited at 500 nm, the excitation wavelength of YFP, showing the equal concentration of the YFP-SNAP protein present and no excitation of the discotics at this wavelength.

The conjugation of the discotic to both YFP-SNAP and CFP-SNAP was also analyzed by SDS-PAGE and LC-MS, confirming covalent attachment of the protein to the discotic. The SDS gel of a ligation mixture shows the two bands of both ligated and non-ligated protein. Only the band with higher molecular weight features fluorescence when excited at 350 nm, resulting from the conjugated **1Benzylguanine-Disc** (Figure 4.3). Two protein peaks can as well be observed with LC-MS corresponding to ligated and non-ligated protein (Figure 4.4, retention time of 6.75 and 6.25 minutes respectively).

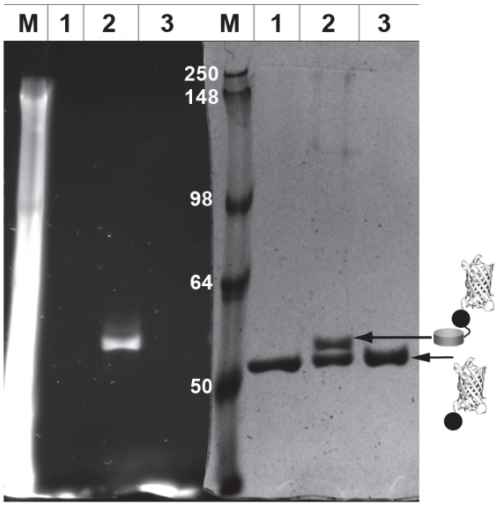

Figure 4.3: SDS-PAGE of YFP-SNAP (1), YFP-SNAP and **1Benzylguanine-Disc** (2), YFP-SNAP and **Inert-Disc** (3) after incubation for 3 h at 37 °C. Left: UV illumination (350 nm), right: Coomassie blue staining, M = marker.

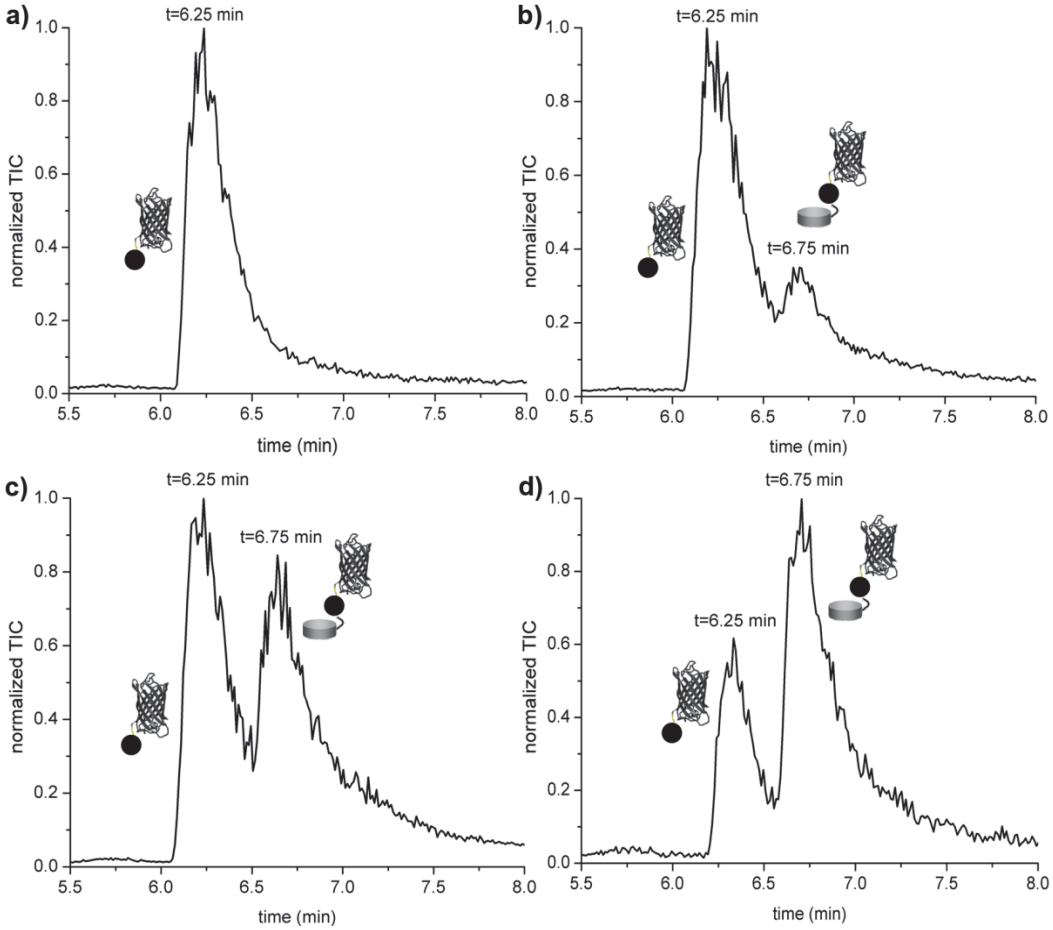

Figure 4.4: LC-MS spectra of the CFP-SNAP protein alone (a, R_t = 6.25 min) and the CFP-SNAP (10 μM) protein ligated with 1 equiv. (b), 3 equiv. (c) and 10 equiv. (d) of **1Benzylguanine-Disc** after 3 hours of ligation at 37 °C.

Further, the ligation was performed in presence of increasing concentration of **1Benzylguanine-Disc** to study if complete functionalization of proteins with discotics can be achieved (Figure 4.4). A protein conjugation reaction with a 10-fold excess of **1Benzylguanine-Disc** resulted in a maximum conversion leading to approximately 60 % of the protein conjugated to the discotics. A larger excess of the **1Benzylguanine-Disc** or longer reaction times did not lead to an enhanced functionalization. Considering the 50 kDa mass of the protein and the 3.5 kDa mass of the discotics, a highly protein-decorated supramolecular assembly is obtained, which most probably controls the partial functionalization of the discotics.

4.2.3 *Inducing protein-protein interactions*

Display of multiple proteins on the supramolecular wire was investigated via simultaneous conjugation with the YFP/CFP FRET-pair. At 410 nm the CFP protein can be selectively excited over the discotics and YFP (Figure 4.5).

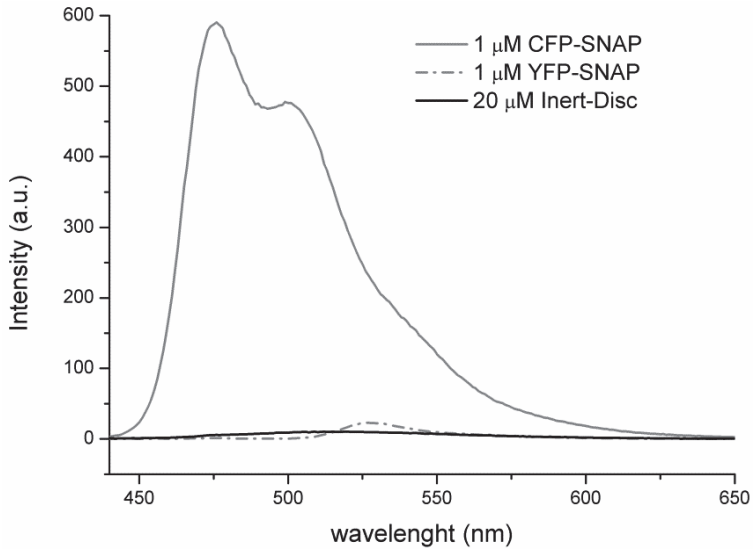

Figure 4.5: Fluorescence emission spectra (λ_{ex} = 410 nm) of 1 μM CFP-SNAP (gray), 1 μM YFP-SNAP (gray, dash-dot) and of 20 μM **Inert-Disc** (black) at 20°C. Excitation wavelength is 410 nm, the excitation wavelength for CFP. At this wavelength only negligible excitation of YFP-SNAP (gray, dash-dot) and hardly any excitation of the **Inert-Disc** (black) is observed.

Only when CFP is in close proximity to YFP the excited-state energy of CFP is transferred to YFP, resulting in an increase in fluorescence intensity at 527 nm, the emission wavelength of YFP, and a decrease at 475 nm, the emission wavelength of CFP. A 1:1 mixture of YFP-SNAP and CFP-SNAP was added to the **1Benzylguanine-Disc** and as control to the **Inert-Disc**. After 3 h incubation at 37 °C, only the mixture with **1Benzylguanine-Disc** showed energy transfer from CFP to YFP, resulting in a I_{527nm}/I_{475nm} ratio of 0.65 (Figure 4.6). The control mixture with **Inert-Disc** featured only CFP fluorescence, with an I_{527nm}/I_{475nm} ratio of 0.48. These results show that the monovalent protein-discotic conjugates self-assemble into supramolecular wires on which

different proteins can interact with each other. The close proximity of the proteins on the supramolecular framework leads to the occurrence of efficient energy transfer.[35]

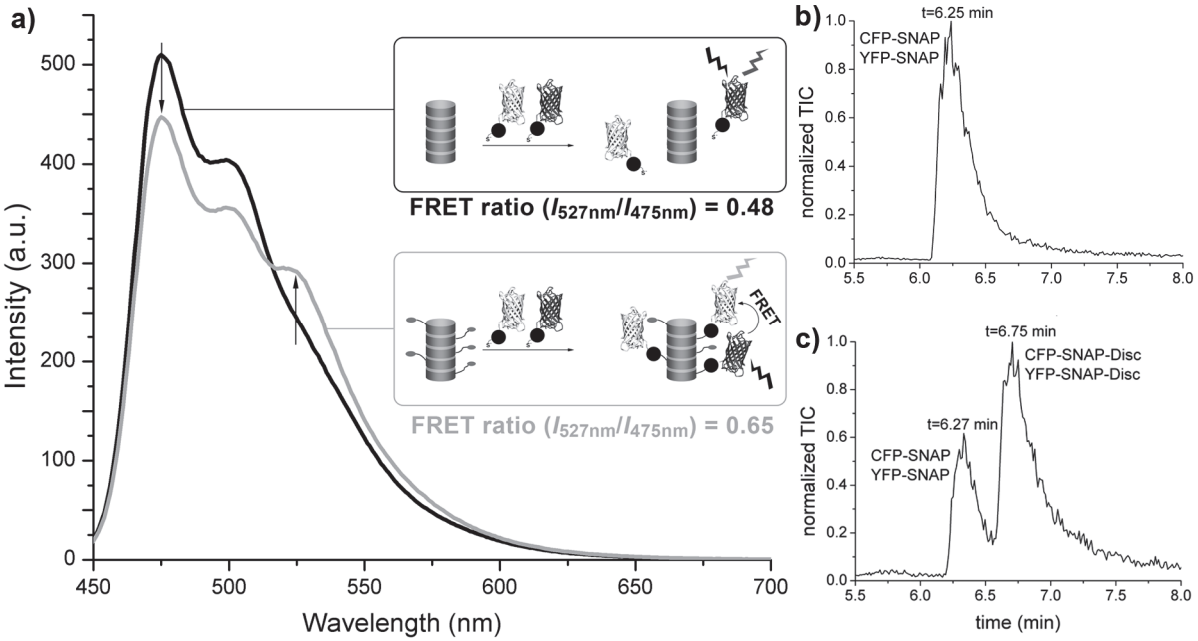

Figure 4.6: a) Fluorescence emission spectra (λ_{exc} = 410 nm) of 1:1 mixtures of YFP-SNAP (1 μM) and CFP-SNAP (1 μM) reacted for 3 h at 37°C with either the **1Benzylguanine-Disc** (20 μM; gray trace) or **Inert-Disc** (20 μM; black trace). The black trace corresponds to the experiment depicted in the black box; the gray trace represents the experiment depicted in the gray box. b) LC-MS spectrum of the ligation of a 1:1 mixture of CFP-SNAP and YFP-SNAP with the **Inert-Disc** after 3 h at 37 °C. c) LC-MS spectrum of the ligation of a 1:1 mixture of CFP-SNAP and YFP-SNAP with **1Benzylguanine-Disc** after 3 h at 37 °C. The concentration of both discotics was 200 μM and 10 μM of each protein was added for the ligation. Deconvoluting the LC-MS spectra confirmed that both proteins were ligated to the **1Benzylguanine-Disc** at nearly equal amounts (see experimental section, Table S1).

4.2.4 *Dynamic intermixing*

To investigate the dynamic monomer exchange of this supramolecular protein-decorated polymer, YFP and CFP were first each conjugated separately to **1Benzylguanine-Disc**, and subsequently these solutions were mixed (concept, see Figure 4.1 c). Any non-ligated protein was blocked after 3 hours using an excess of O^6-(4-glutaryl-amidomethyl)-benzylguanine. As a control the same mixtures were again prepared with **Inert-Disc**. The appearance of FRET, due to exchange of protein-conjugated discotics between the assemblies, was followed over time (Figure 4.7). The intermixing will bring the two different proteins in close proximity, which can be visualized with FRET.

Indeed, a time-dependent increase in FRET is observed when mixing **1Benzylguanine-Disc** conjugated to CFP with **1Benzylguanine-Disc** conjugated to YFP. This evidences that the discotics decorated with large proteins are capable of intermixing between the different

supramolecular protein wires. The control mixture containing the **Inert-Disc** and the proteins does not feature any FRET, indicating that energy transfer because of dynamic intermixing requires covalent attachment of the proteins to the supramolecular columns.

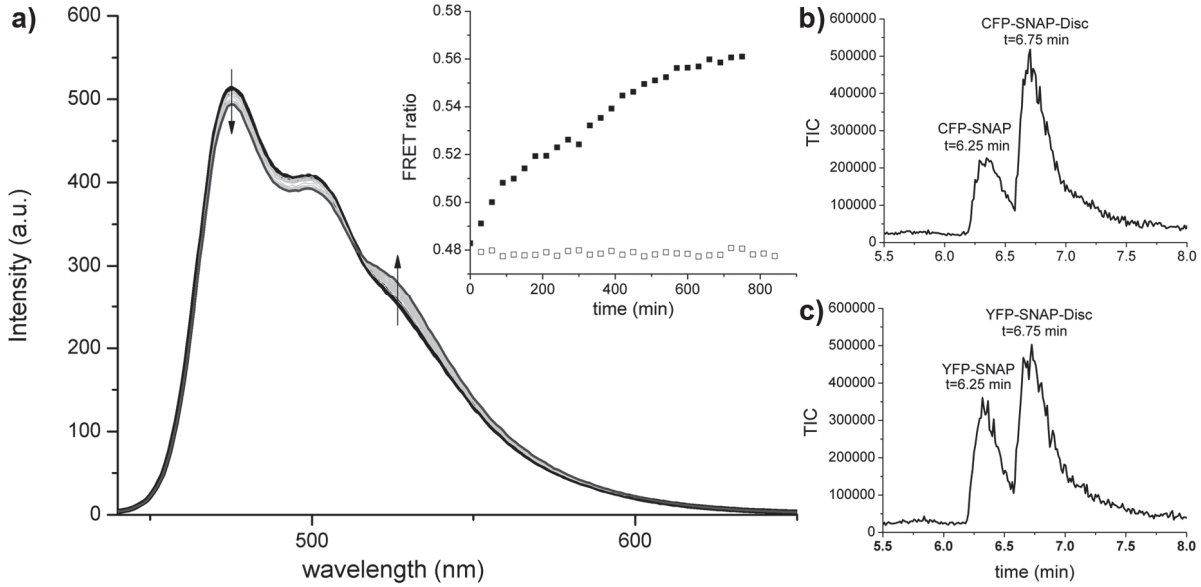

Figure 4.7: a) Fluorescence emission spectra (λ_{exc}= 410 nm) over the time course of 12 h of a 1:1 mixture of two protein-discotic mixtures consisting of YFP-SNAP and **1Benzylguanine-Disc** and of CFP-SNAP and **1Benzylguanine-Disc**; t = 0 min (black), t = 750 min (dark gray). The ligation reactions were incubated for 3 h at 37 °C before mixing. Inset: FRET ratio ($I_{527\ nm}/I_{475\ nm}$) over the time course of 12 h of a 1:1 mixture of two protein-discotic mixtures consisting of YFP-SNAP and **1Benzylguanine-Disc** and of CFP-SNAP and **1Benzylguanine-Disc** (■); and of the 1:1 mixture of CFP-SNAP with **Inert-Disc** and YFP-SNAP with **Inert-Disc** (□), (λ_{exc} = 410 nm). The intermixing of different protein-functionalized stacks leads to a heterovalent supramolecular polymer containing both, CFP and YFP, resulting in an increase in FRET ratio over time in case of proteins conjugated to **1Benzylguanine-Disc**. b) LC-MS spectrum of the ligation of **1Benzylguanine-Disc** with CFP-SNAP after 3 h at 37 °C just before mixing. c) LC-MS spectrum of the ligation of **1Benzylguanine-Disc** with YFP-SNAP after 3 h at 37 °C just before mixing. The concentration of the **1Benzylguanine-Disc** is 100 μM and the concentration of the corresponding protein is 10 μM.

4.3 Conclusions

The functionalization of the **1NH$_2$-Disc** with O^6-benzylguanine provides access to monovalent discotic molecules with functionalities for protein conjugation, which self-assemble into supramolecular wires in water. This supramolecular system allows for site-specific covalent conjugation of fluorescent proteins to the columnar wires, which results in energy transfer from the fluorescent discotic building blocks to the YFP proteins. The protein conjugation to the discotics seems not to interfere with the discotic self-assembly, but rather enables the self-assembly process to bring fluorescent proteins into close proximity on the supramolecular wire.

In case of attaching two different proteins to the intrinsically monovalent discotics, the supramolecular wires act as dynamic framework on which these different proteins can assemble and exchange in a dynamic manner, leading to effective protein interactions, as observed by FRET. The self-assembled protein-conjugated discotics are still capable of intermixing, which allows the formation of hetero-functionalized supramolecular protein-conjugated polymers via simple mixing of building blocks. We envision that this synthetic supramolecular architecture enables to bridge the gap between synthetic and biological architectures, allowing to create dynamic multivalent systems with a responsive nature.

4.4 Experimental

The synthesis of all discotics used is described in chapter 2. CFP-SNAP and YFP-SNAP proteins were expressed and purified as described elsewhere.[32]

General LC-MS analysis: samples were analyzed using a Shimadzu SCL-10 AD VP series HPLC coupled to a diode array detector (Finnigan Surveyor PDA Plus detector, Thermo Electron Corporation) and an Ion-Trap (LCQ Fleet, Thermo Scientific). Analyses were performed using a reversed phase HPLC column (C4 Jupiter, 150 x 2 mm, 5 μm), using an injection volume of 1-4 μL, a flow rate of 0.20 mL/min and typically a gradient (20% to 90% in 10 min, held at 90% for 1 more minute) of acetonitrile in water (both containing 0.1% formic acid) at 298K. Prior to LC-MS the protein samples have been desalted using DyeEx 2.0 Spin Columns (Qiagen). Deconvolution of mass spectra was performed using the ProMassXcali software. Protein concentrations were measured with NanoDrop V3.5.2 using A515 and a molar extinction coefficient of 84 000 $M^{-1}cm^{-1}$ for YFP-SNAP[36] and A435 and a molar extinction coefficient of 32 5000 $M^{-1}cm^{-1}$ for CFP-SNAP[37].

Fluorescence spectra were recorded on a Varian Cary Eclipse photoluminescence spectrometer equipped with a Perkin–Elmer PTP-1 Peltier temperature control system. All fluorescence measurements were performed in phosphate buffer (25 mM, pH 7.5 containing 50 mM NaCl) in quartz cuvettes of 10 mm light path (Hellma) and 2 mL minimal volume at 20°C. Samples were excited at 410 nm for CFP, 500 nm for YFP or 340 nm for the discotics. The FRET ratio (YFP/CFP) was calculated by dividing the emission of YFP at 527 nm and the emission of CFP at 475 nm. The change in FRET ratio is defined as the difference between the FRET ratio at a later measuring point and the FRET ratio at the beginning.

Ligation of a 1:1 mixture of CFP-SNAP and YFP-SNAP with **1Benzylguanine-Disc** or **Inert-Disc**:

Final volume of ligation reaction was 420 μL, containing 100 μM **1Benzylguanine-Disc** and a 1:1 mixture of 5 μM CFP-SNAP and 5 μM YFP-SNAP. After 3 h of shaking at 37°C the reaction was stopped through addition of a large excess of *O*^{6}-(4-glutaryl-amidomethyl)-benzylguanine. 400 μL of this ligation reaction was diluted with 1600 μL of buffer to have a final volume of 2 mL and a final concentration of 20 μM of **1Benzylguanine-Disc** and 1 μM of each protein. Under the same conditions the 1:1 mixture of 5 μM CFP-SNAP and 5 μM YFP-SNAP was ligated to the **Inert-Disc** (100 μM). The fluorescence spectra were measured at the excitation wavelength of 410 nm at 20°C (Figure 4.6).

Table S1: Masses found after deconvoluting TIC traces of Figure 4.6 b&c.

	protein	$Mw_{decon.}$ (Da)	relative abundance (%)	R_t (min)
Ligation with **Inert Disc**	CFP-SNAP	49146	100	6.25 min
	YFP-SNAP	49233	98	
Ligation with **1Benzylguanine-Disc**	CFP-Disc	52666	77	6.75 min
	YFP-Disc	52767	100	

Ligation CFP-SNAP or YFP-SNAP with **1Benzylguanine-Disc** and subsequent mixing:

Final volume of ligation reaction was 210 μL, containing 100 μM **1Benzylguanine-Disc** and 10 μM CFP-SNAP. After 3 h of shaking at 37° C the reaction was stopped through addition of a large excess of O^6-(4-glutaryl-amidomethyl)-benzylguanine. Under the same conditions YFP-SNAP was ligated to **1Benzylguanine-Disc**. 200 μL of each ligation reaction were mixed and diluted with 1600 μL of buffer to have a final volume of 2 mL and a final concentration of 20 μM of **1Benzylguanine-Disc** and 1 μM of each protein. Using the remaining 10 μL the conversion of the ligation was monitored with LC-MS (Figure 4.7 b&c). The fluorescence spectra were measured every 30 minutes over the course of 12.5 h at 20°C at the excitation wavelength of 410 nm (Figure 4.7 a).

4.5 References

1. Pawson, T.; Nash, P. Assembly of Cell Regulatory Systems Through Protein Interaction Domains. *Science* **2003**, *300*, 445 –452.
2. Kueh, H. Y.; Mitchison, T. J. Structural Plasticity in Actin and Tubulin Polymer Dynamics. *Science* **2009**, *325*, 960 –963.
3. Borukhov, S.; Nudler, E. RNA Polymerase: The Vehicle of Transcription. *Trends Microbiol.* **2008**, *16*, 126–134.
4. Finnigan, G. C.; Hanson-Smith, V.; Stevens, T. H.; Thornton, J. W. Evolution of Increased Complexity in a Molecular Machine. *Nature* **2012**, *481*, 360–364.
5. Fegan, A.; White, B.; Carlson, J. C. T.; Wagner, C. R. Chemically Controlled Protein Assembly: Techniques and Applications. *Chem. Rev.* **2010**, *110*, 3315–3336.
6. Ringler, P.; Schulz, G. E. Self-Assembly of Proteins into Designed Networks. *Science* **2003**, *302*, 106-109.
7. Burazerovic, S.; Gradinaru, J.; Pierron, J.; Ward, T. R. Hierarchical Self-Assembly of One-Dimensional Streptavidin Bundles as a Collagen Mimetic for the Biomineralization of Calcite. *Angew. Chem. Int. Ed.* **2007**, *46*, 5510–5514.
8. Kluger, R.; Zhang, J. Hemoglobin Dendrimers: Functional Protein Clusters. *J. Am. Chem. Soc.* **2003**, *125*, 6070–6071.
9. Breurken, M.; Lempens, E. H. M.; Temming, R. P.; Helms, B. A.; Meijer, E. W.; Merkx, M. Collagen Targeting Using Multivalent Protein-functionalized Dendrimers. *Bioorg. Med. Chem.* **2011**, *19*, 1062–1071.
10. Hernández-Rocamora, V. M.; Reulen, S. W. A.; Waal, B. de; Meijer, E. W.; Sanz, J. M.; Merkx, M. Choline Dendrimers as Generic Scaffolds for the Non-covalent Synthesis of Multivalent Protein Assemblies. *Chem. Commun.* **2011**, 5997-5999.

11. Gac, S. Le; Schwartz, E.; Koepf, M.; Cornelissen, J. J. L. M.; Rowan, A. E.; Nolte, R. J. M. Cysteine-Containing Polyisocyanides as Versatile Nanoplatforms for Chromophoric and Bioscaffolding. *Chem. Eur. J.* **2010**, *16*, 6176–6186.
12. Boyer, C.; Bulmus, V.; Liu, J.; Davis, T. P.; Stenzel, M. H.; Barner-Kowollik, C. Well-Defined Protein−Polymer Conjugates via in Situ RAFT Polymerization. *J. Am. Chem. Soc.* **2007**, *129*, 7145–7154.
13. Heredia, K. L.; Bontempo, D.; Ly, T.; Byers, J. T.; Halstenberg, S.; Maynard, H. D. In Situ Preparation of Protein−"Smart" Polymer Conjugates with Retention of Bioactivity. *J. Am. Chem. Soc.* **2005**, *127*, 16955–16960.
14. Griffith, B. R.; Allen, B. L.; Rapraeger, A. C.; Kiessling, L. L. A Polymer Scaffold for Protein Oligomerization. *J. Am. Chem. Soc.* **2004**, *126*, 1608–1609.
15. Uhlenheuer, D. A.; Petkau, K.; Brunsveld, L. Combining Supramolecular Chemistry with Biology. *Chem. Soc. Rev.* **2010**, *39*, 2817-2826.
16. Stupp, S. I. Self-Assembly and Biomaterials. *Nano Lett.* **2010**, *10*, 4783-4786.
17. Besenius, P.; Goedegebure, Y.; Driesse, M.; Koay, M.; Bomans, P. H. H.; Palmans, A. R. A.; Dankers, P. Y. W.; Meijer, E. W. Peptide Functionalised Discotic Amphiphiles and Their Self-assembly into Supramolecular Nanofibres. *Soft Matter* **2011**, *7*, 7980–7983.
18. Gasiorowski, J. Z.; Collier, J. H. Directed Intermixing in Multicomponent Self-Assembling Biomaterials. *Biomacromolecules* **2011**, *12*, 3549–3558.
19. Reulen, S. W. A.; Dankers, P. Y. W.; Bomans, P. H. H.; Meijer, E. W.; Merkx, M. Collagen Targeting Using Protein-Functionalized Micelles: The Strength of Multiple Weak Interactions. *J. Am. Chem. Soc.* **2011**, *131*, 7304–7312.
20. Algar, W. R.; Prasuhn, D. E.; Stewart, M. H.; Jennings, T. L.; Blanco-Canosa, J. B.; Dawson, P. E.; Medintz, I. L. The Controlled Display of Biomolecules on Nanoparticles: A Challenge Suited to Bioorthogonal Chemistry. *Bioconjugate Chem.* **2011**, *22*, 825–858.
21. Kitagishi, H.; Kakikura, Y.; Yamaguchi, H.; Oohora, K.; Harada, A.; Hayashi, T. Self-Assembly of One- and Two-Dimensional Hemoprotein Systems by Polymerization Through Heme-Heme Pocket Interactions. *Angew. Chem. Int. Ed.* **2009**, *48*, 1271–1274.
22. Brunsveld, L.; Lohmeijer, B. G. G.; Vekemans, J. A. J. M.; Meijer, E. W. Chirality Amplification in Dynamic Helical Columns in Water. *Chem. Commun.* **2000**, 2305–2306.
23. Müller, M. K.; Brunsveld, L. A Supramolecular Polymer as a Self-Assembling Polyvalent Scaffold. *Angew. Chem. Int. Ed.* **2009**, *48*, 2921–2924.
24. Müller, M. K.; Petkau, K.; Brunsveld, L. Protein Assembly Along a Supramolecular Wire. *Chem. Commun.* **2010**, 310–312.
25. Mori, Y.; Minamihata, K.; Abe, H.; Goto, M.; Kamiya, N. Protein Assemblies by Site-specific Avidin–biotin Interactions. *Org. Biomol. Chem.* **2011**, *9*, 5641–5644.
26. Ma, M.; Bong, D. Protein Assembly Directed by Synthetic Molecular Recognition Motifs. *Org. Biomol. Chem.* **2011**, *9*, 7296–7299.
27. Lemercier, G.; Gendreizig, S.; Kindermann, M.; Johnsson, K. Inducing and Sensing Protein–Protein Interactions in Living Cells by Selective Cross-linking. *Angew. Chem. Int. Ed.* **2007**, *46*, 4281–4284.
28. Keppler, A.; Gendreizig, S.; Gronemeyer, T.; Pick, H.; Vogel, H.; Johnsson, K. A General Method for the Covalent Labeling of Fusion Proteins with Small Molecules in Vivo. *Nat Biotech* **2003**, *21*, 86–89.
29. Juillerat, A.; Gronemeyer, T.; Keppler, A.; Gendreizig, S.; Pick, H.; Vogel, H.; Johnsson, K. Directed Evolution of O^6-alkylguanine-DNA Alkyltransferase for Efficient Labeling of Fusion Proteins with Small Molecules in Vivo. *Chem. Biol.* **2003**, *10*, 313–317.
30. Maurel, D.; Comps-Agrar, L.; Brock, C.; Rives, M.-L.; Bourrier, E.; Ayoub, M. A.; Bazin, H.; Tinel, N.; Durroux, T.; Prezeau, L. *et al.* Cell-surface Protein-protein Interaction Analysis with Time-resolved FRET and Snap-tag Technologies: Application to GPCR Oligomerization. *Nat Meth* **2008**, *5*, 561–567.
31. Srikun, D.; Albers, A. E.; Nam, C. I.; Iavarone, A. T.; Chang, C. J. Organelle-Targetable Fluorescent Probes for Imaging Hydrogen Peroxide in Living Cells via SNAP-Tag Protein Labeling. *J. Am. Chem. Soc.* **2010**, *132*, 4455–4465.

32. Uhlenheuer, D. A. Supramolecular Control over Protein Assembly, Technische Universiteit Eindhoven, **2011**.
33. Petkau-Milroy, K.; Uhlenheuer, D. A.; Spiering, A. J. H.; Vekemans, J. A. J. M.; Brunsveld, L. Dynamic Protein Assembly Through Site-Selective Attachment and Display on a Supramolecular Wire. *submitted*.
34. For chemical structure of Inert-Disc see chapter 2.
35. Huebsch, N. D.; Mooney, D. J. Fluorescent Resonance Energy Transfer: A Tool for Probing Molecular Cell-biomaterial Interactions in Three Dimensions. *Biomaterials* **2007**, *28*, 2424–2437.
36. Patterson, G.; Day, R. N.; Piston, D. Fluorescent Protein Spectra. *J. Cell Sci.* **2001**, *114*, 837 –838.
37. Cubitt, A. B.; Woollenweber, L. A.; Heim, R. Understanding Structure-function Relationships in the Aequorea Victoria Green Fluorescent Protein. *Methods Cell Biol.* **1999**, *58*, 19–30.

5

Supramolecular polymers as dynamic multi-component cellular uptake carriers

Abstract. Supramolecular synthesis provides a flexible entry for the generation of dynamic multicomponent materials with tunable properties, as the supramolecular synthesis can generate heterovalent polymers with differing ligand composition by simple intermixing of a variety of discotic monomers. Here we show that these dynamic multi-component polymers provide rapid entry to novel materials of diverse compositions with cellular uptake properties. Discotics featuring several peripheral amine functionalities endow the supramolecular polymer with cellular uptake capabilities. Co-assembly with these cell-penetrating discotics enables the cellular uptake of other, non cell-permeable discotics, via co-transport by virtue of the supramolecular assembly. Dynamic multi-component and multi-functional supramolecular polymers represent a novel and unique platform for modular cellular uptake systems.

Adapted with permission from: K. Petkau-Milroy, M. H. Sonntag, A. H. A. M. van Onzen, L. Brunsveld, *J. Am. Chem. Soc.*, **2012,** DOI: 10.1021/ja3029075. Copyright (2012) American Chemical Society.

5.1 Introduction

The plasma membrane, a highly selectively permeable barrier, is essential to cell survival and function. At the same time, it presents a major challenge for intracellular delivery of cargo.[1] For example imaging agents, therapeutics, and reporter molecules require cellular internalization via crossing of the plasma membrane. Two strategies are generally applied to deliver cargos inside a cell: making use of a ligand-receptor interaction[2] or by functionalizing the cargo with cell-penetrating peptides (CPPs)[3,4]. A common feature of the in the late 80s discovered CPPs[5,6] is their high content of cationic amino acids such as arginine and lysine, which makes them highly positively charged. This positive charge favors binding to cell membrane associated proteoglycans leading to cellular uptake via endocytosis.[7,8] A peptidic scaffold is thereby not crucial as positively charged polyamine dendrimers[9,10], foldamers[11,12] and polymers[13,14] were shown similarly capable to cross the cell membrane. However, synthetic supramolecular polymers[15] haven't been explored as intracellular carriers, although their self-assembling nature provides highly appealing properties, due to their modular synthetic accessibility, as successfully shown for liposomal systems[16–18]. Dynamic and adaptable multifunctional and multivalent self-assembling scaffolds can be prepared conveniently without the need for repeated syntheses[19–21], as required for example for conventional polymers. We envisioned that non-covalent supramolecular synthesis of supramolecular polymers via a combination of cell-penetrating monomers and other non cell-permeable monomers, should allow cellular uptake of the complete intermixed system (Figure 5.1).

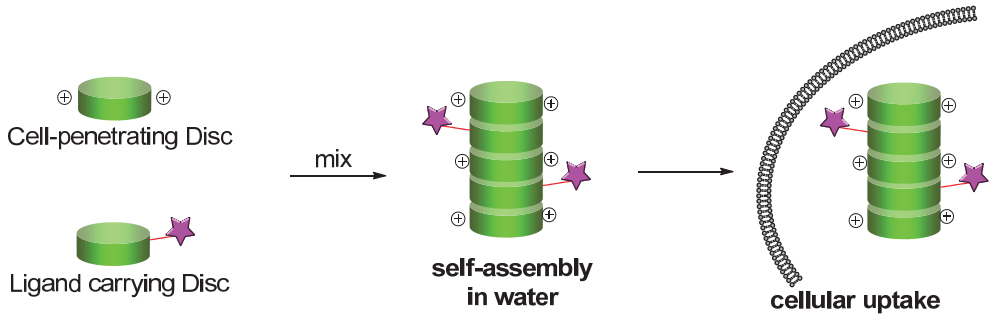

Figure 5.1: Concept of supramolecular cellular uptake carriers.

5.2 Results and Discussion

5.2.1 *Design and synthesis*

The supramolecular polymers used herein are C_3-symmetrical amphiphilic discotics, which self-assemble into columnar stacks at dilute micromolar concentrations in water.[22] The monomers consist of an aromatic core shielded by nine biocompatible and water soluble poly(ethylene)glycol (PEG) chains. Their self-assembly induces a strong auto-fluorescence with a large Stokes shift[23,24], practical for cellular imaging. At the periphery of these PEG chains different

functional groups can be introduced, for example as attachment points for bioactive ligands.[25,26] For this study we designed a library of discotics with diverse peripheral amine densities (**1NH$_2$-Disc**, **3NH$_2$-Disc, 9NH$_2$-Disc**, Figure 5.2) to enable cellular uptake. Together with intrinsically non-cell permeable discotic monomers, featuring either a single fluorescein fluorophore, or three biotins, or only inert glycol side-chains (**1Fluorescein-Disc**, **3Biotin-Disc**, **Inert-Disc**) a library of six supramolecular discotic monomers was synthesized (for synthesis see chapter 2).

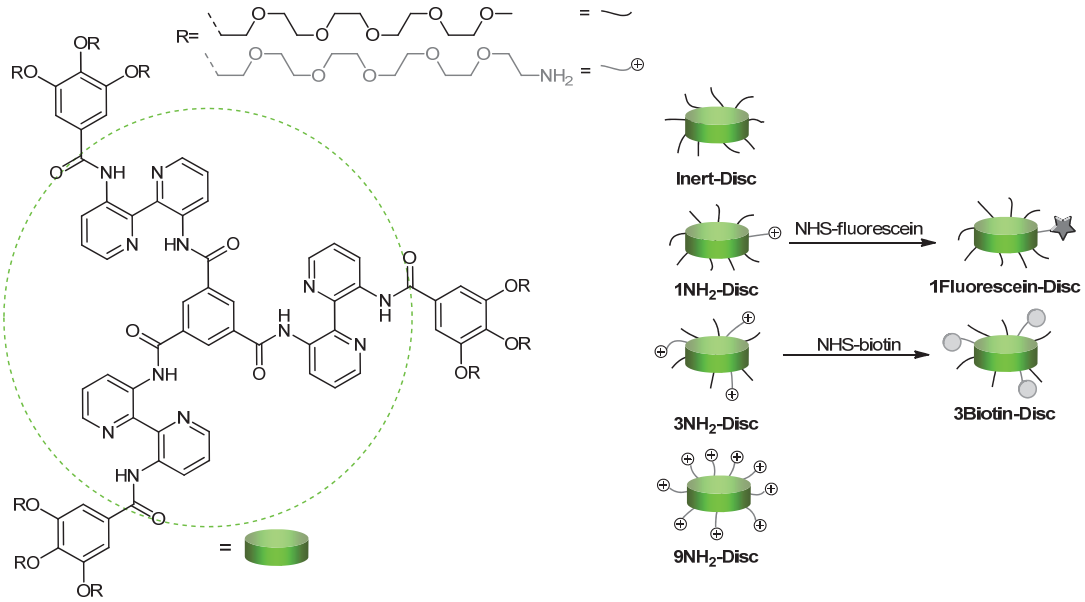

Figure 5.2: Library of discotics used in this chapter. For synthesis see chapter 2.

5.2.2 *Cellular uptake of poly-amine discotics*

The cellular uptake of four different supramolecular homopolymers, differing in amine content, was evaluated via multiphoton fluorescence microscopy using adherent HeLa cells. The multiphoton excitation with its highly localized excitation results in reduction of the out-of-plane background signal. At the same time, excitation using far-red wavelengths, here 760 nm, reduces photo-damage and facilitates imaging due to near-transparency of many tissues in this spectral range.[27,28] HeLa cells were incubated for 1 hour with different concentrations of **Inert-Disc**, **1NH$_2$-Disc**, **3NH$_2$-Disc** and **9NH$_2$-Disc** and imaged after washing. Even at high concentrations (5 μM) no uptake could be observed for the **Inert-** and **1NH$_2$-Disc**, in line with the inert nature / low number of amines of these discotics. The cells incubated with **3NH$_2$-** and **9NH$_2$-Discs**, however, featured discotic fluorescence even at concentrations as low as 0.5 μM (Figure 5.3). The effectiveness of the cellular uptake did not significantly differ for the **3NH$_2$-** and the **9NH$_2$-Disc** at the concentration range from 0.5 μM to 10 μM.

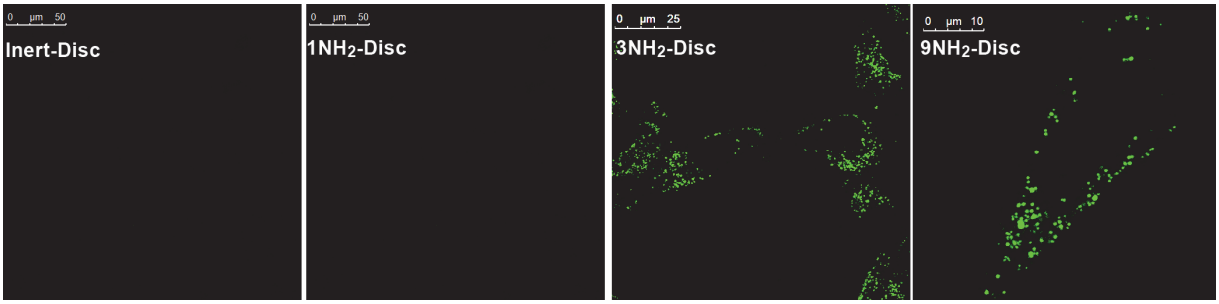

Figure 5.3: Confocal microscopy images of the cellular uptake of **Inert-**, **1NH$_2$-**, **3NH$_2$-**, and **9NH$_2$-Discs** (all 5 µM) by HeLa cells.

At first glance the cellular uptake of the **3NH$_2$-Disc** might look surprising, as the discotic molecule itself only displays three positive charges. However, the self-assembly into columnar stacks increases the density of charges on the periphery of the supramolecular polymers. This is in accordance with literature, where a systematic study performed with poly-arginine peptides revealed a minimum of 7-8 arginines for cellular uptake[29,30] whereas, when presented on self-assembling vesicles, 3 arginines were as effective as the natural Tat sequence.[31] The supramolecular assembly thus allows for the generation of an overall high density of positive charges and effective cellular uptake, even using discotic monomers featuring a low number of amines.

The toxicity of these supramolecular homopolymers (0.5 µM to 25 µM) on the growth of the HeLa cells was evaluated using the MTT assay, a standard colorimetric assay for measuring mitochondrial activity (Figure 5.4).The discotic scaffold itself (**Inert-Disc**) shows no toxicity, probably due to the shielding of the aromatic core by the non-toxic biocompatible PEGs.[32–34] In agreement with literature the cell viability decreases with the increased amount of charges.[35,36] However, the cell viability decrease is very modest and at 5 µM, the concentration used for all further experiments, no toxic effects were observed, showing the potential of the scaffold for biological applications.

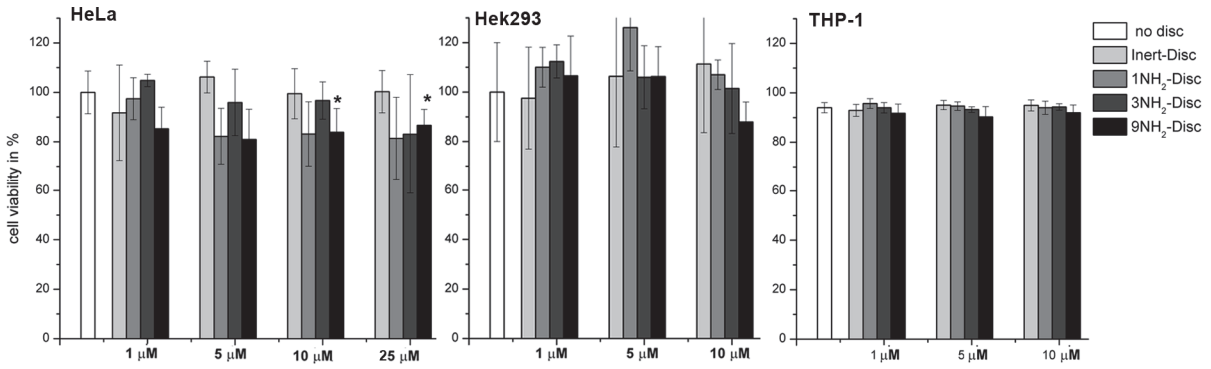

Figure 5.4: Cell viability of HeLa and Hek293 cells after incubation for 1 hour with different concentrations of different discotics determined using the MTT assay. Cell viability of THP-1 cells incubated for 1 hour with different concentrations of different discotics measured with the Guava easyCyte 8HT Base System.

The cellular uptake of the supramolecular polymers and their potential cytotoxicity has been further investigated with two additional cell-lines: Hek293 and one difficult to transfect suspension cell line, THP-1. Both cell lines showed similar effective uptake results and low toxicity as observed for the HeLa cells (Figure 5.4 and Figure S 5.1-S 5.2). These results underline the general cellular applicability of the supramolecular polymers.

To determine the subcellular localization of the supramolecular polymers, time-lapse confocal microscopy was performed (Figure 5.5 a). Within the first 5 minutes the **3NH$_2$-** and **9NH$_2$-Discotics** were binding to the outside of the cell, most probably through electrostatic interactions with the cell membrane associated proteoglycans.[8] After 15 minutes, additionally to membrane bound fluorescence, auto-fluorescence of the discotics inside the cell could be observed. The uptake increased over time, leading to more intracellular fluorescence in the cytoplasm of the cell in form of vesicles. After 24 hours all the fluorescence was localized around the perinuclear region. Co-staining with DIO, a membrane and endosomal marker, and LysoTracker Red, a lysosomal marker, confirmed the endocytotic uptake of the positively charged supramolecular polymer (Figure 5.5 b and Figure S 5.3). Additional to the efficient uptake of amine functionalized discotics, introduction of guanidinium groups could possibly even enhance the uptake and modulate localization as has been seen for CPPs.[37,38]

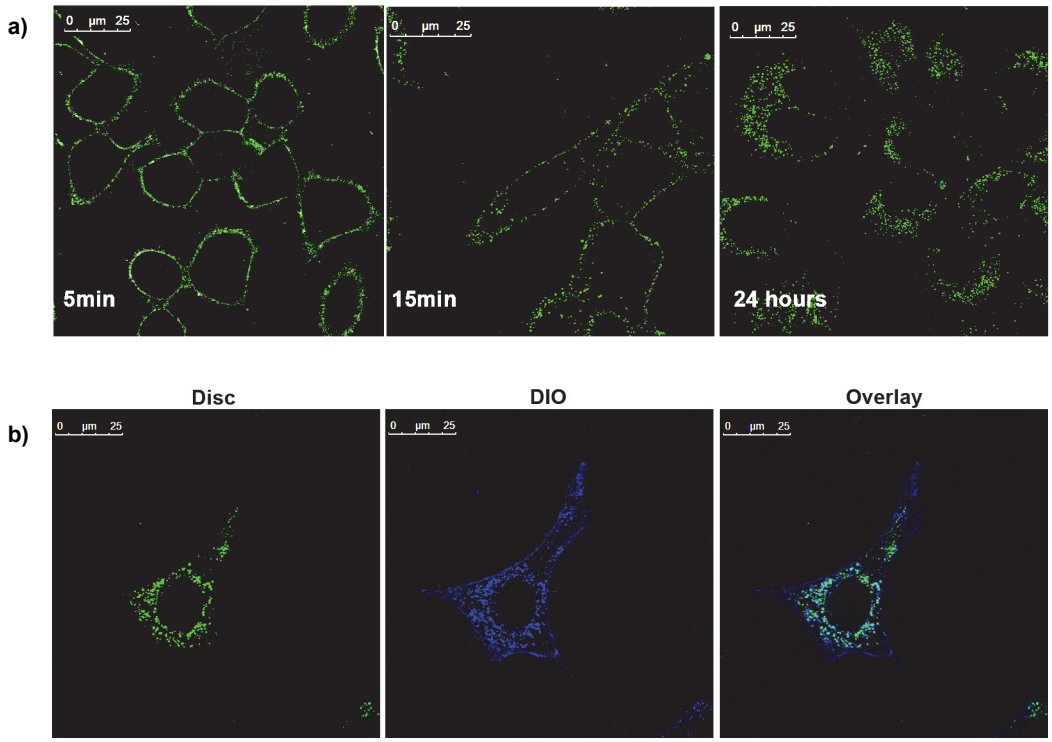

Figure 5.5: a) Cellular uptake of **3NH$_2$-Disc** (5 µM) by HeLa cells over time. b) Confocal microscopy image of HeLa cells incubated with **3NH$_2$-Disc** (5 µM) overnight and co-stained with DIO, a marker for cellular membranes staining early endosomes as well as the membrane.

5.2.3 *Supramolecular co-polymers as cellular uptake carriers*

A major advantage of supramolecular polymers over conventional polymers and small molecules is their dynamic, multicomponent nature. As shown in chapter 3 and chapter 4, the dynamic intermixing of supramolecular polymers is leading to supramolecular heterovalent copolymers with a dynamic behavior.[39–41] To investigate the potential of this concept, supramolecular copolymers were prepared via simple mixing of a cell-penetrating discotic monomer (**3NH$_2$-** and **9NH$_2$-Disc**) with a non cell-permeable monomer. When effective, the amine functionalized discotics should act as carriers for the cellular uptake of different non cell-permeable discotics, by virtue of their combined presence in the copolymer. The **1Fluorescein-Disc** alone was neither taken up by HeLa cells, nor was there any unspecific binding to the cell membrane (Figure S 5.4-S 5.5). HeLa cells were therefore incubated with different copolymers of **9NH$_2$-** and **1Fluorescein-Disc**. To ensure intermixing the discotic mixtures were pre-incubated overnight at room temperature.[42] Cellular imaging 30 minutes after the addition of the supramolecular copolymers showed, in contrast to the observation with the **1Fluorescein-Disc** alone, a clear signal along the cell membrane of both the discotic fluorophore and of the fluorescein (Figure 5.6).

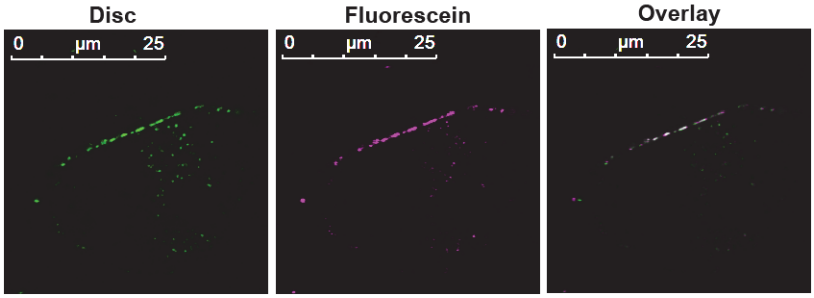

Figure 5.6**:** HeLa cells incubated with a 5 µM 80:20 mixture of **9NH$_2$-** and **1Fluorescein-Disc** and imaged 30 minutes after addition without a washing step in-between.

Subsequently, the cells were washed and imaged 24 hours after incubation. The copolymers had internalized and co-localization of the discotic and fluorescein signal was observed inside the cell (Figure 5.7). Similar results were observed for experiments on Hek293 cells or when using **3NH$_2$-Disc** (Figure 5.8 and Figure S 5.6). These results show that the **1Fluorescein-Disc** requires the interaction with the **9NH$_2$-Disc** within the supramolecular assembly to be internalized into the cell.

To prove that the uptake is caused by the supramolecular copolymerization of the discotic monomers and not via for example permeabilization of the membrane through the addition of **9NH$_2$-Disc**, cells were incubated with a mixture of **9NH$_2$-Disc** and the carboxy fluorescein fluorophore alone. Using the same incubation and imaging procedure as before, no fluorescein signal could be detected inside the cell (Figure 5.7).

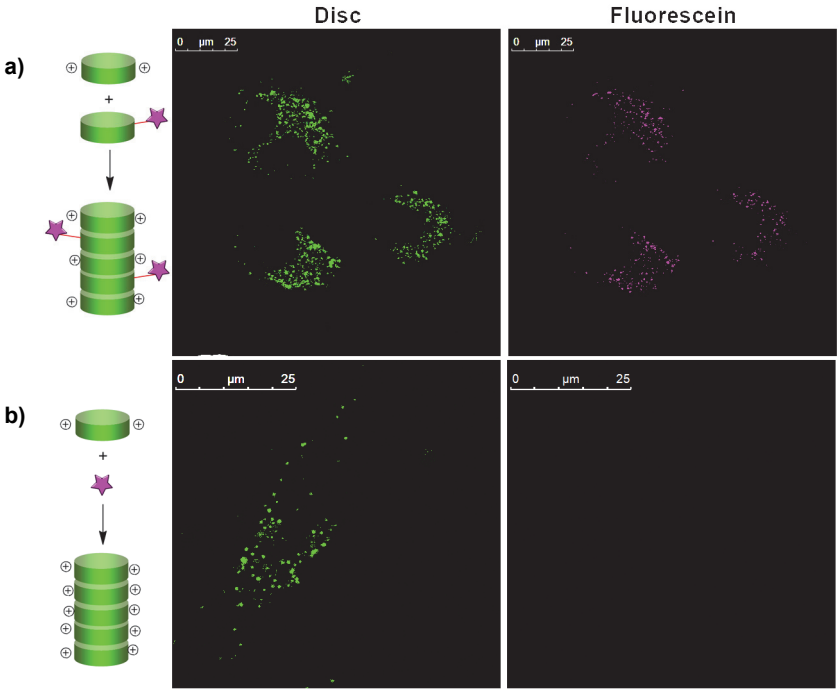

Figure 5.7**:** Discotic copolymers as cellular uptake carriers: a) Confocal images of living HeLa cells which were incubated for 1 hour with a 5 µM mixture of **9NH$_2$-** and **1Fluorescein-Disc** (80:20) and imaged 24 hours later; b) HeLa cells incubated with a 80:20 mixture of **9NH$_2$-Disc** and carboxy fluorescein, both 5 µM, for 1 hour, washed and imaged 24 hours later. The dye mixed with **9NH$_2$-Disc** is not taken up by the HeLa cells.

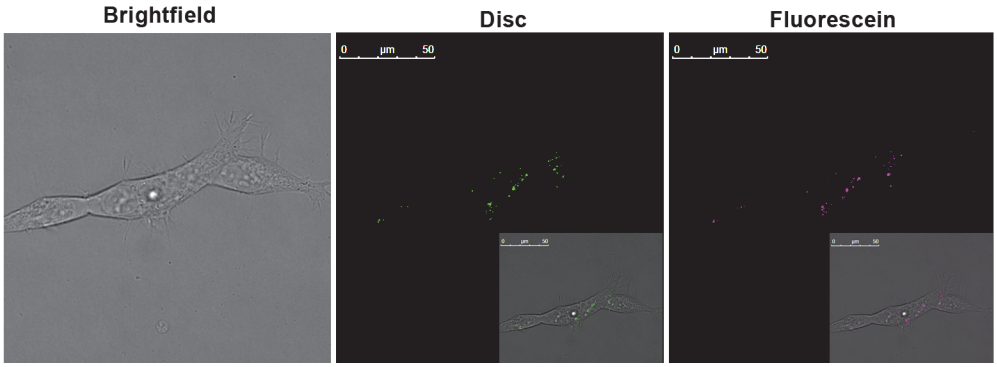

Figure 5.8: Hek293 cells incubated with a 5 µM 80:20 mixture of **9NH$_2$-** and **1Fluorescein-Disc** for 1 hour, washed and imaged 24 hours later. Insets: overlay of the according channel with Brightfield.

A **3Biotin-Disc**, which is non cell-permeable on its own (Figure S 5.7), was as well successfully taken up, when present in a supramolecular copolymer with the **9NH$_2$-Disc**. To visualize cellular uptake of the biotin-functionalized discotic, the cells were fixed and stained with a Cy5-labelled anti-biotin antibody (Figure 5.9).

A variety of copolymers were prepared, with different ratios for the cell-permeable discotics (**9NH$_2$-**and **3NH$_2$-Disc**) to non cell-permeable **1Fluorescein-** or **3Biotin-Disc** (50:50, 80:20, 95:5). For all of these copolymers internalization of the non cell-permeable discotic was observed. Using

the 95:5 mixtures obviously led to a low but detectable ligand signal. Less cellular uptake was observed when using the 50:50 mixtures, probably through dilution of the amine-density on the surface. The 80:20 mixtures provided the best results in terms of uptake and visualization.

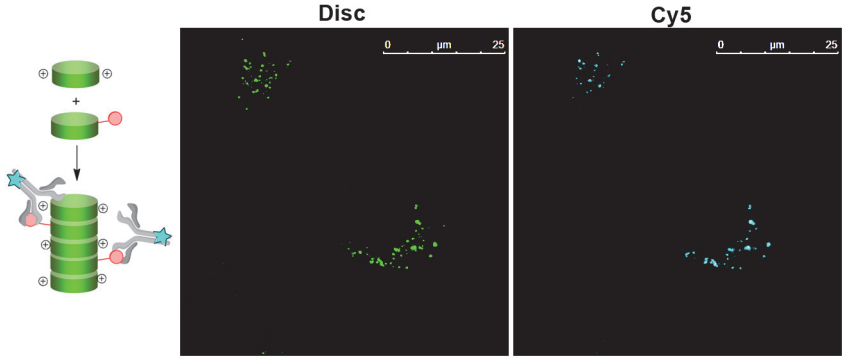

Figure 5.9: Discotic copolymers as cellular uptake carriers: Confocal images of fixed HeLa cells. The cells were incubated for 1 hour with a 5 µM mixture of **9NH$_2$-** and **3Biotin-Disc** (80:20) and fixed and stained with a Cy5-labelled anti-biotin antibody 24 hours later.

In a final experiment, to highlight the potential and versatility of the approach, supramolecular copolymers consisting of three different discotics: **9NH$_2$-**, **1Fluorescein-** and **3Biotin-Disc** (80:10:10) were prepared and evaluated. The copolymers were added to the cells and incubated for 1 hour after which the cells were washed and fixed and immunostained 24 hours later. Confocal microscopy revealed the presence and co-localization of all three fluorescent signals from the discotic scaffold, fluorescein and biotin inside the cell (Figure 5.10). These results show that the supramolecular synthesis approach is highly flexible and effective, and enables each discotic monomer to express its functionality in the combined system.

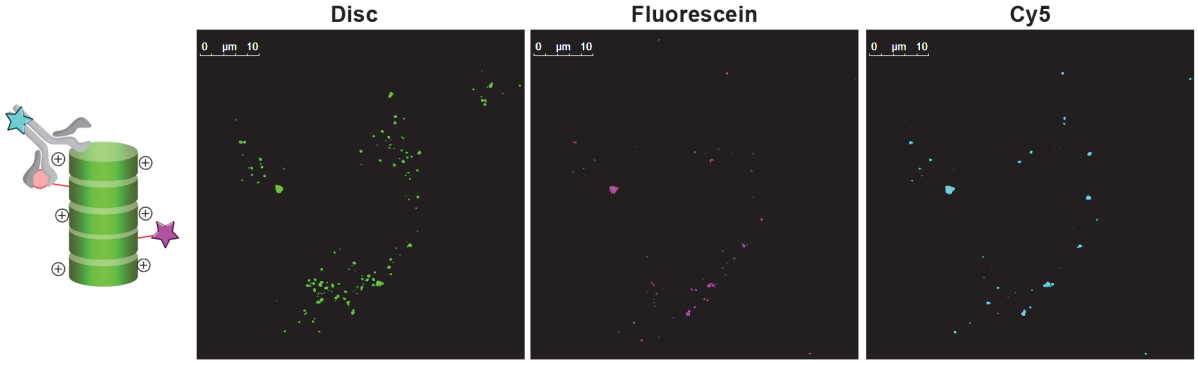

Figure 5.10: Confocal images of HeLa cells incubated for 1 hour with a 5 µM mixture of **9NH$_2$-**, **1Fluorescein-** and **3Biotin-Disc** (80:10:10). After 24 hours the cells were fixed and stained with a Cy5-labelled anti-biotin antibody.

5.3 Conclusions

In conclusion, a library of cell-permeable and non cell-permeable ligand-functionalized discotic molecules was synthesized for the supramolecular synthesis of a variety of dynamic

multicomponent copolymers with tunable properties. Supramolecular homopolymers of amine functionalized discotics featured efficient cellular uptake, detectable by their auto-fluorescence using live cell multiphoton fluorescence microscopy. The translocation through the plasma membrane of non cell-permeable ligand-functionalized discotics was induced by combining them with the amine functionalized discotics into cell-permeable supramolecular copolymers. The supramolecular synthesis approach allows rapid generation of copolymers with differing composition by simple intermixing of a variety of discotic monomers. This led to multi-functional supramolecular polymers consisting of up to three different discotic monomers. After efficient cellular uptake, each of the components could be individually visualized, demonstrating the potential of dynamic multi-component supramolecular polymers. In this example the supramolecular polymers represent a unique and flexible platform for modular cellular uptake systems, but other applications can similarly be envisioned

5.4 Experimental

The synthesis of all discotics used is described in chapter 2.
Thiazolyl blue tetrazolium bromide (MTT), bovine serum albumine (BSA), Nonidet40 and phoshate buffer saline (PBS) tablets were purchased from Sigma-Aldrich. Paraformaldehyd was purchased from Acros. Fetal bovine serum (FBS), 3,3'-dioctadecyloxacarbocyanine perchlorate ('DiO'; DiOC18(3)), LysoTracker® Red DND-99, Penicillin – Streptomycin solution (Pen/Strep) and DMEM phenol red free cell culture media have been purchased from Invitrogen. Cy5-labelled anti-biotin antibody was purchased from Jackson ImmunoResearch. Aqua-Poly/Mount mounting media was purchased from Polysciences Inc. and glass slides for cell fixing from VWR. Guava ViaCount was purchased from Millipore. HeLa cells have been a kind gift from Moniek de Liefde, TU Eindhoven. Human embryonic kidney (HEK) 293 cells (accession no.: ACC 305) were obtained from the German Collection of Microorganisms and Cell Cultures (DSMZ, Germany). TPH-1 cells have been purchased from the American Type Culture Collection (ATCC, accession no.: TIB-202).

For the MTT assay, cells were seeded in a Nunc 96 well Microwell plate. Absorbance of MTT was read out on a multiscan ascent plate reader from Thermo Electron Corporation. The viability of the suspension cell line THP-1 has been measured on the Guava easyCyte 8HT Base System from Millipore.

For confocal imaging, cells were seeded in uncoated 24 glass bottom wells purchased from MatTeK. The cells were imaged on a Leica TCS SP5 AOBS equipped with an HCX PL APO CS x63/1.2 NA water immersion lens and a temperature-controlled incubation chamber maintained at 37°C. Discotics were excited with a Chameleon Multiphoton laser using 760 nm laser pulses. DiO, LysoTracker Red, fluorescein and Cy5 were excited with a Whitelight laser (DiO at 488 nm, LysoTracker Red at 577 nm, fluorescein at 488 nm, Cy5 at 633 nm). During imaging with Multiphoton laser the pinhole was fully opened, whereas otherwise it was closed to 1 airy unit. Fluorophore emission bands were detected in the following ranges: discotics, 500–550 nm; DiO, 495–520 nm; LysoTracker Red, 585-600 nm; fluorescein, 496–520 nm; Cy5, 665-715 nm.

General imaging protocol:

For imaging, cells were seeded in 24-well glass-bottom wells (HeLa and HEK 293: 75000 cells/well, THP-1: 1000000 cells/well) and cultured in DMEM media supplemented with 10% FBS and 1% Pen/Strep at 37 °C, 5% CO_2. When the confluency had reached about 70%, the media was removed and replaced by discotics dissolved in media. After 1 h of incubation at 37 °C, 5% CO_2 the disc solution was removed; the cells were washed 5x with 2 mL PBS and incubated in fresh media at 37 °C, 5% CO_2. The cells were imaged 14 h later.

Time-lapse imaging:

For time-lapse imaging, the media was replaced by media containing discotic solutions and the cells were imaged directly without any washing steps.

Co-staining:

To stain the membrane as well as the endosomes, DiO (5 μM) was added to the cells in media 1 h prior to imaging. To stain the lysosomes, LysoTracker® Red (75 nM) was added to the cells 1 h prior to imaging.

Fixation and antibody staining:

When staining with antibody and fixation was required, HeLa cells were seeded on glass slides in 24-well plates and cultured in DMEM media supplemented with 10% FBS and 1% Pen/Strep at 37 °C, 5% CO_2. When the confluency reached about 70%, the media was removed and replaced by discotics dissolved in media. After 1 h of incubation, disc-containing media was removed. After washing the cells 5 times with 2 mL PBS, the cells were fixed with 4% paraformaldehyde in PBS for 30 minutes at RT. The supernatant was discarded and the cells were washed 3 times 5 min with 2 mL Tris (50 mM, pH 8.0), NaCl (100 mM) and 1 time 10 min with 2 mL 20 mM Glycine in PBS. The cells were permeabilized for 15 minutes at room temperature with 0.1 % TritonX-100 in PBS and consequently washed 3 times for 5 minutes with 2 mL PBS. Afterwards the cells were blocked with 5% BSA in PBS for 30 minutes at room temperature. To stain the 3Biotin-Disc the supernatant was removed and Cy5-conjugated monoclonal mouse anti-biotin antibody (1:600 diluted in PBS) was added and incubated with the cells at room temperature in the dark for 45 minutes. After the staining, the cells were washed 5 times with PBS, mounted with aqua polymer on a glass slide and dried for 1 h in dark at room temperature before imaging.

MTT assay:

HEK 293 and HeLa cells were seeded in 96 well plates (1000 cells/well) cultured in DMEM media supplemented with 10% FBS and 1% Pen/Strep at 37 °C, 5% CO_2 overnight. The next day the media was removed and 100 μL of discotic solutions dissolved in media were added and incubated at 37 °C, 5% CO_2. After 1 h incubation, the discotic solutions were removed, the cells were washed 1 time with 100 μL PBS and 120 μL media containing 20% MTT solution were added to each well. The MTT solution was removed after an incubation time of 3.5 h at 37 °C, 5% CO_2, replaced with 150μL MTT solvent (4 mM HCl, 0.1% Nonidet P-40 (NP40) in isopropanol) and incubated on a shaker for 15 to 60 minutes at room temperature. The absorbance was read out on a multiskan ascent plate reader at 590 nm.

THP-1 viability assay:

The viability of the THP-1 cells was determined using the ViaCount reagent from Millipore. The reagent is based on the differential permeation of (two) DNA intercalating dyes and allows not only to distinguish between live and dead cells, but also between live and apoptotic cells. To determine the viability of the THP-1 cells, 25 μL cells (100 cells/μL) were mixed with 25 μL of discotics dissolved in DMEM media supplemented with 10% FBS and 1% Pen/Strep. After 1 h of incubation at 37 °C, 25 μL of the cell/discotic solutions were added to 225 μL ViaCount reagent and the viability was determined immediately using the Guava easyCyte 8HT Base System.

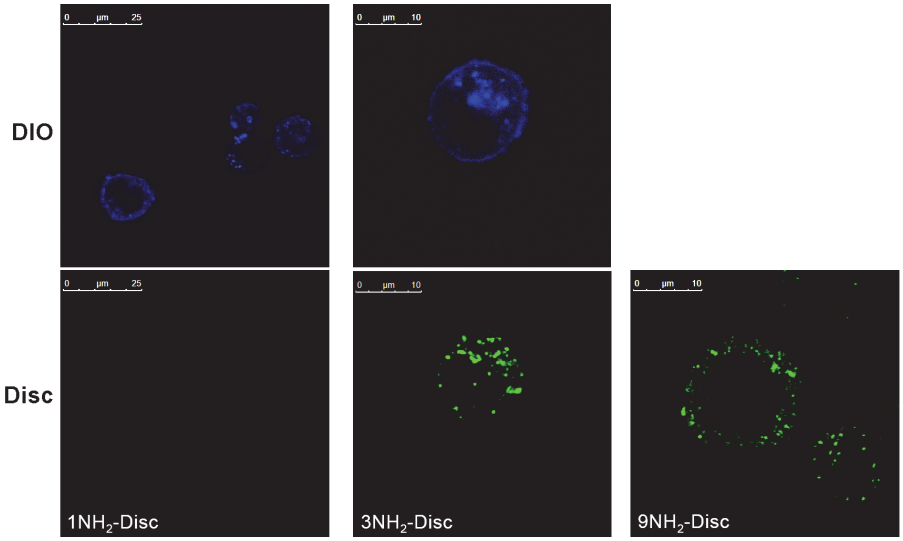

Figure S 5.1: THP-1 cells incubated with different discotics for 1 h, washed and imaged 14 h later after co-staining the cells with DiO. Top row: DiO channel (blue), lower row: disc channel (green).

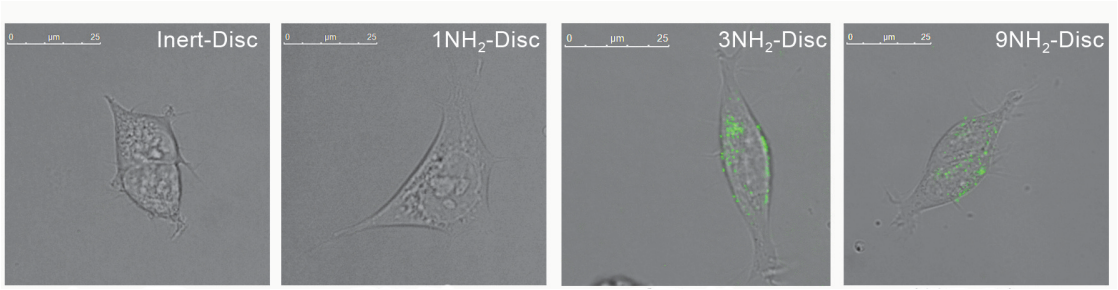

Figure S 5.2: Hek293 cells incubated with different discotics for 1 h, washed and imaged 14 h later. Overlay of Brightfield and Disc-fluorescence channel.

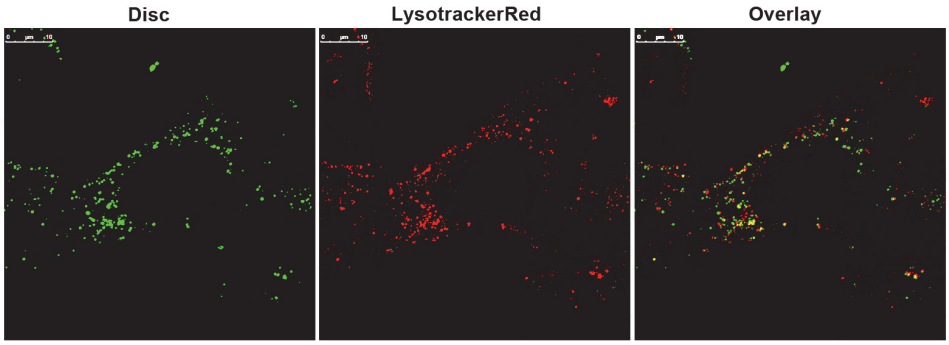

Figure S 5.3: Confocal microscopy image of HeLa cells incubated with **9NH₂-Disc** (5 µM) overnight and co-stained with LysoTracker Red, a lysosomal marker.

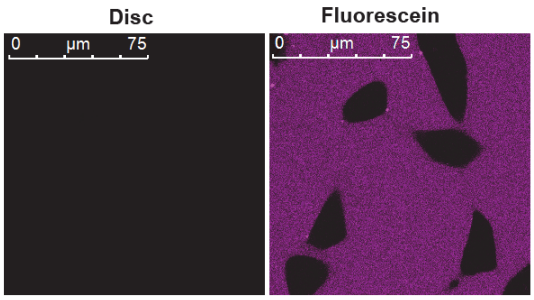

Figure S 5.4: HeLa cells incubated with carboxy fluorescein (5 µM). The cells were imaged 15 minutes after addition of the dye. Carboxy fluorescein does not bind to cell membranes and is not excited under the settings used to image the discotics

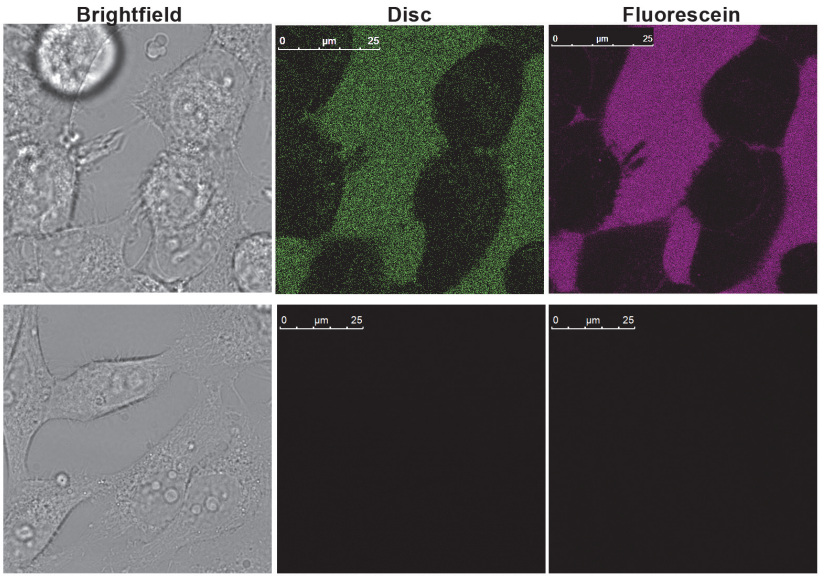

Figure S 5.5**:** HeLa cells incubated with **1Fluorescein-Disc** (5 µM): Top): Imaged 30 minutes after addition; only diffuse fluorescence between the cells can be observed. Bottom): After 1 h of incubation, the cells were washed and imaged 16 h later. No fluorescence signal was observed, confirming no unspecific binding.

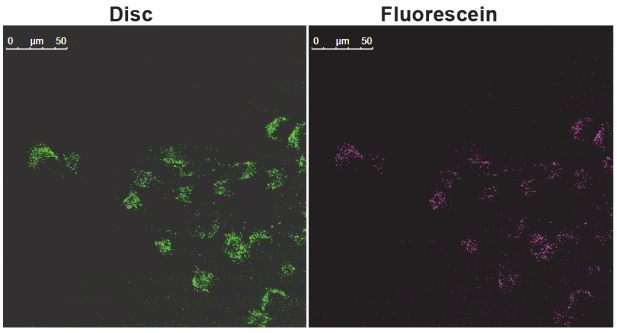

Figure S 5.6: HeLa cells incubated with a 5 µM 80:20 mixture of **3NH$_2$-** and **1Fluorescein-Disc** for 1 h, washed and imaged 16 h later.

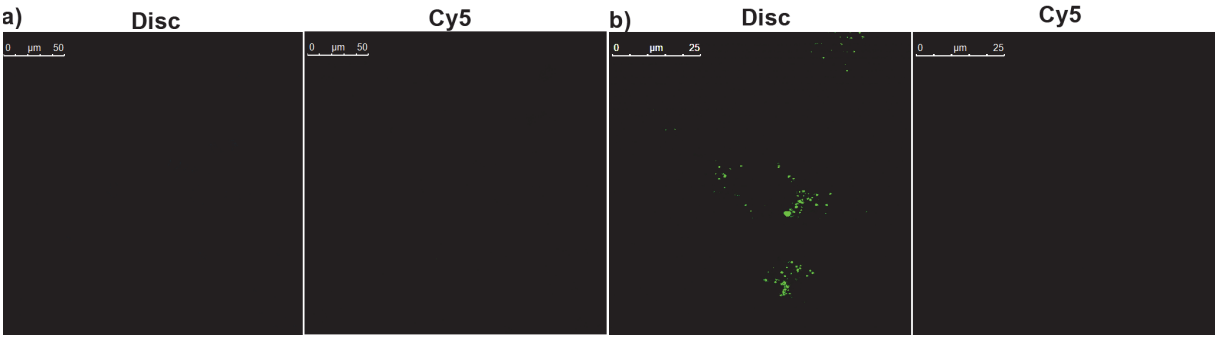

Figure S 5.7**:** a) HeLa cells incubated with **3Biotin-Disc** (5 µM) for 1 hour, washed, incubated overnight, fixed, stained with Cy5-lableled anti-biotin antibody and imaged. b) HeLa cells incubated with **9NH$_2$-Disc** (5 µM) for 1 hour, washed, incubated overnight, fixed, stained with Cy5-lableled anti-biotin antibody and imaged. **3Biotin-Disc** is not able to penetrate the cell on its own and the **9NH$_2$-Disc** is not unspecificly stained by the antibody.

5.5 References

1. Torchilin, V. P. Recent Approaches to Intracellular Delivery of Drugs and Dna and Organelle Targeting. *Annu. Rev. Biomed. Eng*. **2006**, 8, 343–375.
2. Blanka, Ř. Receptor-mediated Targeted Drug or Toxin Delivery. *Adv. Drug Deliver. Rev.* **1998**, 29, 273–289.
3. Fonseca, S. B.; Pereira, M. P.; Kelley, S. O. Recent Advances in the Use of Cell-penetrating Peptides for Medical and Biological Applications. *Adv. Drug Deliver. Rev.* **2009**, 61, 953–964.
4. Stewart, K. M.; Horton, K. L.; Kelley, S. O. Cell-penetrating Peptides as Delivery Vehicles for Biology and Medicine. *Org. Biomol. Chem*. **2008**, 6, 2242–2255.
5. Green, M.; Loewenstein, P. M. Autonomous Functional Domains of Chemically Synthesized Human Immunodeficiency Virus Tat Trans-activator Protein. *Cell* **1988**, 55, 1179–1188.
6. Frankel, A. D.; Pabo, C. O. Cellular Uptake of the Tat Protein from Human Immunodeficiency Virus. *Cell* **1988**, 55, 1189–1193.
7. Fischer, P. M. Cellular Uptake Mechanisms and Potential Therapeutic Utility of Peptidic Cell Delivery Vectors: Progress 2001–2006. *Med. Res. Rev.* **2007**, 27, 755–795.
8. Nakase, I.; Tadokoro, A.; Kawabata, N.; Takeuchi, T.; Katoh, H.; Hiramoto, K.; Negishi, M.; Nomizu, M.; Sugiura, Y.; Futaki, S. Interaction of Arginine-Rich Peptides with Membrane-Associated Proteoglycans Is Crucial for Induction of Actin Organization and Macropinocytosis. *Biochemistry* **2006**, 46, 492–501.
9. Amir, R. J.; Albertazzi, L.; Willis, J.; Khan, A.; Kang, T.; Hawker, C. J. Multifunctional Trackable Dendritic Scaffolds and Delivery Agents. *Angew. Chem. Int. Ed.* **2011**, 50, 3425–3429.
10. Albertazzi, L.; Serresi, M.; Albanese, A.; Beltram, F. Dendrimer Internalization and Intracellular Trafficking in Living Cells. *Mol. Pharmaceutics* **2010,** 7, 680–688.
11. Gillies, E. R.; Deiss, F.; Staedel, C.; Schmitter, J.-M.; Huc, I. Development and Biological Assessment of Fully Water-Soluble Helical Aromatic Amide Foldamers. *Angew. Chem.* **2007**, 119, 4159–4162.
12. Iriondo-Alberdi, J.; Laxmi-Reddy, K.; Bouguerne, B.; Staedel, C.; Huc, I. Cellular Internalization of Water-Soluble Helical Aromatic Amide Foldamers. *Chem.: Eur. J.* **2010**, 11, 1679–1685.
13. Moon, J. H.; McDaniel, W.; MacLean, P.; Hancock, L. F. Live-Cell-Permeable Poly(p-phenylene Ethynylene). *Angew. Chem. Int. Ed.* **2007**, 46, 8223–8225.
14. Kolonko, E. M.; Kiessling, L. L. A Polymeric Domain That Promotes Cellular Internalization. *J. Am. Chem. Soc.* **2008**, 130, 5626–5627.
15. Brunsveld, L.; Folmer, B. J. B.; Meijer, E. W.; Sijbesma, R. P. Supramolecular Polymers. *Chem. Rev.* **2001**, 101, 4071–4098.
16. Mulder, W. J. M.; Strijkers, G. J.; Tilborg, G. A. F. van; Cormode, D. P.; Fayad, Z. A.; Nicolay, K. Nanoparticulate Assemblies of Amphiphiles and Diagnostically Active Materials for Multimodality Imaging. *Acc. Chem. Res.* **2009**, 42, 904–914.
17. Al-Jamal, W. T.; Kostarelos, K. Liposomes: From a Clinically Established Drug Delivery System to a Nanoparticle Platform for Theranostic Nanomedicine. *Acc. Chem. Res*. **2011**, 44, 1094–1104.
18. Forssen, E.; Willis, M. Ligand-targeted Liposomes. *Adv. Drug. Deliver. Rev*. **1998**, 29, 249–271.
19. See chapter 3.2.3.
20. Silva, G. A.; Czeisler, C.; Niece, K. L.; Beniash, E.; Harrington, D. A.; Kessler, J. A.; Stupp, S. I. Selective Differentiation of Neural Progenitor Cells by High-Epitope Density Nanofibers. *Science* **2004**, 303, 1352–1355.
21. Cui, H.; Webber, M. J.; Stupp, S. I. Self-assembly of Peptide Amphiphiles: From Molecules to Nanostructures to Biomaterials. *Biopolymers* **2010**, 94, 1–18.
22. Brunsveld, L.; Lohmeijer, B. G. G.; Vekemans, J. A. J. M.; Meijer, E. W. Chirality Amplification in Dynamic Helical Columns in Water. *Chem. Commun.* **2000**, 2305–2306.
23. Brunsveld, L.; Zhang, H.; Glasbeek, M.; Vekemans, J. A. J. M.; Meijer, E. W. Hierarchical Growth of Chiral Self-Assembled Structures in Protic Media. *J. Am. Chem. Soc*. **2000,** 122, 6175–6182.

24. Toele, P.; Gorp, J. J. van; Glasbeek, M. Femtosecond Fluorescence Studies of Self-Assembled Helical Aggregates in Solution. *J. Phys. Chem. A* **2005**, 109, 10479–10487.
25. Müller, M. K.; Petkau, K.; Brunsveld, L. Protein Assembly Along a Supramolecular Wire. *Chem. Commun*. **2011**, 310-312.
26. Müller, M. K.; Brunsveld, L. A Supramolecular Polymer as a Self-Assembling Polyvalent Scaffold. *Angew. Chem. Int. Ed.* **2009**, 48, 2921–2924.
27. Denk, W.; Strickler, J. H.; Webb, W. W. Two-photon Laser Scanning Fluorescence Microscopy. *Science* **1990**, 248, 73–76.
28. Zipfel, W. R.; Williams, R. M.; Webb, W. W. Nonlinear Magic: Multiphoton Microscopy in the Biosciences. *Nat Biotech* **2003**, 21, 1369–1377.
29. Kosuge, M.; Takeuchi, T.; Nakase, I.; Jones, A. T.; Futaki, S. Cellular Internalization and Distribution of Arginine-Rich Peptides as a Function of Extracellular Peptide Concentration, Serum, and Plasma Membrane Associated Proteoglycans. *Bioconjugate Chem* **2008**, 19, 656–664.
30. Futaki, S.; Suzuki, T.; Ohashi, W.; Yagami, T.; Tanaka, S.; Ueda, K.; Sugiura, Y. Arginine-rich Peptides. *J. Biol. Chem.* **2001**, 276, 5836 –5840.
31. Yoon, Y.-R.; Lim, Y.; Lee, E.; Lee, M. Self-assembly of a Peptide Rod–coil: a Polyproline Rod and a Cell-penetrating Peptide Tat Coil. *Chem. Commun.* **2008**, 1892–1894.
32. Allen, T. M.; Cullis, P. R. Drug Delivery Systems: Entering the Mainstream. *Science* **2004**, 303, 1818 – 1822.
33. Karakoti, A. S.; Das, S.; Thevuthasan, S.; Seal, S. PEGylated Inorganic Nanoparticles. *Angew. Chem. Int. Ed.* **2011**, 50, 1980–1994.
34. Knop, K.; Hoogenboom, R.; Fischer, D.; Schubert, U. S. Poly(ethylene Glycol) in Drug Delivery: Pros and Cons as Well as Potential Alternatives. *Angew. Chem. Int. Ed*. **2010**, 49, 6288–6308.
35. Malik, N.; Wiwattanapatapee, R.; Klopsch, R.; Lorenz, K.; Frey, H.; Weener, J. .; Meijer, E. .; Paulus, W.; Duncan, R. Dendrimers:: Relationship Between Structure and Biocompatibility in Vitro, and Preliminary Studies on the Biodistribution of 125I-labelled Polyamidoamine Dendrimers in Vivo. *J. Control. Release* **2000**, 65, 133–148.
36. Rodrigo, A. C.; Rivilla, I.; Pérez-Martínez, F. C.; Monteagudo, S.; Ocaña, V.; Guerra, J.; García-Martínez, J. C.; Merino, S.; Sánchez-Verdú, P.; Ceña, V. et al. Efficient, Non-Toxic Hybrid PPV-PAMAM Dendrimer as a Gene Carrier for Neuronal Cells. *Biomacromolecules* **2011**, 12, 1205–1213.
37. Thoren, P. Uptake of Analogs of Penetratin, Tat(48-60) and Oligoarginine in Live Cells. *Biochem. Bioph. Res. Co.* **2003**, 307, 100–107.
38. Mitchell, D. J.; Steinman, L.; Kim, D. T.; Fathman, C. G.; Rothbard, J. B. Polyarginine Enters Cells More Efficiently Than Other Polycationic Homopolymers. *J. Pept. Res.* **2000**, 56, 318–325.
39. Besenius, P.; Goedegebure, Y.; Driesse, M.; Koay, M.; Bomans, P. H. H.; Palmans, A. R. A.; Dankers, P. Y. W.; Meijer, E. W. Peptide Functionalised Discotic Amphiphiles and Their Self-assembly into Supramolecular Nanofibres. *Soft Matter* **2011**, 7, 7980–7983.
40. Gasiorowski, J. Z.; Collier, J. H. Directed Intermixing in Multicomponent Self-Assembling Biomaterials. *Biomacromolecules* **2011**, 12, 3549–3558.
41. Petkau-Milroy, K.; Uhlenheuer, D. A.; Spiering, A. J. H.; Vekemans, J. A. J. M.; Brunsveld, L. Dynamic Protein Assembly Through Site-Selective Attachment and Display on a Supramolecular Wire. submitted.
42. See chapter 4.

6

Pre- and post-functionalized self-assembled π-conjugated fluorescent organic nanoparticles for dual targeting

Abstract. There is currently a high demand for novel approaches to engineer fluorescent nanoparticles with precise surface properties suitable for various applications, including imaging and sensing. To this end, a facile and highly reproducible one-step method for generating functionalized fluorescent organic nanoparticles via self-assembly of pre-functionalized π-conjugated oligomers is reported. The engineered design of the nonionic amphiphilic oligomers enables the introduction of different ligands at the extremities of inert ethylene glycol side-chains without interfering with the self-assembly process. The intrinsic fluorescence of the nanoparticles permits the measurement of their surface properties and binding to dye labeled target molecules via Förster resonance energy transfer (FRET). Co-assembly of differently functionalized oligomers is also demonstrated, which enables the tuning of ligand composition and density. Furthermore, nanoparticle pre-functionalization has been combined with subsequent post-modification of azide-bearing oligomers via click chemistry. This allows for expanding ligand diversity at two independent stages in the nanoparticle fabrication process. The practicability of the different methods entails greater control over surface functionality. Through labeling with different ligands, selective binding of proteins, bacteria and functionalized beads to the nanoparticles has been achieved. This, in combination with the absence of unspecific adsorption, clearly demonstrates the broad potential of these nanoparticles for selective targeting and sequestration. Therefore, controlled bi-functionalization of fluorescent π-conjugated oligomer nanoparticles represents a novel approach with high applicability to multi-targeted imaging and sensing in biology and medicine.

Reprinted with permission from: K. Petkau, A. Kaeser, I. Fischer, L. Brunsveld, A. P. H. J. Schenning, *J. Am. Chem. Soc.*, **2011**, 133 (42), 17063–17071. Copyright (2011) American Chemical Society.

6.1 Introduction

The ability to actively target specific receptors and, as a result, cells is a prerequisite for the use of fluorescent nanoparticles as molecular imaging probes, diagnostics, and therapeutic delivery vehicles.[1–3] Targeting is typically achieved through surface functionalization of the nanoparticles with high affinity ligands, such as small molecules, peptides, and antibodies. Multiple ligands can be attached leading to high binding affinities due to multivalent interactions, which are necessary to achieve maximal selectivity in diagnostics.[4,5] This at the same time requires chemical control over the ligand functionalization of nanoparticle surfaces via pre- or post-functionalization.

Several classes of nanoparticles have been developed in the last few decades starting from the first liposomes in 1960s[6] via inorganic quantum dots[7,8], to organic nanoparticles[9–11]. Due to their intrinsic fluorescence with high quantum yields, especially quantum dots are currently widely used as fluorescent imaging probes.[12] Having no intrinsic aqueous solubility, these inorganic nanoparticles require a relatively thick encapsulation layer to ensure biocompatibility and stability. These so-called caps not only solubilize and protect the inorganic core, but as well carry reactive groups, which serve as points of covalent attachment for biomolecules via post-functionalization.[13] Liposomes, which are based on self-assembled lipid amphiphiles, are prepared from pre-functionalized building blocks.[14] However, sensitive targeting ligands like proteins are attached to liposomes via post-functionalization.[15] Additionally, in order to construct fluorescent liposomes dye molecules are introduced, for example, via the polar head groups of the lipids on the outside of the liposome.

Fluorescent organic nanoparticles based on π-conjugated systems combine the features of inorganic nanoparticles and liposomes in being self-assembling amphiphiles with high fluorescence brightness and photostability.[16–20] The functionalization of these particles with biomolecules, which will be crucial for their use in sensing and imaging applications, has scarcely been reported. π-Conjugated polymer dots have been co-assembled with polymers bearing carboxylic acids as attachment points for post-functionalization by McNeill, Chiu and coworkers. In this way, the nanoparticle surface was functionalized on the one hand with ethylene glycol chains to provide a biocompatible layer that minimizes non-specific adsorption and on the other hand with biomolecules to afford specific targeting.[21,22] Interestingly, these particles were used as probes for in vivo cell labeling and tumor imaging.[21,23] Using a large variation of π-conjugated oligomers, an extensive pioneering structural study has been performed by Lee and coworkers. Mannose pre-functionalized oligomers were designed to assemble into bioactive nanostructures of different shapes showing enhanced binding affinities due to multivalency.[24] Although the nanoparticles were not fluorescent, the encapsulation of a dye was possible, which could even trigger changes in the structure of these dynamic aggregates.[25]

Recently, Schenning and coworkers have reported on self-assembled fluorescent nanoparticles based on π-conjugated fluorene oligomers in water.[26] Via the co-assembly of the different

fluorene based amphiphiles, fluorescent nanoparticles with tunable emission colors covering the entire visible range (including white)[27] were obtained. Here, a facile and flexible approach to prepare (multi)functional fluorescent organic nanoparticles for targeted imaging is reported.

Via the co-assembly of synthetically accessible pre-functionalized π-conjugated oligomers a library of functionalized nanoparticles was generated. The amphiphilic oligomers were on the one hand pre-functionalized with ligands for biological targeting, such as mannose, and on the other with azides to allow post-functionalization of pre-formed nanoparticles (Figure 6.1). The binding behavior of these nanoparticles has been evaluated using Förster resonance energy transfer (FRET) between nanoparticles and fluorescently labeled proteins that target the introduced ligands. The nanoparticles were capable of selective binding to bacteria and to magnetic beads, which led to nanoparticle-target clustering and, in the case of magnetic beads, to complete removal from solution. Our results show that the self-assembly of pre-functionalized amphiphiles enabled the reliable tuning of ligand density at the nanoparticle surface. Via copper catalyzed azide-alkyne cycloaddition (CuAAC) ligands were as well successfully introduced at the nanoparticle surface after nanoparticle formation. Multi-targeting of the fluorescent organic nanoparticles was demonstrated through functionalization of the same nanoparticle with different ligands, which were recognized by their corresponding protein partners. Our results reveal synthetic pathways and self-assembly protocols to prepare tunable functionalized fluorescent multivalent nanoparticles for biological multi-target imaging applications.

6.2 Results and Discussion

6.2.1 *Design and Synthesis*

The studied amphiphilic fluorene oligomers **1**, **2** and **3** (Figure 6.1 and Scheme 6.1) consist of the same π-conjugated core of two fluorene units connected by a benzothiadiazole linker. The hydrophobic chromophore has been decorated with gallic acid derivatives bearing at one end alkyl tails and ethylene glycol chains at the other. These hydrophilic ethylene glycol chains are not only necessary for phase segregation, but should also prevent unspecific adsorption of biological matter to the surface of the resulting nanoparticles.[28] Furthermore, polyethylene glycols have an excellent water solubility and low toxicity and are now extensively used in clinical applications.[29,30]

To functionalize the surface of the nanoparticles our strategy was to introduce ligands at the periphery of hydrophilic ethylene glycol chains. This should ensure the exposure of the ligands to the aqueous environment.[31,32] Two functionalities, a mannose and an azide group were selected for the pre-functionalization of the oligomers (Figure 6.1, compound **2** and **3**, respectively). Mannose is used to evaluate the binding to biological structures such as *E. Coli* bacteria[33] and the lectin concanavalin A (ConA)[34], while the azide moiety allows the preparation of nanoparticles for post-functionalization via the copper catalyzed azide-alkyne cycloaddition reaction.[35,36]

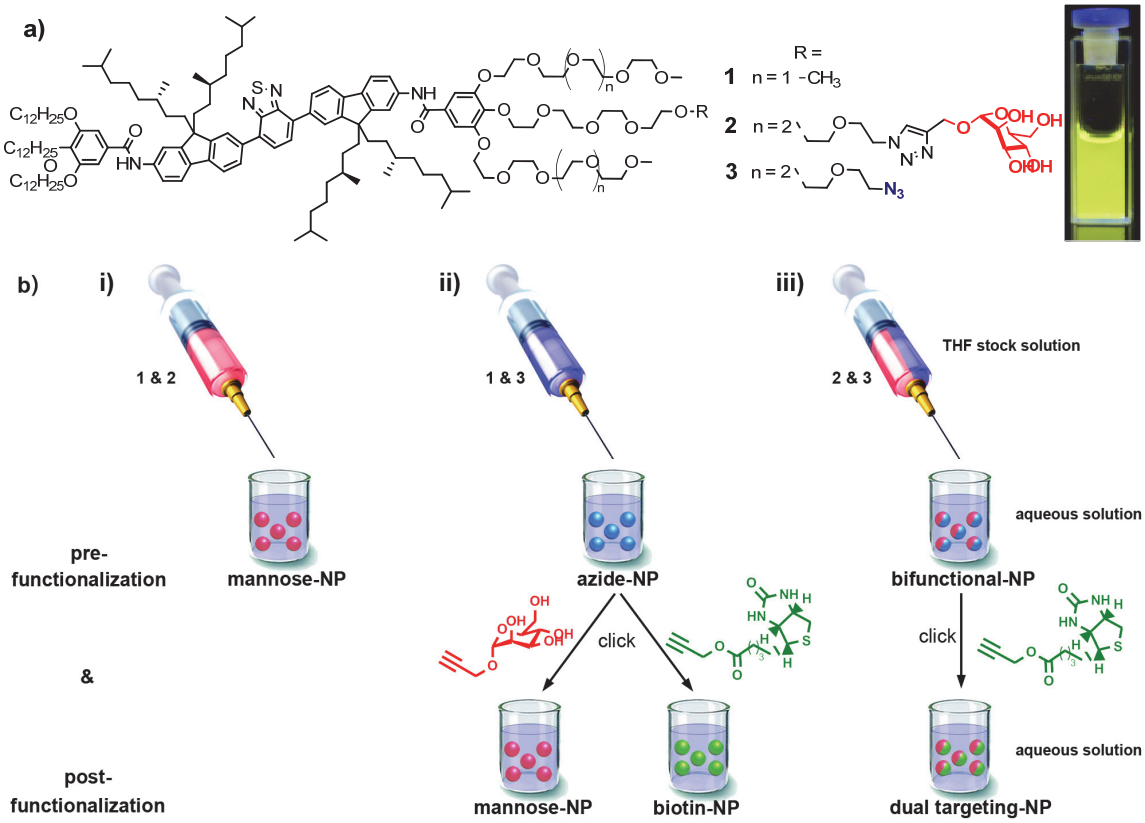

Figure 6.1: a) Chemical structures of amphiphiles used in this study and a photograph of a 0.3 μM nanoparticle solution under UV light (λ_{ex} = 360 nm). b) i) Generation of nanoparticles pre-functionalized with mannose using mixtures of **1** and **2**. ii) Generation of nanoparticles pre-functionalized with azides using mixtures of **1** and **3** and subsequent post-functionalization via copper catalyzed azide-alkyne cycloaddition with alkyne derivatives of either mannose or biotin. iii) Generation of bi-functional nanoparticles containing azides and mannose using mixtures of **2** and **3** and subsequent post-functionalization via copper catalyzed azide-alkyne cycloaddition with alkyne derived biotin yielding dual targeting mannose and biotin labeled nanoparticles.

The synthesis of amphiphile **1** and the building block **7** is based on an earlier reported method.[26] For the synthesis of amphiphile **2** and **3**, the azide functionalized gallic acid derivative **4** was synthesized in a multistep process as described previously.[31] Reacting this building block with propargyl mannose **5** in the presence of copper sulfate and sodium ascorbate yielded **6**. For the final acylation step, the azide functionalized gallic acid derivative **4** was transformed into an acid chloride in situ using oxalyl chloride and reacted with **7**. The mannose functionalized gallic acid derivative **6** was pre-activated using *O*-benzotriazole-*N*,*N*,*N*′,*N*′-tetramethyl-uronium-hexafluoro-phosphate (HBTU) and coupled to **7**. Both activation strategies led to the desired amphiphiles (Scheme 6.1).

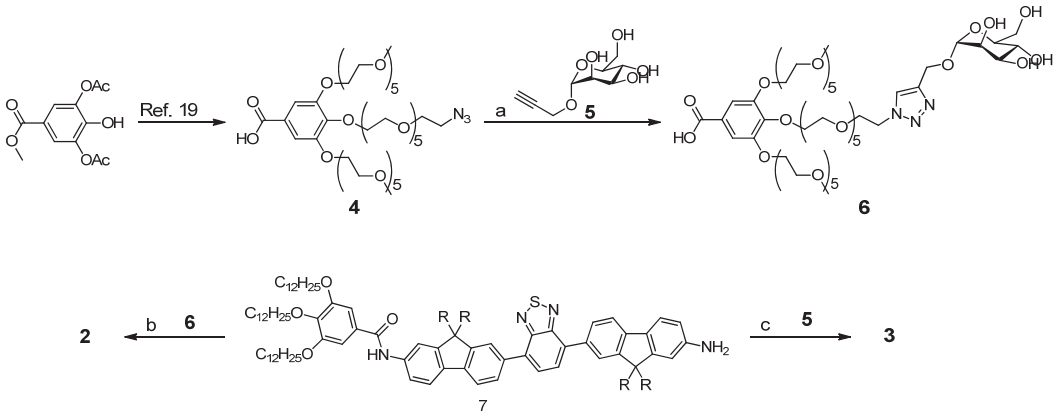

Scheme 6.1: Synthesis of the mannose and azide amphiphiles **2** and **3**.Reagents and conditions: (a) $CuSO_4$, sodium ascorbate, H_2O/tBuOH, 1:1, rt, 56%, (b) HBTU, DIPEA, DMF, 40 °C, 47%, (c) i) $(COCl)_2$, Et_3N, CH_2Cl_2, 0 °C to rt, quant.; ii)Et_3N, CH_2Cl_2, 0 °C to rt, 55%.

6.2.2 *Formation and characterization of pre-functionalized nanoparticles*

Nanoparticles from the π-conjugated oligomers were prepared using the reprecipitation method[37] via rapid injection of 15 µL of a 1 mM THF stock solution of the oligomer, or mixtures of oligomers, into 5 mL of water (Figure 6.1 b). In this way, by premixing known volumes of THF stock solutions of the oligomers **1**, **2** and **3** before injection, nanoparticles with equal emission colors but different functional group compositions were generated and their properties studied (Table 6.1). These preparations contained as well non-functionalized nanoparticles (**NP**) of **1** only, and functionalized nanoparticles consisting out of 50% of **1** and either 50% of azide amphiphile **3** (**azide-50-NP**) or 50% of mannose amphiphile **2** (**mannose-50-NP**). Dynamic Light Scattering (DLS) measurements showed for all nanoparticles a similar average hydrodynamic radius of 40 to 50 nm, which is in good agreement with the size of the spherical nanoparticles observed with transmission electron microscopy (TEM) (Figure 6.2). The oligomers thus self-assemble into spherical nanoparticles and the TEM images suggest an amorphous internal morphology.

Table 6.1: Overview over the prepared nanoparticles and their sizes

name	**1**	**3**	**2**	r (nm) (DLS)
NP	100%	-	-	40
mannose-10-NP	90%		10%	53
mannose-25-NP	75%	-	25%	45
mannose-50-NP	50%	-	50%	35
mannose-75-NP	25%	-	75%	43
mannose-90-NP	10%	-	90%	38
azide-50-NP	50%	50%	-	50
bi-functional-NP	-	50%	50%	87

The **NP**, **azide-50-NP** and **mannose-50-NP** systems all showed identical absorption maxima at around 334 nm and 430 nm and an emission maximum at 542 nm similar to the previously reported nanoparticles based on self-assembled bolaamphiphilic fluorene benzothiadiazole derivatives[26] (Figure 6.2 a). Additionally, the different nanoparticles all had high quantum yields between 80 and 90 %.[38] These results show that the introduction of mannose and azide functionalities into the π-conjugated oligomers does not alter the size and optical and fluorescence properties of the nanoparticles. Most likely the self-assembly and optical properties are dominated by the core structure of these amphiphiles, which is not influenced by the introduced functionalities, since these compounds contain the same chromophore, and the hydrophilic/hydrophobic ratio is hardly changed.

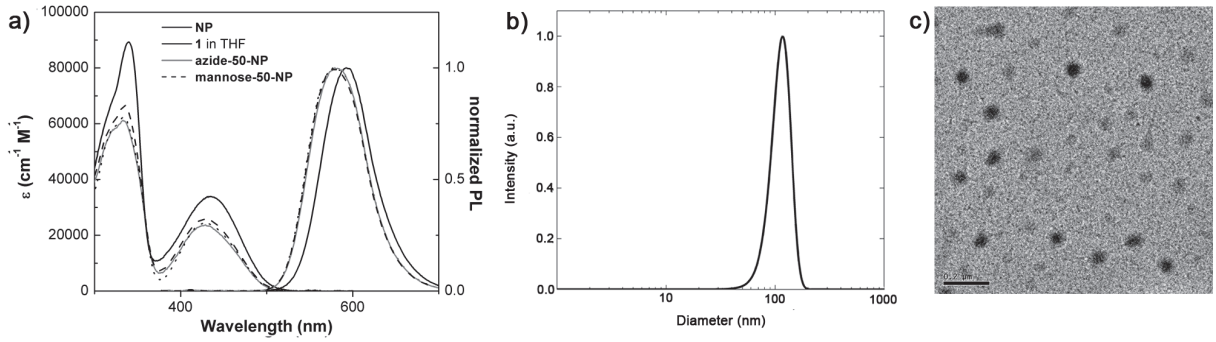

Figure 6.2**:** a) Absorption and emission spectra of self-assembled NP, **azide-50-NP** and **mannose-50-NP** in water and of molecularly dissolved amphiphile **1** in THF (amphiphile concentration for absorption measurement 3 μM, for emission spectra 1.5 μM). b) Hydrodynamic diameter of **azide-50-NP** (0.3 μM in phosphate buffer) measured by dynamic light scattering. c) Transmission electron microscopy image of **azide-50-NP**. Scale bar represents 200 nm.

To investigate the bio-availability of the introduced mannose, **mannose-50-NP**s were incubated with *E. Coli* bacteria since it is know that mannose specifically binds to the FimH receptor of *E. Coli* bacteria.[39] After incubation and washing, the bacterial pellet was yellow fluorescent under UV illumination showing that the mannose functionalized particles bind to the bacteria. At the same time, the incubation of *E. Coli* with **azide-50-NP** did not stain the bacterial pellet (Figure 6.3 a). Additionally, the hydrodynamic radius of these nanoparticles before and after the addition of mannose binding lectin ConA was measured with DLS (Figure 6.3 b). The addition of ConA to **mannose-50-NP**s significantly increased the hydrodynamic radius of the particles in solution, presumably via the cross-linking of the nanoparticles upon binding to the tetrameric lectin. In contrast, no increase in the size of **azide-50-NP**s was observed via DLS upon addition of ConA (Figure 6.3c) indicating that the azide functionality does not lead to unspecific binding. Our results show therefore, that targeting organic nanoparticles can be prepared via a simple co-assembly process. Targeting is solely induced through the appending ligand and unspecific adsorption is prevented by the shielding ethylene glycol chains. At the same time, the

introduction of a ligand at the extremities of the π-conjugated oligomers does not affect the optical and self-assembly properties.

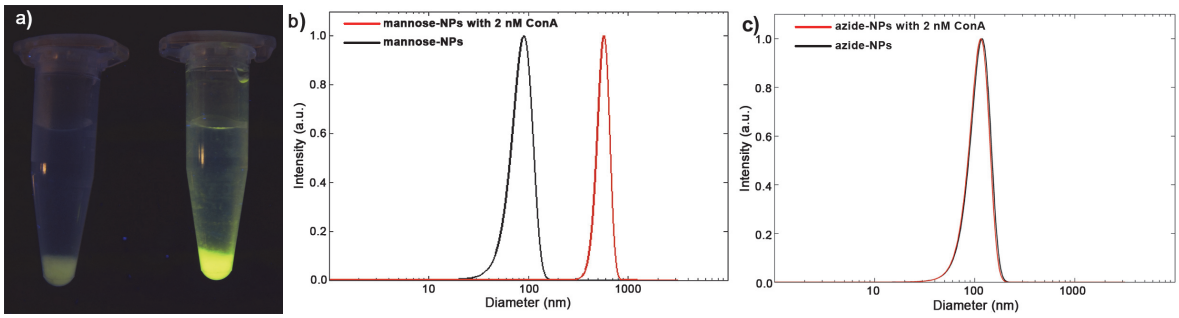

Figure 6.3: a) Photograph of washed *E. Coli* bacteria under UV illumination after incubation with (left) **azide-50-NP** and (right) **mannose-50-NP** (both 3 μM). b) Hydrodynamic diameter of **mannose-50-NP**s (0.3 μM) before and after the addition of the lectin ConA (2 nM) measured by dynamic light scattering in phosphate buffer (with 0.1 mM $CaCl_2$ and 0.1 mM $MnCl_2$, pH = 7.0) at 82°. c) Hydrodynamic diameter of **azide-50-NP**s (0.3 μM) before and after the addition of the lectin ConA (2 nM) measured by dynamic light scattering in phosphate buffer (with 0.1 mM $CaCl_2$ and 0.1 mM $MnCl_2$, pH = 7.0) at 82°.

6.2.3 *Control over nanoparticle ligand density*

An important feature of nanoparticles generated via self-assembly of pre-functionalized building blocks should be the facile and reproducible control over ligand density.[40] To investigate the effect of nanoparticle ligand densities on ConA binding, particles containing different amounts of mannose amphiphile **2** were subsequently prepared, ranging from 10% (**mannose-10-NP**) to 90% (**mannose-90-NP**) of **2** (Figure 6.4 & Table 6.1).[41]

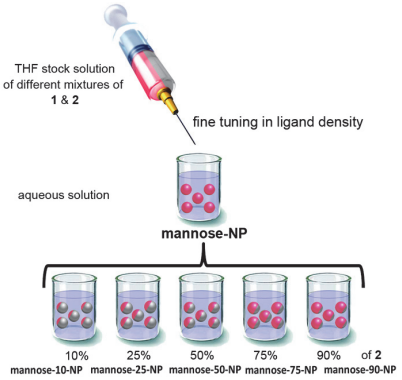

Figure 6.4: Generation of pre-functionalized mannose nanoparticles with different densities of mannose on the nanoparticle surface using mixtures of **1** and **2**.

Förster resonance energy transfer (FRET) studies were performed using dye labeled ConA to determine the influence of ligand density on protein binding. Alexa Fluor 633 (AF633) was the dye of choice as its absorbance spectrum overlaps with the emission spectrum of the nanoparticles. The binding of ConA to mannose on the nanoparticle surface should bring the

nanoparticle and the dye-labeled protein in close proximity and enable energy transfer from the fluorene benzothiadiazole donor chromophore to the acceptor dye AF633. Thus, addition of AF633 labeled ConA (ConA-AF633) indeed resulted in a decrease in the emission of **mannose-NP** (λ_{max} = 542 nm) and the appearance of AF633 acceptor emission (λ_{max} = 648 nm) (Figure 6.5 a).[39] In contrast, when AF633 labeled ConA was added to **azide-50-NP**, no energy transfer was observed, indicating that the mannose molecules attached to the nanoparticles are crucial for binding to ConA. Interestingly, a clear correlation between the energy transfer and the percentage of used mannose amphiphile **2** could be observed, with the highest FRET ratio in the case of **mannose-90-NP**s (Figure 6.5 b). A higher mannose density leads to a higher recruitment of proteins to the nanoparticle surface, resulting in an increase in FRET. The tuning of ligand density during the nanoparticle preparation therefore modulates the extent of protein binding to the nanoparticles.

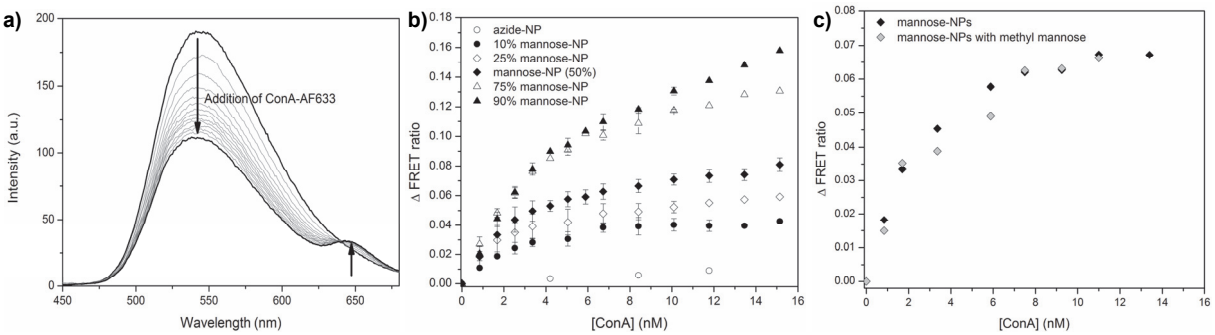

Figure 6.5: a) Change in emission spectra of **mannose-90-NP** upon addition of AlexaFluor633 labeled concanavalin A (ConA-AF633; 0.8 -15 nM) caused by energy transfer between nanoparticles and ConA-AF633. b) Change in FRET ratio of different nanoparticles upon addition of ConA-AF633 shown as the mean value of at least 3 measurements. The determined nanoparticle-protein energy transfer ratio was constant for different batches of nanoparticles prepared from different stock solutions, underlining the reproducibility of the generated ligand densities. c) Change in FRET ratio of **mannose-50-NP**s upon addition of ConA-AF633 without and in the presence of 125 μM methyl mannose. All spectra measured in phosphate buffer (with 0.1 mM $CaCl_2$ and 0.1 mM $MnCl_2$) at pH 7.0 using a nanoparticle concentration of 0.3 μM and an excitation wavelength of 350 nm.

Remarkably, FRET studies in the absence and presence of a 500-fold excess of competing methyl mannose did not lead to changes in FRET ratio (Figure 6.5 c). Methyl mannose is thus not capable of competing with the nanoparticles for ConA binding, showing the strength of lectin ConA binding to the nanoparticles. This indicates that a high ligand density of a low affinity ligand (mannose) leads to increased effective binding affinities of the nanoparticles.[42,43] This multivalency effect has not been observed for molecular dissolved mannose-containing π-conjugated systems[44] and shows the advantage of using self-assembled π-conjugated nanoparticles. The ability to control and tune the ligand density in a single preparation step opens up the possibility to screen for optimal surface functionalization for a given application in a simple and reliable way.

6.2.4 *Post-functionalization via azide-alkyne cycloaddition*

Nanoparticles with surface accessible azides enable the introduction of diverse ligands via the copper(I)-catalyzed azide-alkyne cycloaddition (CuAAC) reaction after nanoparticle formation (Figure 6.1b ii).[21,45,46] First, the azide nanoparticles, **azide-50-NP**, were post-functionalized with mannose to compare the degree of functionalization via the pre- and post-functionalization methods.

The cycloaddition reaction of azide nanoparticles was performed in degassed water using copper (II) sulfate, copper wire, bathophenanthroline, sodium ascorbate and an excess of alkyne mannose. The copper salts did not cause any significant quenching of nanoparticle fluorescence.[38] The cycloaddition reaction was performed over 18 h, and the excess of ligand and more importantly the cytotoxic copper salts were removed either by dialysis or PD-10 sephadex desalting column, both purification methods leading to the same results. The functionalization was confirmed by mass spectrometry (MALDI-ToF), where, in addition to the mass of the azide amphiphile **3**, the mass of the mannose functionalized amphiphile **2** could be detected (Figure 6.6 a). After CuAAC functionalization of azide-50-NPs with propargyl mannose **5**, changes in the FRET ratio of the post-functionalized nanoparticles upon addition of ConA-AF633 were measured and correlated with changes in the FRET ratios of pre-functionalized **mannose-50-NP**s. The post-functionalization was successful as observed by the energy transfer from nanoparticle to the dye-labeled protein. When compared with the pre-functionalized **mannose-50-NP**s the FRET experiments revealed a significantly lower degree of ligand density for the post-functionalization strategy (Figure 6.6 b). Based on the observed FRET ratios for the pre-functionalized mannose nanoparticles (Figure 6.5 b) less than 10% of the azide moieties in the **azide-50-NP**s were functionalized with mannose using typical aqueous CuAAC conditions. The lower degree of functionalization via the post-functionalization method compared with the pre-functionalization is not surprising, as the accessibility and therewith the degree of amphiphile functionalization will be significantly lower for pre-formed nanoparticles.

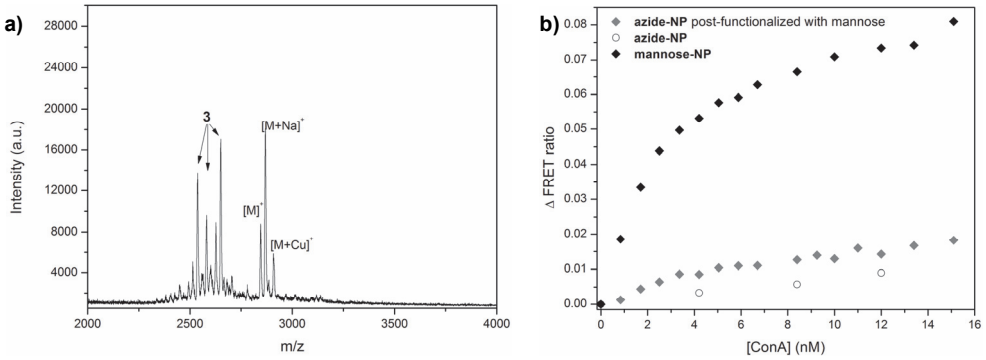

Figure 6.6: a) Changes in FRET ratio upon addition of ConA-AF633 to pre-functionalized **mannose-50-NP**s, **azide-50-NP**s or **azide-50-NP**s post-functionalized with mannose.[47] In phosphate buffer (with 0.1 mM $CaCl_2$ and 0.1 mM $MnCl_2$) at pH = 7.0 using an excitation wavelength of 350 nm. The nanoparticle concentration was 0.3 μM. b) MALDI-TOF spectrum of the azide amphiphile **3** after the cycloaddition reaction in water with propargyl mannose.

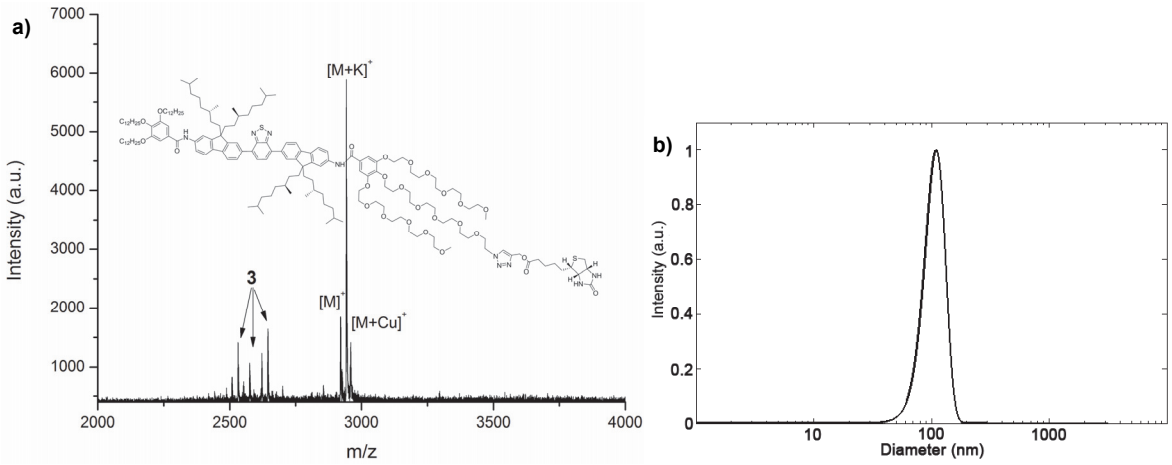

Figure 6.7: a) MALDI-TOF spectrum of the azide amphiphile **3** after the cycloaddition reaction in water with biotin alkyne. b) DLS data at 82° of **biotin-NP**s after cycloaddition of biotin alkyne to **azide-50-NP**s and purification.

Subsequently, biotin was chosen as a second biomolecule to investigate the post-functionalization of the azide nanoparticles. With a suitable alkyne derivative, biotin could also be successfully introduced onto the nanoparticle surface via CuAAC reaction at room temperature (Figure 6.1 b ii). The functionalization was confirmed by MALDI-ToF, where both the azide amphiphile **3** and the biotinylated amphiphile were detected (Figure 6.7 a). Furthermore, DLS and TEM measurements showed no significant changes in the size and shape of the biotin functionalized nanoparticles (**biotin-NP**s) compared with **azide-50-NP**, as still spherical particles with a somewhat larger hydrodynamic radius of 60 nm were observed (Figure 6.7 b). FRET studies between the post-functionalized biotin-NPs and Alexa Fluor 633 labeled streptavidin (SA-AF633), revealed energy transfer from the fluorene benzothiadiazole donor chromophore to the acceptor dye AF633 (Figure 6.8 b). No energy-transfer was observed for non-reacted **azide-50-NP**s (Figure 6.8 a). The increase in acceptor emission upon binding to the nanoparticles led to a strong color change of the nanoparticle solution when illuminated with UV light (λ_{ex} = 360 nm), allowing simple optical detection (Figure 6.8, insets). The addition of the lectin ConA-AF633 did not lead to energy transfer (Figure S 6.1) suggesting that non-specific binding does not occur. The energy transfer efficiency was higher for the streptavidin - **biotin-NP** system than for the concanavalin A - **mannose-NP** system (Figure 6.8 versus Figure 6.5). This might be explained by the shorter distance between the **biotin-NP** and the Alexa Fluor 633 dye attached to streptavidin, as SA is smaller than ConA and additionally possesses a stronger binding constant to its corresponding ligand.

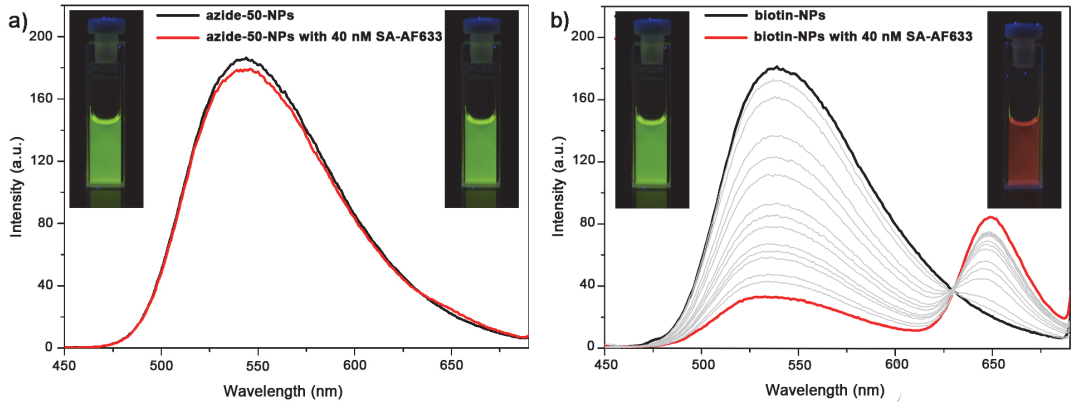

Figure 6.8: Emission spectra of a) **azide-50-NP**s and b) **biotin-NP**s before and after addition of 40 nM Alexa Fluor 633 labeled streptavidin (SA-AF633) showing that only the presence of biotin induces energy transfer. The insets show photographs of the corresponding nanoparticle solutions before (left) and after (right) the addition of 40 nM SA-AF633 under illumination with UV light (λ_{ex} = 360 nm). Energy transfer from **biotin-NP** to SA-AF633 leads to a strong color change. Spectra were measured in phosphate buffer (with 0.1 mM $CaCl_2$ and 0.1 mM $MnCl_2$) at pH 7.0 using an excitation wavelength of 350 nm. The concentration of nanoparticles was 0.3 µM.

The isolation of self-assembled post-functionalized **biotin-NP**s by magnetic streptavidin beads was also investigated.[48] After incubation with these beads and subsequent extraction using a magnet, the solution of **azide-50-NP**s remained fluorescent, suggesting no unspecific binding to the beads. In contrast, the fluorescent **biotin-NP**s were not visible in solution, indicating that the nanoparticles are effectively sequestered from solution (Figure 6.9).[49] The lack of fluorescence in solution simultaneously underlines the stability of these self-assembled nanoparticles.

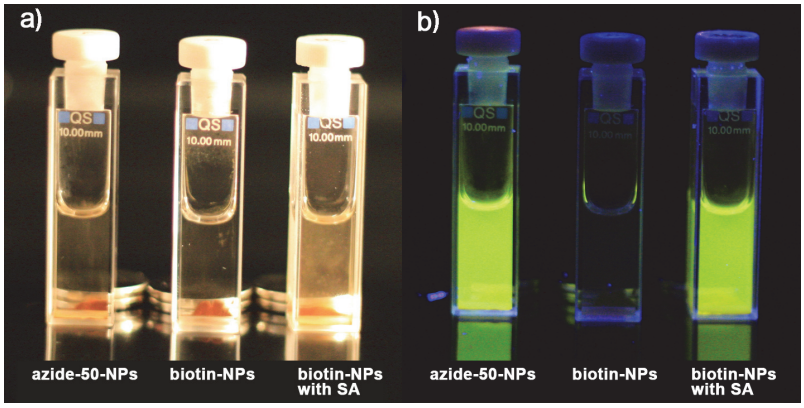

Figure 6.9: Photographs of **azide-50-NP** and **biotin-NP** under visible light (a) and UV light (b) after incubation with 150 µL of magnetic streptavidin beads (for preparation see supporting information) followed by magnetic separation after 40 minutes of incubation.

Our results show that the **azide-50-NP**s can be successfully post-functionalized with mannose and biotin via CuAAC reaction. Although, as expected, the post-functionalization was less efficient than the pre-functionalization of nanoparticles, the post-functionalization can

successfully be applied with high affinity ligands to, for example, target specific proteins or extract nanoparticles from solution by magnetic beads. This should not only enable the separation of specifically modified nanoparticles in solution but as well control circulation times *in vivo* via an avidin-induced clearance strategy.[50]

6.2.5 *Dual targeting nanoparticles*

The self-assembly of π-conjugated oligomers enables direct access to bi-functional nanoparticles, which can be used for dual targeting with possible synergistic effects.[51] For this purpose the pre- and post-functionalization strategies were combined. First, via self-assembly of pre-functionalized oligomers, **bi-functional-NP**s consisting of 50% mannose functionalized amphiphile **2** and 50% azide functionalized amphiphile **3** were prepared (Figure 6.1 b iii). To evaluate the surface availability of azides for subsequent bioconjugation, the cycloaddition reaction was performed using the alkyne derivative of biotin yielding mannose and biotin containing **dual targeting NP**s. The dual targeting properties of these particles were evaluated by measuring the energy transfer between these **dual targeting-NP**s and both, ConA-AF633 and SA-AF633. FRET studies showed that the **dual targeting-NP**s bind both to ConA and to SA (Figure 6.10). When compared with the pure **biotin-NP**s and **mannose-50-NP**s a similar binding behavior was observed (Figure 6.10 versus Figure 6.5 and Figure 6.8), proving the same effective introduction and availability of the targeting ligands. Our results show that a portfolio of pre- and post-functionalization strategies significantly broadens the flexibility of these nanoparticles in terms of ligand modification and in multitargeting applications.

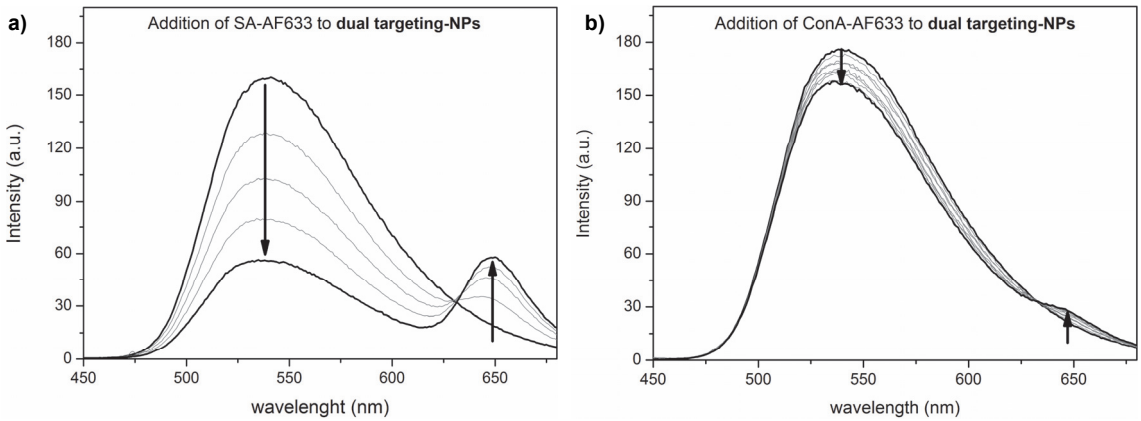

Figure 6.10: Emission spectra of **dual targeting-NP**s (0.3 μM), which contain both biotin and mannose upon addition of SA-AF633 (a; 1-5 nM) and of ConA-AF633 (b; 0.8-15 nM) measured in phosphate buffer at pH 7.0 using an excitation wavelength of 350 nm. Energy transfer was observed for both ligands.

6.3 Conclusions

We have demonstrated facile methods to generate (multi)targeted fluorescent nanoparticles based on the self-assembly of π–conjugated amphiphilic oligomers in water. Azide and mannose groups were introduced at the periphery of the ethylene glycol chains of the amphiphile. Using these building blocks a library of differently pre-functionalized nanoparticles was generated. Additionally, the nanoparticle pre-functionalization was combined with subsequent post-fuctionalization of azide bearing nanoparticles via the copper catalyzed azide-alkyne cycloaddition (CuAAC) reaction, thus expanding the ligand diversity at two independent stages in the nanoparticle fabrication process. The intrinsic fluorescence of these organic nanoparticles enables the simple evaluation of recognition events and surface properties via FRET, showing, for example, their capability and potential for multi-targeting. Decoration of nanoparticles with specific ligands induced the selective binding of proteins, bacteria and magnetic beads to the nanoparticles, which, in combination with the absence of unspecific adsorption and their stability, proves their broad potential as selective biological targeting tools. The successfully combined pre- and post-functionalization of fluorescent oligomer nanoparticles represents a novel opportunity to apply these versatile nanoparticles with readily tailored optical properties to imaging applications in biology and medicine.

6.4 Experimental

O-Benzotriazole-*N*,*N*,*N*′,*N*′-tetramethyl-uronium-hexafluoro-phosphate (HBTU) and *N*,*N*´-diisopropylethylamine (DIPEA) were purchased from Biosolve. Copper (II) sulfate, dry *N*,*N*´-dimethylformamide (DMF), (+)-sodium L-ascorbate, dry triethylamine (TEA), concanavalin A, and streptavidin were purchased from Sigma-Aldrich. Oxalylchloride, bathophenanthrolinedisulfonic acid disodium salt hydrate and copper turnings was purchased from Acros. Calcium chloride, manganese (II) chloride and *tert*-Butanol were obtained from Merck. Alexa Fluor 633 labeled streptavidin (3 moles dye per mole), Alexa Fluor 633 labeled concanavalin A (2 moles dye per mole) and streptavidin coated magnetic beads (Dynabeads® MyOne™ Streptavidin T1) were purchased from Invitrogen. Deuterated solvents were bought from Cambridge Isotope Laboratories. PD-10 sephadex desalting columns were purchased from GE Healthcare. All solvents and chemicals were used as received. Water was demineralized prior to use. Dry dichloromethane (DCM) and tetrahydrofuran (THF) were obtained from distillation over Merck molecular sieves (4 Å). Analytical thin layer chromatography (TLC) was carried out using Merck pre-coated silica gel plates (60F-254) using ultraviolet light irradiation at 254 or 365 nm. Manual column chromatography was carried out using Merck 60 Å pore size silica gel (particle size: 63-200 μm). Flash chromatography was performed using Biotage SP1 equipped with Biotage SNAP FLASH purification silica cartridges (particles size: 50 μm). General LC-MS analysis: samples were analyzed using a Shimadzu SCL-10 AD VP series HPLC coupled to a diode array detector (Finnigan Surveyor PDA Plus detector, Thermo Electron Corporation) and an Ion-Trap (LCQ Fleet, Thermo Scientific). Analyses were performed using a reversed phase HPLC column (GraceSmart PP18, 50 mm x 2.1 mm, 3μm), using an injection volume of 1-4 μL, a flow rate of 0.20 mL/min and a typically a gradient (5% to 100% in 10 min, held at 100% for 1 more minute) of acetonitrile in water (both containing 0.1% formic acid) at 298K. Reversed phase high-pressure liquid

chromatography (RP-HPLC) was performed on a Shimadzu LC-8A HPLC system by using a Gemini 5u C18 column. A gradient of water in acetonitrile, both containing 0.1% formic acid was used to elute products. Detection was performed by a Shimadzu SPD-10AV UV-detector (λ = 240 nm). Preparative recycling GPC was performed using a Shimadzu system equipped with a Shimadzu LC-10ADvp pump, a Jai-Gel 2.5 H and a Jai-Gel 2 H column in series and a Shimadzu SPD-10AVvp UV/Vis detection system performing detection at 254 nm and 340 nm. HPLC grade chloroform was used as the eluent (with a flow of 3.5 ml/min and manual injection was performed with a volume of 2 ml. One cycle through the system took 1 hour.) Matrix assisted laser desorption/ionisation time of flight mass spectra (MALDI-TOF-MS) were measured on a PerSeptive Biosystems Voyager-DE PRO spectrometer with a Biospectrometry workstation using 2-[(2E)-3-(4-tert-butylphenyl)-2-methylprop-2-enylidene] malononitrile (DCTB) as matrix material. M/z values are given in gram/mol. ^{1}H and ^{13}C NMR spectra were recorded using a Varian Mercury Vx 400 MHz (100 MHz for 13C) NMR spectrometer at 298 K. Chemical shifts are given in parts per million (ppm) and the spectra are calibrated to residual solvent signals of $CDCl_3$ (7.26 ppm (^{1}H) and 77.0 ppm (^{13}C)). Splitting patterns are labeled as s, singlet; d, doublet; dd, double doublet; t, triplet; m, multiplet and br stands for broad. UV-vis and PL spectra were measured on a Jasco V-650 spectrophometer and a Jasco FP-6500 spectrofluorometer, respectively. Dynamic light scattering experiments (DLS) were performed on an ALVCGS-3 Compact Goniometer, in the angular range of 25 to 151 degrees. The incident beam was produced by a HeNe laser operating at 632 nm. The intensity signal was sent to an ALV5000 digital correlator, using a typical acquisition time of 100 s for each angle. The calculation of the particle size distribution was performed using cumulant analysis. The nanoparticle solutions were prepared via the reprecepitation method as described before followed by a filtration via a 0.4 μm pore size cellulose filter to remove dust particles. Visualization by transmission electron microscopy (TEM) was done with a Technai G2 Sphera by FEI, working at a voltage of 200 kV on a CCD chip of 1024 x 1024 pixels. Samples were prepared by dropcasting a 3 μM solution of nanoparticles on a carbon film on a 400 square mesh copper grid for 1 min. Fluorescence spectra were recorded on a Varian Cary Eclipse fluorescence spectrophotometer equipped with a Perkin–Elmer PTP-1 Peltier temperature control system. All fluorescence measurements were performed in phosphate buffer (10 mM, pH 7.0 containing 0.1 mM $CaCl_2$ and 0.1 mM $MnCl_2$) in quartz cuvettes of 10 mm light path (Hellma) and 2 mL minimal volume at 20°C with an excitation wavelength of 350 nm. Wavelengths are given in nm, and absorptions in $Lmol^{-1}cm^{-1}$. Protein concentrations were determined using NanoDrop V3.5.2 by measuring the absorbance at 280 nm using extinction coefficients (and molecular weight) of non-labeled proteins (streptavidin Mw=53 kDa, ε =200 $M^{-1}cm^{-1}$, concanavalin A $Mw_{tetramer}$=110 kDa, ε1%=13.7 $g^{-1}cm^{-1}$x0.1L). The FRET ratio was calculated by dividing the emission of Alexa Fluor 633 at 648 nm and the emission of fluorescent nanoparticles at 542 nm, respectively. The change in FRET ratio is defined as the difference between the FRET ratio at a later measuring point and the FRET ratio before the addition of dye labeled protein. Preparation of nanoparticles, UV-PL, TEM and DLS measurements were performed by Dr. Adrien Kaeser and Irén Fischer.

The compounds **4**[31] and **5**[31] were synthesized as described previously. Compounds **1**, **7** and **3** were provided by Dr. Adrien Kaeser.[38] Compound **8** was provided by Irén Fischer.[38]

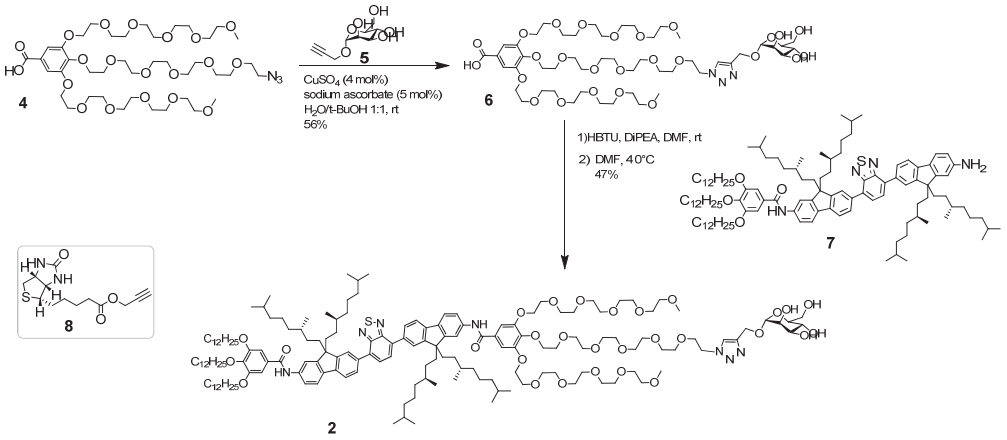

Scheme S 6.1. Synthesis of mannose functionalized amphiphile **2**.

(**6**) **4** (0.5 g, 0.55 mmol, 1 eq.) was dissolved in a one to one mixture of water and *tert*-butanol and subsequently **5** (0.141 g, 0.65 mmol, 1.2 eq.), copper (II) sulfate (1.35 mg, 0.0054 mmol, 1 mol%) and sodium ascorbate (5.3 mg, 0.027 mmol, 5 mol%) were added. After stirring the reaction mixture at room temperature overnight, the excess of educt was extracted with diethyl ether and the aqueous phase was freeze dried. The crude product purified using HPLC (40% to 65% acetonitrile in water in 10 minutes) yielding **6** (0.363 g, 56%) as a clear oil. ^{1}H NMR (400 MHz, $CDCl_3$) δ 7.79 (s, 1H, triazole), 7.29 (s, 2H, benzyl), 4.90 (s, 1H, mannose), 4.81 – 4.34 (m, 12H, mannose), 4.28 – 4.10 (m, 6H, OCH_2CH_2), 3.69 (d, *J* = 140.2 Hz, 58H, glycol chains), 3.35 (s, 6H, OCH_3); ^{13}C NMR (100 MHz, $CDCl_3$) δ 168.36 (C=O), 152.09 (benzyl), 143.71 (benzyl), 142.44 (triazole), 125.11 (triazole), 124.48 (benzyl), 109.32 (benzyl), 99.40 (α-C mannose), 72.66, 72.19, 71.83 (glycol), 71.41, 70.67-70.35 (glycol), 69.62 (glycol), 69.24 (mannose), 68.75 (glycol), 66.81, 61.27 (mannose), 60.02 (mannose), 58.92 (OCH_3), 50.21 (CH_2-triazole); LC-MS: calc. $[M]^+$ 1145.56, found $[M+H]^+$ 1146.75; R_t = 4.85 min.

(**2**) **6** (77mg, 67 μmol, 1.05 eq.) was pre-activated using HBTU (25.6 mg, 67 μmol, 1.05 eq.) and DIPEA (11.5 μL, 0.13 mmol, 2 eq.) in DMF at room temperature for 30 minutes and subsequently added to **7** (100 mg, 64 μmol, 1 eq), which was dissolved in DMF. The reaction mixture was heated up to 40 °C for 48 hours. After evaporating the solvent, the final product was purified via column chromatography (silica, 0% up to 20% MeOH in CH_2Cl_2) yielding **2** (86 mg, 47%) as a yellow solid. ^{1}H NMR (400 MHz, $CDCl_3$) δ 9.07 (s, 1H), 8.03 (d, *J* = 6.8 Hz, 2H), 7.93 (d, *J* = 8.0 Hz, 2H), 7.87 – 7.66 (m, 11H), 7.55 (d, *J* = 8.4 Hz, 1H), 7.39 – 7.34 (m, 1H), 7.31 (s, 2H), 7.10 (s, 2H), 4.94 (s, 1H), 4.77 (d, *J* = 12.4 Hz, 1H), 4.63 (d, *J* = 12.2 Hz, 1H), 4.52 (t, *J* = 4.8 Hz, 2H), 4.24 (d, *J* = 4.1 Hz, 6H), 4.05 (m, 6H), 3.93 (s, 1H), 3.83 (m, 12H), 3.61 (m, 53H), 3.34 (s, 6H), 2.18-1.96 (m, 8H), 1.88-1.73 (m, 6H), 1.53-0.64 (m, 154H); ^{13}C NMR (100 MHz, $CDCl_3$) δ 165.46, 165.42, 154.34, 153.23, 152.52, 152.25, 150.95, 150.92, 143.94, 141.55, 141.17, 140.94, 140.89, 138.14, 137.49, 137.19, 136.86, 135.83, 135.64, 133.60, 133.48, 130.70, 130.03, 128.41, 128.17, 127.74, 127.70, 126.23, 125.85, 124.43, 123.81, 120.29, 120.15, 119.30, 118.81, 117.41, 115.09, 114.69, 111.11, 107.44, 105.91, 99.35, 73.54, 72.49, 72.28, 71.79, 71.44, 70.64, 70.48, 70.41, 70.35, 70.31, 70.24, 69.63, 69.51, 69.27, 68.86, 67.26, 61.54, 60.30, 58.90, 55.26, 55.21, 50.20, 39.19, 37.75, 37.48, 36.82, 36.77, 36.58, 36.53, 33.05, 32.97, 32.91, 31.89, 30.77, 30.68, 30.30, 29.71, 29.66, 29.61, 29.55, 29.36, 29.33, 27.86, 26.06, 24.77, 24.68, 24.58, 24.55, 22.65, 22.62, 22.52, 22.49, 19.69, 19.65, 19.41, 19.35, 14.08; MALDI TOF MS: calc. $[M]^+$ 2838.90, found $[M+H]^+$ 2839.58, $[M+Na]^+$ 2863.51, $[M+K]^+$ 2879.4, R_f = 0.3 (Silica, 15 % MeOH in CH_2Cl_2).

Formation and properties of nanoparticles: Preparation of nanoparticles: Injection of 15 μL of 1 mM THF stock solutions into 5 mL of water results in a 3 μM nanoparticle solution.[26]

Binding studies with E. coli: A single colony of *E. coli* strain BL 21 was picked from an agar plate and grown overnight in 5 ml LB media with ampicillin (0.1 mg/mL) in a shaker at 37 °C. The OD_{600} was measured and the culture was diluted to reach an OD_{600} of 1.5. The bacterial culture was split in portions of 1 mL and centrifuged for 10 min at 1700 rpm. The supernatant was removed and the pellet was re-suspended in 400 μL of PBS buffer and washed three times with this buffer. Finally the pellet was re-suspended in 400 μL PBS containing $MnCl_2$ and $CaCl_2$ (0.1 mM) and 300 μL of 3 μM nanoparticle solution, either of **mannose-50-NP** or **azide-50-NP,** were added. The bacteria were incubated with the nanoparticles for 30 min at rt. Subsequently the bacteria were washed with PBS buffer as described. The pellet was re-suspended in 1 mL PBS and pictures were taken under UV illumination at 340 nm.
Binding studies with ConA-AF633: For FRET measurements (in phosphate buffer (with 0.1 mM $CaCl_2$ and 0.1 mM $MnCl_2$) at pH 7.0 using 350 nm for excitation) nanoparticles were diluted ten folds to reach the final concentration of 0.3 μM and equilibrated in the spectrophotometer at 20°C for 30 minutes before titration.

CuAAC of azide-50-NPs: Using degassed water 5 mL of a 3 μM stock solution were prepared as described previously. Subsequently, using 1 mM stock solutions, 5eq of biotin alkyne (**8**, 75 μL) or propargyl mannose (**5**, 75 μL), 4 eq of sodium ascorbate (60 μL) and 0.4 eq of copper (II) sulfate (6 μL) were added. In some cases, during the addition of reactants, aggregation occurred, which could be diminished via good stirring and bubbling of Argon through the solution during addition. If no aggregation occurred during addition, the reaction mixture did not aggregate during overnight reaction. After up to 24 hours at room temperature, the excess of alkyne ligand and the cytotoxic copper salts were removed using a PD-10 sephadex desalting column or via dialysis using a 3.5-5 kDa MWCO membrane.[38] To increase the efficiency of a CuAAC reaction of propargyl mannose (6) and azide-50-NPs, several factors can usually be changed: concentration, solvent, temperature and addition of a copper (I) stabilizing ligand. Being restricted to pure water as solvent and as well to a 3 μM concentration, the post-functionalization of the nanoparticles was conducted in presence of copper (I) stabilizing ligand (bathophenanthrolinedisulfonic acid disodium salt trihydrate (0.4 eq)). Additionally, the CuAAC reaction has been conducted at 40° C in presence and in absence of this copper (I) stabilizing ligand. None of the strategies enhanced the yields. Generally, for post-functionalization of nanoparticle surfaces an excess of ligand is necessary to drive the reaction, leading to batch to batch variations and making it difficult to adjust surface properties. Therefore, in cases where pre-functionalization is not possible, due to the poor solubility of ligands in organic solvents, the success of the bioconjugation via the CuAAC reaction needs to be controlled using binding assays.
For MALDI measurement, molecularly dissolved amphiphiles were achieved by dissolving the nanoparticles from several CuAAC reactions in THF after evaporation of water.

Incubation with magnetic streptavidin beads: Dynabeads T1 were thoroughly vortexed and 500 μL of the beads suspension were washed three times with 500 μL phosphate buffer (containing 0.1 mM $CaCl_2$ and 0.1 mM $MnCl_2$) prior to use. In the end the beads were resuspended in 600 μL buffer. After addition to nanoparticles, the magnetic beads were collected with a magnet after 40 minutes of incubation.

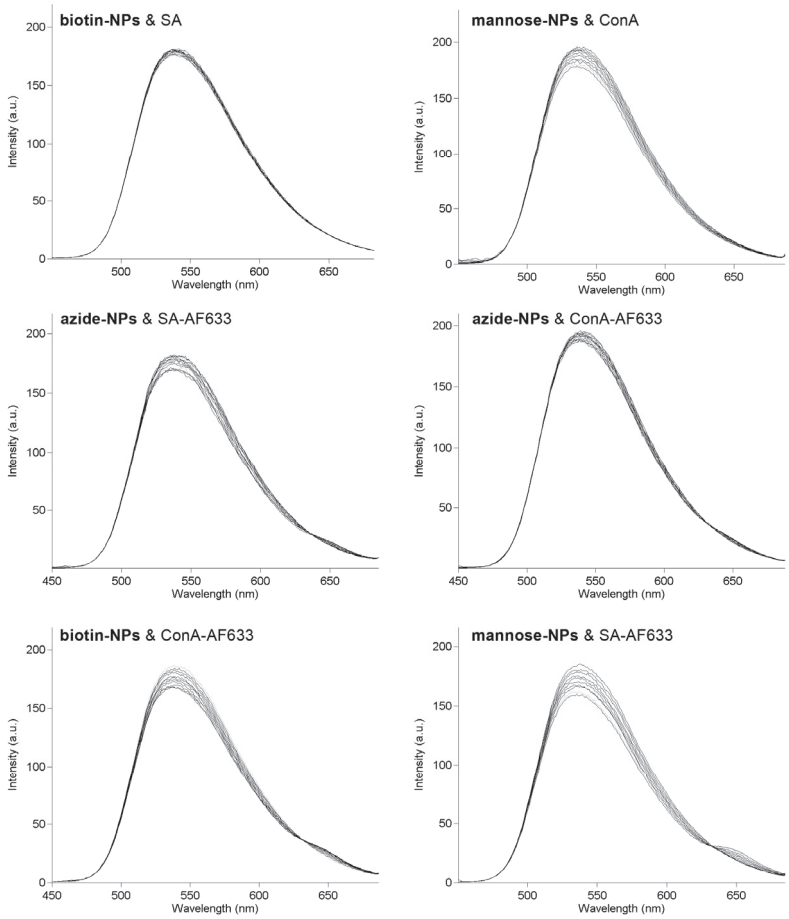

Figure S 6.1: Control measurements to show that there is no unspecific adsorption: Emission spectra of either **azide-**, **mannose-** or **biotin-NPs** upon addition of labeled and non-labeled protein. Addition of non-labeled protein as expected does not lead to a decrease in emission. No unspecific interaction is observed between both labeled proteins and **azide-NPs**. Addition of labeled SA to **mannose-NPs** and of labeled ConA to **biotin-NPs** did not feature strong FRET, indicating that FRET is specifically induced through binding to the appropriate ligand. Concentration of nanoparticles was 0.3 μM, maximum concentration of added proteins varied between 14 and 45 nM.[38] The samples were excited at 350 nm.

6.5 References

1. Davis, M. E.; Chen, Z. (Georgia); Shin, D. M. Nanoparticle Therapeutics: An Emerging Treatment Modality for Cancer. *Nat Rev Drug Discov* **2008**, *7*, 771–782.
2. R. Subbiah; M. Veerapandian; K. S. Yun Nanoparticles: Functionalization and Multifunctional Applications in Biomedical Sciences. *Curr. Med. Chem* **2010**, *17*, 4559–4577.
3. Shi, J.; Votruba, A. R.; Farokhzad, O. C.; Langer, R. Nanotechnology in Drug Delivery and Tissue Engineering: From Discovery to Applications. *Nano Lett.* **2010**, *10*, 3223–3230.
4. Zhou, Y.; Drummond, D. C.; Zou, H.; Hayes, M. E.; Adams, G. P.; Kirpotin, D. B.; Marks, J. D. Impact of Single-chain Fv Antibody Fragment Affinity on Nanoparticle Targeting of Epidermal Growth Factor Receptor-expressing Tumor Cells. *J. Mol. Biol.* **2007**, *371*, 934–947.
5. Montet, X.; Funovics, M.; Montet-Abou, K.; Weissleder, R.; Josephson, L. Multivalent Effects of RGD Peptides Obtained by Nanoparticle Display. *J. Med. Chem.* **2006**, *49*, 6087–6093.

6. Bangham, A. D.; Horne, R. W. Negative Staining of Phospholipids and Their Structural Modification by Surface-active Agents as Observed in the Electron Microscope. *J. Mol. Biol.* **1964**, *8*, 660–668, IN2–IN10.
7. Medintz, I. L.; Uyeda, H. T.; Goldman, E. R.; Mattoussi, H. Quantum Dot Bioconjugates for Imaging, Labelling and Sensing. *Nat Mater* **2005**, *4*, 435–446.
8. Zrazhevskiy, P.; Sena, M.; Gao, X. Designing Multifunctional Quantum Dots for Bioimaging, Detection, and Drug Delivery. *Chem. Soc. Rev.* **2010**, *39*, 4326-4354.
9. Wu, C.; Bull, B.; Szymanski, C.; Christensen, K.; McNeill, J. Multicolor Conjugated Polymer Dots for Biological Fluorescence Imaging. *ACS Nano* **2008**, *2*, 2415–2423.
10. Tuncel, D.; Demir, H. V. Conjugated Polymer Nanoparticles. *Nanoscale* **2010**, *2*, 484-494.
11. Pecher, J.; Mecking, S. Nanoparticles of Conjugated Polymers. *Chem. Rev.* **2010**, *110*, 6260–6279.
12. Biju, V.; Itoh, T.; Ishikawa, M. Delivering Quantum Dots to Cells: Bioconjugated Quantum Dots for Targeted and Nonspecific Extracellular and Intracellular Imaging. *Chem. Soc. Rev.* **2010**, *39*, 3031-3056.
13. Oh, J. K. Surface Modification of Colloidal CdX-based Quantum Dots for Biomedical Applications. *J. Mater. Chem.* **2010**, *20*, 8433-8445.
14. Mulder, W. J. M.; Strijkers, G. J.; Tilborg, G. A. F. van; Cormode, D. P.; Fayad, Z. A.; Nicolay, K. Nanoparticulate Assemblies of Amphiphiles and Diagnostically Active Materials for Multimodality Imaging. *Acc. Chem. Res.* **2009**, *42*, 904–914.
15. Strijkers, G. J.; Kluza, E.; Tilborg, G. A. F.; Schaft, D. W. J.; Griffioen, A. W.; Mulder, W. J. M.; Nicolay, K. Paramagnetic and Fluorescent Liposomes for Target-specific Imaging and Therapy of Tumor Angiogenesis. *Angiogenesis* **2010**, *13*, 161–173.
16. Moon, J. H.; McDaniel, W.; MacLean, P.; Hancock, L. F. Live-Cell-Permeable Poly(p-phenylene Ethynylene). *Angew. Chem. Int. Ed.* **2007**, *46*, 8223–8225.
17. Wu, C.; Szymanski, C.; Cain, Z.; McNeill, J. Conjugated Polymer Dots for Multiphoton Fluorescence Imaging. *J. Am. Chem. Soc.* **2007**, *129*, 12904–12905.
18. Kaeser, A.; Schenning, A. P. H. J. Fluorescent Nanoparticles Based on Self-Assembled π-Conjugated Systems. *Adv. Mater.* **2010**, *22*, 2985–2997.
19. For molecularly dissolved π-conjugated polymers and oligomers in imaging and sensing see: a) Feng, X.; Liu, L.; Wang, S.; Zhu, D. Water-soluble Fluorescent Conjugated Polymers and Their Interactions with Biomacromolecules for Sensitive Biosensors. *Chem. Soc. Rev.* **2010**, *39*, 2411; b) Herland, A.; Inganäs, O. Conjugated Polymers as Optical Probes for Protein Interactions and Protein Conformations. *Macromol. Rapid Commun.* **2007**, *28*, 1703–1713; c) Thomas, S. W.; Joly, G. D.; Swager, T. M. Chemical Sensors Based on Amplifying Fluorescent Conjugated Polymers. *Chem. Rev.* **2007**, *107*, 1339–1386; d) Xue, C.; Velayudham, S.; Johnson, S.; Saha, R.; Smith, A.; Brewer, W.; Murthy, P.; Bagley, S. T.; Liu, H. Highly Water-Soluble, Fluorescent, Conjugated Fluorene-Based Glycopolymers with Poly(ethylene glycol)-Tethered Spacers for Sensitive Detection of Escherichia Coli. *Chem. Eur. J.* **2009**, *15*, 2289–2295; e) Duarte, A.; Pu, K.-Y.; Liu, B.; Bazan, G. C. Recent Advances in Conjugated Polyelectrolytes for Emerging Optoelectronic Applications. *Chem. Mater.* **2011**, *23*, 501–515; f) Phillips, R. L.; Kim, I.-B.; Tolbert, L. M.; Bunz, U. H. F. Fluorescence Self-Quenching of a Mannosylated Poly(p-phenylene ethynylene) Induced by Concanavalin A. *J. Am. Chem. Soc.* **2008**, *130*, 6952–6954.
20. Functionalization of π-conjugated systems with biomolecules has as well been used to structure the self-assembly: a) Jatsch, A.; Schillinger, E.-K.; Schmid, S.; Bäuerle, P. Biomolecule Assisted Self-assembly of π-conjugated Oligomers. *J. Mater. Chem.* **2010**, *20*, 3563-3578; b) Ruiz-Carretero, A.; Janssen, P. G. A.; Kaeser, A.; Schenning, A. P. H. J. DNA-templated Assembly of Dyes and Extended π-conjugated Systems. *Chem. Commun.* **2011**,4340-4347.
21. Wu, C.; Schneider, T.; Zeigler, M.; Yu, J.; Schiro, P. G.; Burnham, D. R.; McNeill, J. D.; Chiu, D. T. Bioconjugation of Ultrabright Semiconducting Polymer Dots for Specific Cellular Targeting. *J. Am. Chem. Soc.* **2010**, *132*, 15410–15417.
22. Wu, C.; Jin, Y.; Schneider, T.; Burnham, D. R.; Smith, P. B.; Chiu, D. T. Ultrabright and Bioorthogonal Labeling of Cellular Targets Using Semiconducting Polymer Dots and Click Chemistry. *Angew. Chem. Int. Ed.* **2010**, *49*, 9436–9440.

23. Wu, C.; Hansen, S. J.; Hou, Q.; Yu, J.; Zeigler, M.; Jin, Y.; Burnham, D. R.; McNeill, J. D.; Olson, J. M.; Chiu, D. T. Design of Highly Emissive Polymer Dot Bioconjugates for In Vivo Tumor Targeting. *Angew. Chem. Int. Ed.* **2011**, *50*, 3430–3434.
24. Kim, B.-S.; Hong, D.-J.; Bae, J.; Lee, M. Controlled Self-Assembly of Carbohydrate Conjugate Rod−Coil Amphiphiles for Supramolecular Multivalent Ligands. *J. Am. Chem. Soc.* **2005**, *127*, 16333–16337.
25. Ryu, J.-H.; Lee, E.; Lim, Y.; Lee, M. Carbohydrate-Coated Supramolecular Structures: Transformation of Nanofibers into Spherical Micelles Triggered by Guest Encapsulation. *J. Am. Chem. Soc.* **2007**, *129*, 4808–4814.
26. Abbel, R.; Weegen, R. van der; Meijer, E. W.; Schenning, A. P. H. J. Multicolour Self-assembled Particles of Fluorene-based Bolaamphiphiles. *Chem. Commun.* **2009**, 1697-1699.
27. Abbel, R.; der Weegen, R. van; Pisula, W.; Surin, M.; Leclère, P.; Lazzaroni, R.; Meijer, E. W.; Schenning, A. P. H. J. Multicolour Self-Assembled Fluorene Co-Oligomers: From Molecules to the Solid State via White-Light-Emitting Organogels. *Chem. Eur. J.* **2009**, *15*, 9737–9746.
28. Zalipsky, S. Chemistry of Polyethylene Glycol Conjugates with Biologically Active Molecules. *Adv. Drug. Deliver. Rev.* **1995**, *16*, 157–182.
29. Caliceti, P.; Veronese, F. M. Pharmacokinetic and Biodistribution Properties of Poly(ethylene Glycol)-protein Conjugates. *Adv. Drug. Deliver. Rev.* **2003**, *55*, 1261–1277.
30. Karakoti, A. S.; Das, S.; Thevuthasan, S.; Seal, S. PEGylated Inorganic Nanoparticles. *Angew. Chem. Int. Ed.* **2011**, *50*, 1980–1994.
31. Müller, M. K.; Brunsveld, L. A Supramolecular Polymer as a Self-Assembling Polyvalent Scaffold. *Angew. Chem. Int. Ed.* **2009**, *48*, 2921–2924.
32. Ryu, J.-H.; Hong, D.-J.; Lee, M. Aqueous Self-assembly of Aromatic Rod Building Blocks. *Chem. Commun.* **2008**, 1043–1054.
33. Karlsson, K. A. Bacterium-host Protein-carbohydrate Interactions and Pathogenicity. *Biochem. Soc. Trans* **1999**, *27*, 471–474.
34. Wood, E. *Concanavalin A as a Tool*; **1977**; Vol. 5.
35. Rostovtsev, V. V.; Green, L. G.; Fokin, V. V.; Sharpless, K. B. A Stepwise Huisgen Cycloaddition Process: Copper(I)-Catalyzed Regioselective "Ligation" of Azides and Terminal Alkynes. *Angew. Chem. Int. Ed.* **2002**, *41*, 2596–2599.
36. Tornøe, C. W.; Christensen, C.; Meldal, M. Peptidotriazoles on Solid Phase: [1,2,3]-Triazoles by Regiospecific Copper(I)-Catalyzed 1,3-Dipolar Cycloadditions of Terminal Alkynes to Azides. *J. Org. Chem.* **2002**, *67*, 3057–3064.
37. Kasai, H.; Nalwa, H. S.; Oikawa, H.; Okada, S.; Matsuda, H.; Minami, N.; Kakuta, A.; Ono, K.; Mukoh, A.; Nakanishi, H. A Novel Preparation Method of Organic Microcrystals. *Jpn. J. Appl. Phys.* **1992**, *31*, L1132–L1134.
38. Petkau, K.; Kaeser, A.; Fischer, I.; Brunsveld, L.; Schenning, A. P. H. J. Pre- and Postfunctionalized Self-Assembled π-Conjugated Fluorescent Organic Nanoparticles for Dual Targeting. *J. Am. Chem. Soc.* **2011**, *133*, 17063–17071.
39. Disney, M. D.; Zheng, J.; Swager, T. M.; Seeberger, P. H. Detection of Bacteria with Carbohydrate-Functionalized Fluorescent Polymers. *J. Am. Chem. Soc.* **2004**, *126*, 13343–13346.
40. Gu, F.; Zhang, L.; Teply, B. A.; Mann, N.; Wang, A.; Radovic-Moreno, A. F.; Langer, R.; Farokhzad, O. C. Precise Engineering of Targeted Nanoparticles by Using Self-assembled Biointegrated Block Copolymers. *PNAS* **2008**, *105*, 2586 –2591.
41. DLS and TEM studies revealed aggregation for nanoparticles consisting of pure (100%) **2** only, probably through intermolecular hydrogen bonding of carbohydrates. This outcome is in agreement with the literature, e.g. the intermolecular hydrogen bonds of carbohydrates were used by Bäuerle et al. to self-assemble carbohydrate functionalized oligothiophenes into higher order structures (ref.20a). In our case, the undesired aggregation could be prevented in a simple manner for our nanoparticles, by simply reducing the number of incorporated mannose functionalized amphiphiles by mixing in

amphiphile **1**. Reduction to 90% was found to be enough to overcome unspecific aggregation, as evidenced by DLS.

42. This strong multivalent binding manifested itself as well during the incubation with *E.Coli*, which lead to a strong cross-linking of the bacterial pellet.
43. Binding constants of these multivalent interactions could not be determined as the starting concentration of the nanoparticle solution was too low for enzyme linked lectin assay (ELLA) and hemagglutination assays.
44. Schmid, S.; Mishra, A.; Bäuerle, P. Carbohydrate-functionalized Oligothiophenes for Concanavalin A Recognition. *Chem. Commun.* **2011**, *47*, 1324-1326.
45. Cutler, J. I.; Zheng, D.; Xu, X.; Giljohann, D. A.; Mirkin, C. A. Polyvalent Oligonucleotide Iron Oxide Nanoparticle "Click" Conjugates. *Nano Lett.* **2010**, *10*, 1477–1480.
46. Dongen, S. F. M. van; Nallani, M.; Schoffelen, S.; Cornelissen, J. J. L. M.; Nolte, R. J. M.; Hest, J. C. M. van A Block Copolymer for Functionalisation of Polymersome Surfaces. *Macromol. Rapid Commun.* **2008**, *29*, 321–325.
47. The Figures for post-functionalized nanoparticles represent a typical curve obtained after post-functionalization. In contrast to reproducible ligand densities achieved via the pre-functionalization approach, the reproducibility of ligand densities via the post-functionalization approach was less favorable.
48. Haukanes, B.-I.; Kvam, C. Application of Magnetic Beads in Bioassays. *Nat Biotech* **1993**, *11*, 60–63.
49. The intrinsic nanoparticle fluorescence can be used to determine the optimal biotin-NPs/magnetic streptavidin beads ratio to completely remove the nanoparticles from solution (see Reference 38).
50. Kobayashi, H.; Kawamoto, S.; Star, R. A.; Waldmann, T. A.; Brechbiel, M. W.; Choyke, P. L. Activated Clearance of a Biotinylated Macromolecular MRI Contrast Agent from the Blood Pool Using an Avidin Chase. *Bioconjugate Chem.* **2003**, *14*, 1044–1047.
51. Kluza, E.; Schaft, D. W. J. van der; Hautvast, P. A. I.; Mulder, W. J. M.; Mayo, K. H.; Griffioen, A. W.; Strijkers, G. J.; Nicolay, K. Synergistic Targeting of Avβ3 Integrin and Galectin-1 with Heteromultivalent Paramagnetic Liposomes for Combined MR Imaging and Treatment of Angiogenesis. *Nano Lett.* **2010**, *10*, 52–58.

Self-assembling auto-fluorescent amphiphiles

Nano-sized platform technology for multi-purpose cellular targeting

Amphiphilic molecules emerged as versatile building blocks for the generation of nano-sized architectures in water, as they can be programmed to self-assemble into a wide range of different topologies. In this thesis the generation of auto-fluorescent heterovalent nano-sized structures was explored using two types of amphiphilic scaffolds: disc-shaped and linear amphiphiles self-assembling in water into columnar polymers or into amorphous spherical nanoparticles, respectively.

Numerous applications for self-assembling nanostructures were reported in literature based on amphiphilic molecules, ranging from imaging to diagnostics, and from drug delivery to tissue engineering. Many of these applications require the capability of the supramolecular system to actively target specific cell surface receptors. This is typically achieved through decoration with bioactive epitopes such as small molecules, peptides, and proteins. As discussed in chapter 1, the bioactive epitopes can either already be part of the monomeric supramolecular building blocks (pre-functionalization) or introduced after self-assembly via covalent attachment to appending reactive groups (post-functionalization).

Selective and multivalent binding of disc-shaped amphiphiles to bacterial receptors was previously shown through the introduction of three functional groups at the periphery of the ethylene oxide tails and subsequent functionalization with bioactive ligands. Here, to expand the library of scaffolds, amphiphiles containing either nine amine functionalities or a single amine, azide and propargyl group were synthesized. Their decoration with bioactive ligands such as peptides, carbohydrates, small molecules and fluorescent dyes using both amide coupling and copper-catalyzed azide-alkyne cycloaddition is described in chapter 2. The orthogonality of the copper-catalyzed azide-alkyne cycloaddition allowed the functionalization with unprotected ligands. Whereas the functionalization of discotics with a carbohydrate was quantitative, the coupling of peptides proceeded with at best 40% conversion. This was probably due to steric crowding of peripheral functionalities in the self-assembly inducing solvent, which is required for solubility of unprotected ligands. In contrast, discotics bearing a single amine emerged as a versatile non-sterically hindered scaffold for ligand attachment as they were rapidly and quantitatively functionalized with a range of peptidic- and non-peptidic ligands using both NHS ester and HBTU activation techniques under non-assembling solvent conditions.

The ability to fine-tune the density and display of bioactive epitopes and thereby creating more complex dynamic and heterovalent structures without interfering with the self-assembling process is a key prerequisite for the development of a platform technology for targeting. A versatile and non-sterically hindered scaffold for ligand attachment, such as the presented discotic bearing a single amine, might constitute the basis for such a technology. The functionalization of this discotic leads to monovalent ligand functionalized discotics. The display

of multiple ligands, which is important for enhanced binding affinities, will be accomplished upon self-assembly into columnar stacks. This so-called multivalency upon self-assembly has been probed with a number of monovalent ligand-functionalized discotics in chapter 3. Enzyme-linked lectin assay revealed a three-fold increase in binding activity compared with the non self-assembling counterpart. The self-assembly into a columnar stack and the accompanied display of multiple ligands was as well confirmed studying the binding of monovalent streptavidin to discotics functionalized with a single biotin using Förster resonance energy transfer and SDS-PAGE. The formation of heterovalent supramolecular polymers through dynamic intermixing of different functionalized building blocks was shown using mixtures of biotin and fluorescein functionalized discotics incubated with streptavidin coated magnetic beads. Thus the self-assembly into supramolecular polymers not only generates a multivalent, but as well a heterovalent system.

The possibility to generate heterovalent supramolecular polymers via simple intermixing of discotics has a great potential in view of advanced biological applications, for example in the field of targeted imaging. To gain further inside into the dynamics of this intermixing process, discotics bearing a single O^6-benzylguanine moiety were covalently post-functionalized with two FRET-pairing fluorescent proteins. Firstly, the covalent post-functionalization with proteins, ligands which are incompatible with the pre-functionalization strategy, was confirmed with several analytical techniques such as SDS-PAGE and LC-MS in chapter 4. The covalent protein conjugation at the same time leads to Förster resonance energy transfer from the auto-fluorescent discotic scaffold to the yellow fluorescent protein and allows on-line monitoring of the conjugation. At the same time the protein conjugation does not interfere with the self-assembling process, leading to a multivalent protein display on a supramolecular wire, as visualized via energy transfer from the cyan to the yellow fluorescent protein. Secondly, the system maintains its intermixing dynamics, which allows the formation of hetero-functionalized supramolecular protein-conjugated polymers through exchange of the protein-functionalized discotics over time. The supramolecular wires act as dynamic framework on which the two proteins can assemble and exchange in a dynamic manner, leading to effective protein interactions, as observed by energy transfer.

The cellular uptake of amine-decorated discotics and the dependence of cellular uptake on the peripheral amine density were explored in chapter 5. Using the auto-fluorescence of the discotic scaffolds, their internalization was studied using live cell multiphoton fluorescence microscopy Discotics bearing three or nine amine groups at their periphery efficiently translocated through the plasma membrane via endocytosis. Additionally, the knowledge about the formation of intermixed supramolecular polymers obtained in chapter 3 and 4 was applied to generate multi-functional supramolecular polymers consisting of up to three different cell-permeable and non cell-permeable discotic monomers. Through intermixing with cell-permeable discotic monomers in the supramolecular polymer, the cellular uptake of non-cell permeable discotics was induced

and each of the components could be individually visualized, demonstrating the potential of dynamic multi-component supramolecular polymers.

The functionalization of self-assembling π-conjugated nanoparticles with bioactive epitopes, a prerequisite for applications in targeted multimodal imaging, was investigated in the last chapter. Upon microinjection into water, these linear and auto-fluorescent amphiphiles self-assemble into highly-fluorescent amorphous nanoparticles of 80-100 nm. Azide and mannose groups were introduced at the periphery of the ethylene glycol chains of the amphiphile and did not interfere with the self-assembly process. The binding of mannose functionalized nanoparticles to proteins and bacteria confirmed the accessibility of the introduced ligand. Co-assembly of different amphiphiles enabled the fine-tuning of ligand density, which was confirmed with Förster resonance energy transfer. Additionally, using copper catalyzed azide-alkyne cycloaddition reaction, azide bearing nanoparticles were post-functionalized with different ligands. Successful combination of both functionalization strategies via intermixing of mannose and azide bearing amphiphiles and subsequent copper catalyzed azide-alkyne cycloaddition led to heterovalent nanoparticles.

Nano-sized columnar and spherical supramolecular assemblies were functionalized with a wide range of ligands such as carbohydrates, peptides, and proteins using both pre- and post-functionalization strategies. This allowed for expanding the ligand diversity at two independent stages in the fabrication process of these bioactive nano-structures. Supramolecular synthesis enabled the facile generation of complex heterovalent bioactive assemblies; in the case of nanoparticles via co-assembly of different amphiphiles and in the case of discotics via dynamic intermixing of building blocks between the supramolecular stacks. With this knowledge in hand advanced applications of complex multitargeting and multimodal supramolecular nano-sized structures in imaging can be envisioned; carrying for example several targeting ligands as well as an alternative imaging probe. The ability to tune the optical properties in the case of the nanoparticles should additionally enable multi-color imaging. At the same time, the self-assembling nature of these nanoparticles allows the incorporation of hydrophobic (drug) molecules and functionalized lipids, expanding the scope of functionalization strategies and with it of possible applications. The absence of unspecific adsorption of the bare scaffolds of both the disc-shaped and linear amphiphiles proves their broad potential as selective biological targeting tools.

List of publications

D.A. Uhlenheuer, K. Petkau, L. Brunsveld, Combining supramolecular chemistry with biology, *Chem. Soc. Rev.*, **2010**, 39, 2817-2826

M.K. Müller, K. Petkau, L. Brunsveld, Protein assembly along a supramolecular wire, *Chem. Commun.*, **2011**, 310-312

K. Petkau, A. Kaeser, I. Fischer, L. Brunsveld, A.P.H.J. Schenning, Pre- and postfunctionalized self-assembled π-conjugated fluorescent organic nanoparticles for dual targeting, *J. Am. Chem. Soc.*, **2011**, 133, 17063-17071.

K.Petkau-Milroy, M.H. Sonntag, A.H.A.M van Onzen, L. Brunsveld, Supramolecular polymers as dynamic multi-component cellular uptake carriers, *J. Am. Chem. Soc*, **2012**, DOI: 10.1021/ja3029075

K. Petkau-Milroy, D.A. Uhlenheuer, A.J.H. Spiering, J.A.J.M. Vekemans, L. Brunsveld, Dynamic protein assembly through site-selective attachment and display on a supramolecular wire, submitted.

Curriculum vitae

Katja Petkau-Milroy was born on September 26th 1982 in Frunze (Kyrgyzstan). After emigrating to Germany in December 1993 she continued her primary education at the Reinoldus und Schiller Gymnasium in Dortmund. In 2003, after finishing her secondary education, she went on to study Chemistry at the Technische Universität Dortmund (Germany). As part of her studies she participated in the Erasmus exchange program with the Universidad Complutense de Madrid (Spain), working on cell culture techniques and biocompatibility studies of poly(ε-caprolactone) films in the group of prof. dr. M.T. Portolés and dr. R. Pagani. In 2008, she received the degree of 'Diplom-Chemikerin' after having finished a research project entitled 'peptides used in nuclear receptor - co-factor interaction' under the guidance of prof. dr. H. Waldmann and dr. ir. L. Brunveld at the Max Planck Institute of Molecular Physiology in Dortmund (Germany). From July 2008 she started a PhD project at the Technische Universiteit Eindhoven (the Netherlands) under the supervision of prof. dr. ir. L. Brunsveld. Her research focused on the synthesis and biological evaluation of multivalent supramolecular polymers as dynamic platforms for protein assembly and cell surface recognition. The most important results of this work are presented in this dissertation.

Acknowledgement

The last words of this thesis are dedicated to those people who contributed to the described research and supported me during the last four years.

First of all, I would like to thank my promoter, Prof. Dr. Luc Brunsveld, for giving me the opportunity to work on this exciting project. Luc, hartelijk dank voor jouw begeleiding en ondersteuning. In de laatste 5 jaren heb ik vooral jouw vertrouwen in mij en de vrijheid, die jij me gaf, gewaardeerd. Hierdoor kon ik mijn eigen ideeën en initiatieven nastreven en het was de perfecte combinatie voor mij om te groeien en mezelf te ontwikkelen.

I would like to thank the members of my committee Prof. Dr. Jan van Hest, Dr. Ivan Huc, Prof. Dr. Klaas Nicolay, Dr. Albert Schenning for reading and approving this thesis as well as for their valuable feedback. Prof. Dr. Holger Grüll and Dr. Leo van Ijzendoorn are acknowledged for taking part in the extended defense committee.

The fruitful collaboration with Albert Schenning, Adrien Kaeser and Iren Fischer introduced me to the world of organic nanoparticles. Albert, thanks a lot for your support and input, especially as you mostly offered a different perspective on things. Adrien, it took us a while to get the nanoparticle project working, but I am very glad that we kept at it. Merci et beaucoup de succès. Irén, thanks for continuing this collaboration and countless nanoparticle preparations and TEM measurements. Viel Erfolg für das vor dir liegende Jahr.

The switching from nuclear receptors to supramolecular chemistry between my master's and my PhD project was greatly facilitated by Marion Müller, whose PhD work laid the basis for this thesis. Marion, vielen Dank für deine wertvolle Vorarbeit und Unterstützung. Within our group I have enjoyed working together with Dana Uhlenheuer and Michael Sonntag, who contributed to the work described in chapter 4 and 5. Furthermore, Michel van Houtem and Jolanda Spiering are acknowledged for providing me with the precursor for the mono-functionalized discotics. This compound built the basis for several chapters and saved me a lot of time in the chemistry lab. Additionally, I had the pleasure to guide several students. I would like to thank Neslihan Bozkurt for her support with the peptide synthesis. Alexander Colditz is acknowledged for the expression of monovalent streptavidin and the help with FRET and SDS-PAGE experiments described in chapter 3. I would like to thank Thuur van Onzen for his contribution towards the supramolecular cellular uptake carriers, which are described in chapter 5. In those rather stressful last months I was as well working with Yvonne Dorland and Mark van 't Erve (thanks for being so understanding and Mark thanks for repairing my bike!). Thank you all for your input and a lot of success for the future. Marcel Koenigs is acknowledged for the cryoTEM measurements of the discotics, finally directly proving their self-assembly into long stacks in water. Additionally, I would like to thank Jeff Vekemanns en Bas de Waal for the possibility to discuss synthetic questions and the analytical team for taking care of all the equipment. A special thank you goes

to Lou Xianwen and Ralph Bovee for measuring countless MALDI spectra for me. Henk Janssen and SyMO-Chem are acknowledged for providing me with several ligands.

I would like to acknowledge the whole Brunsveld group which since the beginning of my 'Diplomarbeit' in 2007 more or less became my second family and, judging by the amount of hours spent here, as well my second home. Working in an interdisciplinary group with people from different scientific and geographical backgrounds created a fascinating, instructive and enjoyable environment. From my time in the Brunsveld group at the Max Planck Institute and the Chemical Genomics Center in Dortmund I would like to thank Belén, Dana, Dodo, Esther, Hoang, Hülya, Jacqui, Li, Maëlle, Marion, Marta, Sabine, Trang and Vasanth. Following Luc to Eindhoven for my PhD project meant as well to move from the small labs full of people in Dortmund into the spacious and empty chemistry lab in Eindhoven. The help of Hans Damen was irreplaceable in the process of equipping and starting up the chemistry lab as well as for quick and reliable ordering of the chemicals over the last four years. I would like to thank Joke Rediker for organizing all the official paperwork, group activities and for simply keeping everything running. In the beginning the whole Brunsveld group in Eindhoven was occupying a single office (Dana, Dung, Maëlle and me) but quickly expanded. I want to thank Andrea, Christian, Dana, Dung, Inga, Ingrid, Lech, Lidia, Matthew, Michael, Parisa, Ralph, Sascha, and Wencke for the nice working atmosphere in the 'Eindhoven edition' of the Brunsveld group. Without the people from Schubert's group it would have been quite empty at the beginning and without Christoph my compounds would still be trapped in desiccators. Thanks for your warm welcome. After the Schubert's group left, the lab was fortunately filled with life by people from Rint's group and by the time the discotics were synthesized, I have enjoyed working in the biolab together with the people from Merkx's group. Our joint chemical biology meetings were an excellent platform for detailed project discussions.

Dana, wir kannten uns kaum als wir plötzlich in Eindhoven nicht nur das Labor und das Büro, sondern auch die Wohnung und unsere Freizeit teilten. Zu unserer Überraschung hat es aber super geklappt und ich habe eine sehr gute Freundin dazu gewonnen, wahrscheinlich weil wir so verschieden sind. Deswegen war es umso verwunderlicher, dass wir andauernd verwechselt wurden, das letzte Mal am Tage deiner Verteidigung. Mal sehen ob es auf meiner Verteidigung, wo du meine Paranymphe sein wirst, auch wieder vorkommt. Das letzte halbe Jahr hat es mir sehr gefehlt mich einfach im Büro umzudrehen um mit dir etwas zu besprechen. Vielen Dank für Alles.

Micha, „mein" Biologe, wegen deiner unkomplizierten Art hat das Arbeiten mit dir immer Spaß gemacht, vor allem das Entdecken des neuen Mikroskops, das ich alleine erst mal wohl eher aus der Ferne betrachtet hätte. Vielen Dank für all die Unterstützung, die tolle Rundreise durch Israel und dafür, dass du mein Paranymph sein wirst. Viel Erfolg beim Abrunden deiner Doktorarbeit.

I would like to thank many great colleagues with whom I have spent quality time inside and outside the lab. I want to especially acknowledge Abidin, Adrien (for joining to the movie

concerts in Plaza Futura), Ashish, Brian, Christoph, Dana, Dodo & Pascal (for keeping in touch), Dung (for watering my plants whenever I wasn't there), Ewelina, Floris, Ilknur, Inga (fürs 'kletsen'), Irén, Jan, Lars, Laurens & Targol, Marcel (for sharing with me the pleasure of being the bad and the good cop in the lab), Marie-France, Melissa (for our very interesting trips to several dancing workshops), Matt & Tess, Micha, Michel, Misha Golynskiy (for sharing вареники with me), Oliver, Pol, Remco, Seda, Sascha (for being Sascha and for bringing life to Eindhoven with you hyper energetic, generous and spontaneous personality), Tamara, Tristan, Wencke, and Yulan. Thanks for all the diners, parties, concerts, sport activities, nights out and Sascha's 'berühmt und berüchtigt' parties (including my first and only Oktoberfest-party, I had to come to the Netherlands for this!).

Conchi y Julia, muchas gracias por enseñarme el mundo de las células en 2007, por los tres meses increíbles en Madrid y por vuestra amistad durante todos estos años.

Natürlich möchte ich mich auch bei meinen "alten" Freunden bedanken (Bianca & Thomas, Dagi & Nils, Kai & Levi, Lucas & Rebekka, Marius & Sven, Miriam, Rebecca, Sandra & Christoph, Thomas, Tini & Lucas). Wir haben uns in der letzten Zeit leider etwas selten gesehen. Doch was ich an eurer Freundschaft sehr schätze, ist, dass, wann immer wir uns wieder sehen, ich nie das Gefühl habe, weg gewesen zu sein. Vielen Dank für eure Unterstützung über all die Jahre. Ich wünsche euch das Beste für eure Zukunft und hoffe, dass, egal wohin uns das Leben verstreut, wir trotzdem in Kontakt bleiben.

Я хочу поблагодарить мою семью. Ich möchte mich bei meiner Familie bedanken. I would like to thank my family. Besonders möchte ich mich bei meinen Eltern bedanken. Ihr habt dafür gesorgt, dass es mir an nichts fehlt und mit dem Umzug nach Deutschland sehr vieles aufgegeben, damit eure Kinder eine bessere Zukunft haben. Ich möchte mich für eine wundervolle, behütete Kindheit bedanken, für eure Liebe, euer Verständniss und eure volle Unterstützung. Мама и папа, я достигла многого блогодаря вам. Спасибо за вашу безграничную любовь и поддержку!

The very last lines are dedicated to Lech. Лёха, I simply enjoy every second we spend together. Thanks for your love and support. You mean the world to me.

Катя